UNIVERSIDAD COMPLUTENSE DE MADRID

FACULTAD DE FARMACIA

TESIS DOCTORAL

Nanopartículas de sílice mesoporosa sensibles a ultrasonido para aplicaciones biomédicas

Ultrasound-responsive Mesoporous Silica nanoparticles for biomedical applications

MEMORIA PARA OPTAR AL GRADO DE DOCTOR

PRESENTADA POR

Juan Luis Paris Fernández de la Puente

Directores

María Victoria Cabañas Criado
Miguel Manzano García

Madrid, 2018

Nanopartículas de sílice mesoporosa sensibles a ultrasonido para aplicaciones biomédicas

Ultrasound-Responsive Mesoporous Silica Nanoparticles for Biomedical Applications

Juan Luis Paris Fernández de la Puente

Memoria para optar al grado de Doctor por la Universidad Complutense de Madrid

Departamento de Química Inorgánica y Bioinorgánica
Facultad de Farmacia, UCM
Madrid 2017
Directores: María Victoria Cabañas Criado
Miguel Manzano García

Departamento de Química Inorgánica y Bioinorgánica
Facultad de Farmacia

UNIVERSIDAD
COMPLUTENSE
MADRID

Nanopartículas de sílice mesoporosa sensibles a ultrasonido para aplicaciones biomédicas

---

Memoria presentada por

Juan Luis Paris Fernández de la Puente

Directores

María Victoria Cabañas Criado

Miguel Manzano García

Para optar al grado de Doctor con Mención Internacional por la Universidad Complutense de Madrid

Madrid 2017

UNIVERSIDAD
COMPLUTENSE
MADRID

AUTORIZACIÓN DEL DIRECTOR DE TESIS

PARA SU PRESENTACIÓN

Dra. María Victoria Cabañas Criado con DNI 02211553B como Directora de la Tesis Doctoral

Nanopartículas de sílice mesoporosa sensibles a ultrasonido para aplicaciones biomédicas

realizada en el **Departamento de Química Inorgánica y Bioinorgánica** por el doctorando **Juan Luis Paris Fernández de la Puente**, autorizo la presentación de la citada Tesis Doctoral, dado que reúne las condiciones necesarias para su defensa.

En Madrid, a 16 de octubre de 2017

LA DIRECTORA DE TESIS

Fdo.: **María Victoria Cabañas Criado**

UNIVERSIDAD
COMPLUTENSE
MADRID

AUTORIZACIÓN DEL DIRECTOR DE TESIS

PARA SU PRESENTACIÓN

Dr. Miguel Manzano García con DNI 33519758H como Director de la Tesis Doctoral

Nanopartículas de sílice mesoporosa sensibles a ultrasonido para aplicaciones biomédicas

realizada en el **Departamento de Química Inorgánica y Bioinorgánica** por el doctorando **Juan Luis Paris Fernández de la Puente**, autorizo la presentación de la citada Tesis Doctoral, dado que reúne las condiciones necesarias para su defensa.

En Madrid, a 16 de octubre de 2017

EL DIRECTOR DE TESIS

Fdo.: **Miguel Manzano García**

Agradecimientos

Siempre es difícil despedir las etapas bonitas de la vida, especialmente aquellas que definen parte de quién eres. Mi tesis doctoral, con todos sus altibajos, ha sido extremadamente gratificante tanto en lo profesional como en lo personal. Me gustaría agradecer a todas las personas que han contribuido a que este documento exista hoy, pero me temo que con ello podría llenar más páginas de las que tiene toda la tesis, y aun así es posible que me quedara corto. Por ello, quiero empezar disculpándome por las ausencias imperdonables que, seguramente, contenga este apartado.

Empezaré agradeciendo a la Profesora María Vallet Regí por acogerme en su grupo de investigación y darme la oportunidad de aprender y desarrollarme en un campo apasionante.

A mis directores de tesis, Victoria Cabañas y Miguel Manzano, quiero agradecerles toda la dedicación y esfuerzo a lo largo de estos años y, especialmente, en la última etapa de redacción de la tesis. Siento todas las prisas por llegar a tiempo a todo. Vicky me ha transmitido una pasión por la ciencia que me acompañará el resto de mi vida, y con ella he aprendido a pensar, y a tener una sed de entendimiento que, desgraciadamente, casi nunca se sacia del todo. Gracias a Miguel por facilitarme oportunidades increíbles de desarrollo personal y profesional, que me han conducido a expandir mis horizontes y a ser un científico más completo.

Gracias al Ministerio de Economía y Competitividad por la concesión de un contrato de formación de doctores, así como de financiación para estancias breves en el extranjero, gracias a los cuales todo este trabajo ha sido posible.

Al Departamento de Química Inorgánica y Bioinorgánica, a la Facultad de Farmacia y a la Universidad Complutense de Madrid. Después de 5 años de carrera y 4 de doctorado, esta facultad, y este departamento, son mi segunda casa. Esté donde esté, esta institución y lo que representa formarán parte de todo lo que haga. Procuraré estar a la altura con todas mis fuerzas. En este departamento he coincidido con gente excepcional que han hecho de cada momento único. La experiencia sin ellos habría sido radicalmente diferente. Juan Carlos, como director del departamento, ha hecho todo lo posible para que nuestra situación fuese inmejorable. Pili y Jose han sido auténticos guías y expertos en resolución de todos los problemas que, con buena intención pero mala ejecución, hemos ido causando. A todos los profesores y resto de personal del departamento, he aprendido cosas de todos ellos. Antonio, Montse, Isa, Dani, Blanca, Ana, África, María Teresa, Maribel, Antonio Luis y tantos otros. Gracias a Jose también, sin todos los cafés y chascarrillos, esta tesis no estaría aquí. O por lo menos, no hoy. Gracias también a los distintos Centros de Apoyo a la Investigación, especialmente al Centro Nacional de Microscopía Electrónica y el CAI de Difracción de Rayos X.

A Jesús Román y Juan Peña. Tras muchos años de relación profesional y personal con los dos son, junto con Vicky, parte fundamental de mi familia científica.

Las cosas no siempre salen como uno las planea, pero las personas que te marcan te acompañan para siempre, no importa las vueltas que dé el camino. Sin ellos tres, no estaría donde me encuentro hoy.

A todos los compañeros de trinchera con quienes he luchado en búsqueda de la verdad, ese ser esquivo cuya presencia solo se intuye la mayor parte de las veces. A Edu, que para mí ha sido como ese niño que va dos cursos por delante en el colegio, y que siempre consideraste que tenía una personalidad "magnética". A Marina, con su maravillosa personalidad jovial y su risa contagiosa, que ha sido la "luz" en las tinieblas en tantas ocasiones. A Nati, cuya tesis ha discurrido en paralelo a la mía, y que en multitud de ocasiones ha sido el "andamio" sobre el que apoyarme. A Gonzalo, con quien he entablado una "sólida" amistad, y con quien hablando de camino al trabajo se han solucionado no pocos problemas de esta tesis. A Alejandro, por todas las charlas de ciencia en el laboratorio, despachos y mil situaciones más, que de tanto "estímulo" me han servido. A Rocío, compañera de despacho inmejorable, que "encapsula" en su persona prácticamente todas las características de los grandes científicos. A Miguel (Maño), que ha hecho algunos días interminables mucho más fáciles gracias a su humor, a veces "ácido", y casi siempre absurdo. A Sergio, que ha sido un compañero genial en las últimas etapas de mi tesis, y que vale su peso en "oro". A Ángel, que en lo personal, científico y musical, se merece un disco de "platino". A Fer, que como amigo y profesional, es lo "máximo". A Marta, que en su paso por aquí fue una compañera fantástica, a quien deseo toda la suerte del mundo, sin tomar decisiones "precipitadas". También a Patricia, que nunca pierdas tu alegría y empuje. A Sandra, con quien pasé mis primeros momentos como "profesor". A Ana (Fonti), por esas tertulias, sándwiches y visitas a bodegas, siempre geniales. A Dani, por todas esas placas, y el poco tiempo con el que te he avisado de algunas de ellas. A Rafa, que siempre está dispuesto a ayudar a todo el mundo. A todos los demás que han pasado y siguen pasando por aquí y que han hecho de esta experiencia lo que ha sido (Mónica, Okan, Talelli, Rebeca, Nuria, Noemí y muchos más). A los nuevos doctorandos con este camino aún por delante de ellos, también gracias y ofreceros un consejo: Disfrutad de la tesis, se acaba mucho antes de lo que parece.

Al Instituto de Investigación 12 de octubre y al grupo de medicina regenerativa: Ana Flores y Paz de la Torre, conoceros ha sido increíble, y el trabajo que hemos hecho constituye una parte fundamental de esta tesis. Gracias también a todos sus estudiantes con los que he tenido la suerte de ir coincidiendo en estos años.

To Professor Daniel S. Kohane and his wonderful research group, especially Alina and Bruce, for an amazing stay of 4 months surrounded by great people. Gracias también a Joaquín, Rocío y Ema, con los que tuve la tremenda suerte de coincidir en Boston y con quienes espero volver a coincidir en multitud de nuevas ocasiones.

To Professor Constantin C. Coussios and everyone in his research group, especially Christophoros Mannaris. They made me appreciate the wonders and beauty of engineering during my 3 months in Oxford. Once a BUBBL, always a BUBBL!.

A mis amigos de (casi) toda la vida, Pablo, Jose, José Pablo, Migui, Esther, y a aquellos que ya parece que llevan toda una vida (te estoy mirando a ti, Rebeca). Hemos crecido juntos a lo largo de todos estos años, pero no puedo evitar cerrar esta etapa de mi vida sintiéndome un poco un niño jugando a ser adulto. Gracias por estar ahí todo este tiempo.

A mi familia. A Luisa, mi madre, y a mis hermanas Sonsoles y Leyre, por su inmensa paciencia y su infinita ternura. Soy quien soy gracias a ellas. Nunca podré enumerar todo lo que han hecho por mí, ni pedir perdón por todos los disgustos que, de nuevo sin mala fe, les he causado a lo largo de los años. Por las noches sin dormir, las tardes de cine en películas para ellas aburridísimas, la casa llena de "amigotes", las horas encerrado en un libro sin hacer caso a nadie, las tardes dando vueltas por Atocha, los ensayos interminables con una baraja en la mano, por pasar conmigo las frustraciones de la vida, los nervios antes de un examen, por haber podido caminar hacia el altar a vuestro lado, por saber que siempre estáis ahí. Gracias mamá por darme una infancia tremendamente feliz, a pesar de todo. Gracias también a mis cuñados Iván y Rubén, y unas gracias tremendamente especiales a mis sobrinos, Emma, Samuel, Adrián, Mateo, Alejandra… y los que vengan. El mundo es un lugar mucho más maravilloso porque vosotros estáis en él, y mi vida mucho más feliz. Gracias a mis abuelas, que espero tengan hueco en su estantería para un ejemplar de esta tesis. Gracias también a todos los demás miembros de mi familia, los que siguen aquí y los que ya no están. Siempre os llevo conmigo, especialmente al padre excepcional que tuve la suerte de que me fuera dado, a pesar del poco tiempo que pudimos pasar juntos.

Gracias a Fuen, mi compañera de vida a quien tuve la tremenda suerte de conocer en esta mi segunda casa, hace ya más de 8 años. El proyecto de vida que tenemos por delante me llena de ilusión y expectación. Gracias por ser quien eres y por todos esos momentos en los que he podido escapar de las dificultades a tu lado. Recorreremos el camino juntos, por siempre y para siempre. Gracias también a tus padres y a tu hermana Loles, que me han acogido en su familia con los brazos abiertos.

Gracias por último a todos aquellos lectores que se enfrentan ahora a esta tesis, espero que leyéndola podáis percibir al menos una ínfima parte de las alegrías y desvelos que he vivido a lo largo de su desarrollo.

ABREVIATURAS

Abreviaturas empleadas en la tesis doctoral, explicadas en inglés y en español.

BET: Brunauer–Emmett–Teller

CTAB: Hexadecyltrimethylammonium bromide/ Bromuro de hexadeciltrimetilamonio

DLS: Dynamic light scattering/ Dispersión de luz dinámica

DMSCs: Decidua-derived MSCs/ MSCs de decidua

EPR: Enhanced permeation and retention/ Permeabilidad y retención aumentadas

FRP: Free radical polymerization/ Polimerización por radicales libres

FTIR: Fourier-transformed infrared/ Infrarrojo con transformada de Fourier

GPC: Gel permeation chromatography/ Cromatografía por permeación de gel

HIFU: High intensity focused ultrasound/ Ultrasonido focalizado de alta intensidad

LCST: Lower critical solution temperature/ Temperatura crítica inferior de disolución

MAA: Methacrylic acid/ Ácido metacrílico

MEO_2MA: 2-(2-methoxyethoxy) ethyl methacrylate/ 2-(2-metoxiethoxi) etilmetacrilato

MI: Mechanical index/ Índice mecánico

MSCs: Mesenchymal stem cells/ Células madre mesenquimales

MSN: Mesoporous silica nanoparticles/ Nanopartículas mesoporosas de sílice

NIR: Near infrared/ Infrarrojo cernano

NMR: Nuclear magnetic resonance/ Resonancia magnética nuclear

PEG: Polyethylene glycol/ Polietilenglicol

PEI: Polyethyleneimine/ Polietilenimina

RAFT: Reversible addition−fragmentation chain-transfer/ Adición fragmentación y transferencia de cadena reversible

RGD: Arginylglycylaspartic acid/ Ácido arginilglicilaspártico

ROS: Reactive oxygen species/ Especies reactivas de oxígeno

SEM: Scanning electron microscopy/ Microscopía electronica de barrido

TEM: Transmission electron microscopy/ Microscopía electronica de transmisión

TEOS: Tetraethyl orthosilicate/ Tetraetilortosilicato

TGA: Thermogravimetric analysis/ Análisis termogravimétrico

THPMA: 2-tetrahydropyranyl methacrylate/ 2-tetrahidropiranilmetacrilato

US: Ultrasound/ Ultrasonido

XRD: X-Ray diffraction/ Difracción de rayos X

ÍNDICE

Resumen

Esta tesis doctoral se centra en el estudio de nanopartículas de sílice mesoporosa (MSNs) en combinación con ultrasonido (US) para su uso en biomedicina, y más concretamente, en el contexto de la oncología.

La elevada toxicidad de los fármacos antitumorales tras su administración sistémica hace necesaria la búsqueda de nuevas estrategias terapéuticas con un mejor perfil de seguridad para el paciente. El uso de nanopartículas como transportadores de estos fármacos podría permitir una acumulación más selectiva de los mismos en el tumor, disminuyendo así la distribución al resto del organismo y los efectos secundarios asociados. La acumulación selectiva de nanopartículas en tumores sólidos se debe a su estructura vascular anómala, que permite la extravasación y retención de macromoléculas y partículas de hasta varios cientos de nanómetros. Este efecto de permeabilidad y retención aumentadas (EPR), que se denomina comúnmente "vectorización pasiva" constituyó la principal motivación en el desarrollo de la nanomedicina aplicada al cáncer, como es el caso del Doxil®, primera nanomedicina oncológica comercializada.

En la presente tesis doctoral se ha elegido como nanotransportador de dichos fármacos las MSNs debido a su estabilidad físicoquímica y sus propiedades texturales, elevada área superficial y volumen de poro, que proporcionan una elevada capacidad de carga de fármacos. El US se ha elegido como estímulo porque presenta una gran capacidad para penetrar hasta zonas profundas del organismo de forma no invasiva, y puede producir efectos tanto mecánicos como térmicos en el medio biológico sobre el que se aplique.

La tesis doctoral está dividida en tres bloques. Primero, se lleva a cabo el desarrollo y la evaluación de MSNs para liberación de fármacos inducida por US. Posteriormente, se plantean dos tipos de aproximaciones para lograr el transporte selectivo de las MSNs hacia tumores, bien mediante estrategias físico-químicas de vectorización o bien empleando como vehículos de las MSNs células capaces de migrar al tejido tumoral.

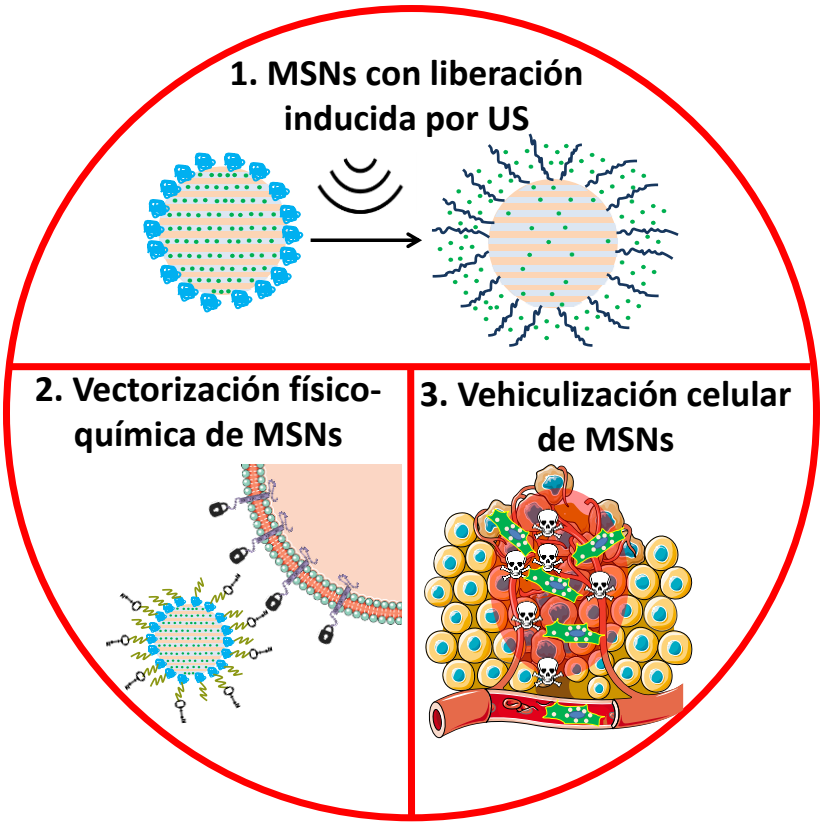

Resumen gráfico de las partes en que se encuentra dividida la presente tesis doctoral.

El **primer bloque** de la tesis versa sobre el desarrollo de MSNs con liberación de fármacos sensible a US (MSNs-US). La porosidad abierta de las MSNs implica que cualquier fármaco que se cargue en su interior va a empezar a ser liberado al medio en el momento en el que las nanopartículas se encuentren dispersas en un fluido. Esto no solo disminuiría la cantidad de fármaco capaz de alcanzar el órgano diana, sino que además puede dar lugar a toxicidad en tejidos sanos debido a esta liberación inespecífica. Para atajar este problema, se ha desarrollado una compuerta polimérica que impida la liberación prematura del fármaco. La compuerta polimérica, sintetizada mediante polimerización por radicales libres (FRP), es un copolímero aleatorio compuesto de los monómeros metoxietoxietilmetacrilato (MEO_2MA) y tetrahidropiranilmetacrilato (THPMA). El THPMA proporciona al copolímero final la capacidad de respuesta a US, ya que se produce su hidrólisis al exponerlo a US de alta frecuencia, dando lugar a ácido metacrílico. Este cambio en el copolímero desencadenará la liberación de la carga en el material final. El copolímero sensible a ultrasonido obtenido fue anclado a la superficie de MSNs, para dar lugar a MSNs-US. La capacidad de retener la carga en su interior a temperatura fisiológica, y de liberarla en respuesta a la aplicación de US fue comprobada empleando dos moléculas modelo:

fluoresceína y un complejo fluorescente de rutenio ($[Ru(bipy)_3]^{2+}$). Posteriormente, se comprobó que las nanopartículas híbridas obtenidas no son citotóxicas cuando no están cargadas con ningún fármaco. Cuando las nanopartículas fueron cargadas con el antitumoral doxorrubicina, fueron capaces de inducir toxicidad dosis-dependiente en células tumorales de próstata (LNCaP) sólo cuando el material había sido expuesto a US, demostrando su capacidad de matar células tumorales bajo estímulo de US.

A continuación se llevó a cabo la evaluación del mecanismo de apertura de las MSNs-US. Esto es, si la apertura de la compuerta se debe a los efectos térmicos o mecánicos causados por el US. Para ello, se emplearon tres frecuencias de US focalizado diferentes, 0.5, 1 y 3.3 MHz. Se introdujo un termopar en el recipiente de la muestra para monitorizar la temperatura durante el experimento, mientras que un detector pasivo de cavitación permitió distinguir la presencia de cavitación acústica (como principal efecto mecánico evaluado). Los resultados mostraron que la aplicación de una cierta intensidad de cavitación acústica inercial, aún sin calentamiento apreciable a escala macroscópica, es capaz de producir la liberación de la carga desde el material. Por otro lado, el tratamiento térmico de la muestra o la aplicación de US con incremento de temperatura, pero sin presencia significativa de cavitación, no fueron capaces de inducir la liberación de la carga. Por lo tanto, el mecanismo de apertura de las MSNs-US parece estar ligado a la cavitación acústica, sin necesidad de un incremento de la temperatura del medio, lo que permitiría utilizar nuestros transportadores de una forma segura, ya que van a liberar el fármaco sin aumento de temperatura en los tejidos circundantes.

En el **segundo bloque** de la tesis se analizan tres estrategias físico-químicas diferentes para lograr la vectorización selectiva de las MSNs hacia tumores.

Primero se anclaron a las MSNs-US descritas en el bloque 1 una capa de polietilenglicol (PEG) y moléculas de vectorización activa. Tal y como se describe en la literatura, la decoración de la superficie de nanopartículas con cadenas de PEG (PEGilación) permite aumentar el tiempo de circulación de las partículas en el torrente sanguíneo, con el objetivo de lograr una mayor acumulación de las mismas en el tumor. Los agentes de vectorización activa son moléculas capaces de interaccionar con algún componente sobreexpresado en la membrana de las células diana facilitando su internalización en las mismas. Así, el fármaco antitumoral se liberará en el interior de la célula diana, aumentando su concentración local y maximizando su efecto. Para ser capaces de obtener este nuevo material PEGilado y con vectorización activa, se

desarrollaron diferentes estrategias químicas. Primero, el método de obtención de la compuerta polimérica fue modificado, empleando en este caso la polimerización por adición fragmentación y transferencia de cadena reversible (RAFT). Este método permitió obtener un copolímero con dos extremos funcionales diferentes, anclándolo por un extremo a las MSNs, y uniendo el otro extremo al PEG con el agente de vectorización. Se comprobó que este nuevo material retenía su capacidad de respuesta al estímulo de ultrasonido. El empleo de la cicloadición 1,3-dipolar de Huisgen utilizando un alquino tensionado permitió obtener un material PEGilado modular al que poder anclar distintos agentes de vectorización activa. Empleando la secuencia peptídica RGD, capaz de interaccionar con integrinas en la membrana celular para aumentar su internalización, se llevaron a cabo estudios *in vitro* con células tumorales HeLa. La internalización de las nanopartículas con RGD fue mucho mayor que en el sistema sin vectorización activa. Finalmente, en un experimento con nanopartículas cargadas con doxorrubicina, se observó que la aplicación de US era capaz de inducir un incremento en la toxicidad de las nanopartículas, indicando un aumento en la liberación del fármaco en respuesta al estímulo.

Uno de los problemas potenciales de la vectorización activa es el efecto conocido como barrera del sitio de unión. Una vez que las nanopartículas con vectorización activa han alcanzado el tumor, las células tumorales en la primera línea del tejido captan la gran mayoría de las nanopartículas, impidiendo su distribución a zonas más profundas, y limitando su efecto terapéutico. El empleo de estrategias de vectorización jerarquizada puede ayudar a disminuir este inconveniente. En dichas estrategias, las nanopartículas circulan por el torrente sanguíneo con algún agente de vectorización oculto al medio externo. Una vez en la zona deseada, la presencia de un estímulo, interno o externo, permite exponer al medio dicho agente, produciéndose la captación de las partículas por las células tumorales. En el siguiente trabajo de esta tesis, se utilizaron los efectos térmicos del US para desarrollar MSNs con vectorización jerarquizada. Estas nanopartículas poseen oculto bajo una capa de PEG un agente que inducirá su internalización. El PEG se encuentra unido a las MSNs mediante un enlace termosensible. El aumento de temperatura producido por el US provoca que la capa de PEG se separe del material, exponiendo grupos aminopropilo cargados positivamente que favorecen su internalización en células de osteosarcoma humano (HOS). Experimentos de citotoxicidad empleando nanopartículas cargadas con el antitumoral

topotecan mostraron un destacado incremento en la muerte de las células HOS cuando se emplearon nanopartículas que habían sido expuestas a US.

Todas las estrategias de vectorización utilizadas hasta el momento en este bloque dependen en primera instancia del efecto EPR. Una vez que las partículas se han acumulado de forma pasiva en el tumor, la interacción de su superficie con la membrana celular permite la actuación de las estrategias de vectorización activa o de vectorización jerarquizada. Sin embargo, el efecto EPR no es un fenómeno homogéneo en todos los tipos de tumores, ni en las distintas zonas de un mismo tumor. Además, la única fuerza motriz actuando sobre las nanopartículas durante su acumulación pasiva es la difusión, la cual se ve dificultada por la elevada presión intersticial del tumor. Por ello, el siguiente paso en esta tesis fue el uso de US para favorecer la acumulación y penetración de MSNs en tumores. Se utilizó un modelo que simula el tejido tumoral empleando un gel de agarosa con canales, por los que se hace pasar una suspensión de MSNs. La aplicación de US se realizó de forma focalizada en distintos puntos de cada canal, evaluando la extravasación de las nanopartículas al gel de agarosa empleando distintas frecuencias de US (0.5 y 1.6 MHz). Se observó extravasación de las MSNs en las condiciones empleadas, obteniendo mayor direccionalidad a 1.6 MHz y una extravasación de mayor magnitud aplicando presiones más elevadas. La extravasación de nanopartículas cargadas con el fluoróforo rodamina B fue también evaluada en el mismo modelo, obteniendo resultados similares a los previamente observados en MSNs sin carga. Por último, la combinación de MSNs con núcleos de cavitación poliméricos (NCs) que faciliten la generación de cavitación inercial fue estudiada, consiguiendo extravasación de las MSNs a la mitad de la presión necesaria sin la combinación con NCs. Así, los NCs serían co-inyectados con MSNs cargadas con el fármaco de interés. Los NCs serían activados por US focalizado en la zona del tumor, generando cavitación inercial e induciendo la extravasación de ambos tipos de partículas. Una vez embebidas en el tejido, las MSNs actuarían como un reservorio del fármaco, liberándolo lentamente en su zona de actuación.

El **tercer bloque** de esta tesis doctoral se centra en el uso de vehículos celulares para transportar las MSNs-US. Esta estrategia se plantea como una alternativa a la vectorización físico-química de nanopartículas, la cual ha tenido hasta ahora un limitado éxito en su transferencia al entorno clínico. Esta aproximación nos va a permitir transportar de forma selectiva hacia tumores las MSNs-US, superando además la mayoría de las limitaciones previamente mencionadas de las estrategias clásicas de

vectorización de nanopartículas. Es bien conocida la existencia de varios tipos de células que poseen capacidad migratoria hacia tumores y otros tejidos patológicos. Entre ellos, cabe destacar las células madre mesenquimales (MSCs) por haber sido ampliamente estudiadas. Las MSCs pueden proceder de distintas fuentes, tales como la médula ósea, el tejido adiposo o la placenta. Las MSCs procedentes de la decidua de la placenta humana (DMSCs) son especialmente prometedoras, ya que son fáciles de obtener en grandes cantidades, constituyen una población homogénea, no son inmunogénicas y han demostrado previamente su capacidad de migrar hacia tumores de mama en un modelo *in vivo* de rata. Son además capaces de ralentizar el crecimiento de tumores de mama primarios y de afectar también al desarrollo de tumores secundarios.

En el primer capítulo de este bloque se evalúa la interacción de las DMSCs con MSNs con carga superficial positiva o negativa. La captación de nanopartículas con carga positiva fue más eficiente, demostrando además su retención en el interior de la célula durante al menos 5 días. Las MSNs no afectaron a la viabilidad ni a la capacidad migratoria de las DMSCs *in vitro*. También se observó el transporte de MSNs hacia tumores de mama *in vivo*, al observar la fluorescencia de las MSNs en cortes histológicos del tumor. Finalmente, se introdujeron MSNs cargadas con doxorrubicina en las DMSCs, que fueron entonces co-cultivadas con células tumorales de mama (NMU). La liberación del fármaco desde las MSNs en el interior de las DMSCs fue capaz de inducir la muerte de las células NMU en co-cultivo con las células transportadoras.

Los resultados de la combinación de las MSNs con DMSCs muestran que este tipo de estrategias pueden ser prometedoras para la terapia de tumores sólidos. Sin embargo, dado que las MSNs empleadas en el trabajo anterior carecían de ningún tipo de compuerta, la liberación del fármaco durante el proceso de migración de la célula transportadora podría comprometer su viabilidad y capacidad migratoria. Por ello, el siguiente paso fue evaluar la combinación de las DMSCs con las MSNs-US desarrolladas en el bloque 1. Para lograr la internalización eficaz de las nanopartículas, éstas tuvieron que ser recubiertas con un policatión, polietilenimina (PEI), para dotarlas de una carga superficial positiva. Se comprobó que las nanopartículas recubiertas con PEI mantenían su comportamiento sensible a US, tanto *in vitro* como *in vivo*. Las partículas fueron internalizadas de forma eficiente por las DMSCs, y fueron retenidas en su interior durante al menos 6 días. En ausencia del estímulo de US, las nanopartículas cargadas con doxorrubicina no eran tóxicas para las DMSCs durante al menos 3 días

tras la internalización, ni tampoco afectaban a su comportamiento migratorio hacia homogenado de tumor *in vitro*. En un co-cultivo de DMSCs con células tumorales NMU, se observó muerte de las células tumorales solo cuando DMSCs transportando MSNs-US cargadas con doxorrubicina habían sido expuestas a US, demostrando la capacidad de respuesta al estímulo externo.

La eficacia de distintos tipos de nanopartículas en aplicaciones biomédicas puede mejorarse empleando estrategias duales, en las que distintos mecanismos de acción se combinan para lograr un efecto sinérgico. Un ejemplo de este tipo de combinaciones es el desarrollo de nanopartículas con capacidad de transfección génica además de ser empleadas como transportadores de fármacos. En el último capítulo de esta tesis doctoral, se ha aprovechado el recubrimiento de PEI sobre las MSNs-US para proporcionar una nueva funcionalidad al material: como agente de transfección génica, al introducir genes insertados en dicho recubrimiento. Así, se puede lograr que las células transportadoras DMSCs puedan expresar algún gen de interés terapéutico, cuyo efecto se añadiría al de la doxorrubicina transportada en el interior de las nanopartículas. La capacidad de transfección de las nanopartículas fue evaluada con PEI de dos pesos moleculares diferentes: 2 y 5 kDa. Empleando un plásmido que codifica la proteína verde fluorescente, se comprobó que la capacidad de transfección génica es mayor con el PEI de mayor tamaño. Posteriormente, se introdujo un plásmido que codifica dos genes suicidas empleados para terapia antitumoral: citosina desaminasa y uracil fosforribosiltransferasa. Estas dos proteínas actúan de forma secuencial, siendo capaces de convertir el profármaco no tóxico 5-fluorocitosina (5-FC) en una especie tóxica. Tras la transfección de las DMSCs con los genes suicidas empleando las nanopartículas, se observó una gran toxicidad al añadir 5-FC en el medio. La producción de esta especie tóxica también fue capaz de inducir la muerte de células tumorales NMU co-cultivadas con las células DMSCs.

Todos los resultados obtenidos en la presente tesis doctoral muestran el gran potencial del ultrasonido para inducir distintas respuestas por parte de nanopartículas de sílice mesoporosa en el contexto del cáncer, pudiendo controlar tanto la liberación de fármacos, como la captación de las nanopartículas por parte de células o su extravasación en el tumor.

Summary

This PhD thesis is focused on studying the use of mesoporous silica nanoparticles (MSNs) in combination with ultrasound (US) for biomedical applications, and more specifically, in the context of oncology.

The high toxicity of anticancer drugs after their systemic administration makes necessary looking for new therapeutic strategies with a better safety profile for the patient. The use of nanoparticles as carriers of these drugs could allow a more selective accumulation of the drug in the tumor, decreasing the distribution to the rest of the organism and the associated side effects. The selective accumulation of nanoparticles in solid tumors is due to their anomalous vasculature, which allows the extravasation and retention of macromolecules and particles up to a few hundred nanometers. This enhanced permeation and retention (EPR) effect, which is commonly referred to as "passive targeting", has constituted the main motivation driving the development of cancer nanomedicine, as was the case for Doxil®, the first cancer nanodrug commercialized.

In the present doctoral thesis, MSNs were selected as drug nanocarriers due to their physicochemical stability and their textural properties, high surface area and pore volume, which provide a high drug loading capacity. US was chosen as the stimulus because it presents the capacity to non-invasively penetrate deep into the body, and it can produce thermal and mechanical effects in the biological medium.

The doctoral thesis is divided in three parts. First, the development and evaluation of mesoporous silica nanoparticles with ultrasound-induced drug release was carried out. Then, two different approaches to achieve selective transport of MSNs towards tumors were evaluated, either through physicochemical targeting or employing tumor-tropic cells as vehicles of the mesoporous silica nanoparticles.

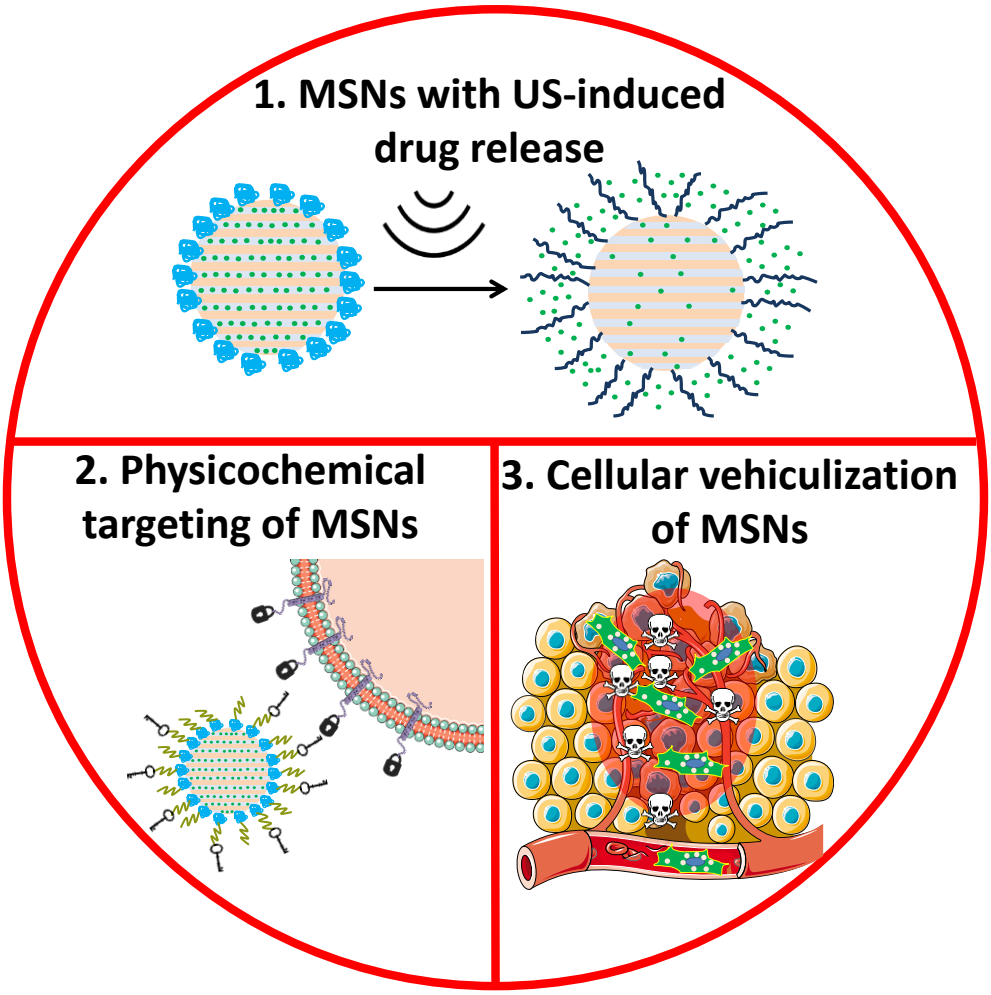

Graphical summary of the parts in which the present doctoral thesis is divided.

The **first part** of the thesis deals with the development and evaluation of MSN with ultrasound-sensitive drug release (MSNs-US). The open porosity of MSNs implies that any drug loaded into the pores will start to diffuse out from the moment the nanoparticles are dispersed in a fluid. This will not only decrease the amount of drug able to reach the target organ, but it can also give rise to toxicity in healthy tissues due to this premature release. To solve this issue, a polymeric gate was developed to prevent premature release of the drug. The polymeric gate, synthesized by free radical polymerization (FRP), is a random copolymer composed of the monomers 2-(2-methoxyethoxy) ethyl methacrylate (MEO_2MA) and 2-tetrahydropyranyl methacrylate (THPMA). THPMA will provide US-responsiveness to the final copolymer, undergoing hydrolysis when exposed to high frequency ultrasound. This change in the copolymer will trigger the cargo release from the final material. The US-responsive copolymer was grafted on the surface of MSNs to obtain MSNs-US. Its capacity to retain a cargo at physiological temperature and release it in response to US application was verified

employing two model molecules: fluorescein and a fluorescent ruthenium complex ($[Ru(bipy)_3]^{2+}$). Then, the obtained hybrid nanoparticles were checked not to be cytotoxic when they were not loaded with any drug. When the nanoparticles were loaded with the anticancer drug doxorubicin, the particles could induce dose-dependent toxicity to prostate cancer cells (LNCaP) only when the material had been exposed to US, demonstrating its capacity to kill cancer cells under US stimulus.

Then, the evaluation of the opening mechanism of the MSNs-US was evaluated, which can be due to the thermal or mechanical effects of US. To do that, three different frequencies of focused US, 0.5, 1 and 3.3 MHz, were used. A thermocouple was introduced in the sample holder to monitor bulk temperature during the experiment, while a passive cavitation detector allowed us to evaluate the onset of acoustic cavitation (as the main mechanical effect being evaluated). The results showed that the application of a certain intensity of inertial acoustic cavitation, even without significant bulk heating, was capable of inducing cargo release from the material. On the other hand, thermal treatment of the sample, or the application of US with bulk heating but without significant presence of cavitation were not able to induce cargo release. Therefore, the mechanism behind the opening of the MSNs-US appears to be linked to acoustic cavitation, without the need for an increase in the bulk temperature of the medium, what would allow us to use our nanocarriers in a safe manner, since they will release the drug without a temperature increase in the surrounding tissues.

In the **second part** of this thesis, three different physicochemical strategies to achieve selective MSN delivery to tumor were analyzed.

First, MSNs-US were grafted with a polyethylene glycol (PEG) chain and with active targeting molecules. As it has been described in the literature, decorating the nanoparticle surface (PEGylation) increases the circulation time of nanoparticles in the bloodstream, achieving a greater accumulation of the particles in the tumor. Active targeting agents are able to interact with some component overexpressed on the target cell membrane to facilitate their uptake. That way, the anticancer drug will be released within the target cell, increasing its local concentration and maximizing its effect. To obtain this new PEGylated and actively-targeted hybrid material, different chemical strategies were developed. First, the method to synthesize the polymeric gate was modified, employing in this case reversible addition−fragmentation chain-transfer (RAFT) polymerization. This method allowed us to obtain a copolymer with two different functional ends, grafting it to the MSNs through one of them, and linking the

other end to the PEG chain with the targeting agent. This new material retained its ultrasound-responsive behavior. Copper-free click chemistry was used to obtain a modular hybrid material to which different active targeting agents can be coupled. Employing the RGD peptide sequence, capable of interacting with integrins on the cell membrane to increase their uptake, *in vitro* experiments were performed with HeLa cancer cells. The internalization of RGD-targeted nanoparticles was greatly superior to that of the non-targeted system. Finally, in an experiment with doxorubicin-loaded nanoparticles, US application was observed to increase the toxicity of the nanoparticles, indicating an increase in drug release in response to the stimulus.

The next problem an actively-targeted nanoparticle will find is the effect known as the binding site barrier. Once the actively-targeted nanoparticles have reached the tumor, the first line of cancer cells will uptake the majority of the nanoparticles, preventing their distribution to deeper areas and limiting their therapeutic effect. Hierarchical targeting strategies can help reduce this problem. In such strategies, nanoparticles travel through the bloodstream with an active targeting agent hidden from the environment. Once in the desired area, the presence of a stimulus, internal or external, will expose that agent to the environment, promoting nanoparticle uptake by cancer cells. In the next work in this thesis, the thermal effects of US were used to develop MSNs with hierarchical targeting. These nanoparticles possess an agent that will induce their uptake, hidden under a PEG layer. The PEG chains are attached to the MSNs through a thermosensitive linker. An US-induced temperature increase will provoke the detachment of the PEG chains, exposing positively-charged aminopropyl groups that favour their internalization in human osteosarcoma (HOS) cells. Cytotoxicity experiments employing nanoparticles loaded with the anticancer drug topotecan showed a great increase in HOS cell death when nanoparticles exposed to US were employed.

All of the nanoparticle delivery strategies used up to this point in this part of the thesis rely on the EPR effect. Once the nanoparticles have passively accumulated in the tumor, the interaction of their surface with cell membranes allows active or hierarchical targeting. However, the EPR effect is not a homogeneous phenomenon in all types of tumors, or even in different parts of the same tumor. Besides, the only force acting upon the nanoparticles during their passive accumulation is diffusion, which is hindered by the high interstitial pressure of the tumor. For these reasons, the next step in this thesis consisted in favouring the accumulation and penetration of MSNs in tumors. A tumor

tissue-mimicking model employing an agarose gel with channels through which MSNs are flowed was used. US application was performed in a focused manner at different points in each channel, evaluating the extravasation of the nanoparticles to the agarose gel employing different frequencies (0.5 and 1.6 MHz). MSN extravasation was observed under the conditions used, obtaining a greater directionality at 1.6 MHz and a greater extravasation at higher pressures. The extravasation of nanoparticles loaded with the fluorophore rhodamine B was also evaluated in the same model, obtaining similar results as previously observed for non-loaded MSNs. Last, the combination of MSNs with polymeric cavitation nuclei (NCs) to ease the onset of inertial cavitation was studied. That way, NCs would be co-injected with MSNs loaded with the drug of interest. NCs would be activated by focused US in the tumor area, generating inertial cavitation and inducing the extravasation of both types of particles. Once embedded in the tissue, MSNs would act as a reservoir of drug, slowly releasing it close to its site of action.

The **third part** of this doctoral thesis is focused on using cellular vehicles to transport MSNs-US. This strategy is presented as an alternative to physicochemical targeting of nanoparticles, which so far has had a limited success on its translation to the clinical setting. This approach will allow us to selectively transport MSNs-US to tumors overcoming most of the limitations previously mentioned related to classical nanoparticle targeting strategies. Several types of cells possess migratory properties towards tumors and other pathological tissues. Mesenchymal stem cells (MSCs) can be highlighted as one of the types of tumor-tropic cells more thoroughly studied. MSCs can be obtained from different sources, such as bone marrow, adipose tissue or placenta. MSCs from the *decidua* of the human placenta (DMSCs) appear as especially promising, since they are easy to obtain in large quantities, they constitute a homogeneous population, they are low- or non-immunogenic and they have been previously shown to migrate towards mammary tumors in an *in vivo* rat model. They are also able to slow down the growth or primary tumors, and also affect the development of secondary tumors.

The first chapter in this part of the thesis evaluates the interaction of DMSCs with MSNs with positive or negative surface charge. Nanoparticle uptake was more efficient for positively-charged nanoparticles, while they were also retained inside the cells for at least 5 days. MSNs did not affect DMSC viability, nor their migration capacity *in vitro*. MSN transport towards mammary tumors was also observed *in vivo*,

by detecting MSN fluorescence in tumor histology samples. Finally, doxorubicin-loaded MSNs were introduced inside DMSCs, which were then co-cultured with mammary cancer cells (NMU). Drug release from MSNs inside DMSCs was capable of inducing the killing of the co-cultured NMU cancer cells in co-culture with the vehicle cells.

The results on the combination of MSNs with DMSCs show that this kind of strategies can be promising for solid tumor therapy. However, since the MSNs employed in the above work lacked of any king of gating mechanism, drug release during migration of the vehicle cell might compromise their viability and migration capacity. For that reason, the next step was to evaluate the combination of DMSCs with the MSNs-US developed in the first part of the thesis. To achieve a successful internalization of the nanoparticles, these had to be coated with a polycation, polyethyleneimine (PEI), to provide a positive surface charge. PEI-coated nanoparticles maintained their US-responsive behavior, both *in vitro* and *in vivo*. The nanoparticles were efficiently internalized in DMCSs, and they were retained within the vehicle cells for at least 6 days. In the absence of US stimulus, doxorubicin-loaded nanoparticles were shown not to be toxic for DMSCs for at least 3 days after nanoparticle uptake, as well as they did not affect their migratory behavior towards tumor homogenate *in vitro*. In a co-culture with NMU cancer cells, cancer cell death was only observed when DMSCs carrying doxorubicin-loaded MSNs-US had been exposed to US.

The efficacy of different types of nanoparticles for biomedical application can be enhanced by employing dual strategies, in which different mechanisms of action are combined to achieve a synergetic effect. An example of this type of combinations is the development of nanoparticles with gene transfection capacity besides being employed as drug carriers. In the last chapter of this doctoral thesis, the PEI coating previously developed on MSNs-US was employed to provide a new capacity to the material: gene transfection, by introducing genes inserted in the PEI coating. That way, we can induce the expression of a therapeutically useful gene by DMSCs, adding its effect to the one of the doxorubicin being carried. Gene transfection capacity of the nanoparticles was evaluated with PEI coatings of two different molecular weights: 2 and 5 kDa. Employing a plasmid encoding green fluorescent protein, gene transfection capacity was shown to be greater for the higher molecular weight PEI. Then, a plasmid encoding two suicide genes for anticancer therapy was introduced: cytosine deaminase and uracil phosphoribosyl transferase. These two proteins act in a sequential manner, converting the non-toxic prodrug 5-fluorocytosine (5-FC) into a toxic molecule. After DMSC

transfection with the suicide genes employing the nanoparticles, a great toxicity was observed when 5-FC was added to the medium. The production of this toxic molecule was also able to kill cancer NMU cells co-cultured with the DMSCs.

All of the results obtained in the present doctoral thesis show the great potential of ultrasound to induce different responses by mesoporous silica nanoparticles in the context of cancer, enabling us not only to control drug release, but also the uptake of nanoparticles by cells and their extravasation in the tumor.

1. INTRODUCCIÓN

La cosa más hermosa que podemos experimentar es el misterio. Es la fuente de todo arte y toda ciencia

Albert Einstein

La Introducción está dividida en tres capítulos centrados en los distintos aspectos a tratar en el desarrollo de la presente tesis doctoral.

El Capítulo 1.1 presenta una introducción general al campo de la nanomedicina, con una visión global de los tres campos principales de actuación de la misma: diagnóstico *in vitro*, diagnóstico *in vivo* y terapia. Durante este capítulo se introducirán los tipos de nanopartículas más empleados en nanomedicina, así como una breve revisión de sus principales aplicaciones en diagnóstico *in vitro* e imagen *in vivo*. También se explican los principales fundamentos de la nanomedicina en la terapia del cáncer, introduciendo conceptos como la vectorización pasiva y activa, estrategias terapéuticas basadas en el propio material utilizado o en el transporte de fármacos, el desarrollo de materiales sensibles a estímulos y una breve descripción de la aplicación de nanopartículas en otras patologías. Este capítulo (que se presenta en inglés) se encuentra recogido como un capítulo de libro aceptado para su publicación en "Handbook of nanoparticles and architectural nanostructured materials" de la editorial Elsevier.

Posteriormente, el Capítulo 1.2 contiene una introducción a la síntesis, caracterización y propiedades del tipo de nanopartículas seleccionado para el desarrollo de la tesis doctoral: nanopartículas de sílice mesoporosa.

Finalmente, en el Capítulo 1.3 se explican brevemente los principios fundamentales del estímulo externo elegido para este trabajo, el ultrasonido, así como los principales efectos que el ultrasonido puede provocar en el medio biológico.

1.1 Nanostructures for imaging, medical diagnostics and therapy

Juan L. Paris and María Vallet-Regí*.

Dpto. Química Inorgánica y Bioinorgánica, Facultad de Farmacia, UCM, Instituto de Investigación Sanitaria Hospital 12 de Octubre i+12, 28040-Madrid, Spain. Centro de Investigación Biomédica en Red de Bioingeniería, Biomateriales y Nanomedicina (CIBER-BBN), Spain. *Corresponding author, e-mail: vallet@ucm.es

1. Introduction

The application of nanotechnology for diagnostic or therapeutic application is called nanomedicine (Jain & Stylianopoulos 2010). Nanomedicine is an interdisciplinary field in which biology, medicine, chemistry, physics and other disciplines are brought together in order to develop nanomaterials suitable for biomedical application (Wicki et al. 2015). Nanoparticle size (in the range from a few nanometers to a few hundred nanometers) allows them to interact with biological entities in a fundamentally different manner than non-nanostructured materials (Albanese et al. 2012). Some of those size-dependent properties derive from the surface to volume ratio being much higher than for non-nanostructures materials. These properties can be exploited to design nanostructures that can be used to diagnose or treat different pathologies. Some examples would be the unique thermal, electrical, magnetic and optical properties that present different types of nanoparticles and that greatly differ from the properties of non-nanostructured materials with similar chemical composition (Chen et al. 2016).

The design of nanoparticles is essential to allow their correct function for biomedical application. Amongst the most important parameters to consider are nanoparticle size, chemical composition and surface characteristics (Chen et al. 2016). For example, nanoparticle size is critical for *in vivo* imaging as well as for therapeutic application of nanoparticles. As it will be explained later in this chapter, nanoparticles tend to accumulate in tumor tissue, due to an enhanced permeation and retention (EPR). In that context, if the particles are too big, they will not be able to reach the diseased tissue and, therefore, they will not achieve their function. On the other hand, if the nanoparticles are too small (less than 10 nm), they will be excreted in the urine, potentially preventing accumulation in the desired target, which would lead to, again, the material not achieving its function. For *in vitro* diagnostics, the size of nanoparticles is also a fundamental parameter, since it often determines the optical properties of the nanoparticle suspension (for example, in plasmonic gold nanoparticles), and a

modification in size will lead to changes in the measured response after exposure to a sample containing the analyte.

This chapter is divided in three parts. In the first one, some of the most important types of nanoparticles proposed for biomedical application will be classified based on their chemical composition. Then, the rationale for their use in medicine will be explored in two different applications, each with their needs and particularities: diagnostics (*in vitro* diagnostics and *in vivo* imaging) and therapy (or the combination of diagnostic and therapeutic nanoparticles: theranostics) (**Figure 1**).

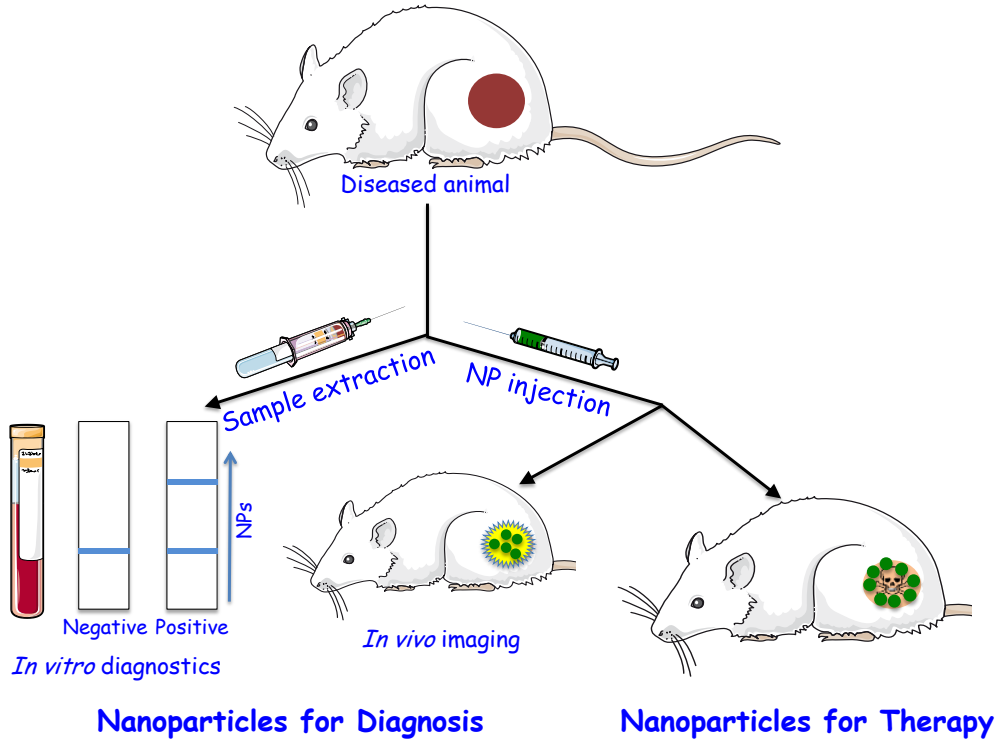

Figure 1. Representation of the three applications of nanostructures in medicine that will be described in this chapter: *In vitro* diagnostics, *in vivo* imaging and therapy.

2. Types of nanoparticles for nanomedicine.

A wide variety of nanoparticle types have been proposed for nanomedicine, some of the most important ones are going to be highlighted in this chapter. These types of nanoparticles will be classified based on their chemical composition in organic or inorganic nanoparticles (**Figure 2**). However, nowadays a very high percentage of the nanoparticles under evaluation are actually hybrid nanoparticles, joining organic and inorganic structures to yield multifunctional materials. These materials will be treated

inside the section regarding the organic or inorganic core nanoparticle used to obtain the hybrid.

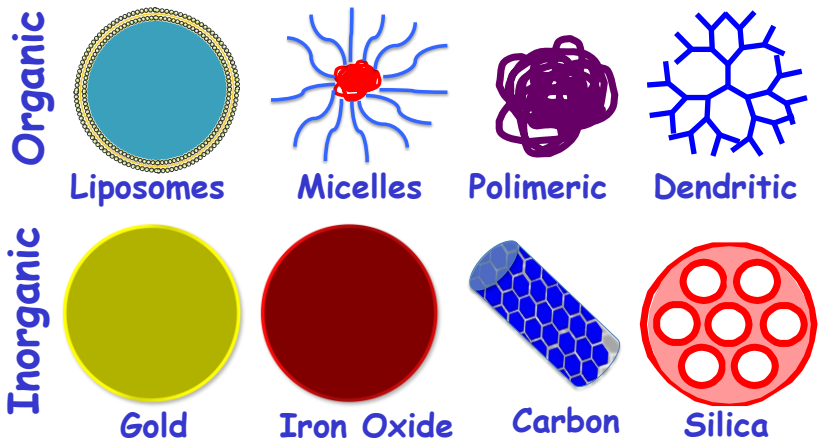

Figure 2. Schematic representation of some of the most important types of nanoparticles used for nanomedicine, divided by their chemical composition.

2.1 Organic nanoparticles

2.1.1 Liposomes and lipid nanoparticles

Liposomes are one of the most widely evaluated types of nanoparticles for biomedical application, and they have already reached clinical use (Bozzuto & Molinari 2015). Liposomes consist of amphiphilic lipids arranged in vesicles with an aqueous cavity surrounded by one or more lipid bilayers.

Liposomes can be prepared by different methods, being the most common ones reverse phase evaporation or vesicle extrusion (Bozzuto & Molinari 2015). They can be produced with natural or synthetic lipids and their chemical composition, size, lipid bilayer structure and surface charge (amongst other parameters) will determine the formulation characteristics, from the stability to the drug release behavior. For example, the stability of liposomes can be increased by the incorporation of cholesterol in their structure, which induces a denser packing of the hydrophobic chains inside the lipid bilayer. On the other hand, drug release from unilamellar liposomes is usually faster than from multilamellar ones, since the drug has to diffuse through more lipid bilayers in the second case. Liposomes can load hydrophilic molecules in the inner aqueous compartment (as is usually the case in unilamellar liposomes) or hydrophobic ones, in that case inserted in the lipid bilayer (mostly used in multilamellar liposomes). The combination of liposomes with other types of nanoparticles can yield multifunctional

systems that allow simultaneous therapy and diagnosis (theranostic materials), for example, by conjugating the liposomes with nanoparticles with imaging capabilities, like quantum dots (optical imaging) or superparamagnetic iron oxide nanoparticles (magnetic resonance imaging). All of these characteristics, together with their high biocompatibility, easy preparation with tunable sizes and high loading capacity make them the most successful nanostructured drug delivery system to date (Bozzuto & Molinari 2015). However, they present a rather low physicochemical stability compared to other nanoparticles. To increase nanoparticle stability, solid lipid nanoparticles can be obtained by using high-melting lipids. These lipid nanoparticles can be stabilized in aqueous suspension by adding surfactants or other functionalities (Bozzuto & Molinari 2015).

2.1.2 Micelles and solid polymeric nanoparticles

Polymeric micelles are also amongst the most studied nanocarriers. They are colloidal nanoparticles with a size around 5-100 nm, constituted by an amphiphilic block copolymer that self-assembles in aqueous medium (Oerlemans et al. 2010). At low concentrations, amphiphilic molecules are dissolved in the aqueous medium, but with increasing concentration, once the critical micellar concentration (CMC) is reached, the amphiphiles self-assemble, forming a hydrophobic core with a hydrophilic shell stabilizing the particles by hydrogen bonding with the surrounding water. The CMC of polymeric micelles is usually very low, which allows the presence of micelles at almost any dilution (Oerlemans et al. 2010). The polymer composition determines the micelle characteristics, like the drug molecules that can be loaded or the stability and biodistribution of the formulation. For example, the most common hydrophilic block is a chain of polyethyleneglycol (PEG), because it can stabilize the micelles and prevent the rapid uptake by the Reticuloendothelial system (RES) after injection. The polymer composition can also be modified to provide different functionalities to the material. A targeting moiety can also be included in the hydrophilic shell, as well as different components that provide imaging capabilities (like superparamagnetic iron oxide nanoparticles) to obtain theranostic nanodevices. Micelles can efficiently carry high amounts of hydrophobic drugs within their core, preventing the use of toxic adjuvants that would be necessary to administer the free hydrophobic drug. However, they have poor stability and cannot carry high amounts of hydrophilic molecules.

Other polymeric nanoparticles can also be prepared from natural or synthetic, biodegradable or non-biodegradable polymers (Kumari et al. 2010). Amongst them, biodegradable nanoparticles are preferred, due to a better safety profile. These particles have higher stability and the vast amount of polymers available make them a very versatile choice to develop particles for nanomedicine. Some of the most common methods to obtain polymeric nanoparticles are emulsification-diffusion, solvent emulsion-evaporation, nanoprecipitation, interfacial deposition and inotropic gelation (for example, in the case of polycations). They can load different types of drugs depending on the chemical nature of the chosen polymer; however, the loading efficiency is usually lower than with other types of nanocarriers. The most commonly biodegradable polymers used to develop nanoparticles for nanomedicine are: Poly-D,L-lactide-co-glycolide (PLGA), Polylactic acid (PLA), Poly-ε-caprolactone (PCL), chitosan and gelatin (Kumari et al. 2010). Protein nanoparticles (like those made of albumin) have also attracted great attention, because of the high biocompatibility and biodegradability behavior, and their high chemical versatility due to the large amount of different free functional groups throughout the biopolymer structure.

2.1.3 Dendritic nanoparticles

Dendrimers are hyperbranched polymers that can be obtained with different functional groups. They can be prepared in a highly defined way (with a polydispersity index close to 1) (Khandare et al. 2012). Some of the most used dendritic molecules are polyamidoamine (PAMAM), poly(propylene imine) and polyglycerol. Branched polymers present several advantages for biomedical application, for example, they have shown a longer blood circulation half-life than linear polymers with similar molecular weight and chemistry (Khandare et al. 2012). The obtention of polycationic dendrimers allows gene therapy application (due to the interaction with negatively-charged nucleic acid molecules). An important disadvantage of these types of materials might be the significant cytotoxicity found for highly charged polycations.

2.2 Inorganic nanoparticles:

2.2.1 Metal-based nanoparticles

A wide variety of metallic nanoparticles can be obtained for biomedical application. The synthesis of these nanoparticles is in general very tunable and allows the

preparation of monodisperse nanoparticles that can be easily modified afterwards (Boisselier & Astruc 2009). **Gold nanoparticles** in particular have been extensively studied for diagnostics and therapy. Gold nanoparticles ranging from 3 to more than 120 nm present a phenomenon called surface plasmon resonance, which allows their use for photodiagnostics and photothermal therapy. Moreover, not only spherical nanoparticles can be synthesized, but gold nanorods with different aspect ratios (ratio of length between long and short axis of the nanoparticle) can be obtained, with profound impact in the properties of those colloidal nanoparticles. **Silver nanoparticles** with plasmonic behavior can also be obtained. One of the most promising applications of silver nanoparticles is in antibacterial nanodevices, due to the bactericidal effect of the ion Ag^{+} (Boisselier & Astruc 2009).

Fluorescent semiconductor nanocrystals **(Quantum dots,** QDs) are inorganic fluorophores with very small diameter (2-10 nm) composed of a are single crystal of a semiconductor (like CdS, PbSe) or core/shell structures of two semiconductors (like CdSe/ZnS) (Azzazy & Mansour 2009; Michalet 2005). Compared to organic dyes, quantum dots have a broad-range excitation spectrum and a very narrow emission band, and their photostability is much higher. They have been studied very extensively for *in vitro* diagnostics and *in vivo* imaging. Near-Infrared (NIR)-emitting QDs hold great promise for *in vivo* imaging, since NIR light is known to penetrate more in living tissue and shows much better signal-to-noise ratio (due to less autofluorescence in that range), however, most NIR-emitting QDs currently known are significantly less stable than visible-light emitting QDs. An important concern with QDs is regarding their potential toxicity *in vivo* after the metal ions they are composed of are released from the material. For this reason, heavy metal-free quantum dots are gathering great interest for their biomedical use (Yaghini et al. 2016).

Nanoparticles for photon **upconversion** can also be prepared from rare earth ions (for example Er^{3+} or Yb^{3+}) dispersed in a dielectric lattice (Azzazy & Mansour 2009). These kinds of particles can be excited by two or more low-energy photons (usually in the NIR range) and emit one higher energy photon (generally in the ultraviolet or visible region). Therefore, they present many advantages for biomedical use, as they can be excited deep inside the organism (by highly-penetrating NIR light) and then emit UV or visible light to elicit the desired biological effect. They present very high photostability and low toxicity. Many formulations have been developed by

joining upconversion nanoparticles with other particles or functionalities that can respond to the emission from these particles after NIR irradiation.

Superparamagnetic nanoparticles (like maghemite, γ-Fe_2O_3, and magnetite, Fe_3O_4, nanoparticles) present very interesting properties for their use in biomedicine (Banerjee et al. 2010). When these types of nanoparticles have less than 50 nm in diameter, the whole nanoparticle acts as a single magnetic domain, showing superparamagnetic behavior. Without an applied magnetic field, the particles do no present macroscopic magnetization, what eliminates the possibility of agglomeration of the nanoparticles due to their magnetic behavior, which is of outmost importance if the nanoparticles are to be injected in a living organism. Superparamagnetic iron oxide nanoparticles have been extensively studied as *in vivo* imaging tools (Through magnetic resonance imaging, for example) and therapeutic agents, due to their capacity to induce a rise in the local temperature when exposed to an alternating magnetic field. These types of nanoparticles can also be induced to accumulate in the diseased area by the application of a magnetic field that can slow down nanoparticle flow at the desired site, easing extravasation. While these types of nanoparticles are well tolerated and generally considered to be non-toxic, some toxicity may be derived from the generation of Reactive Oxygen Species (ROS) from iron oxide nanoparticles *via* the Fenton reaction (Baeza 2014).

2.2.2 Carbon-based nanoparticles

Different carbon-based materials have been proposed for biomedical application. Fullerenes and carbon nanotubes are hollow structures that consist of one or several graphene-like sheets shaped as a sphere (fullerene) or a cylinder (carbon nanotube) (Ji et al. 2010). The structure of sp^2-bonded carbon atoms confers graphene, carbon nanotubes and fullerenes unique electrical properties. Graphene oxide has also been proposed for drug delivery and gene transfection (Shen et al. 2012). Mesoporous carbon nanoparticles and luminescent carbon dots have also been proposed for biomedical application. In order to give stable suspensions in aqueous environment, these carbon-based materials have to be modified with hydrophilic moieties on their surface. They have a high physicochemical stability and their size and morphology can be finely tuned. The particular electrical properties of carbon nanotubes can be exploited in the design of biosensors. However, issues regarding their toxicity may hinder their translation to the clinical setting for *in vivo* application. The safety profile of carbon-

based nanoparticles is a matter of discussion, as it appears that particle parameters such as size and surface properties can affect the toxicological characteristics of the material (Zhang et al. 2014).

2.2.3 Silica nanoparticles

Silicon oxide (silica) nanoparticles have been thoroughly studied as model nanoparticles for a wide variety of applications. Silica is not cytotoxic and its excellent physicochemical stability allows multiple functionalization strategies. Mesoporous Silica Nanomaterials have attracted a lot of interest in the context of drug delivery, since their very high surface area enables them to load high amounts of drugs within their pores (Mamaeva et al. 2013; Vallet-Regi et al. 2001). The textural parameters of the nanoparticles, such as surface area and pore size can be finely tuned depending on the needed characteristics for a particular application. Surface functionalization to ensure nanoparticle suspension stability is needed to allow these nanoparticles to achieve their function *in vivo*. Mesoporous Silica Nanoparticles for therapeutic and diagnostic applications have been developed, in most cases by obtaining hybrid nanoparticles by modifying the inner or outer structure of the silica particles with other nanoparticles or molecules that provide the desired function to the material (Mamaeva et al. 2013; Li et al. 2012). Also, Mesoporous Silica is known to undergo dissolution under physiological conditions, giving rise to non-toxic products that can be excreted from the organism. A potential drawback of these materials might be their high rigidity, which may obstruct their penetrability in solid tissues.

3. Nanoparticles for diagnostics

A promising approach in nanomedicine is the use of nanoparticles to develop diagnostic tools. Nanoparticles can be used for *in vitro* detection of pathologically relevant analytes. They can also be used as imaging agents for *in vivo* imaging.

3.1 *In vitro* diagnostics

The size of nanoparticles (typically bellow 100 nm) is in the same range as that of many biomolecules (enzymes, antibodies, other proteins). This fact allows an intimate interaction between both structures, which can be seized to develop *in vitro* setups that enable the detection of a wide variety of analytes. The high surface to volume ratio of nanoparticles allows the interaction of a large number of biomolecules with a single

nanoparticle, potentially enabling detection of the analyte with very high sensitivity (Chen et al. 2016). Besides the potential implications of these strategies in the evolution and growth of analytical chemistry, the highly sensitive detection of pathologically relevant analytes in biological fluids could dramatically improve the diagnosis of several diseases, potentially improving the prognosis of many patients thanks to an early diagnosis (Azzazy & Mansour 2009). Amongst the plethora of nanoparticles that have been developed for *in vitro* diagnostics, we will only review a few of them in order to illustrate some of the most common strategies.

Inorganic nanoparticles are of particular interest for *in vitro* diagnostics, especially gold nanoparticles, quantum dots and superparamagnetic nanoparticles (Azzazy & Mansour 2009). Different strategies developed for *in vitro* diagnostics can be divided by the parameter measured as well as by the types of nanoparticles that are used for that detection.

3.1.1 Assays based on fluorescent nanoparticles

A wide variety of methods can be used to develop fluorescent nanoparticles that act as sensors for different molecules (Chen et al. 2016). For example, an organic fluorophore can be introduced in the nanoparticles, either as part of the structure or loaded within them. An archetype of this type of systems are the so called "probes encapsulated by biologically localized embedding" or PEBBLEs. These systems have been adapted to be able to detect changes in pH, oxygen concentration and temperature, among others, by means of a change in fluorescence after exposure to the particular stimulus (Azzazy & Mansour 2009).

QDs have also been very thoroughly evaluated for this application, since they present much higher photostability and a much narrower emission band than organic dyes. Also, one of their main disadvantages for other biomedical applications, the potential toxicity due to heavy metals in their structure, is not relevant in this application, since the nanoparticles would never enter in contact with the organism of the patient. Sensors based on QDs have been developed to measure pH, temperature and different analytes (Azzazy & Mansour 2009). For example, a sensor to detect maltose was developed by grafting a maltose-binding protein to the surface of QDs (Medintz et al. 2003). Then, a dark quencher conjugated with a cyclodextrin was used to occupy the maltose-binding site of the protein, eliminating the fluorescence of the QDs by Fluorescence Resonance Energy Transfer (FRET). Then, after addition of the analyte,

maltose displaced the dark quencher from the protein, allowing the recovery of nanoparticle fluorescence, enabling a straightforward measurement of maltose concentration. Similar concepts have been evaluated to determine the concentration of specific proteases and other molecules (Azzazy & Mansour 2009).

Upconversion nanoparticles are also promising for *in vitro* diagnostics because the excitation of the sample can be performed with NIR light, thus avoiding many potential interferences from molecules in the biological fluids that might be found when exciting the sample in the ultraviolet of visible range (where background signal is commonly found). Then, the emission in the visible part of the spectrum could be easily measured to determine the result of the test. Also, the excitation and emission spectra of upconversion nanoparticles are relatively independent of their environment, making them a good choice for detection of analytes in biological fluids that are often very complex. Upconversion nanoparticles have been used to develop detection methods for temperature, oxygen, nucelic acids, antigens and many other biomolecules (Azzazy & Mansour 2009).

3.1.2 Assays based on plasmonic nanoparticles

Plasmonic nanoparticles have been very extensively evaluated as the main component to develop *in vitro* diagnostic systems (mainly based on gold nanoparticles)(Chen et al. 2016). Localized Surface Plasmon Resonance (LSPR) is a phenomenon due to collective electron charge oscillations in the surface of some metallic (for example, gold) nanoparticles when they are excited by light. Since it is a surface phenomenon, any change in the surface of the nanoparticle (or its size, since it is a highly size-dependent phenomenon) will induce a change in the LSPR and, therefore, in the optical properties of the nanoparticle suspension, which can be then detected by a colorimetric method. The surface of the plasmonic nanoparticles can be modified to include a recognition molecule for the analyte of interest. After the interaction with the desired molecule, a modification on the surface due to the interaction with the recognition ligand will lead to a change in the color of the sample, which can be measured and analyzed to give a concentration of the analyte present in the medium. An excellent example is the home pregnancy test, which is a colorimetric assay for the detection of human gonadotropic hormone, and is based on gold nanoparticles (Azzazy & Mansour 2009). Gold nanosensors have also been developed to determine biomolecules due to nanoparticle aggregation when the analyte is present in the sample. The change in

nanoparticle size and shape due to aggregation induces a change in the LSPR peak of a magnitude such that it is usually detectable by the naked eye. For example, systems for detecting DNA in the medium by decorating gold nanoparticles with complementary single strand DNA, inducing aggregation and a sharp change in the LSPR peak (Azzazy & Mansour 2009; Chen et al. 2016).

The interaction of plasmonic nanoparticles with fluorophores can also be utilized to develop different types of nanosensors. When a florescent molecule is in close proximity to the surface of a plasmonic nanoparticle, there is a dipole-induced quenching of the fluorophore. After being removed from the surface, the molecule will recover its fluorescence, which can be detected in the sample. A system based on this effect was developed to detect proteins in the sample, due to the specific displacement of a fluorescent polymer from the surface of gold nanoparticles caused by the analyte (You et al. 2007; Chen et al. 2016).

Another type of sensors for *in vitro* diagnostics are those based on Surface Enhanced Raman Scattering (SERS), which can provide very high sensitivity and also giving information about the conformation of the analyte. For this reason, they are under extensive evaluation for immunoassays, amongst other applications (Chen et al. 2016).

3.1.3 Assays based on superparamagnetic nanoparticles.

A wide variety of superparamagnetic nanoparticles (especially iron oxide nanoparticles) have been developed for *in vitro* detection (Azzazy & Mansour 2009). Upon exposure to an external magnetic field, superparamagnetic nanoparticles can be employed to capture different analytes that are bound to them (by interactions with recognition ligands decorating their surface), separating them from the sample medium. An example is an immunoassay detection method for C-reactive protein (CRP) based on this kind of nanoparticles (Kriz et al. 2006). A monoclonal antibody for CRP was grafted to the nanoparticle surface. A policlonal anti-CRP antibody was also conjugated to silica microparticles (to ease sedimentation). The increase in magnetic permeability of the sediment correlated with the amount of CRP in the sample (Azzazy & Mansour 2009).

Superparamagnetic nanoparticles can also be used to separate pathogenic cells from healthy ones by decorating the nanoparticles with antibodies for specific markers of the pathogenic cells, which can then be separated from the rest of the sample by

applying an external magnetic field or with the use of a magnetic needle (Azzazy & Mansour 2009; Bryant et al. 2007).

3.1.4 Assays based on electric properties of nanostructures

The particular electric properties of different nanoparticles (like carbon nanotubes) can also be exploited to develop *in vitro* nanosensors. The high surface area of single wall carbon nanotubes (SWNTs), up to 1600 m^2/g allows grafting a vast amount of antibodies on their surface. The very efficient electric conductivity of SWNTs along their longitudinal axis (often referred to as ballistic electron conduction) enables the development of nanosensors with the desired performance. Such methods have allowed, for example, the development of a Prostate Specific Antigen (PSA) detection kit with better performance than commercial immunodetection assays, with a detection limit of 4 pg/mL (Ji et al. 2010; Rusling et al. 2009).

While all of the different strategies that have been briefly collected here are very exciting and promising for their application in clinical diagnostics, several problems are still to be addressed before the majority of them will reach the clinical setting. One of the most important ones is getting the nanoparticle-based diagnostic assays to work properly in real complex biological fluids like those that are found in the clinical setting.

3.2 *In vivo* imaging

Another promising field for nanotechnology application in medicine, and still in the diagnostic context, is the use of nanoparticles as imaging agents *in vivo*. Due to several characteristics of diseased tissues, like tumors, nanoparticles can be preferentially located in those pathological locations. If the nanoparticle is designed in order to be detected generating some kind of image, then the clinician can take advantage of that selective accumulation of nanoparticles to provide a diagnosis or a prognosis of the pathological situation of a particular patient, or can be used to assess the evolution of the pathology throughout the treatment or the success of a surgical intervention.

There are several means by which nanoparticles can be used to generate a diagnostic image *in vivo*, depending on the physical phenomenon in which those nanoparticles will be involved. They can be divided in optical imaging, magnetic resonance imaging (MRI), radioisotope imaging and X-Ray computed tomography (CT) imaging. In the last years, the preparation of nanoparticles that enable the use of different imaging modalities simultaneously has been extensively evaluated. This

multimodality can allow a single nanoparticle formulation to combine the advantages of the different techniques. Again, Inorganic nanoparticles will be of outmost importance in this context.

3.2.1 Optical imaging

Optical imaging methods are based on the difference in the optical properties of the contrast nanoparticle and the background signal from the surrounding tissue. Most of the current optical imaging nanodevices are based on fluorescent nanoparticles. Fluorescent nanoparticles (like QDs of dye-doped silica nanoparticles) present several advantages over traditional organic dyes, such as improved photostability (with greatly diminished photobleaching effect) and the capability to accumulate in the desired tissues by targeting strategies. The development of highly efficient NIR-emitting nanoparticles is a rising strategy in this context. QDs are specially promising due to their narrow emission spectrum in a finely tunable region (and heavy-metal free QDs would be highly desirable due to toxicity issues related to nanoparticles containing heavy-metal).

Photoacoustic imaging is another strategy for optical bioimaging. It is based on the generation of an acoustic wave as a consequence of heat generated by light absorption by the contrast nanoparticles (Chen et al. 2016). It presents several advantages, since it combines the higher contrast of optical imaging with the higher penetration and spatial resolution of ultrasound imaging. One example of this strategy is the development of indocyanine green-loaded nanoparticles to provide photoaccoustic imaging *in vivo* (Witte et al. 2008).

Upconversion imaging can be performed with upconversion nanoparticles, which show a significantly better safety profile than QDs. The excitation of these nanoparticles is generally in the NIR region, allowing the excitation of nanoparticles located deep inside the body. Besides, the imaging background can be diminished by using short-pass filters, since the emitted light is significantly shifted from the excitation source (Chen et al. 2016). Upconversion nanoparticles in which both the excitation and the emission wavelengths are in the Infrared region seem very promising for this application, since they allow the imaging of deep tissues and organs with a low background noise. An example of this kind of particles was developed with $NaYF_4$ nanocrystals doped with Yb^{3+} and Tm^{3+}, showing an excitation wavelength of 975 nm and an emission one of 802 nm (Nyk et al. 2008).

3.2.2 Magnetic Resonance Imaging

There are two modalities of MRI: T_1 (relying on spin-lattice relaxation of protons in the organ/tissue) and T_2 (dependent on spin-spin relaxation of protons in the organ/tissue). It creates images with good spatial resolution, but contrast agents are often needed to improve the sensitivity of the technique. These contrast agents are magnetically active species that can be divided in T_1 or T_2 agents depending on which of the modalities provides a better contrast with that particular contrast agent.

The most common T_1 contrast agents are species containing Gd (III) as the magnetic agent, chelated with either diethylamine pentaacetic acid (DTPA) or tetraazacyclododecane tetraacetic acid (DOTA)(Chen et al. 2016). These are the most widely used MRI contrast agents in the clinical setting, even though there is some concern about the toxicity of Gd (III) ions that can be released. Modifying the surface of nanocarriers with DTPA or DOTA in order to chelate Gd (III) is a very common and successful way to provide MRI capabilities to virtually any type of nanodevice that could be used simultaneously with therapeutic purpose. This kind of strategies allow for real-time monitoring of the therapy. Gd (III) ions can also be incorporated into an inorganic matrix of different types of nanoparticles (like upconversion nanoparticles) to provide MRI contrast ability. The use of nanoparticles capable of providing different imaging capabilities is promising, since they would allow taking advantage of the benefits of the different imaging modalities with a single formulation (Chen et al. 2016). Superparamagnetic iron oxide (Fe_3O_4) nanoparticles can be used as negative T_2 contrast agents (since they reduce the spin-spin relaxation of the proton and therefore, give a dark contrast). They have been used in clinical MRI and their lack of toxicity is one of their biggest advantages. However, the contrast that these types of particles provide is rather low, and has to be improved in order to be more extensively used (Chen et al. 2016).

Another option would be using nanoparticles to produce magnetic resonance imaging using spin transitions of the nucleus of other species, like ^{19}F. This isotope can be introduced in the structure of different nanoparticles in a fairly easy manner, allowing MRI with increased sensitivity and very low background noise, due to the lack of ^{19}F in the organism. This promising strategy would only need minor modification in existing MRI devices to allow their use for ^{19}F detection (Chen et al. 2016).

3.2.3 Radioisotope imaging

The incorporation of radioactive isotopes in different types of nanoparticles allows their use for *in vivo* imaging. The radioactive isotopes to be used are chosen to emit low energy species, so that there will not be any radiotoxicity derived from their use for bioimaging. The most common modalities of radioisotope imaging are positron emission tomography (PET) and single photon emission computed tomography (SPECT)

In PET imaging, a radioisotope (like ^{124}I or ^{64}Cu) emits γ rays that after detection, are used to generate a three dimensional image. Nanoparticles allow a large number of radioisotope labeling, providing a great sensitivity and reducing the amount of contrast agent needed to perform the imaging. The most common ways to obtain nanoparticles for PET imaging are the use of chelators in the surface of the nanoparticles and radiolabeling by ion exchange within the nanoparticle matrix. SPECT imaging is based on a similar rationale, and suitable radioisotopes (like ^{125}I) can also be included in a nanoparticle structure to evaluate nanoparticle distribution with whole-body *in vivo* SPECT imaging (Chen et al. 2016).

3.2.4 X-ray Computed Tomography

CT imaging is based on using several X-Ray scans to produce a tomographic image after being processed by a computer program. CT contrast is very high for hard tissues, but it is not sufficient when the objective is to image soft tissues, where a contrast agent is needed. Atoms with large atomic number provide high contrast in X-ray images, and are therefore used for CT imaging. For this reason, gold nanoparticles with different shapes have been extensively studied for CT imaging. Some of the main reasons are, besides the high contrast in X-ray, their easy synthetic procedures, biocompatibility and the capacity to finely tune their optical properties in order to combine CT imaging with other optical modalities. Other inorganic nanoparticles, like upconversion nanoparticles containing Yb have also been studied for this application (and also in combination with optical imaging modalities) (Chen et al. 2016; Liu et al. 2012).

4. Nanoparticles for therapy

Nanoparticles can be designed for therapeutic application based on two different (but compatible) approaches: either the nanoparticle itself is the therapeutic agent that will

exert the desired function (material-based therapy) or the nanoparticle is used as a carrier for a therapeutic molecule (constituting a nano-Drug Delivery System, nano-DDS). Nano-DDS can overcome many of the problems related to traditional drugs for the treatment of several diseases. They are particularly useful when dealing with toxic drugs of hydrophobic ones that are difficult to administer in a stable formulation. Therefore, nanomedicine can improve the bioavailability, and increase the target specificity while decreasing the systemic toxicity of a wide variety of drugs. The inclusion of drugs inside a nanocarrier can also protect the drug from degradation that might take place when exposed to the physiological environment (such as enzymatic degradation) (Chen et al. 2016). This can potentially allow the use of drugs that would otherwise be unable to reach the clinic, either due to poor solubility, systemic toxicity of lack of chemical stability.

Multifunctional nanosystems can be obtained by adding therapeutic capabilities to the *in vivo* diagnostic nanoparticles already discussed, developing theranostic nanodevices. Nanoparticles can be used for a wide variety of pathological conditions, including infection, osteoporosis, gene therapy, cancer treatment and others (Chen et al. 2016). However, most of the research has been focused on the use of nanoparticles for cancer treatment.

4.1 Cancer nanomedicine

The most important reason why the vast majority of nanomedicine research has been focused on cancer is what has been called the Enhanced Permeation and Retention (EPR) effect (**Figure 3**). By that name, Maeda defined in the 1980s the preferential accumulation in tumor tissues of macromolecules and nanosized structures (Matsumura & Maeda 1986). This effect is possible due to the fast and chaotic growth of most solid tumors. During that indiscriminate growth, the tumor cells are capable of inducing the formation of blood vessels (in a process called angiogenesis) in order to receive enough nutrients and remove waste products from their metabolism. However, and in contrast to the formation of healthy blood vessels, this angiogenesis is fast and disorganized, leading to imperfect blood vessels, leaving pores in the walls of capillaries that are bigger than those in healthy tissues and organs. The presence of those pores or fenestrations allows the extravasation of large macromolecules and nanoparticles to the diseased site, what would not be possible in a healthy tissue (enhanced permeation). Besides that, solid tumors are generally very compact structures with a high interstitial

pressure. Under those conditions, the lymphatic vessels present in the tissue will be blocked, preventing the drainage of extravasated particles (enhanced retention). The discovery of this phenomenon in the 1980s lead to the proposal of using nanoparticles to treat tumors, since the enhanced accumulation would allow the delivery of higher doses of antitumor drugs in the tumors, potentially reducing the dose of the drug and, therefore, reducing side effects without compromising the efficacy of the treatment. The EPR effect became then the main justification for the development of nanomedicine, and would provide what would be known in the field as a "passive targeting".

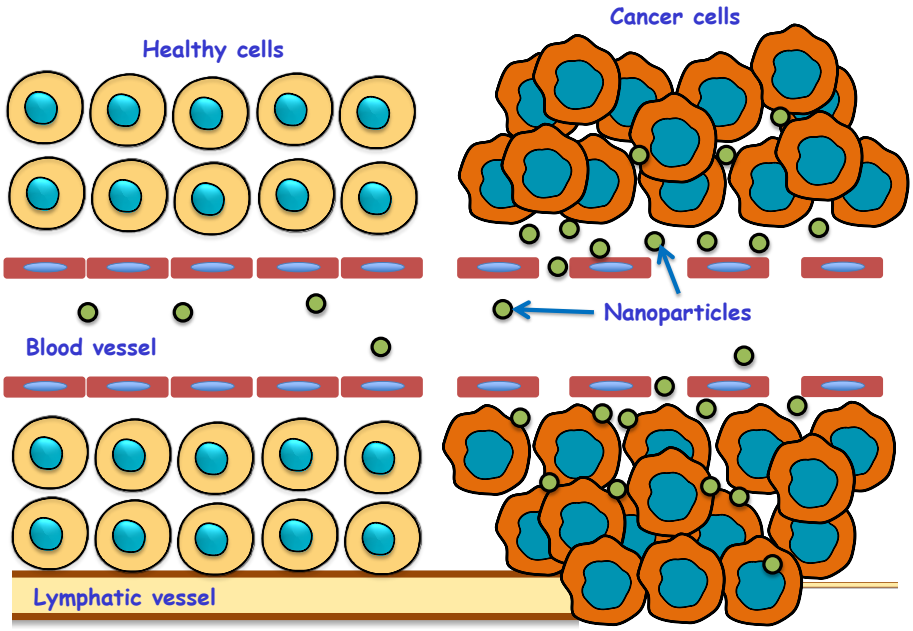

Figure 3. Schematic representation of the enhanced permeation and retention (EPR) effect.

Nanoparticle accumulation in the tumor area by the EPR effect relies on the circulation time of the nanoparticles in the bloodstream. After intravenous injection of the nanoparticles, a series of steps must take place to allow the EPR effect to take place. First, the nanoparticles have to be stable in suspension while circulating in the blood. Otherwise, nanoparticle aggregation will lead to the obstruction of blood vessels, potentially compromising the patient´s life. Then, the nanoparticles have to remain in the bloodstream long enough to extravasate to the tumor in a sufficient amount to elicit the therapeutic effect. One key aspect to consider regarding nanoparticle circulation time is the opsonization of the nanoparticles (Wicki et al. 2015). Opsonization is a process by which a pathogen or foreign body is surrounded by a type of proteins called opsonins. Opsonins act as a label for phagocitic cells to ingest the labeled structure in

order to destroy it. When nanoparticles without any surface modification are put in contact with the blood, they are covered by a mixture of different proteins (forming what is called the protein corona). The formation of this protein corona can accelerate very dramatically the clearance of the nanoparticles from systemic circulation due to the presence of opsonins in its composition. One of the most employed strategies to slow down the formation of the protein corona consists on modifying their surface with highly hydrophilic moieties that will hinder protein adsorption on the nanoparticle surface. The most common molecule to achieve this is polyethyleneglicol (PEG), and the process of coating a nanoparticle with PEG has been called PEGylation.

PEGylation has been shown to significantly increase circulation time of nanoparticles and, therefore, their accumulation in tumors (Wicki et al. 2015). However, the protein corona will eventually form (although more slowly), and the nanoparticles that have not yet reached the diseased site will be removed from the circulation by the organs of the reticuloendothelial system (RES, mainly liver and spleen). It has been recently estimated that the amount of nanoparticles that arrive to the tumor tissue is in average less than 1% of the injected dose (Wilhelm et al. 2016). Even though that number seems low, it is greatly superior to the percentage of free drug that would reach the tumor site without the nanocarrier (Lammers et al. 2016). Moreover, several strategies can be applied to further improve nanoparticle accumulation in tumors, like injecting angiotensin II (a vasoconstrictor) to increase the systemic blood pressure and facilitate nanoparticle leakage to tumors (Maeda et al. 2013), normalizing tumor vasculature to diminish interstitial pressure within the tumor (Chauhan et al. 2012) or destabilizing the blood vessels in the tumor by hyperthermia or ultrasound to increase their permeability (O'Neill et al. 2009).

4.1.1 Active targeting of nanoparticles

In order to improve the efficacy of nanoparticles for therapy, a second strategy of nanoparticle targeting was then developed, the one known as "active targeting". Active targeting is based on decorating the nanoparticle surface with molecules that would induce selective internalization in tumor cells, and decreasing the amount of particles that would reach healthy cells. When the release of the cytotoxic agent takes place inside the tumor cell, the high local concentration of the drug would increase its efficacy, lowering even more the required dose of the highly toxic antitumor drug. The most studied types of molecules used for active targeting are either nutrients (for which

the tumor cells overexpress receptors, due to their high demand to allow their rapid growth) or antibodies (for specific antigens present in the tumor cell membrane). These targeting molecules can be small molecules (like folic acid (Stella et al. 2000) or biotin (Yang et al. 2009)) or macromolecules (like the protein transferrin) (Greish et al. 2014). Another step of nanoparticle targeting can take place after cellular uptake of the nanodevice. In this case, the surface of the nanoparticles is also decorated with moieties that can drive nanoparticle accumulation in a particular subcellular structure or organelle. For example, nanoparticles presenting triphenyl phosphonium moieties on their surface are known to target the mitochondria, and are often used to carry drugs that act at the mitochondria, increasing the therapeutic efficacy of the nanodevice.

It is worth noting that, since active targeting strategies involve the interaction of nanoparticle with a receptor in the target cell membrane, this strategy relies on passive accumulation first, which would bring the particles close enough to the cells so that active targeting can take place. Once the nanoparticle has reached the tumor environment and has interacted with the tumor cell receptors, another consideration must be taken. If the interaction with the cell receptor is very efficient in inducing nanoparticle uptake, a paradoxical effect can appear. The first line of cells in the tumor will internalize all of the nanoparticles, preventing their penetration to deeper areas. This might hinder the therapeutic efficacy of the nanoparticles, since most of the tumor will not be exposed to them. In order to try to solve this issue, hierarchical targeting strategies are being developed (Wang et al. 2016). In these strategies, the targeting moiety is hidden until the nanoparticles are already distributed in the tumor. Then, the presence of an internal or external stimulus will induce the exposure of the targeting moiety, allowing particle uptake by the tumor cells. These kinds of strategies would also be useful to increase the circulation time of those targeted nanoparticles, since the presence of targeting moieties on the surface of PEGylated nanoparticles has been shown to facilitate their removal from the bloodstream by the RES (Wang et al. 2016). If the targeting ligand is hidden until after the nanoparticles have accumulated in the tumor, the nanoparticles will be able to remain in the circulation for longer periods of time. After extravasation to the tumor tissue, PEGylated nanoparticles are poorly internalized in tumor cells (due to what has been called the "PEGylation dilemma") (Hatakeyama et al. 2013). However, with these hierarchical targeting strategies, the exposure of the targeting molecule will allow their successful internalization in tumor cells, increasing their therapeutic efficacy (Wang et al. 2016).

Besides this problem, other considerations must be taken into account. First, nanoparticle diffusion in tumor tissues is hindered by the high interstitial pressure. Therefore, the size of the nanoparticles will be a key factor in determining whether the particles can reach deeper areas of the diseased tissue. To attack this problem, size-changing materials are being developed to allow for a deeper penetration once the nanoparticles have reached the tumor (Wang et al. 2016). Besides, strategies directed to reducing interstitial pressure are also interesting approaches with potential to obtain very positive results (like using collagenase prior to nanoparticle injections) (Goodman et al. 2007).

All the strategies we have discussed so far depend on the EPR effect to induce selective accumulation of the nanoparticles in the tumor microenvironment. However, it is well established that the EPR effect presents a very high variability, even amongst tumors of the same type, and it changes greatly when discussing different tumor types (Greish et al. 2014). Two possibilities arise from this perspective: either developing methods that would allow for a selection of patients that are most likely to respond to nanoparticle-mediated therapy (by determining whether their particular tumor presents a strong EPR effect or not), or developing new strategies to induce nanoparticle accumulation in tumors that do not rely on the EPR effect (Greish et al. 2014; Hu et al. 2010).

4.1.2 Material-based therapeutic approaches

Several approaches have been studied to induce therapeutic effects by using nanoparticles without relying on drug release, because the nanomaterial itself is responsible for the desired response. These effects are often used in combination with drug release from the same nanoparticles, looking for a synergistic effect between them. Some of the most important ones will be briefly mentioned here.

Photodynamic therapy (PDT): PDT is a type of therapy involving two components: light and a molecule called photosensitizer. None of them are toxic individually, but they are capable of inducing cell death when they are combined. Photosensitizers (generally porphyrin molecules) can be excited by light (at different wavelengths depending on the particular photosensitizer) into a triplet state. This excited photosensitizer in its triplet state can transfer its energy to oxygen in the medium, producing highly reactive singlet oxygen (Chen et al. 2016). The short half-live of

singlet oxygen implies that only the cells very close to the photosensitizer will be affected by the generation of those reactive oxygen species (ROS). Since photosensitizers share many shortcomings with other drugs regarding their poor solubility and difficulty to get high concentrations in the tumor tissue, the use of nanoparticles to transport them to the desired area of the body has emerged as a very powerful tool to increase the efficacy of PDT (Chen et al. 2016). As PDT will happen independently of whether the photosensitizer is free in solution or inside a nanoparticle, the sensitizer can be included in the formulation without having to be released to induce the desired effects.

Photothermal Therapy (PTT): In PTT, the nanoparticle itself is responsible for the biological effects of the therapy. PTT is mainly based on the plasmonic absorption of metallic nanoparticles. Metallic nanostructures can be designed to absorb Near-Infrared (NIR) or Infrared (IR) light, generating heat as a consequence. If the nanoparticles are embedded inside a tumor mass, the increase in the temperature will eventually cause cell death by necrosis (cancer cells are more vulnerable to hyperthermia than healthy cells, in a temperature range 40-43ºC)(Chen et al. 2016; Hildebrandt 2002). Gold nanorods are amongst the most studied nanoparticles for PTT, since they can generate heat very efficiently when exposed to NIR light, while also having an easy and finely tunable synthesis. Another type of nanoparticles that is under extensive evaluation for PTT is graphene oxide, which has been shown to generate heat when exposed to 800 nm lasers. Also, incorporating NIR dyes or porphyrins in the structures of different nanoparticles not only allows their use for imaging, but also the generation of PTT (obtaining theranostic nanodevices) (Chen et al. 2016).

Magnetic hyperthermia: Besides the possibility to increase accummulation of superparamagnetic nanoparticles in tumors by the application of an external magnetic field (magnetic targeting), these nanoparticles can also generate heat when exposed to an alternating magnetic field (Chen et al. 2016). In the same way as for PTT, the local heating caused by magnetic hyperthermia can cause the death of cancer cells without the need for any drug molecules to be released from the material. The possibility of obtaining theranostic nanodevices for magnetic hyperthermia is also exciting, since superparamagnetic iron oxide nanoparticles that can be employed to induce it can also be used to provide MRI capabilities.

4.1.3 Nano-Drug Delivery Systems

Most of the work that has been developed about the therapeutic application of nanoparticles involves using them as DDS, so that they can improve the pharmacokinetic parameters of different active molecules, getting them to the site of action. Once the nanoparticles are located in the tumor area, nanoparticles carrying cytotoxic drugs will have to release them so that they can perform their action. The nanoparticles acting as nano-DDS can be designed to present a controlled release of the drugs they contain. Nanoparticles can be prepared to provide prolonged release of the drug, for example by introducing the active molecule in a biodegradable matrix (PLGA nanoparticles are a typical example of this strategy) (Chen et al. 2016). As the nanoparticle degrades, the drug is released to the medium, and carries out its function. However, since anticancer drugs are highly toxic, it would be very interesting to develop a nanocarrier that can release such drug only in the diseased site, without any drug loss during transport. In that context, as plethora of stimuli-responsive materials have been evaluated (most of them *in vitro*, although many *in vivo* evaluations have also been performed). In these materials, drug release is hindered by some component in the formulation that can respond to differences in its environment, inducing a change in the formulation that will lead to drug release. The different stimuli that can be employed to this end can be divided in internal and external stimuli (**Figure 4**).

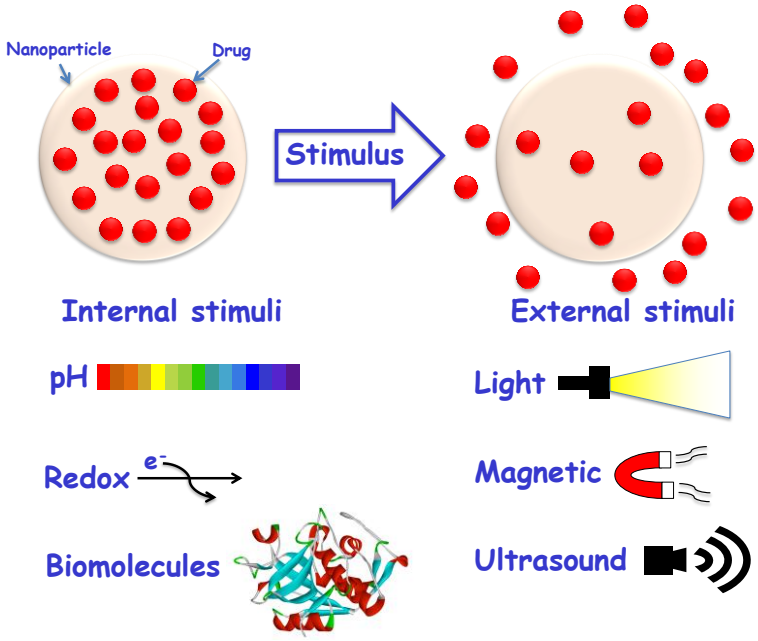

Figure 4. Concept of stimuli-responsive drug release. Different stimuli reported in the literature divided in internal or external stimuli.

Internal stimuli are differences in tumor tissues or tumor cells that are not present in the healthy counterparts (or are much less intense). Therefore, once the nanoparticle is in the tumor, the presence of such stimulus will induce some change that will provoke drug release. Typical examples of internal stimuli in cancer therapy are pH (tumors possess a lower pH than healthy tissues, and the pH in some intracellular compartments, like lysosomes, is also much lower than in the extracellular medium) (Liu et al. 2010), redox potential (which also presents significant changes in the intracellular compartment compared to extracellular media) (Z.-Y. Li et al. 2015), and the presence of different proteins or signaling molecules (like Matrix MetaloProteases, MMPs) (Singh et al. 2011). For example, pH-responsive mesoporous silica nanoparticles can be obtained by grafting gold nanoparticles acting as gatekeeper through a pH-labile acetal group (Liu et al. 2010). Once the nanoparticles are exposed to an acidic pH, the acetal linker is cleaved and the cargo inside the nanoparticle pores can be released. Another example are redox-responsive polymeric nanoparticles that can be obtained by the introduction of disulfide bonds inside the polymer structure (Song et al. 2011). Once in the reducing intracellular environment, the disulfide bonds are broken and the nanoparticle releases its cargo. An advantage of internal stimuli is that once the nanoparticle is administered, no further action is needed from the clinician. This would in theory ease the translation of these strategies. However, a general piece of criticism towards these stimuli is that most of the differential characteristics between healthy and tumor tissues are not as exacerbated in reality as it is supposed in most research articles dealing with them, what would hamper the correct behavior of the material in real clinical situations.

On the other hand, external stimuli have also been extensively evaluated. External stimuli are not present in the organism and they are not a consequence of the pathology. They are exogenous agents that the clinician might apply to the diseased site after the administration of the nanocarrier and would then interact with the formulation, inducing drug release. Examples of external stimuli that have been evaluated are light (Martínez-Carmona et al. 2015), magnetic field (Guisasola et al. 2015) or ultrasound (Grüll & Langereis 2012; Schroeder et al. 2009; Li et al. 2016; Paris et al. 2015). For example, light-responsive liposomes can be obtained by taking advantage of the same effect as the one used for photodynamic therapy. A photosensitizer can be included in the formulation, as well as an unsaturated lipid. Once the formulation is exposed to light, ROS are generated, inducing the peroxidation of the unsaturated lipid component

of the lipid bilayer (Carter et al. 2014). The lipid bilayer permeability is therefore modified, inducing drug release. As an example of magnetic-responsive drug release, superparamagnetic nanoparticles embedded in a mesoporous silica matrix can be employed to induce an increase in the local temperature when exposed to an alternating magnetic field, what can then induce a conformational change in a temperature-responsive polymeric gate, allowing cargo release from the material (Guisasola et al. 2015). An advantage of these kinds of stimuli is that, since they are not present in the organism, designing formulations that are sensitive to them will provide a high selectivity in the material response. On the other hand, there are several concerns about their use, like the poor penetration of the stimulus in the organism (for example, with light), difficulty to focus the stimulus in the tumor or toxicity associated to the stimulus alone.

4.2 Nanomedicine for other applications

4.2.1 Infection: Nanoparticles can be used to deliver different antimicrobial drugs to treat different infectious diseases, by developing the so-called "nanoantibiotics" (Huh & Kwon 2011). Nanoantibiotics can be developed by using nanoparticles with inherent antimicrobial activities (like Ag nanoparticles, fullerenes or chitosan nanoparticles) or by acting as drug delivery vehicles that can release antimicrobial drugs (Huh & Kwon 2011). Antibiotic-loaded mesoporous Silica Nanoparticles have been proposed for intracellular pathogens like *Francisella tularensis* (Z. Li et al. 2015). The main rationale for this work was the fact that *F. tularensis* is found in macrophages of the infected host. Macrophages are professional phagocytes that tend to engulf large amounts of nanoparticles after they are injected in the bloodstream. Once nanoparticles have undergone uptake by them, the antibiotic moxifloxacin was released, killing the bacteria inside the macrophages and showing promising *in vivo* results for the treatment of Lethal Pneumonic Tularemia (Z. Li et al. 2015). Antimicrobial nanomedicine has gained great attention due to antibiotic resistance. Nanoantibiotics can be used to deal with this problem either by taking advantage of different mechanisms of action (less likely to induce resistance, like using silver or other metal nanoparticles), by better targeting the diseased site or by employing combinations of different drugs in a single formulation (combination therapy).

4.2.2 Osteoporosis: Osteoporosis is nowadays one of the main reasons of morbidity in the aging population (Luhmann et al. 2012). Nanoparticles have been proposed for the treatment of osteoporosis in order to try to improve the efficacy of anabolic (increasing bone production) and anti-resorptive (decreasing bone elimination) therapy (Luhmann et al. 2012). This could happen mainly by increasing the local concentration of the drugs of interest in the diseased site. For that reason, different strategies have been developed to improve bone targeting of nanomedicines, mainly by decorating the nanoparticle surface with different bisphosphonates (that present a strong interaction with calcium present in the inorganic phase of bone, hydroxyapatite) or with the collagen binding domain of different proteins (targeting therefore collagen, the main organic component of bone) (Luhmann et al. 2012). Once located in the diseased bone, the nanoparticles can be used to release different therapeutic agents, like Parathyroid Hormone (PTH) or Bone Morphogenetic Proteins (BMPs), which are growth factors that have been extensively studied for bone regenerative therapy (Luhmann et al. 2012).

4.2.3 Gene Therapy: A great number of diseases are caused by a malfunction of one or several genes, and gene therapy implies a modification in the structure or expression of such genes to treat the pathologies that arise from that malfunction. The main barriers that gene vectors encounter to allow effective gene therapy are: prevention of degradation of the nucleic acid (DNA or RNA), efficient uptake by the target cells, release of the nucleic acid in the cytoplasm and outside of the endolysosomal system, entering the nucleus and producing sufficient gene expression (Chen et al. 2016). The use of a targeted nanocarrier that can protect the nucleic acid during transport and can release it in the proper location can therefore overcome most of those concerns. Especially appealing is the strategy of delivering small interference RNA (siRNA) to modify the expression of different genes of interest. The most common way of introducing nucleic acids in a nanoformulation is through the electrostatic interaction between the negatively charged nucleic acid (DNA or RNA) and a positively charged nanostructure, generally by using polycationic polymers. Among all the available polycations, the ones that are most widely used are polyethyleneimine (PEI, either linear or branched), PAMAM and chitosan (Chen et al. 2016). Besides polymeric nanoparticles composed of these kinds of polycations, liposomes with positively charged lipids are also very widely used for this application. The use of nanoparticles with high positive charges presents another advantage: lysosomal escape capacity.

Nanoparticles with protonable groups under acidic conditions are capable of inducing lysosomal escape *via* the Proton Sponge Effect. Once the nanoparticles are inside the lysosomes after endocytosis, at the lysosomal low pH, the protonable groups acquire a high positive charge, which would tend to be neutralized by the entrance of chloride anions. These osmotically active ions enter the lysosomes accompanied by water, making the lysosome swell until it bursts, releasing the nanoparticles in the cytoplasm (Sahay et al. 2010). The nanoparticles can also be modified by endosomolytic agents to induce lysosomal escape of the nucleic acid-carrying nanoparticles (Chen et al. 2016).

5. Conclusion

Nanomedicine is a multidisciplinary field aimed to develop diagnostic and therapeutic tools based on nanoparticles with different chemical compositions. The selection of a particular nanoparticle type and their further modifications are selected based on the particular application of interest.

The great versatility of nanotechnology enables the design and preparation of highly sensitive and specific diagnostic assays that could allow early detection of different pathologies, hopefully improving the prognosis of the patients.

Nanoparticles can also be used *in vivo* for the diagnosis and treatment of several diseases (sometimes at the same time, by developing theranostic nanoparticles). With the help of nanoparticles, more sensitive imaging contrast agents can be obtained for their use with different imaging techniques. Recently, great attention has been attracted by nanoparticles that can act as contrast agents for several imaging techniques simultaneously. At the same time, nanoparticles can constitute powerful tools for the treatment of those same diseases, either by their own intrinsic characteristics, or by using them as carriers of different drugs. It is worth noting that, for each particular application, the pathological characteristics of the diseased tissues and cells have to be taken into account.

The evolution of the field of nanomedicine in the last decades holds great promise, and their use could revolutionize the practice of medicine in a wide variety of clinical situations. However, before that can happen, all of the problems of current strategies have to be carefully addressed by the nanomedicine scientific community.

Acknowledgements

Authors thank the funding from the European Research Council through the Advanced Grant VERDI (ERC-2015 AdG Proposal no. 694160). Financial support from Ministerio de Economía y Competitividad, (MEC), Spain (Project MAT2015-64831-R) is gratefully acknowledged. Images from Servier Medical Art (and their Powerpoint image bank) have been employed to produce the figures included in this chapter.

References

Albanese, A., Tang, P.S. & Chan, W.C.W., 2012. The Effect of Nanoparticle Size, Shape, and Surface Chemistry on Biological Systems. *Annual Review of Biomedical Engineering*, 14(1), pp.1–16.

Azzazy, H.M.E. & Mansour, M.M.H., 2009. In vitro diagnostic prospects of nanoparticles. *Clinica Chimica Acta*, 403(1–2), pp.1–8.

Baeza, A., 2014. Ceramic Nanoparticles for Cancer Treatment. In *Bio-Ceramics with Clinical Applications* (ed M. Vallet-Regí), John Wiley & Sons, Ltd, Chichester, UK.

Banerjee, R. et al., 2010. Nanomedicine: Magnetic Nanoparticles and their Biomedical Applications. *Current Medicinal Chemistry*, 17(27), pp.3120–3141.

Boisselier, E. & Astruc, D., 2009. Gold nanoparticles in nanomedicine: preparations, imaging, diagnostics, therapies and toxicity. *Chemical Society Reviews*, 38(6), p.1759.

Bozzuto, G. & Molinari, A., 2015. Liposomes as nanomedical devices. *International Journal of Nanomedicine*, 10, p.975.

Bryant, H.C. et al., 2007. Magnetic needles and superparamagnetic cells. *Physics in Medicine and Biology*, 52(14), pp.4009–4025.

Carter, K. a et al., 2014. Porphyrin-phospholipid liposomes permeabilized by near-infrared light. *Nature communications*, 5, p.3546.

Chauhan, V.P. et al., 2012. Normalization of tumour blood vessels improves the delivery of nanomedicines in a size-dependent manner. *Nature Nanotechnology*, 7(6), pp.383–388.

Chen, G. et al., 2016. Nanochemistry and Nanomedicine for Nanoparticle-based Diagnostics and Therapy. *Chemical Reviews*, 116(5), pp.2826–2885.

Goodman, T.T., Olive, P.L. & Pun, S.H., 2007. Increased nanoparticle penetration in collagenase-treated multicellular spheroids. *International journal of nanomedicine*, 2(2), pp.265–274.

Greish, K. et al., 2014. Nanomedicine for drug targeting: strategies beyond the enhanced permeability and retention effect. *International Journal of Nanomedicine*, p.2539.

Grüll, H. & Langereis, S., 2012. Hyperthermia-triggered drug delivery from temperature-sensitive liposomes using MRI-guided high intensity focused ultrasound. *Journal of Controlled Release*, 161(2), pp.317–327.

Guisasola, E. et al., 2015. Magnetic-Responsive Release Controlled by Hot Spot Effect. *Langmuir*, 31(46), pp.12777–12782.

Hatakeyama, H., Akita, H. & Harashima, H., 2013. The Polyethyleneglycol Dilemma: Advantage and Disadvantage of PEGylation of Liposomes for Systemic Genes and Nucleic Acids Delivery to Tumors. *Biological and Pharmaceutical Bulletin*, 36(6), pp.892–899.

Hildebrandt, B., 2002. The cellular and molecular basis of hyperthermia. *Critical Reviews in Oncology/Hematology*, 43(1), pp.33–56.

Hu, Y.-L. et al., 2010. Mesenchymal stem cells: a promising targeted-delivery vehicle in cancer gene therapy. *Journal of controlled release : official journal of the Controlled Release Society*, 147(2), pp.154–62.

Huh, A.J. & Kwon, Y.J., 2011. "Nanoantibiotics": A new paradigm for treating infectious diseases using nanomaterials in the antibiotics resistant era. *Journal of Controlled Release*,

156(2), pp.128–145.
Jain, R.K. & Stylianopoulos, T., 2010. Delivering nanomedicine to solid tumors. *Nature Reviews Clinical Oncology*, 7(11), pp.653–664.
Ji, S. et al., 2010. Carbon nanotubes in cancer diagnosis and therapy. *Biochimica et Biophysica Acta (BBA) - Reviews on Cancer*, 1806(1), pp.29–35.
Khandare, J. et al., 2012. Multifunctional dendritic polymers in nanomedicine: opportunities and challenges. *Chem. Soc. Rev.*, 41(7), pp.2824–2848.
Kriz, K. et al., 2006. Rapid one-step whole blood C-reactive protein magnetic permeability immunoassay with monoclonal antibody conjugated nanoparticles as superparamagnetic labels and enhanced sedimentation. *Analytical and Bioanalytical Chemistry*, 384(3), pp.651–657.
Kumari, A., Yadav, S.K. & Yadav, S.C., 2010. Biodegradable polymeric nanoparticles based drug delivery systems. *Colloids and Surfaces B: Biointerfaces*, 75(1), pp.1–18.
Lammers, T. et al., 2016. Cancer nanomedicine: is targeting our target? *Nature Reviews Materials*, 1(9), p.16069.
Li, F. et al., 2016. Ultrasound responsive block copolymer micelle of poly(ethylene glycol)–poly(propylene glycol) obtained through click reaction. *Ultrasonics Sonochemistry*, 30, pp.9–17.
Li, Z. et al., 2012. Mesoporous silica nanoparticles in biomedical applications. *Chemical Society Reviews*, 41(7), pp.2590–2605.
Li, Z. et al., 2015. Mesoporous Silica Nanoparticles with pH-Sensitive Nanovalves for Delivery of Moxifloxacin Provide Improved Treatment of Lethal Pneumonic Tularemia. *ACS Nano*, 9(11), pp.10778–10789.
Li, Z.-Y. et al., 2015. A redox-responsive drug delivery system based on RGD containing peptide-capped mesoporous silica nanoparticles. *J. Mater. Chem. B*, 3(1), pp.39–44.
Liu, R. et al., 2010. pH-responsive nanogated ensemble based on gold-capped mesoporous silica through an acid-labile acetal linker. *Journal of the American Chemical Society*, 132, pp.1500–1501.
Liu, Y. et al., 2012. A high-performance ytterbium-based nanoparticulate contrast agent for in vivo X-ray computed tomography imaging. *Angewandte Chemie - International Edition*, 51(6), pp.1437–1442.
Luhmann, T. et al., 2012. Bone targeting for the treatment of osteoporosis. *Journal of Controlled Release*, 161(2), pp.198–213.
Maeda, H., Nakamura, H. & Fang, J., 2013. The EPR effect for macromolecular drug delivery to solid tumors: Improvement of tumor uptake, lowering of systemic toxicity, and distinct tumor imaging in vivo. *Advanced Drug Delivery Reviews*, 65(1), pp.71–79.
Mamaeva, V., Sahlgren, C. & Lindén, M., 2013. Mesoporous silica nanoparticles in medicine--recent advances. *Advanced drug delivery reviews*, 65(5), pp.689–702.
Martínez-Carmona, M. et al., 2015. Mesoporous silica nanoparticles grafted with a light-responsive protein shell for highly cytotoxic antitumoral therapy. *J. Mater. Chem. B*, 3(28), pp.5746–5752.
Matsumura, Y. & Maeda, H., 1986. A New Concept for Macromolecular Therapeutics in Cancer Chemotherapy: Mechanism of Tumoritropic Accumulation of Proteins and the Antitumor Agent Smancs. *Cancer Research*, 46(12 Part 1).
Medintz, I.L. et al., 2003. Self-assembled nanoscale biosensors based on quantum dot FRET donors. *Nature Materials*, 2(9), pp.630–638.
Michalet, X., 2005. Quantum Dots for Live Cells, in Vivo Imaging, and Diagnostics. *Science*, 307(5709), pp.538–544.
Nyk, M. et al., 2008. High Contrast in Vitro and in Vivo Photoluminescence Bioimaging Using Near Infrared to Near Infrared Up-Conversion in Tm 3+ and Yb 3+ Doped Fluoride Nanophosphors. *Nano Letters*, 8(11), pp.3834–3838.
O'Neill, B.E. et al., 2009. Pulsed High Intensity Focused Ultrasound Mediated Nanoparticle Delivery: Mechanisms and Efficacy in Murine Muscle. *Ultrasound in Medicine & Biology*, 35(3), pp.416–424.
Oerlemans, C. et al., 2010. Polymeric Micelles in Anticancer Therapy: Targeting, Imaging and

Triggered Release. *Pharmaceutical Research*, 27(12), pp.2569–2589.
Paris, J.L. et al., 2015. Polymer-Grafted Mesoporous Silica Nanoparticles as Ultrasound-Responsive Drug Carriers. *ACS Nano*, 9(11), pp.11023–11033.
Rusling, J.F., Sotzing, G. & Papadimitrakopoulosa, F., 2009. Designing nanomaterial-enhanced electrochemical immunosensors for cancer biomarker proteins. *Bioelectrochemistry*, 76(1–2), pp.189–194.
Sahay, G., Alakhova, D.Y. & Kabanov, A. V., 2010. Endocytosis of nanomedicines. *Journal of Controlled Release*, 145(3), pp.182–195.
Schroeder, A. et al., 2009. Ultrasound triggered release of cisplatin from liposomes in murine tumors. *Journal of Controlled Release*, 137(1), pp.63–68.
Shen, H. et al., 2012. Biomedical Applications of Graphene. *Theranostics*, 2(3), pp.283–294.
Singh, N. et al., 2011. Bioresponsive mesoporous silica nanoparticles for triggered drug release. *Journal of the American Chemical Society*, 133(49), pp.19582–5.
Song, N. et al., 2011. Preparation and in vitro properties of redox-responsive polymeric nanoparticles for paclitaxel delivery. *Colloids and Surfaces B: Biointerfaces*, 87(2), pp.454–463.
Stella, B. et al., 2000. Design of folic acid-conjugated nanoparticles for drug targeting. *Journal of Pharmaceutical Sciences*, 89(11), pp.1452–1464.
Vallet-Regi, M. et al., 2001. A New Property of MCM-41: Drug Delivery System. *Chemistry of Materials*, 13(2), pp.308–311.
Wang, S., Huang, P. & Chen, X., 2016. Hierarchical Targeting Strategy for Enhanced Tumor Tissue Accumulation/Retention and Cellular Internalization. *Advanced Materials*, 28(34), pp.7340–7364.
Wicki, A. et al., 2015. Nanomedicine in cancer therapy: Challenges, opportunities, and clinical applications. *Journal of Controlled Release*, 200, pp.138–157.
Wilhelm, S. et al., 2016. Analysis of nanoparticle delivery to tumours. *Nature Reviews Materials*, 1(5), p.16014.
Witte, R.S. et al., 2008. Enhanced photoacoustic neuroimaging with gold nanorods and PEBBLEs. In A. A. Oraevsky & L. V. Wang, eds. *Proceedings of SPIE*. p. 685614.
Yaghini, E. et al., 2016. In vivo biodistribution studies and ex vivo lymph node imaging using heavy metal-free quantum dots. *Biomaterials*, 104, pp.182–191.
Yang, W. et al., 2009. Targeting cancer cells with biotin-dendrimer conjugates. *European Journal of Medicinal Chemistry*, 44(2), pp.862–868.
You, C.-C. et al., 2007. Detection and identification of proteins using nanoparticle-fluorescent polymer "chemical nose" sensors. *Nature nanotechnology*, 2(5), pp.318–323.
Zhang, Y. et al., 2014. Toxicity and efficacy of carbon nanotubes and graphene: the utility of carbon-based nanoparticles in nanomedicine. *Drug Metabolism Reviews*, 46(2), pp.232–246.

1.2 Nanopartículas de sílice mesoporosa

Los materiales porosos, en general, pueden clasificarse en función de su tamaño de poro, dando lugar a tres tipos de materiales: microporosos (poros inferiores a 2 nm), mesoporosos (poros entre 2 y 50 nm) y macroporosos (poros mayores de 50 nm).[1] Los materiales mesoporosos fueron desarrollados a principios de la década de 1990, siendo empleados para múltiples aplicaciones, tales como catálisis, captación de agentes contaminantes o liberación de fármacos.[2–5]

Los materiales mesoporosos de sílice consisten en una matriz de dióxido de silicio (sílice) amorfa a escala atómica que posee porosidad ordenada a escala nanométrica cuyo diámetro de poro se encuentra en el rango mesoporoso. Entre las principales características que hacen de los materiales mesoporosos de sílice una opción atractiva para sistemas de liberación de fármacos destacan sus propiedades texturales, su estabilidad físico-química y su facilidad de modificación química.[6–8] En cuanto a sus propiedades texturales, poseen una elevada área superficial, hasta 1500 m^2/g, y un alto volumen de poro, en torno a 1 cm^3/g, que permiten alojar grandes cantidades de fármacos en el interior de sus poros.[9,10] Además, los materiales mesoporosos de sílice han demostrado ser biocompatibles y capaces de ser eliminados del organismo tras su disolución parcial o total.[11–16] De hecho, desde que en 2001 se propusieron por primera vez como sistemas de liberación de fármacos, su utilización ha crecido exponencialmente.[4]

1.2.1 Síntesis de nanopartículas de sílice mesoporosa.

La síntesis de materiales mesoporosos de sílice se basa en la condensación de precursores de sílice mediante el método sol-gel sobre una serie de plantillas que dirigen la estructura y que posteriormente serán eliminados. Generalmente se lleva a cabo empleando surfactantes, que son polímeros anfifílicos capaces de autoensamblarse en disolución dando lugar a estructuras ordenadas.[17] Esta mesofase o cristal líquido actuará como agente director de estructura sobre el que condensará la materia inorgánica, siendo responsable de la porosidad del material final.[18] La estructura ordenada del material puede modificarse seleccionando diferentes surfactantes, que pueden ser aniónicos o catiónicos, lo cual determinará el tipo de interacción que poseen con el precursor de sílice, así como las condiciones óptimas para llevar a cabo la síntesis.[18] El tamaño de poro también puede ser controlado empleando surfactantes con distinta

longitud de cadena. Posteriormente, la adición de un precursor de sílice que sufrirá la hidrólisis y posterior policondensación en torno al agente director de estructura, dará lugar a la matriz de sílice que constituye el material.[18] Para llevar a cabo la obtención de nanopartículas de sílice mesoporosa, se emplea el método de Stöber[19] modificado, que se basa en realizar la síntesis en condiciones muy diluidas, pudiéndose controlar el tamaño de partícula en función de las condiciones de síntesis, tales como temperatura, concentración del precursor de sílice y agitación. Por último, la eliminación del surfactante por extracción o calcinación, permite dejar los poros vacíos y disponibles para cargar un fármaco en su interior.[20]

En función de las condiciones de síntesis y del surfactante seleccionado, se pueden obtener materiales mesoporosos con distintas estructuras ordenadas de poro, siendo ejemplos típicos los materiales tipo SBA-15 o MCM-41.[20,21] En la presente tesis doctoral, el material seleccionado son nanopartículas de sílice mesoporosa tipo MCM-41 (MSNs). Para obtener dicho material, el surfactante empleado como agente director de estructura es el surfactante catiónico bromuro de hexadeciltrimetil amonio (CTAB por sus siglas en inglés).[7] Así, el procedimiento sintético de obtención del material empleado puede observarse en el Esquema 1.

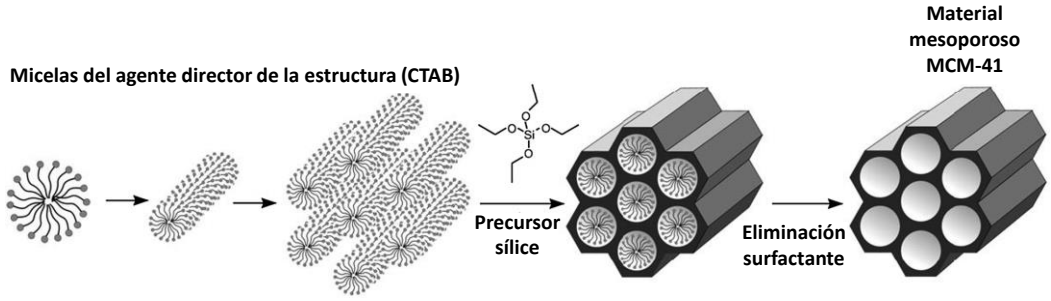

Esquema 1. Obtención de los materiales de sílice mesoporosa empleados en esta tesis doctoral. Adaptada con permiso.[18]

La síntesis de las MSNs empleadas en este trabajo se realiza en medio básico para catalizar la hidrólisis y condensación del precursor de sílice (Tetraetilortosilicato, TEOS) para dar lugar a la matriz del material.[20] El CTAB se elimina del material por medio de extracción por intercambio iónico empleando nitrato de amonio. El motivo de realizar esta eliminación por extracción en lugar de calcinando el material es doble. Por un lado, evitar la agregación irreversible de las nanopartículas debida al tratamiento a alta temperatura. Además, se evita la generación de productos potencialmente tóxicos procedentes de la calcinación del surfactante, ya que la aplicación deseada para el material en este trabajo es en biomedicina.[20] En las condiciones de síntesis empleadas,

el CTAB da lugar a una estructura mesoporosa con orden hexagonal, con poros de diámetro entre 2 y 3 nm, paralelos entre sí y no interconectados.[12]

1.2.2 Caracterización de MSNs.

La obtención del material deseado puede evaluarse mediante múltiples técnicas de caracterización. A continuación se muestran algunos ejemplos representativos de la caracterización básica más habitual de materiales mesoporosos de sílice. En primer lugar, la correcta síntesis de la matriz de sílice por el método sol-gel es comprobada mediante espectroscopía infrarroja con transformada de Fourier (FTIR, por sus siglas en inglés). El espectro FTIR de las MSNs muestra las bandas vibracionales correspondientes a la sílice (490-1090 cm^{-1}, Figura 1), al mismo tiempo que nos permite confirmar la correcta extracción del surfactante (que mostraría una serie de bandas entre 1400-1700 cm^{-1} y 2800-3000 cm^{-1}).[22–24] Posteriormente, la isoterma de adsorción de nitrógeno del material permite apreciar la elevada porosidad del material, así como la estrecha distribución del diámetro de poro, entre 2.5 y 3 nm (Figura 1).[25] La estructura ordenada de los poros del material se confirma mediante el diagrama de difracción de rayos X (XRD por sus siglas en inglés) a bajo ángulo, donde se observan los máximos de difracción característicos de la estructura ordenada hexagonal bidimensional de los poros de materiales tipo MCM-41 (grupo espacial p6mm, Figura 1).[4,26]

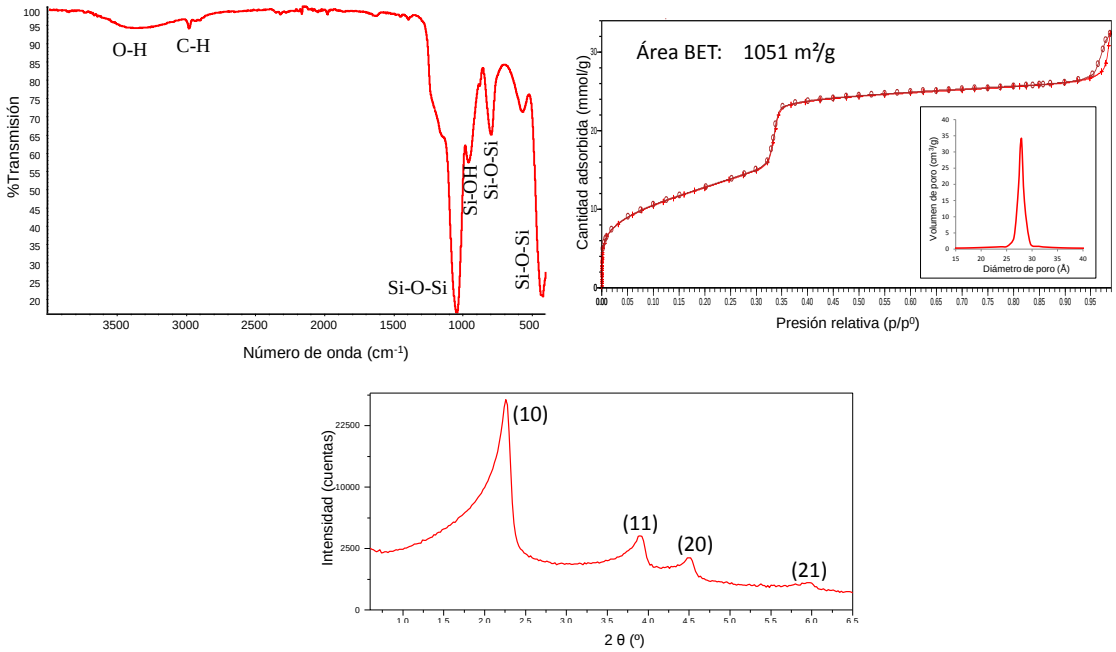

Figura 2. Caracterización típica de MSN. Espectro FTIR (arriba, izquierda), isoterma de adsorción de N_2 y distribución de diámetro de poro por adsorción de nitrógeno (arriba, derecha) y diagrama XRD a bajo ángulo (abajo).

Finalmente, la obtención del material en forma de nanopartículas puede observarse en las micrografías de las MSNs presentadas en la Figura 2, donde se observa la morfología y distribución de tamaños de las nanopartículas (microscopía electrónica de barrido, SEM por sus siglas en inglés), así como su estructura mesoporosa ordenada (microscopía electrónica de transmisión, TEM por sus siglas en inglés). Como se verá más adelante, otra técnica ampliamente empleada para analizar la distribución de tamaños de nanopartículas es la dispersión de luz dinámica (DLS).

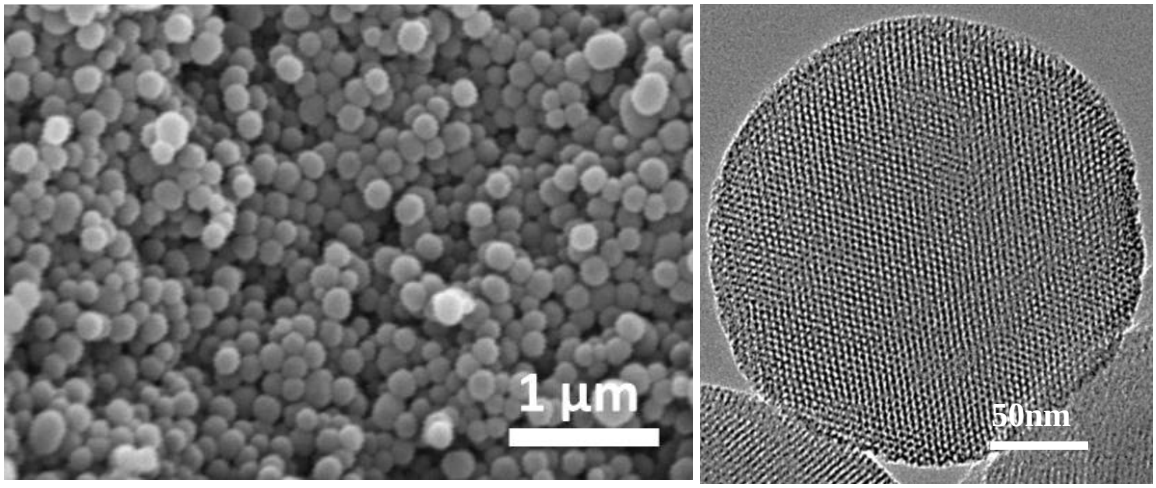

Figura 2. Micrografías de MSNs obtenidas por SEM (izquierda) y TEM (derecha).

1.2.3 Modificación química de MSNs.

La modificación química, o funcionalización, de las MSNs puede emplearse para dotar a las nanopartículas de grupos funcionales en superficie que permitan llevar a cabo modificaciones químicas posteriores o para favorecer la interacción de los grupos funcionales presentes en el poro con un fármaco, de forma que se consiga un proceso de carga y liberación del mismo controlado por dicha interacción.[27] La funcionalización puede realizarse por dos rutas diferentes, en función del momento en el que se realice, durante o tras la síntesis del material, co-condensación o post-síntesis, respectivamente.[28] Durante la presente tesis doctoral, una u otra ruta será elegida en función del objetivo de cada proceso de funcionalización (Esquema 2).

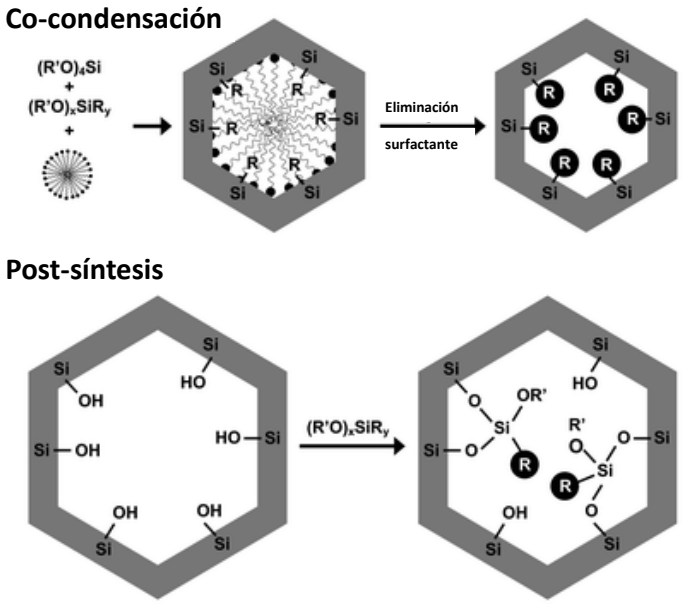

Esquema 2. Representación esquemática de las vías de funcionalización por co-condensación (arriba) y post-síntesis (abajo). Adaptada de [5].

a) Funcionalización por co-condensación

La funcionalización por co-condensación se realiza durante el proceso de obtención de las nanopartículas de sílice mesoporosa. El agente funcionalizante será añadido en forma de organosilano de forma conjunta con el precursor de sílice, de manera que los dos condensarán conjuntamente para dar lugar a la matriz del material.[28] De esta forma, el agente funcionalizante se encontrará repartido por toda la estructura de la partícula de forma homogénea, tanto en la superficie externa de la partícula, como en la superficie expuesta del interior de los poros, así como en el interior de la matriz.[29,30] La principal desventaja de este método es que grandes proporciones del agente funcionalizante pueden afectar a la estructura mesoporosa ordenada, por lo que suele emplearse en porcentajes minoritarios con respecto al TEOS.[31] También obliga a controlar las condiciones de eliminación del agente director de la estructura, para asegurar que el agente funcionalizante no sea dañado en el proceso. La funcionalización por co-condensación ha sido empleada en varias ocasiones en esta tesis doctoral para obtener MSNs con grupos aminopropilo homogéneamente distribuidos por toda su estructura.

b) Funcionalización post-síntesis

La funcionalización post-síntesis se realiza después de la obtención del material mesoporoso, por medio de la reacción del organosilano de interés con grupos silanol

expuestos en la superficie de la nanopartícula.[28] El agente funcionalizante no puede, por lo tanto, incorporarse en la matriz de sílice, y quedará en la superficie externa de la partícula así como en la superficie expuesta del interior de los poros.[26] Si se desea que el agente de funcionalización no esté presente en el interior de los poros, puede llevarse a cabo la funcionalización antes de la extracción del surfactante, o puede emplearse un agente funcionalizante de tal tamaño que éste no entre en el poro por impedimento estérico.[32] Este método permite obtener un mayor grado de funcionalización de la superficie del material sin comprometer la estructura ordenada de los poros, aunque la distribución del agente funcionalizante no es tan homogénea como la obtenida por el método anterior, especialmente en el interior de los poros. Otra desventaja es la necesidad de un paso adicional tras la síntesis de las nanopartículas para la obtención del material funcionalizado. La funcionalización post-síntesis ha sido empleada en esta tesis doctoral para el anclaje de la compuerta polimérica sensible a US en la superficie externa de las MSNs.

1.2.4 MSNs estímulo-respuesta.

Como se ha descrito en el capítulo 1.1, el desarrollo de materiales mesoporosos inteligentes, capaces de inducir la liberación de su carga en presencia de determinados estímulos, ha tenido un amplio desarrollo en los últimos años.[33,34] Debido a la estructura porosa abierta de los materiales de sílice mesoporosa, y con el objetivo de controlar la liberación desde los mismos, se hace necesario el anclaje de un elemento de cierre que actúe a modo de compuerta capaz de regular la liberación del contenido presente en los mesoporos. Para la obtención de MSNs con liberación en respuesta a estímulos, se han elegido en esta tesis doctoral las nanopartículas tipo MCM-41, que poseen poros ordenados no interconectados entre ellos, lo que facilita la obtención de un material con liberación controlada. Esto se debe a que los poros del material que no hayan sido tapados totalmente no influirán en la liberación desde el resto de poros correctamente cerrados. La naturaleza de las compuertas que pueden anclarse a MSNs comprende desde polímeros[35,36] hasta nanopartículas compactas de menor tamaño.[37] El conector por el cual la compuerta esté anclada, o bien alguno de los componentes de la compuerta en sí misma, son diseñados con objeto de producir una respuesta (cambio de conformación, ruptura, u otros) en presencia del estímulo de interés.[21] Mediante este tipo de estrategias, se han desarrollado MSNs sensibles a multitud de estímulos, tanto internos (pH,[36,38] redox,[39] enzimas[40]) como externos (luz,[32,41] campo magnético,[35,42,43] ultrasonido[44]).

La presente tesis doctoral se centra en la obtención de nanopartículas de sílice mesoporosa sensibles a ultrasonido (US) como estímulo externo. Con anterioridad al comienzo del desarrollo de esta tesis doctoral, la combinación de materiales mesoporosos de sílice con la aplicación de ultrasonido en el contexto biomédico había sido muy poco explorada.[44–46] En dichos trabajos, o bien no se empleaban nanopartículas,[45,46] o bien no se evaluaba la liberación de ninguna carga en respuesta al estímulo.[44] Durante el desarrollo de esta tesis, este campo se ha convertido en un área de gran interés, con multitud de artículos de investigación desarrollados sobre el tema en este tiempo,[47–57] e incluso revisiones bibliográficas dedicadas a él.[58] El ultrasonido puede ejercer distintos efectos biológicos que pueden ser aprovechados para diseñar y obtener materiales sensibles a la aplicación del estímulo. El siguiente capítulo de la introducción se centra en las características del US como estímulo y sus efectos biológicos.

Bibliografía

1. Rouquerol, J., Avnir, D., Fairbridge, C. W., Everett, D. H., Haynes, J. M., Pernicone, N., Ramsay, J. D. F., Sing, K. S. W. & Unger, K. K. Recommendations for the characterization of porous solids (Technical Report). *Pure Appl. Chem.* **66,** 1739–1758 (1994).
2. Yanagisawa, T., Shimizu, T., Kuroda, K. & Kato, C. The Preparation of Alkyltriinethylaininonium–Kaneinite Complexes and Their Conversion to Microporous Materials. *Bull. Chem. Soc. Jpn.* **63,** 988–992 (1990).
3. Beck, J. S., Vartuli, J. C., Roth, W. J., Leonowicz, M. E., Kresge, C. T., Schmitt, K. D., Chu, C. T. W., Olson, D. H., Sheppard, E. W., McCullen, S. B., Higgins, J. B. & Schlenker, J. L. A new family of mesoporous molecular sieves prepared with liquid crystal templates. *J. Am. Chem. Soc.* **114,** 10834–10843 (1992).
4. Vallet-Regí, M., Rámila, A., del Real, R. P. & Pérez-Pariente, J. A New Property of MCM-41: Drug Delivery System. *Chem. Mater.* **13,** 308–311 (2001).
5. Walcarius, A. & Mercier, L. Mesoporous organosilica adsorbents: nanoengineered materials for removal of organic and inorganic pollutants. *J. Mater. Chem.* **20,** 4478–4511 (2010).
6. Manzano, M., Colilla, M. & Vallet-Regí, M. Drug delivery from ordered mesoporous matrices. *Expert Opin. Drug Deliv.* **6,** 1383–1400 (2009).
7. He, Q. & Shi, J. Mesoporous silica nanoparticle based nano drug delivery systems: synthesis, controlled drug release and delivery, pharmacokinetics and biocompatibility. *J. Mater. Chem.* **21,** 5845–5855 (2011).
8. Mamaeva, V., Sahlgren, C. & Lindén, M. Mesoporous silica nanoparticles in medicine--recent advances. *Adv. Drug Deliv. Rev.* **65,** 689–702 (2013).
9. Manzano, M. & Vallet-Regí, M. New developments in ordered mesoporous materials for drug delivery. *J. Mater. Chem.* **20,** 5593–5604 (2010).
10. Lin, Y. S., Hurley, K. R. & Haynes, C. L. Critical Considerations in the Biomedical Use of Mesoporous Silica Nanoparticles. *J. Phys. Chem. Lett.* **3,** 364–374 (2012).
11. Tarn, D., Ashley, C. E., Xue, M., Carnes, E. C., Zink, J. I. & Brinker, C. J. Mesoporous Silica Nanoparticle Nanocarriers: Biofunctionality and Biocompatibility. *Acc. Chem. Res.* **46,** 792–801 (2013).
12. Trewyn, B. G., Nieweg, J. A., Zhao, Y. & Lin, V. S.-Y. Biocompatible mesoporous silica nanoparticles with different morphologies for animal cell membrane penetration. *Chem. Eng. J.* **137,** 23–29 (2008).
13. Braun, K., Pochert, A., Beck, M., Fiedler, R., Gruber, J. & Lindén, M. Dissolution kinetics of mesoporous silica nanoparticles in different simulated body fluids. *J. Sol-Gel Sci. Technol.* **79,** 319–327 (2016).
14. Paris, J. L., Colilla, M., Izquierdo-Barba, I., Manzano, M. & Vallet-Regí, M. Tuning mesoporous silica dissolution in physiological environments: a review. *J. Mater. Sci.* **52,** 8761–8771 (2017).
15. Fontecave, T., Sanchez, C., Azaïs, T. & Boissière, C. Chemical Modification As a Versatile Tool for Tuning Stability of Silica Based Mesoporous Carriers in Biologically Relevant Conditions. *Chem. Mater.* **24,** 4326–4336 (2012).
16. Cauda, V., Argyo, C. & Bein, T. Impact of different PEGylation patterns on the long-term bio-stability of colloidal mesoporous silica nanoparticles. *J. Mater. Chem.* **20,** 8693–8699 (2010).
17. Qiao, Z. A, Zhang, L., Guo, M. Y., Liu, Y. L. & Huo, Q. S. Synthesis of Mesoporous Silica Nanoparticles via Controlled Hydrolysis and Condensation of

Silicon Alkoxide. *Chem. Mater.* **21,** 3823–3829 (2009).
18. Hoffmann, F., Cornelius, M., Morell, J. & Fröba, M. Silica-Based Mesoporous Organic–Inorganic Hybrid Materials. *Angew. Chemie Int. Ed.* **45,** 3216–3251 (2006).
19. Stöber, W., Fink, A. & Bohn, E. Controlled growth of monodisperse silica spheres in the micron size range. *J. Colloid Interface Sci.* **26,** 62–69 (1968).
20. Wu, S.-H., Mou, C.-Y. & Lin, H.-P. Synthesis of mesoporous silica nanoparticles. *Chem. Soc. Rev.* **42,** 3862–3875 (2013).
21. Argyo, C., Weiss, V., Bräuchle, C. & Bein, T. Multifunctional Mesoporous Silica Nanoparticles as a Universal Platform for Drug Delivery. *Chem. Mater.* **26,** 435–451 (2014).
22. Chen, J., Liu, M., Chen, C., Gong, H. & Gao, C. Synthesis and Characterization of Silica Nanoparticles with Well-Defined Thermoresponsive PNIPAM via a Combination of RAFT and Click Chemistry. *ACS Appl. Mater. Interfaces* **3,** 3215–3223 (2011).
23. Villaverde, G., Baeza, A., Melen, G. J., Alfranca, A., Ramírez, M. & Vallet-Regí, M. A new targeting agent for the selective drug delivery of nanocarriers for treating neuroblastoma. *J. Mater. Chem. B* **3,** 4831–4842 (2015).
24. Chaudhary, Y. S., Ghatak, J., Bhatta, U. M. & Khushalani, D. One-step method for the self-assembly of metal nanoparticles onto facetted hollow silica tubes. *J. Mater. Chem.* **16,** 3619–3623 (2006).
25. Ishii, Y., Nishiwaki, Y., Al-zubaidi, A. & Kawasaki, S. Pore Size Determination in Ordered Mesoporous Materials Using Powder X-ray Diffraction. *J. Phys. Chem. C* **117,** 18120–18130 (2013).
26. Szegedi, A., Popova, M., Goshev, I., Klébert, S. & Mihály, J. Controlled drug release on amine functionalized spherical MCM-41. *J. Solid State Chem.* **194,** 257–263 (2012).
27. Nieto, A., Balas, F., Colilla, M., Manzano, M. & Vallet-Regí, M. Functionalization degree of SBA-15 as key factor to modulate sodium alendronate dosage. *Microporous Mesoporous Mater.* **116,** 4–13 (2008).
28. Rosenholm, J. M., Sahlgren, C. & Lindén, M. Towards multifunctional, targeted drug delivery systems using mesoporous silica nanoparticles--opportunities & challenges. *Nanoscale* **2,** 1870–1883 (2010).
29. Cauda, V., Schlossbauer, A. & Bein, T. Bio-degradation study of colloidal mesoporous silica nanoparticles: Effect of surface functionalization with organo-silanes and poly(ethylene glycol). *Microporous Mesoporous Mater.* **132,** 60–71 (2010).
30. Hoffman, A. S. Hydrogels for biomedical applications. *Adv. Drug Deliv. Rev.* **54,** 3–12 (2002).
31. Baeza, A., Guisasola, E., Torres-Pardo, A., González-Calbet, J. M., Melen, G. J., Ramírez, M. & Vallet-Regí, M. Hybrid enzyme-polymeric capsules/mesoporous silica nanodevice for in situ cytotoxic agent generation. *Adv. Funct. Mater.* **24,** 4625–4633 (2014).
32. Lai, J., Mu, X., Xu, Y., Wu, X., Wu, C., Li, C., Chen, J. & Zhao, Y. Light-responsive nanogated ensemble based on polymer grafted mesoporous silica hybrid nanoparticles. *Chem. Commun.* **46,** 7370–7372 (2010).
33. Vivero-Escoto, J. L., Slowing, I. I., Trewyn, B. G. & Lin, V. S.-Y. Mesoporous silica nanoparticles for intracellular controlled drug delivery. *Small* **6,** 1952–1967 (2010).
34. Martínez-Carmona, M., Colilla, M. & Vallet-Regí, M. Smart Mesoporous

Nanomaterials for Antitumor Therapy. *Nanomaterials* **5,** 1906–1937 (2015).
35. Baeza, A., Guisasola, E., Ruiz-Hernández, E. & Vallet-Regí, M. Magnetically Triggered Multidrug Release by Hybrid Mesoporous Silica Nanoparticles. *Chem. Mater.* **24,** 517–524 (2012).
36. Popat, A., Liu, J., Lu, G. Q. & Qiao, S. Z. A pH-responsive drug delivery system based on chitosan coated mesoporous silica nanoparticles. *J. Mater. Chem.* **22,** 11173–11178 (2012).
37. Liu, R., Zhang, Y., Zhao, X., Agarwal, A., Mueller, L. J. & Feng, P. pH-responsive nanogated ensemble based on gold-capped mesoporous silica through an acid-labile acetal linker. *J. Am. Chem. Soc.* **132,** 1500–1501 (2010).
38. Niedermayer, S., Weiss, V., Herrmann, A., Schmidt, A., Datz, S., Müller, K., Wagner, E., Bein, T. & Bräuchle, C. Multifunctional polymer-capped mesoporous silica nanoparticles for pH-responsive targeted drug delivery. *Nanoscale* **7,** 7953–7964 (2015).
39. Luo, Z., Cai, K., Hu, Y., Zhao, L., Liu, P., Duan, L. & Yang, W. Mesoporous silica nanoparticles end-capped with collagen: redox-responsive nanoreservoirs for targeted drug delivery. *Angew. Chem. Int. Ed.* **50,** 640–643 (2011).
40. Bernardos, A., Aznar, E., Marcos, M. D., Martínez-Máñez, R., Sancenón, F., Soto, J., Barat, J. M. & Amorós, P. Enzyme-Responsive Controlled Release Using Mesoporous Silica Supports Capped with Lactose. *Angew. Chem. Int. Ed.* **121,** 5998–6001 (2009).
41. Martínez-Carmona, M., Baeza, A., Rodriguez-Milla, M. A., García-Castro, J. & Vallet-Regí, M. Mesoporous silica nanoparticles grafted with a light-responsive protein shell for highly cytotoxic antitumoral therapy. *J. Mater. Chem. B* **3,** 5746–5752 (2015).
42. Guisasola, E., Baeza, A., Talelli, M., Arcos, D., Moros, M., de la Fuente, J. M. & Vallet-Regí, M. Magnetic-Responsive Release Controlled by Hot Spot Effect. *Langmuir* **31,** 12777–12782 (2015).
43. Bringas, E., Köysüren, Ö., Quach, D. V., Mahmoudi, M., Aznar, E., Roehling, J. D., Marcos, M. D., Martínez-Máñez, R. & Stroeve, P. Triggered release in lipid bilayer-capped mesoporous silica nanoparticles containing SPION using an alternating magnetic field. *Chem. Commun.* **48,** 5647–5649 (2012).
44. Kwon, E. J. & Lee, T. G. Surface-modified mesoporous silica with ferrocene derivatives and its ultrasound-triggered functionality. *Appl. Surf. Sci.* **254,** 4732–4737 (2008).
45. Kim, H.-J., Matsuda, H., Zhou, H. & Honma, I. Ultrasound-Triggered Smart Drug Release from a Poly(dimethylsiloxane)– Mesoporous Silica Composite. *Adv. Mater.* **18,** 3083–3088 (2006).
46. Depan, D., Saikia, L. & Singh, R. P. Ultrasound-triggered release of ibuprofen from a chitosan-mesoporous silica composite- A novel approach for controlled drug release. *Macromol. Symp.* **287,** 80–88 (2010).
47. Milgroom, A., Intrator, M., Madhavan, K., Mazzaro, L., Shandas, R., Liu, B. & Park, D. Mesoporous silica nanoparticles as a breast-cancer targeting ultrasound contrast agent. *Colloid Surface B* **116,** 652–657 (2014).
48. Ma, M., Xu, H., Chen, H., Jia, X., Zhang, K., Wang, Q., Zheng, S., Wu, R., Yao, M., Cai, X., Li, F. & Shi, J. A Drug-Perfluorocarbon Nanoemulsion with an Ultrathin Silica Coating for the Synergistic Effect of Chemotherapy and Ablation by High-Intensity Focused Ultrasound. *Adv. Mater.* **26,** 7378–7385 (2014).
49. Lee, S.-F., Zhu, X.-M., Wang, Y.-X. J., Xuan, S.-H., You, Q., Chan, W.-H., Wong, C.-H., Wang, F., Yu, J. C., Cheng, C. H. K. & Leung, K. C.-F.

Ultrasound, pH, and Magnetically Responsive Crown-Ether-Coated Core/Shell Nanoparticles as Drug Encapsulation and Release Systems. *ACS Appl. Mater. Interfaces* **5,** 1566–1574 (2013).

50. Lv, Y., Cao, Y., Li, P., Liu, J., Chen, H., Hu, W. & Zhang, L. Ultrasound-Triggered Destruction of Folate-Functionalized Mesoporous Silica Nanoparticle-Loaded Microbubble for Targeted Tumor Therapy. *Adv. Healthc. Mater.* **6,** 1700354 (2017).
51. Qian, X., Wang, W., Kong, W. & Chen, Y. Hollow periodic mesoporous organosilicas for highly efficient HIFU-based synergistic therapy. *RSC Adv.* **4,** 17950–17958 (2014).
52. Qian, X., Wang, W., Kong, W. & Chen, Y. Organic-Inorganic Hybrid Hollow Mesoporous Organosilica Nanoparticles for Efficient Ultrasound-Based Imaging and Controlled Drug Release. *J. Nanomater.* **2014,** 1–8 (2014).
53. Kempen, P. J., Greasley, S., Parker, K. A., Campbell, J. C., Chang, H.-Y., Jones, J. R., Sinclair, R., Gambhir, S. S. & Jokerst, J. V. Theranostic Mesoporous Silica Nanoparticles Biodegrade after Pro-Survival Drug Delivery and Ultrasound/Magnetic Resonance Imaging of Stem Cells. *Theranostics* **5,** 631–642 (2015).
54. Zhao, Y. & Zhu, Y. Synergistic cytotoxicity of low-energy ultrasound and innovative mesoporous silica-based sensitive nanoagents. *J. Mater. Sci.* **49,** 3665–3673 (2014).
55. Yildirim, A., Chattaraj, R., Blum, N. T. & Goodwin, A. P. Understanding Acoustic Cavitation Initiation by Porous Nanoparticles: Toward Nanoscale Agents for Ultrasound Imaging and Therapy. *Chem. Mater.* **28,** 5962–5972 (2016).
56. Huang, P., Qian, X., Chen, Y., Yu, L., Lin, H., Wang, L., Zhu, Y. & Shi, J. Metalloporphyrin-Encapsulated Biodegradable Nanosystems for Highly Efficient Magnetic Resonance Imaging-Guided Sonodynamic Cancer Therapy. *J. Am. Chem. Soc.* **139,** 1275–1284 (2017).
57. Teng, Z., Wang, R., Zhou, Y., Kolios, M., Wang, Y., Zhang, N., Wang, Z., Zheng, Y. & Lu, G. A magnetic droplet vaporization approach using perfluorohexane-encapsulated magnetic mesoporous particles for ultrasound imaging and tumor ablation. *Biomaterials* **134,** 43–50 (2017).
58. Zhou, Y., Han, X., Jing, X. & Chen, Y. Construction of Silica-Based Micro/Nanoplatforms for Ultrasound Theranostic Biomedicine. *Adv. Healthc. Mater.* **6,** 1700646 (2017).

1.3 Ultrasonido como estímulo externo

El ultrasonido (US) puede ser definido como una onda acústica (mecánica) cuya frecuencia está por encima del límite de audición del ser humano (20 kHz).[1] La onda de US puede ser definida en función de diversos parámetros, tales como frecuencia, potencia, intensidad o presión (Figura 1). La velocidad del US dividido por su longitud de onda da lugar a la frecuencia, que es el parámetro más habitual para describir una onda de US. La velocidad del US en agua, que es el medio por el que se va a transmitir en un organismo vivo, es de 1480 m/s.[2] En función de su frecuencia, puede dividirse en ultrasonido de baja frecuencia (inferior a 1 MHz) o ultrasonido de alta frecuencia (superior a 1 MHz).[1] La potencia del US puede expresarse en vatios (W), aunque en el entorno clínico suele emplearse más el concepto de intensidad (expresada en W/cm^2).[3–5] Dado que se trata de una onda mecánica, la presión generada por la aplicación del US también se emplea de forma habitual para describir las condiciones de US aplicadas.[6]

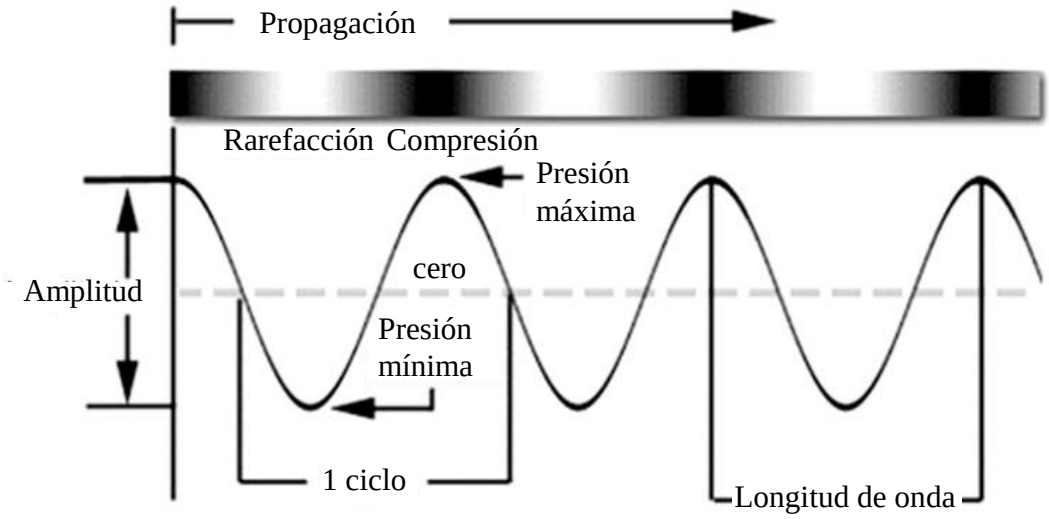

Figura 1. Parámetros que describen una onda de ultrasonido. Adaptado con permiso.[2]

El uso de US en clínica se encuentra ampliamente extendido tanto con fines diagnósticos como terapéuticos.[7] Se ha empleado para multitud de aplicaciones, como en la generación de hipertermia,[8] apertura de la barrera hemato-encefálica,[9] sonoporación,[10] inmunoestimulación,[11] obtención de imagen diagnóstica[12] y en fisioterapia,[4] entre otras muchas. Para su uso diagnóstico suelen emplearse frecuencias altas (generalmente por encima de 3 MHz) trabajando a intensidades bajas.[13] Por otra

parte, para aplicación terapéutica se suelen emplear frecuencias inferiores, trabajando a una mayor intensidad.

La generación de US suele realizarse empleando transductores constituidos por cristales piezoeléctricos, capaces de convertir una señal eléctrica en una onda mecánica que se transmitirá por un fluido.[14] La utilización de transductores con curvatura permite la generación de un punto focal a cierta distancia de la fuente de US de alta frecuencia. Esto posibilita la aplicación de una mayor intensidad del estímulo en el punto de interés a cierta profundidad en el interior del organismo de forma no invasiva, minimizando la intensidad de US a la que estarán expuestos los tejidos sanos circundantes.[8] La posibilidad de focalizar el US a cierta profundidad ha dado lugar al desarrollo de terapias que emplean ultrasonido focalizado de alta intensidad (HIFU por sus siglas en inglés). El uso de HIFU se plantea como alternativa a la cirugía en algunos casos de tumores internos, mediante la destrucción de tejido en el punto focal del US (Esquema 1).[13]

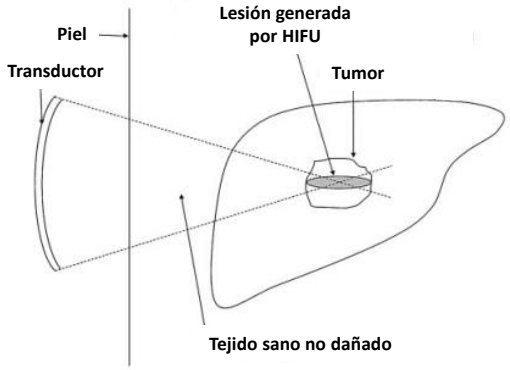

Esquema 1. Representación de terapias ablativas para tumores sólidos basadas en HIFU. Adaptado con permiso.[13]

La elevada capacidad de penetración del US y la posibilidad de aplicarlo de forma focalizada suponen grandes ventajas sobre otros estímulos externos ampliamente estudiados, como es el caso de la luz. El principal inconveniente de la luz en su uso en biomedicina es la poca capacidad de penetración de dicho estímulo en tejidos, haciendo necesario el uso de intensidades elevadas que pueden llegar a causar quemaduras en la piel del paciente.[1,15] El uso de luz del infrarrojo cercano (NIR por sus siglas en inglés) aumenta la capacidad de penetración del estímulo, pero sigue siendo mucho menor que la capacidad de penetración del US.[16] A modo de ejemplo, se realizó durante una estancia predoctoral en el grupo dirigido por el Prof. Daniel S. Kohane (Boston Children´s Hospital, Harvard Medical School), una comparativa de la penetración de luz

NIR (730 nm) frente a US no focalizado de 1 MHz, como puede verse en la Figura 2. Para la determinación de la capacidad de penetración de ambos estímulos, se aplicó cada uno de ellos en músculo, empleando carne de ternera. Se detectó la intensidad del estímulo capaz de atravesar distintos grosores de tejido muscular con un medidor de potencia (luz) o un transductor conectado a un osciloscopio a través de un módulo de detección (US). Como se puede observar en la Figura 2, la capacidad del US de atravesar el músculo es mucho mayor que en el caso de la luz NIR.

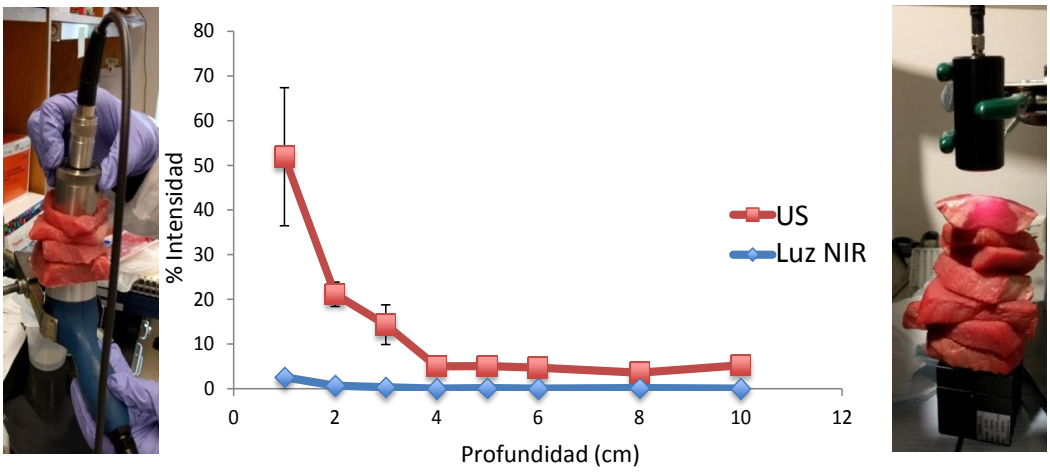

Figura 2. Capacidad de penetración *ex vivo* de luz NIR frente a US en tejidos (centro), imagen del montaje experimental para determinar la capacidad de penetración de US (izquierda) y luz NIR (derecha).

Los efectos biológicos del ultrasonido pueden dividirse en efectos térmicos y efectos mecánicos.[8] Sin embargo, merece la pena mencionar que ambos tipos de efectos se van a producir de forma simultánea, y que en la mayoría de las ocasiones, separar ambos es una tarea compleja, como se va a comentar a continuación.

Efectos térmicos: A medida que una onda de US se propaga por un tejido, parte de su energía puede ser absorbida en forma de calor, incrementando la temperatura en la zona.[8] Así, la hipertermia generada por US puede emplearse para terapias ablativas del cáncer (como en el ejemplo presentado del uso de HIFU en el esquema 1) o para activar nanomateriales sensibles a temperatura.[17] Los efectos térmicos están relacionados de forma directa con la frecuencia de US empleada: mayores frecuencias producen un mayor aumento de temperatura al transmitirse por los tejidos.[4]

Efectos mecánicos: Los efectos mecánicos del US pueden dividirse en efectos no cavitatorios y cavitación acústica.[18] Entre los primeros, el más común es el flujo

acústico (referido en inglés como *acoustic streaming*), que puede ser definido como la generación de movimiento o flujo en un fluido como consecuencia de la exposición del mismo a las ondas mecánicas del US.[19] Por otra parte, la cavitación acústica es debida a la interacción de burbujas de gas en un fluido con las ondas mecánicas del US a las que está expuesto.[20,21] Puede dividirse en tres etapas, pudiendo dar lugar a cavitación estable o cavitación inestable (también denominada inercial) (Figura 3).

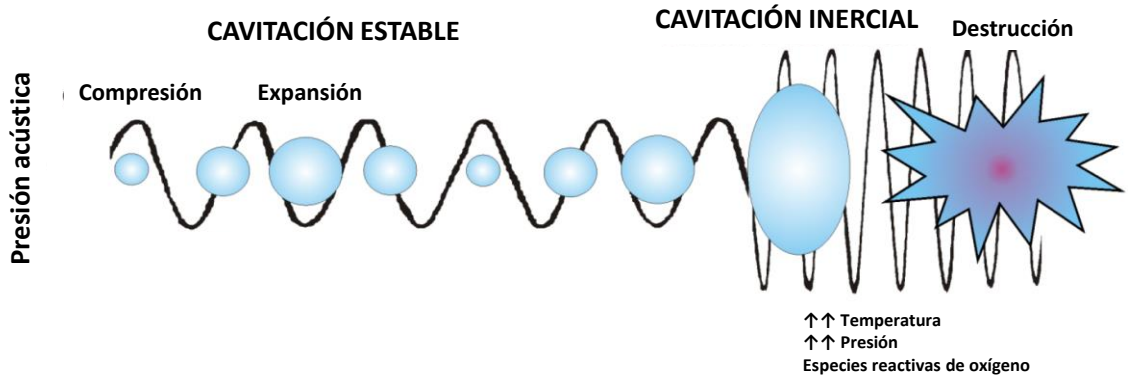

Figura 3. Proceso de cavitación acústica. Adaptado con permiso.[22]

Primero, la exposición a las ondas mecánicas induce la formación de pequeñas burbujas de gas en el fluido. La interacción de estas microburbujas con las ondas de US las hace oscilar de tamaño, expandiéndose y comprimiéndose en la fase de presión positiva y negativa, respectivamente (cavitación estable).[20] Finalmente, si el estímulo alcanza una intensidad suficiente, la superación de un tamaño umbral en la fase de presión negativa induce el colapso catastrófico de la misma en la fase de presión positiva (cavitación inercial).[6] Esta implosión de la microburbuja de gas produce unas condiciones extremas en el entorno local (en la nanoescala), alcanzándose presiones y temperaturas muy altas, del orden de 5000 K, lo que dificulta separar efectos térmicos y mecánicos.[1] Estas condiciones extremas dan lugar a la generación de luz (sonoluminiscencia)[23] y a la formación de especies reactivas de oxígeno (ROS por sus siglas en inglés) debido a la pirolisis de moléculas de agua.[18] El índice mecánico (MI por sus siglas en inglés) es un parámetro que indica la probabilidad de cavitación inercial en un fluido expuesto a US.[24] Se define como el pico de presión negativa generado dividido por la raíz cuadrada de la frecuencia de US empleada. Valores de MI mayores a 0.7 indican una alta probabilidad de cavitación inercial. Por lo tanto, la probabilidad de cavitación será mayor cuanto menor sea la frecuencia utilizada.

La generación de cavitación es considerada como una de las aplicaciones más prometedoras del uso de US en biomedicina, dado que puede generar una gran multitud de efectos biológicos. Se cree que está implicada en la permeabilización de la membrana celular por US (sonoporación),[10] y puede utilizarse para favorecer la penetración de fármacos y nanopartículas.[6] Sin embargo, la presión necesaria para superar el umbral de cavitación *in vivo* puede ser demasiado grande para poder utilizarse de forma segura sin dañar tejidos sanos.[24] Por ello, la utilización de núcleos de cavitación capaces de disminuir el umbral de presión necesario para producir cavitación acústica aparece como una opción conveniente para aplicación biomédica.[20] Entre los agentes de cavitación más empleados se pueden destacar las burbujas lipídicas micrométricas, que ya se utilizan en clínica como agentes de contraste de US,[22] las gotículas submicrométricas de cambio de fase[25] y las partículas poliméricas submicrométricas con capacidad de estabilización de nanoburbujas de gas.[26,27]

Por último, cabe mencionar que los efectos térmicos y mecánicos del US, y especialmente el fenómeno de cavitación inercial, pueden ser empleados para acelerar o inducir reacciones químicas (sonoquímica).[28–33] La inducción de reacciones químicas en presencia de cavitación inercial puede deberse a la generación de especies reactivas de oxígeno que inicien una cadena de reacciones posteriores, al calentamiento en la nanoescala en las proximidades de burbujas en proceso de implosión, a efectos mecánicos como microflujo acústico (también asociado a la cavitación), o a una combinación de todos estos efectos.

Los efectos térmicos,[34] mecánicos[35] y químicos[36] del US pueden emplearse para desarrollar diferentes materiales inteligentes, capaces de desencadenar una respuesta al ser expuestos al estímulo. Así, se han desarrollado liposomas,[14,17,37,38] micelas[29,36,39] y partículas poliméricas[40] sensibles a US. La presente tesis doctoral se centra en el desarrollo de nanopartículas de sílice mesoporosa sensibles a US. A lo largo de la tesis se irán describiendo los distintos tipos de dispositivos de US empleados, algunos comerciales y otros diseñados, tanto focalizados como no focalizados. La puesta a punto de las pruebas de concepto iniciales se llevaron a cabo con un dispositivo comercial de laboratorio empleando un transductor no focalizado de 1.3 MHz con una potencia máxima de trabajo de 100 W. Posteriormente, la evaluación biológica se realizó con un equipo de fisioterapia, no focalizado, de 1 MHz de frecuencia y con una intensidad máxima de 3 W/cm^2. Para los estudios mecanísticos y experimentos de extravasación de nanopartículas se utilizaron equipos de ultrasonido construidos con transductores

focalizados en el rango terapéutico (con frecuencias fundamentales de 0.5, 1 ó 1.1 MHz) o diagnóstico (7.5 MHz), actuando este último como detector pasivo de cavitación.

Bibliografía

1. Timko, B. P., Dvir, T. & Kohane, D. S. Remotely Triggerable Drug Delivery Systems. *Adv. Mater.* **22,** 4925–4943 (2010).
2. Tsaklis, P. Presentation of Acoustic Waves Propagation and Their Effects Through Human Body Tissues. *Hum. Mov.* **11,** 91–95 (2010).
3. Rohr, K. R. & Rooney, J. A. Effect of ultrasound on a bilayer lipid membrane. *Biophys. J.* **23,** 33–40 (1978).
4. Draper, D. O., Castel, J. C. & Castel, D. Rate of Temperature Increase in Human Muscle During 1 MHz and 3 MHz Continuous Ultrasound. *J. Orthop. Sport. Phys. Ther.* **22,** 142–150 (1995).
5. Wang, X. B., Liu, Q. H., Wang, P., Tang, W. & Hao, Q. Study of cell killing effect on S180 by ultrasound activating protoporphyrin IX. *Ultrasonics* **48,** 135–140 (2008).
6. Carlisle, R., Choi, J., Bazan-Peregrino, M., Laga, R., Subr, V., Kostka, L., Ulbrich, K., Coussios, C.-C. & Seymour, L. W. Enhanced Tumor Uptake and Penetration of Virotherapy Using Polymer Stealthing and Focused Ultrasound. *JNCI J. Natl. Cancer Inst.* **105,** 1701–1710 (2013).
7. Wood, A. K. W. & Sehgal, C. M. A Review of Low-Intensity Ultrasound for Cancer Therapy. *Ultrasound Med. Biol.* **41,** 905–928 (2015).
8. van den Bijgaart, R. J. E., Eikelenboom, D. C., Hoogenboom, M., Fütterer, J. J., den Brok, M. H. & Adema, G. J. Thermal and mechanical high-intensity focused ultrasound: perspectives on tumor ablation, immune effects and combination strategies. *Cancer Immunol. Immunother.* **66,** 247–258 (2017).
9. Hynynen, K., McDannold, N., Sheikov, N. A., Jolesz, F. A. & Vykhodtseva, N. Local and reversible blood–brain barrier disruption by noninvasive focused ultrasound at frequencies suitable for trans-skull sonications. *Neuroimage* **24,** 12–20 (2005).
10. Theek, B., Baues, M., Ojha, T., Möckel, D., Veettil, S. K., Steitz, J., van Bloois, L., Storm, G., Kiessling, F. & Lammers, T. Sonoporation enhances liposome accumulation and penetration in tumors with low EPR. *J. Control. Release* **231,** 77–85 (2016).
11. Unga, J. & Hashida, M. Ultrasound induced cancer immunotherapy. *Adv. Drug Deliv. Rev.* **72,** 144–153 (2014).
12. Fenster, A., Downey, D. B. & Cardinal, H. N. Three-dimensional ultrasound imaging. *Phys. Med. Biol.* **46,** R67–R99 (2001).
13. Kennedy, J. E., ter Haar, G. R. & Cranston, D. High intensity focused ultrasound: surgery of the future? *Br. J. Radiol.* **76,** 590–599 (2003).
14. Schroeder, A., Kost, J. & Barenholz, Y. Ultrasound, liposomes, and drug delivery: principles for using ultrasound to control the release of drugs from liposomes. *Chem. Phys. Lipids* **162,** 1–16 (2009).
15. Carregal-Romero, S., Guardia, P., Yu, X., Hartmann, R., Pellegrino, T. & Parak, W. J. Magnetically triggered release of molecular cargo from iron oxide nanoparticle loaded microcapsules. *Nanoscale* **7,** 570–576 (2015).
16. Crucho, C. I. C. Stimuli-Responsive Polymeric Nanoparticles for Nanomedicine. *ChemMedChem* **10,** 24–38 (2015).
17. Grüll, H. & Langereis, S. Hyperthermia-triggered drug delivery from temperature-sensitive liposomes using MRI-guided high intensity focused ultrasound. *J. Control. Release* **161,** 317–327 (2012).

18. Rosenthal, I., Sostaric, J. Z. & Riesz, P. Sonodynamic therapy--a review of the synergistic effects of drugs and ultrasound. *Ultrason. Sonochem.* **11,** 349–363 (2004).
19. Sirsi, S. R. & Borden, M. A. State-of-the-art materials for ultrasound-triggered drug delivery. *Adv. Drug Deliv. Rev.* **72,** 3–14 (2014).
20. Arvanitis, C. D., Bazan-Peregrino, M., Rifai, B., Seymour, L. W. & Coussios, C. C. Cavitation-Enhanced Extravasation for Drug Delivery. *Ultrasound Med. Biol.* **37,** 1838–1852 (2011).
21. O'Neill, B. E., Vo, H., Angstadt, M., Li, K. P. C., Quinn, T. & Frenkel, V. Pulsed High Intensity Focused Ultrasound Mediated Nanoparticle Delivery: Mechanisms and Efficacy in Murine Muscle. *Ultrasound Med. Biol.* **35,** 416–424 (2009).
22. Turánek, J., Miller, A. D., Kauerová, Z., Lukáč, R., Mašek, J., Koudelka, Š. & Raška, M. Lipid-Based Nanoparticles and Microbubbles – Multifunctional Lipid-Based Biocompatible Particles for in vivo Imaging and Theranostics, in *Advances in Bioengineering*, (InTech, 2015).
23. Kuroki, M., Hachimine, K., Abe, H., Shibaguchi, H., Kuroki, M., Maekawa, S., Yanagisawa, J., Kinugasa, T., Tanaka, T. & Yamashita, Y. Sonodynamic therapy of cancer using novel sonosensitizers. *Anticancer Res.* **27,** 3673–3678 (2007).
24. Yildirim, A., Chattaraj, R., Blum, N. T. & Goodwin, A. P. Understanding Acoustic Cavitation Initiation by Porous Nanoparticles: Toward Nanoscale Agents for Ultrasound Imaging and Therapy. *Chem. Mater.* **28,** 5962–5972 (2016).
25. Lee, J. Y., Carugo, D., Crake, C., Owen, J., de Saint Victor, M., Seth, A., Coussios, C. & Stride, E. Nanoparticle-Loaded Protein-Polymer Nanodroplets for Improved Stability and Conversion Efficiency in Ultrasound Imaging and Drug Delivery. *Adv. Mater.* **27,** 5484–5492 (2015).
26. Kwan, J. J., Graham, S., Myers, R., Carlisle, R., Stride, E. & Coussios, C. C. Ultrasound-induced inertial cavitation from gas-stabilizing nanoparticles. *Phys. Rev. E* **92,** 23019 (2015).
27. Kwan, J. J., Myers, R., Coviello, C. M., Graham, S. M., Shah, A. R., Stride, E., Carlisle, R. C. & Coussios, C. C. Ultrasound-Propelled Nanocups for Drug Delivery. *Small* **11,** 5305–5314 (2015).
28. Cintas, P., Tagliapietra, S., Caporaso, M., Tabasso, S. & Cravotto, G. Enabling technologies built on a sonochemical platform: Challenges and opportunities. *Ultrason. Sonochem.* **25,** 8–16 (2015).
29. Li, F., Xie, C., Cheng, Z. & Xia, H. Ultrasound responsive block copolymer micelle of poly(ethylene glycol)–poly(propylene glycol) obtained through click reaction. *Ultrason. Sonochem.* **30,** 9–17 (2016).
30. Li, Y., Wang, P., Zhao, P., Zhu, S., Wang, X. & Liu, Q. Apoptosis induced by sonodynamic treatment by protoporphyrin IX on MDA-MB-231 cells. *Ultrasonics* **52,** 490–496 (2012).
31. Liu, Q., Wang, X., Wang, P., Qi, H., Zhang, K. & Xiao, L. Sonodynamic effects of protoporphyrin IX disodium salt on isolated sarcoma 180 cells. *Ultrasonics* **45,** 56–60 (2006).
32. Dai, Z. J., Li, S., Gao, J., Xu, X. N., Lu, W. F., Lin, S. & Wang, X. J. Sonodynamic therapy (SDT): A novel treatment of cancer based on sonosensitizer liposome as a new drug carrier. *Med. Hypotheses* **80,** 300–302 (2013).
33. McKenzie, T. G., Colombo, E., Fu, Q., Ashokkumar, M. & Qiao, G. G. Sono-

RAFT Polymerization in Aqueous Medium. *Angew. Chemie Int. Ed.* **56,** 12302–12306 (2017).

34. Ernsting, M. J., Worthington, A., May, J. P., Tagami, T., Kolios, M. C. & Li, S.-D. Ultrasound drug targeting to tumors with thermosensitive liposomes. in *2011 IEEE Int. Ultrason. Symp.* 1–4 (IEEE, 2011).
35. Geers, B., Lentacker, I., Sanders, N. N., Demeester, J., Meairs, S. & De Smedt, S. C. Self-assembled liposome-loaded microbubbles: The missing link for safe and efficient ultrasound triggered drug-delivery. *J. Control. Release* **152,** 249–256 (2011).
36. Wang, J., Pelletier, M., Zhang, H., Xia, H. & Zhao, Y. High-Frequency Ultrasound-Responsive Block Copolymer Micelle. *Langmuir* **25,** 13201–13205 (2009).
37. Schroeder, A., Honen, R., Turjeman, K., Gabizon, A., Kost, J. & Barenholz, Y. Ultrasound triggered release of cisplatin from liposomes in murine tumors. *J. Control. Release* **137,** 63–68 (2009).
38. Rwei, A. Y., Paris, J. L., Wang, B., Wang, W., Axon, C. D., Vallet-Regí, M., Langer, R. & Kohane, D. S. Ultrasound-triggered local anaesthesia. *Nat. Biomed. Eng.* **1,** 644–653 (2017).
39. Xuan, J., Boissière, O., Zhao, Y., Yan, B., Tremblay, L., Lacelle, S., Xia, H. & Zhao, Y. Ultrasound-Responsive Block Copolymer Micelles Based on a New Amplification Mechanism. *Langmuir* **28,** 16463–16468 (2012).
40. Papa, A.-L., Korin, N., Kanapathipillai, M., Mammoto, A., Mammoto, T., Jiang, A., Mannix, R., Uzun, O., Johnson, C., Bhatta, D., Cuneo, G. & Ingber, D. E. Ultrasound-sensitive nanoparticle aggregates for targeted drug delivery. *Biomaterials* **139,** 187–194 (2017).

2. OBJETIVOS

Las ideas no duran mucho. Hay que hacer algo con ellas.

Santiago Ramón y Cajal

Objetivos

La presente tesis doctoral se encuentra dividida en 3 bloques, presentando cada uno de ellos sus objetivos principales y secundarios. En líneas generales, los objetivos de esta tesis doctoral son:

1. Desarrollo de nanopartículas de sílice mesoporosa con capacidad de liberación de fármacos inducida por ultrasonido.
    - Síntesis y caracterización de una compuerta polimérica sensible a ultrasonido. Anclaje de dicha compuerta a la superficie de nanopartículas de sílice mesoporosa y caracterización del comportamiento del material híbrido.
    - Evaluación del mecanismo por el cual el ultrasonido induce la liberación en el material híbrido desarrollado, distinguiendo entre efectos térmicos y mecánicos.

A partir de este punto, la tesis doctoral se centra en conseguir un transporte selectivo de nanopartículas de sílice mesoporosa sensibles a ultrasonido por medio de estrategias físico-químicas o mediante estrategias de vehiculización celular.

2. Puesta a punto de estrategias físico-químicas para una conseguir distribución selectiva hacia tumores de nanopartículas de sílice mesoporosa sensibles a ultrasonido.
    - Modificación del material híbrido obtenido en el objetivo 1 para anclar cadenas de polietilenglicol, así como moléculas de vectorización activa que induzcan su internalización selectiva en células tumorales.
    - Desarrollo de un nuevo tipo de nanopartículas de sílice mesoporosa sensibles a ultrasonido para mejorar su distribución en el tumor empleando estrategias de vectorización jerarquizada.
    - Favorecer la extravasación de nanopartículas de sílice mesoporosa empleando ultrasonido. Este trabajo se desarrolla en un modelo *in vitro* de agarosa que simula un tejido tumoral.

3. Evaluación de la vehiculización biológica de nanopartículas de sílice mesoporosa sensibles a ultrasonido hacia tumores.

- Estudio de la introducción de nanopartículas de sílice mesoporosa en células madre mesenquimales de placenta y su capacidad migratoria hacia tumores *in vitro* e *in vivo*.
- Vehiculización celular hacia tumores de nanopartículas de sílice mesoporosa sensibles a ultrasonido (desarrolladas en el objetivo 1), utilizando células madre mesenquimales de placenta.
- Transfección génica de células madre mesenquimales de placenta con genes suicidas empleando nanopartículas de sílice mesoporosa sensibles a ultrasonido modificadas.

Objectives

The present doctoral thesis is divided in 3 parts, having each one of them some primary and secondary objectives. In general terms, the objectives of this thesis are:

1. Development of mesoporous silica nanoparticles with ultrasound-induced drug release capabilities.
    - Synthesis and characterization of an ultrasound-responsive polymeric gate. Grafting of that gate on the surface of mesoporous silica nanoparticles and characterization of the behavior of the hybrid material.
    - Evaluation of the mechanism by which ultrasound induces the release from the hybrid material, distinguishing between thermal and mechanical effects.

Henceforth, the doctoral thesis focuses on achieving selective transport of the ultrasound-sensitive mesoporous silica nanoparticles through physicochemical strategies or through cellular vehiculization strategies.

2. Setting up physicochemical strategies to achieve selective distribution towards tumors of ultrasound-sensitive mesoporous silica nanoparticles.
    - Modification of the hybrid material obtained in objective 1 to achieve the grafting of polyethyleneglycol chains as well as active targeting molecules that induce their selective internalization in cancer cells.
    - Development of a new type of ultrasound-responsive mesoporous silica nanoparticles to improve their distribution in tumors employing hierarchical targeting strategies.
    - Favouring the extravasation of mesoporous silica nanoparticles using ultrasound. This work is carried out in an *in vitro* agarose model that mimics a tumor tissue.

3. Evaluation of biological vehiculization of ultrasound-responsive mesoporous silica nanoparticles towards tumors.
    - Study of the introduction of mesoporous silica nanoparticles inside placental mesenchymal stem cells and their migratory properties towards tumors *in vitro* and *in vivo*.

- Cellular vehiculization towards tumors of ultrasound-responsive mesoporous silica nanoparticles (developed on part 1), using placental mesenchymal stem cells.
- Gene transfection of placental mesenchymal stem cells with suicide genes employing modified ultrasound-responsive mesoporous silica nanoparticles.

3. RESULTADOS Y DISCUSIÓN

Las ciencias aplicadas no existen, sólo las aplicaciones de la ciencia.

Louis Pasteur

En este apartado de la tesis doctoral se describen los aspectos metodológicos relacionados con la síntesis, caracterización y evaluación de los materiales obtenidos, así como los principales resultados y conclusiones de cada trabajo desarrollado.

El apartado de Resultados y Discusión está dividido en tres bloques, conteniendo cada uno de ellos varios capítulos. Cada bloque va además acompañado de una introducción del estado del arte a tratar así como una breve discusión integradora de los capítulos contenidos en el mismo. Los capítulos incluidos en esta sección se presentan en formato de artículo científico en inglés, algunos de ellos publicados en revistas internacionales. Los bloques y capítulos contenidos en esta sección son:

3.1 Desarrollo y evaluación de nanopartículas de sílice mesoporosa con liberación sensible a ultrasonido

3.1.1 Polymer-Grafted Mesoporous Silica Nanoparticles as Ultrasound-Responsive Drug Carriers

3.1.2 Mechanistic evaluation of cargo release from Ultrasound-Responsive Polymer-Grafted Mesoporous Silica Nanoparticles

3.2 Estrategias físico-químicas de vectorización de nanopartículas de sílice mesoporosa sensibles a ultrasonido

3.2.1 From Proof-of-concept Material to PEGylated, Modularly Targeted Ultrasound-Responsive Mesoporous Silica Nanoparticles.

3.2.2 Mesoporous Silica Nanoparticles with Ultrasound-Induced Uptake by Cancer Cells

3.2.3 Ultrasound-Mediated Cavitation-Enhanced Extravasation of Mesoporous Silica Nanoparticles for Controlled-Release Drug Delivery

3.3 Vehiculización celular de nanopartículas de sílice mesoporosa sensibles a ultrasonido

3.3.1 Decidua-Derived Mesenchymal Stem Cells as Carriers of Mesoporous Silica Nanoparticles. In vitro and In vivo Evaluation on Mammary Tumors

3.3.2 Vectorization of Ultrasound-Responsive Nanoparticles in Placental Mesenchymal Stem Cells for Cancer Therapy

3.3.3 Gene Transfection employing Ultrasound-responsive Mesoporous Silica Nanoparticles

Bloque 3.1

Desarrollo y evaluación de nanopartículas de sílice mesoporosa con liberación sensible a ultrasonido

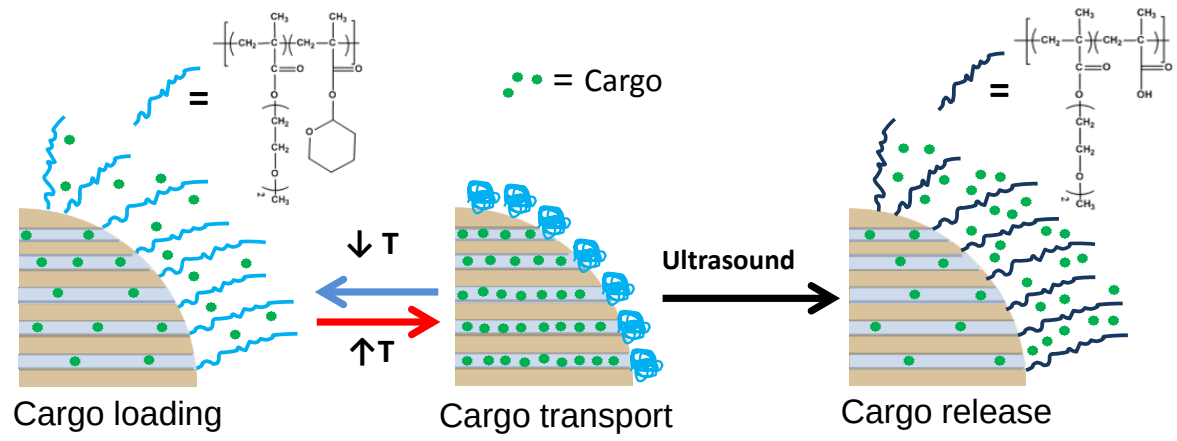

El primer bloque de Resultados y Discusión versa sobre el desarrollo de MSNs con capacidad de retener un fármaco en su interior en condiciones fisiológicas, y liberarlo al entorno en presencia de un estímulo externo de US. El desarrollo de dichas nanopartículas y su evaluación *in vitro* se encuentran recogidos en un artículo científico publicado en la revista ACS Nano (Capítulo 3.1.1).[1] Posteriormente, se muestra la evaluación del mecanismo de apertura de dichas nanopartículas (Capítulo 3.1.2), fruto de una estancia de investigación de 3 meses en la Universidad de Oxford, en el grupo de investigación BUBBL, dirigido por el Prof. Constantin C. Coussios.

Para el desarrollo del nanotransportador estímulo-respuesta, se eligió utilizar una compuerta polimérica anclada a las MSNs para obtener un material híbrido sensible a US. Como se ha mencionado en el capítulo 1.2, el empleo de compuertas poliméricas para obtener materiales de sílice mesoporosa con liberación controlada ha sido estudiado ampliamente. Además, presenta varias ventajas sobre otro tipo de estrategias para cerrar y abrir las entradas de los poros.[2–5] En general, la capacidad de obtener un bloqueo homogéneo de los poros es mayor empleando una compuerta polimérica, ya que es más factible obtener una capa alrededor de todo el contorno de la nanopartícula, que utilizando nanopartículas discretas, que van a dejar parte de la superficie sin ocupar.[6] Además, el peso molecular del polímero puede ser modificado para optimizar la respuesta del nanosistema.[2] Los distintos mecanismos por los que un polímero puede actuar como compuerta en un material híbrido con MSNs serían: el polímero puede separarse de la superficie de la sílice como consecuencia de la ruptura del enlace que los unía,[7] puede destruirse la propia estructura del polímero,[8] o puede producirse un cambio conformacional que permita la salida de la carga.[4] Esta última aproximación puede ser especialmente útil, ya que permite en algunas ocasiones introducir la carga dentro de los mesoporos con el polímero ya anclado, aprovechándonos de ese mismo cambio conformacional que inducirá la liberación.[4,9] Para ello, debe ser posible inducir dicho cambio conformacional de forma reversible. Esta posibilidad dota al material de gran versatilidad, ya que existe la posibilidad de seleccionar el fármaco más adecuado para una aplicación concreta y cargarlo sobre el material ya preparado, sin tener que sintetizar todo el sistema en cada nueva ocasión.

El polímero elegido como compuerta para controlar la liberación en este trabajo fue el poli(metoxietoxietilmetacrilato-co-tetrahidropiranilmetacrilato), p(MEO_2MA-co-THPMA). Para la obtención de este polímero se eligió un método de polimerización por radicales libres (FRP por sus siglas en inglés).[10] En este tipo de polimerización, los

monómeros y un agente iniciador se mezclan en atmósfera inerte en un disolvente en el cual los monómeros, el iniciador y el polímero resultante sean solubles. Para este trabajo se seleccionó como iniciador el ácido 4,4'-azobis(4-ciano)valérico, que es capaz de generar especies radicales por ruptura homolítica al exponerlo a un aumento de temperatura (en torno a 70 ºC en nuestro caso, Esquema 1).[11] La especie radical generada reaccionará con los monómeros, metacrilatos en nuestro caso, dando lugar a una cadena que irá creciendo hasta agotar la cantidad de monómeros en el medio de reacción (Esquema 1). La presencia de un ácido carboxílico en el iniciador permitirá el anclaje del polímero final a la sílice.[12]

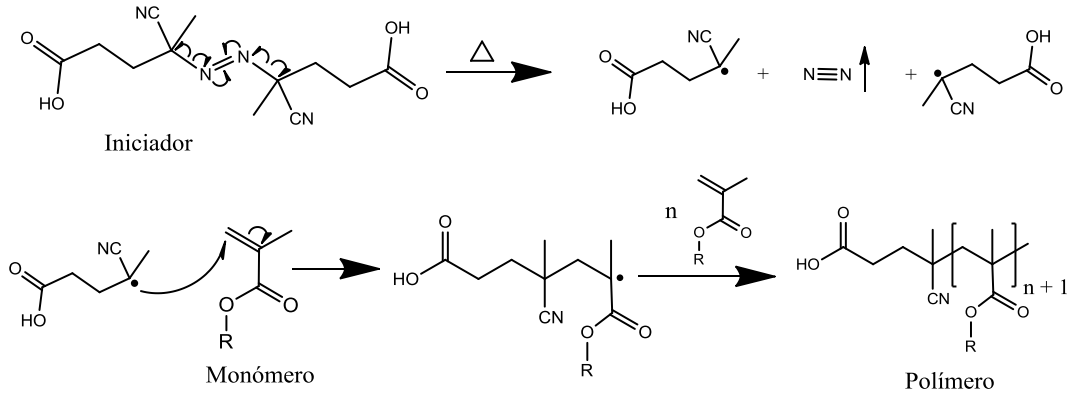

Esquema 1. Generación de radicales por el iniciador (arriba) y posterior crecimiento de la cadena polimérica por FRP (abajo).

El polímero elegido es, como se ha mencionado anteriormente, un copolímero aleatorio constituido por dos monómeros diferentes: tetrahidropiranilmetacrilato (THPMA)[13,14] y metoxietoxietilmetacrilato (MEO_2MA).[15] Los polímeros compuestos de MEO_2MA presentan un comportamiento termosensible con una temperatura crítica inferior de disolución (LCST por sus siglas en inglés).[16] Esto quiere decir que son solubles en agua a temperatura inferior a su LCST, e insolubles (precipitan) por encima de dicha temperatura (Figura 1).[17] Este comportamiento se debe a la diferente contribución de las interacciones del polímero con el medio acuoso y las interacciones hidrofóbicas dentro de la propia cadena del polímero, que se vuelven dominantes a mayor temperatura, y conducen a la deshidratación de la cadena de polímero y a que adopte una conformación globular.[17] Este cambio de conformación reversible es importante ya que nos permitirá cargar de agente terapéutico las nanopartículas híbridas simplemente modificando la temperatura del medio, como se verá más adelante.

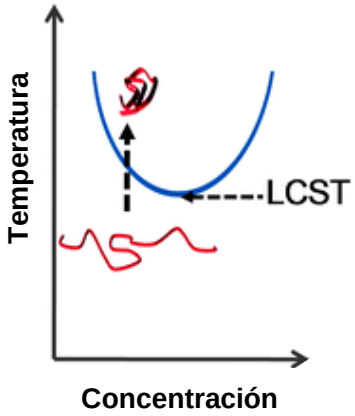

Figura 1. Cambio de conformación de polímeros termosensibles que presentan LCST. Adaptada con permiso.[18]

Una característica importante de este tipo de polímeros es que el valor de la LCST puede modificarse mediante la adición de comonómeros que modifiquen la hidrofilia/lipofilia del polímero en su conjunto.[16] Así, la adición de monómeros hidrofóbicos favorece la precipitación y dará lugar a una disminución de la LCST. Por otro lado, la adición de monómeros hidrofílicos tendrá el efecto contrario, aumentando la temperatura a la cual se producirá el cambio de conformación. En este sentido, el THPMA es un monómero hidrofóbico capaz de romperse cuando es expuesto a US, convirtiéndose en ácido metacrílico (MAA, Figura 2A).[13,14] Este cambio producirá un aumento de la hidrofilia del polímero, aumentando su LCST por encima de valores fisiológicos (Figura 2B) y conduciendo a un cambio de conformación del polímero, en este caso irreversible, causado por la ruptura del monómero THPMA. De este modo, tenemos un sistema que cuando está a temperatura fisiológica (37 ºC) está por encima de la LCST, pero que cuando aplicamos US (a esa misma temperatura fisiológica) estará por debajo de la nueva LCST, con el consiguiente cambio de conformación.

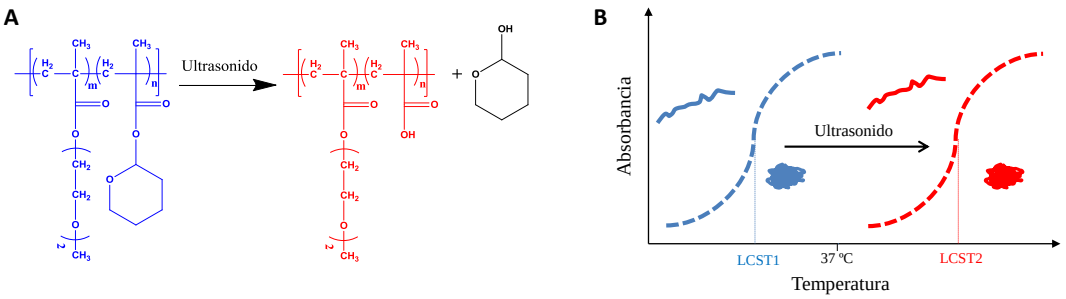

Figura 2. Ruptura del THPMA en el copolímero p(MEO_2MA-co-THPMA) al exponerlo a US, dando lugar a p(MEO_2MA-co-MAA) (A), cambio en la LCST del copolímero al exponerlo a US (B).

Los polímeros termosensibles con LCST se han empleado con anterioridad para obtener materiales híbridos basados en MSNs con liberación controlada.[4,9] En función del método de obtención del material, la compuerta polimérica actuará de forma distinta.[19] Cuando el recubrimiento polimérico se sintetiza desde la propia superficie del material (estrategia conocida en inglés como *grafting from*),[20] la densidad del recubrimiento es mayor, y el polímero actúa como una barrera de difusión cuando las cadenas del mismo están extendidas.[21,22] Así, el material estará "cerrado" por debajo de su LCST. Cuando el polímero colapsa (por encima de la LCST) deja huecos por los que la carga puede liberarse. Por el contrario, cuando se anclan polímeros termosensibles ya preformados a la superficie del material mesoporoso (*grafting to*),[20] las cadenas de polímero colapsadas actúan a modo de tapón, impidiendo la liberación.[9] Cuando las cadenas de polímero están extendidas, el acceso a los poros no está impedido, pudiendo cargar o liberar su contenido. En nuestro material, la segunda estrategia fue elegida, empleando el ácido carboxílico presente en el polímero para anclarlo a la superficie de la sílice mediante química de conjugación con carbodiimidas. Se seleccionó un polímero con una LCST inferior a 37 ºC. Así, el material podrá cargarse con el fármaco en frío (4 ºC), para luego tener su compuerta cerrada a temperatura fisiológica. Cuando se exponga el material a US, el cambio en la LCST del polímero inducirá un cambio de conformación irreversible que provocará la liberación de la carga desde las nanopartículas.

Tal y como se verá en el capítulo 3.1.1, se comprobó que estas nanopartículas no son tóxicas y que pueden ser internalizadas por células tumorales de próstata (LNCaP),[8] manteniendo su comportamiento sensible a ultrasonido en el citoplasma de las células. Las nanopartículas híbridas cargadas con doxorrubicina fueron incubadas con células LNCaP, induciendo su muerte solo cuando las nanopartículas habían sido expuestas a US. Este trabajo demuestra que nuestras nanopartículas híbridas basadas en nanopartículas de sílice mesoporosa pueden ser activadas por un estímulo externo e inducir la muerte de células tumorales, lo cual es de gran importancia para aplicación futura en liberación de fármacos y terapia oncológica.

En el capítulo 3.1.2, se llevó a cabo la evaluación detallada del mecanismo por el cual el US es capaz de inducir la liberación de la carga desde las nanopartículas. Para ello, se estudió la respuesta del material tras ser expuesto a los efectos del US a distintas frecuencias y condiciones experimentales, permitiendo analizar de forma independiente los efectos térmicos y mecánicos del estímulo sobre las nanopartículas híbridas. Los

resultados mostraron que la presencia de cavitación acústica es necesaria para que se induzca la respuesta del material, mientras que los efectos térmicos no fueron ni suficientes ni necesarios para observar la liberación de la carga.

Bibliografía

1. Paris, J. L., Cabañas, M. V., Manzano, M. & Vallet-Regí, M. Polymer-Grafted Mesoporous Silica Nanoparticles as Ultrasound-Responsive Drug Carriers. *ACS Nano* **9,** 11023–11033 (2015).
2. Popat, A., Liu, J., Lu, G. Q. & Qiao, S. Z. A pH-responsive drug delivery system based on chitosan coated mesoporous silica nanoparticles. *J. Mater. Chem.* **22,** 11173–11178 (2012).
3. Niedermayer, S., Weiss, V., Herrmann, A., Schmidt, A., Datz, S., Müller, K., Wagner, E., Bein, T. & Bräuchle, C. Multifunctional polymer-capped mesoporous silica nanoparticles for pH-responsive targeted drug delivery. *Nanoscale* **7,** 7953–7964 (2015).
4. Lai, J., Mu, X., Xu, Y., Wu, X., Wu, C., Li, C., Chen, J. & Zhao, Y. Light-responsive nanogated ensemble based on polymer grafted mesoporous silica hybrid nanoparticles. *Chem. Commun.* **46,** 7370–7372 (2010).
5. Zhang, Y., Ang, C. Y., Li, M., Tan, S. Y., Qu, Q., Luo, Z. & Zhao, Y. Polymer-Coated Hollow Mesoporous Silica Nanoparticles for Triple-Responsive Drug Delivery. *ACS Appl. Mater. Interfaces* **7,** 18179–18187 (2015).
6. Liu, R., Zhang, Y., Zhao, X., Agarwal, A., Mueller, L. J. & Feng, P. pH-responsive nanogated ensemble based on gold-capped mesoporous silica through an acid-labile acetal linker. *J. Am. Chem. Soc.* **132,** 1500–1501 (2010).
7. Saint-Cricq, P., Deshayes, S., Zink, J. I. & Kasko, A. M. Magnetic field activated drug delivery using thermodegradable azo-functionalised PEG-coated core–shell mesoporous silica nanoparticles. *Nanoscale* **7,** 13168–13172 (2015).
8. Gisbert-Garzaran, M., Lozano, D., Vallet-Regí, M. & Manzano, M. Self-immolative polymers as novel pH-responsive gate keepers for drug delivery. *RSC Adv.* **7,** 132–136 (2017).
9. You, Y.-Z., Kalebaila, K. K. & Brock, S. L. Temperature-Controlled Uptake and Release in PNIPAM-Modified Porous Silica Nanoparticles. *Chem. Mater.* **20,** 3354–3359 (2008).
10. Lutz, J. F. Polymerization of oligo(ethylene glycol) (meth)acrylates: Toward new generations of smart biocompatible materials. *J. Polym. Sci. Part A Polym. Chem.* **46,** 3459–3470 (2008).
11. Yorimitsu, H., Wakabayashi, K., Shinokubo, H. & Oshima, K. Radical Addition of 2-Iodoalkanamide or 2-Iodoalkanoic Acid to Alkenes with a Water-Soluble Radical Initiator in Aqueous Media: Facile Synthesis of γ -Lactones. *Bull. Chem. Soc. Jpn.* **74,** 1963–1970 (2001).
12. Sapsford, K. E., Algar, W. R., Berti, L., Gemmill, K. B., Casey, B. J., Oh, E., Stewart, M. H. & Medintz, I. L. Functionalizing nanoparticles with biological molecules: Developing chemistries that facilitate nanotechnology. *Chem. Rev.* **113,** 1904–2074 (2013).
13. Wang, J., Pelletier, M., Zhang, H., Xia, H. & Zhao, Y. High-Frequency Ultrasound-Responsive Block Copolymer Micelle. *Langmuir* **25,** 13201–13205 (2009).
14. Xuan, J., Boissière, O., Zhao, Y., Yan, B., Tremblay, L., Lacelle, S., Xia, H. & Zhao, Y. Ultrasound-Responsive Block Copolymer Micelles Based on a New Amplification Mechanism. *Langmuir* **28,** 16463–16468 (2012).
15. Lutz, J.-F., Hoth, A. & Schade, K. Design of Oligo(ethylene glycol)-Based Thermoresponsive Polymers: an Optimization Study. *Des. Monomers Polym.* **12,** 343–353 (2009).

16. Laloyaux, X., Mathy, B., Nysten, B. & Jonas, A. M. Surface and bulk collapse transitions of thermoresponsive polymer brushes. *Langmuir* **26,** 838–847 (2010).
17. Liu, R., Fraylich, M. & Saunders, B. R. Thermoresponsive copolymers: from fundamental studies to applications. *Colloid Polym. Sci.* **287,** 627–643 (2009).
18. Gibson, M. I. & O'Reilly, R. K. To aggregate, or not to aggregate? considerations in the design and application of polymeric thermally-responsive nanoparticles. *Chem. Soc. Rev.* **42,** 7204–7213 (2013).
19. Guisasola, E., Baeza, A., Talelli, M., Arcos, D. & Vallet-Regí, M. Design of thermoresponsive polymeric gates with opposite controlled release behaviors. *RSC Adv.* **6,** 42510–42516 (2016).
20. Zou, H., Wu, S. & Shen, J. Polymer/Silica Nanocomposites: Preparation, Characterization, Properties, and Applications. *Chem. Rev.* **108,** 3893–3957 (2008).
21. Baeza, A., Guisasola, E., Ruiz-Hernández, E. & Vallet-Regí, M. Magnetically Triggered Multidrug Release by Hybrid Mesoporous Silica Nanoparticles. *Chem. Mater.* **24,** 517–524 (2012).
22. Guisasola, E., Baeza, A., Talelli, M., Arcos, D., Moros, M., de la Fuente, J. M. & Vallet-Regí, M. Magnetic-Responsive Release Controlled by Hot Spot Effect. *Langmuir* **31,** 12777–12782 (2015).

3.1.1 Polymer-Grafted Mesoporous Silica Nanoparticles as Ultrasound-Responsive Drug Carriers

Paris, J. L., Cabañas, M. V., Manzano, M. & Vallet-Regí, M. ACS Nano 9, 11023–11033 (2015). DOI: 10.1021/acsnano.5b04378

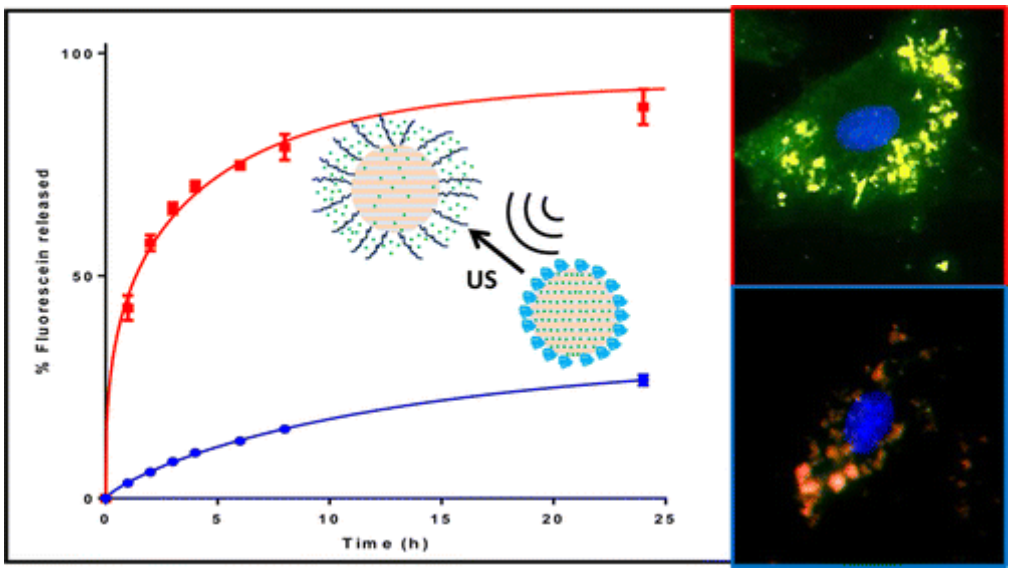

Polymer-Grafted Mesoporous Silica Nanoparticles as Ultrasound-Responsive Drug Carriers

Juan L. Paris,[†,‡] M. Victoria Cabañas,[†] Miguel Manzano,[†,‡] and María Vallet-Regí[*,†,‡]

[†]Dpto. Química Inorgánica y Bioinorgánica, Facultad de Farmacia, UCM, Instituto de Investigación Sanitaria Hospital 12 de Octubre i+12, 28040 Madrid, Spain and
[‡]Centro de Investigación Biomédica en Red de Bioingeniería, Biomateriales y Nanomedicina (CIBER-BBN), 50018 Zaragoza, Spain

ABSTRACT A new ultrasound-responsive system based on mesoporous silica nanoparticles was developed for biomedical applications, grafting a copolymer on their surface that acts as gatekeeper of the pores. The nanoparticles can be loaded with a cargo at low temperature (4 °C), taking advantage of the open conformation that the polymer presents under these conditions. Then, at 37 °C the copolymer collapses closing the pore entrances and allowing the nanoparticles to carry the drugs at physiological temperature without premature release, which is of great importance when dealing with cytotoxic drugs in cancer treatments. Upon ultrasound irradiation, the sensitive polymer changes its hydrophobicity and, therefore, its conformation toward coil-like opening the gates and releasing the cargo. These hybrid nanoparticles have been shown to be noncytotoxic and can be internalized into LNCaP cells retaining their ultrasound-responsive capability in the cytoplasm of the cells. Moreover, doxorubicin-loaded hybrid MSNs were incubated with LNCaP cells to show their capacity to induce cell death only when the nanoparticles had been exposed to ultrasound. This work demonstrates that our hybrid-MSNs can be triggered by remote stimuli, which is of capital importance for future applications in drug delivery and cancer therapy.

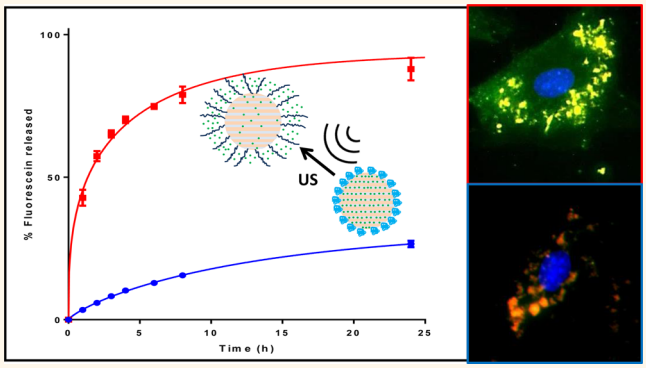

KEYWORDS: mesoporous silica · ultrasound · stimuli-responsive · drug delivery · nanomedicine

Nanotechnology has fully transformed the area of drug delivery thanks to the use of nanocarriers for therapeutics. The reason behind that revolution is the potential for addressing some of the most significant restrictions of conventional medicine, such as poor drug solubility, inadequate pharmacokinetics and diverse side effects. Nanoparticles employed as drug delivery systems have displayed important benefits such as enhanced accumulation of drug molecules at diseased tissues and cells, contributing to the reduction of the systemic toxicity.[1−3]

Among all nanoparticles employed in biomedicine, mesoporous silica nanoparticles (MSNs) are very attractive nanocarriers for diagnostic and therapeutic applications.[4−7] MSNs present unique material properties, such as mechanical and chemical stability, good biocompatibility, and high loading capacity. In fact, the excellent textural properties of mesoporous silica, such as high surface area, high pore volume and tunable pore sizes, guarantee a great loading capacity and efficient encapsulation of an immense variety of cargo molecules.[8−10] Additionally, their chemical composition assures the efficient attachment of organic surface functionalities such as gate keepers to avoid premature release of the cargo, or targeting ligands to favor selective localization of MSNs toward diseased tissues.

However, it is very difficult to actually control the release of the drug from the nanocarriers, which normally relays on the biodegradation of the nanoparticles *in vivo*. One alternative that has been developed in the past few years is the concept of stimuli-responsive drug delivery systems, which allow for tailored release profiles with spatial, temporal and dosage control.[7,10,11] Those stimuli-responsive systems consist of triggering the release of the therapeutic drug at the diseased site through the use diverse entities that are sensitive to exogenous

* Address correspondence to vallet@ucm.es.

Received for review July 15, 2015 and accepted October 11, 2015.

Published online October 11, 2015
10.1021/acsnano.5b04378

stimuli (*i.e.*, temperature, light, magnetic fields, electric fields and ultrasounds) or endogenous stimuli (*i.e.*, changes in pH, redox potential, or the concentrations of enzymes or specific analytes).[12−15]

Among feasible external stimuli, ultrasounds (US) represent a unique and exciting method for achieving spatiotemporal control of the drug release at the desired site.[16] Additionally, US are attractive because of their noninvasiveness, the absence of ionizing radiations, the cost effectiveness and the easy regulation of tissue penetration depth by tuning the frequency, cycles and exposure time. In fact, high-frequency ultrasound can penetrate deep into the body with focused beams, which allows local therapy avoiding adverse side effects to healthy tissues. Moreover, ultrasound stimulus itself presents interesting properties for nanomedicine, as it has been shown to enhance nanoparticle extravasation through blood capillaries, increase cell membrane permeation and even induce an immune response against tumors.[17,18]

Ultrasound waves can induce thermal and/or mechanical effects that could trigger the release of the drug from a collection of nanocarriers, such as liposomes, micelles, microbubbles, *etc.*[16] Moreover, advances in sonochemistry have shown that ultrasound-induced chemical reactions can differ from those carried out by bulk heating, implying mechanical or thermal effects at the nanoscale.[19] US irradiation can also cleave certain chemical bonds, the so-called mechanophores.[20,21] This strategy can be exploited in the design of responsive nanoparticles with ultrasound-labile moieties. In this context, 2-tetrahydropyranyl methacrylate (THPMA) is a hydrophobic monomer bearing a labile acetal group that can be cleaved by ultrasound to yield hydrophilic methacrylic acid (MAA).[20,22] This strategy, phase transformation from hydrophobic to hydrophilic by US irradiation, could be used to develop a polymeric gatekeeper on nanoparticles to avoid premature release of different cargos.

Regarding the cargo of different molecules in MSNs, nanogates based on thermosensitive polymers that exhibit a lower critical solution temperature (LCST), are a versatile option for this purpose. These polymers are soluble in aqueous medium at low temperature, but upon heating, when the system reaches the LCST, the polymer changes to a hydrophobic state, collapsing and giving rise to a suspension in the same aqueous medium. This means that by changing the temperature of the medium, the use of thermosensitive polymers with a LCST allows loading a drug in MSNs after anchoring the polymer nanogates to their surface.[12,13,23,24] This constitutes a great advantage over most stimuli-responsive materials, that must be loaded with the cargo prior to the nanogate grafting.[25]

The combination of a thermoresponsive polymer, such as poly(2-(2-methoxyethoxy)ethyl methacrylate), p(MEO_2MA),[26] with an ultrasound-responsive monomer (THPMA) would result in a dual-responsive copolymer: the thermal response allows us to load and retain the cargo, and the US sensitivity to induce its release at physiological temperature. The US-responsive character empowers the thermoresponsive polymer with the particular property of modulating its phase state by US irradiation at a chosen temperature. Besides, both components of the designed copolymer (MEO_2MA and THPMA) have been shown to present good biocompatibility and interesting properties for biomedical application.[27,28]

The mentioned advantages of US irradiation as extern stimulus motived us to explore a novel smart drug delivery system. In this work, we have combined the possibilities of US stimulus together with the great capabilities of MSNs to design an US stimulus-responsive drug delivery system. Despite the great potential of this strategy, the use of US in mesoporous silica remains largely unexplored.[29,30] Basically, we have developed a nanocarrier based on MSNs with nanogates that allows the encapsulation and transportation of drugs with no premature release to specific locations in the body where the cargo can be released upon externally applied ultrasounds (Scheme 1). To achieve that, we have functionalized MSNs with a copolymer able to open and close the gates of the carrier pores through a nanogate. Copolymer p(MEO_2MA)-*co*-THPMA bearing US-cleavable hydrophobic tetrahydropyranyl moieties, presents a LCST below physiological temperature. At 4 °C, the polymer is in its coil-like conformation, allowing the cargo to be loaded in the mesopores. When the temperature is increased to physiological temperature, the copolymer changes to a collapsed state (insoluble) and the nanogates are closed retaining the cargo into the pores. Upon US irradiation, the hydrophobic tetrahydropyranyl moieties are cleaved, leading to an increase of the hydrophilicity of the polymer and, therefore, an increase of the LCST over physiological temperature. This induces a change in conformation of the polymer to coil-like, opening the gates of the mesopores of the MSNs and allowing the entrapped cargo to be released (Scheme 1).

In this work, we propose and demonstrate a new approach to stimuli-responsive systems by using hybrid mesoporous silica nanoparticles that allow encapsulation of small molecules of any type that would be released only upon external US irradiation.

RESULTS AND DISCUSSION

Hybrid-MSN Nanoparticles. Mesoporous silica nanoparticles, MSNs, with a MCM-41 type structure, diameter of *ca.* 200 and 2 nm mesopores were synthesized by a modification of the well-known Stöber method. The external surface of the MSNs was coated with a copolymer able to open or close the pore entrances under certain stimuli. Thus, preparation and optimization

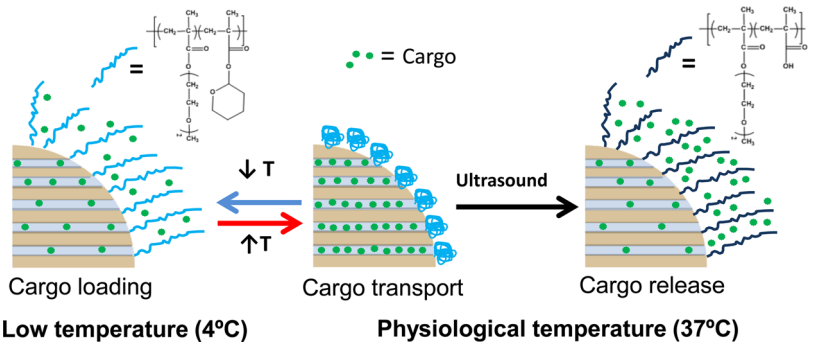

Scheme 1. Schematic illustration of the behavior in aqueous medium of dual responsive release system.

of the copolymer properties was the first task to be completed.

The dual temperature ultrasound-responsive random copolymer poly(2-(2-methoxyethoxy) ethyl methacrylate-*co*-2-tetrahydropyranyl methacrylate, p(MEO_2MA-*co*-THPMA), was synthesized by free radical polymerization from 2-(2-methoxyethoxy) ethyl methacrylate, MEO_2MA (temperature-responsive monomer) and 2-tetrahydropyranyl methacrylate, THPMA (ultrasound-responsive monomer).[26] Different ratios of MEO_2MA and THPMA monomers were evaluated to endow the copolymer with LCST lower (LCST1) and higher (LCST2) than 37 °C before and after ultrasound irradiation, respectively (Table S1, Supporting Information). Optimal results were achieved for a MEO_2MA:THPMA ratio of *ca.* 90:10 (composition estimated by ^{1}H NMR) synthesized from a 87.5:12.5 molar ratio. Lower content in US-responsive monomer lead to LCST2 lower than 37 °C, after 10 min of US irradiation. In fact, the total absence of THPMA in the polymer backbone resulted into a lack of responsiveness upon US irradiation: the LCST and ^{1}H NMR spectrum of the polymer were not modified after US exposure (Figure S1). On the other hand, for higher THPMA contents, the copolymer was insoluble in aqueous solution even at low temperature, which means that the copolymer would be always in a collapsed state closing the gates of the pores. Consequently, it would not be possible to load the cargo in this medium even at 4 °C. Therefore, 90:10 (MEO_2MA:THPMA ratio) was selected for the forthcoming experiments.

The variation of the LSCT of this copolymer as a function of US irradiation time is collected in Figure 1a (the frequency and power of the US beam were fixed at 1.3 MHz and 100 W, respectively). As it can be observed, applied US time had a terrific influence on shifting the LCST of the polymer: the LCST1 of the as-synthesized copolymer was 26 °C, after 3 min of US irradiation it shifted to 36 °C, and after 6 min of US beam the LCST2 went higher than 45 °C. The LCST increase can be attributed to the cleavage of the sensitive part of the copolymer, THPMA, through the tetrahydropyranyl group (Figure 1b).[20,22] This cleavage leads to a change in the composition and hydrophobicity

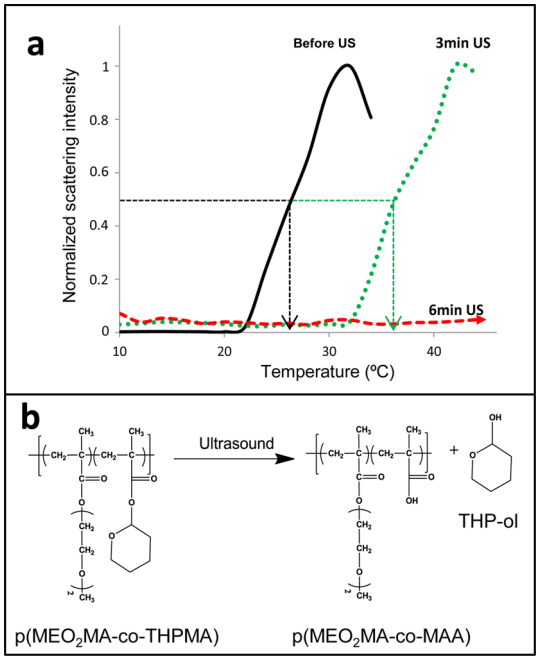

Figure 1. (a) Lower critical solution temperature (LCST) of p(90MEO_2MA-10THPMA) after different periods of time of ultrasound irradiation (1.3 MHz and 100 W). (b) Hydrolysis of dual-responsive p(MEO_2MA-THPMA) into p(MEO_2MA-MAA) and THP-ol (tetrahydropyranol) by ultrasound.

of the copolymer and, therefore, to a LCST shift to temperatures above 37 °C modifying the polymer state toward an extended conformation. The ^{1}H NMR spectrum of the copolymer after US irradiation (Figure S2) confirms the disappearance of the THP moiety. To ensure that THPMA cleavage was not due to bulk heating caused by the US application, a solution of the selected copolymer was heated to 80 °C for 30 min. No modification in the LCST or the ^{1}H NMR spectrum could be found (Figure S2). Also, the THP group was removed by acid catalysis with *p*-toluenesulfonic acid in methanol for 5 h, and the changes in the ^{1}H NMR spectrum were the same as those found when the monomer THPMA was cleaved by US application (Figure S2). These experiments prove that the changes observed are unequivocally due to US irradiation. Then, the ultrasound-induced rise in the LCST makes the tested copolymer and ratio suitable for the desired application.

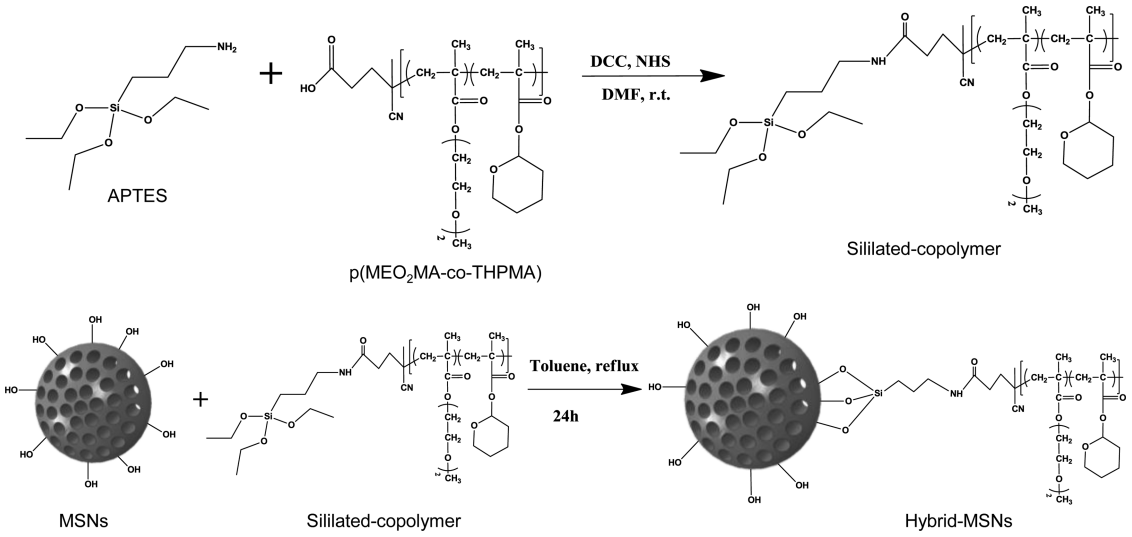

Scheme 2. Preparation of p(MEO_2MA-*co*-THPMA)-SiO_2 nanoparticles (Hybrid-MSNs):APTES conjugation to p(MEO_2MA-*co*-THPMA) (top) and grafting of the sililated-copolymer to mesoporous SiO_2 nanoparticles (bottom).

Once both components of our system, nanocarrier and polymeric nanogates, were produced and optimized, the next step was joining them together. This procedure, described in Scheme 2, was based on functionalizing the copolymer (MEO_2MA-*co*-THPMA) with an alkoxysilane (3-aminopropyl triethoxysilane) through DCC-NHS chemistry to form a sililated polymer, to then graft it to the silica nanoparticles surface through silanol chemistry. The ratio of polymer:nanoparticles together with the coupling reaction conditions were explored to obtain the best possible responsive system. Basically, the amount of grafted copolymer had to be optimized to effectively block the pore entrances of the nanoparticles to avoid any possible premature release. To evaluate that, the already functionalized nanoparticles with different amounts of polymer, hybrid-MSNs from now on, were loaded with fluorescein at 4 °C (extended polymer conformation and open pore entrances) and then temperature was increased up to 37 °C, so the polymer collapsed closing the pore entrances with the dye molecules adsorbed into the mesopores. Then the percentage of dye released in PBS at 37 °C in all the evaluated compositions (Table S2) was measured with a fluorimeter after 24 h of incubation. When the sililated polymer was added in one step to the nanoparticles suspension in a 4:1 ratio (polymer:nanoparticles), the maximum amount of organic matter present in the inorganic nanocarriers measured by thermogravimetric analysis was *ca.* 21%. However, the amount of fluorescein released after 24 h at 37 °C was *ca.* 56%, which means that half of the cargo was being prematurely released without any triggering event, so the copolymer chains were not perfectly closing the gates of the pores. Although increasing the polymer amount might seem as the straightforward solution for properly blocking the pore entrances, we found that 6:1 ratio resulted into even lower functionalization efficiency (*ca.* 15% of organic matter). We hypothesized that high concentration of sililated polymers into the reaction environment could lead to self-condensation rather than condensation with the nanoparticles surface. Consequently, we tested the same ratio, 6:1, but adding the sililated polymer in 3 steps rather than in 1 step, so the polymer concentration was kept low at all times and, therefore, avoiding self-condensation. That approach produced good enough results with *ca.* 30% of organic matter and only 26% of fluorescein released at 37 °C after 24 h.

The successful grafting of copolymer to mesoporous silica nanoparticles to form hybrid-MSNs was confirmed by different characterization techniques (see details in Supporting Information, Figure S3). In this sense, the presence of the typical vibrations bands of silica (between 490 and 1090 cm^{-1}) together with those bands from the polymer (between 1400 and 1800 cm^{-1}) in the FTIR spectra confirmed the functionalization process (Figure S3a). The low-angle XRD pattern of MSNs shows the characteristic ordered MCM-41 type mesostructured with 2D hexagonal (p6m) symmetry (Figure S3b). Similar maxima were observed in hybrid-MSNs, which means that the ordered mesostructured of the particles survived the functionalization process. MSNs showed the characteristic zeta potential of −21 mV at pH = 7, which was shifted to −31.6 mV after copolymer grafting. Thermogravimetry experiments also confirmed the presence of organic matter in hybrid-MSNs, as expected (Figure S3c). Nitrogen adsorption experiments confirmed the size of the mesopores (*ca.* 2.5 nm) and also confirmed the successful grafting of the polymer chains thanks to the reduction of the surface area, from 935 m^2/g in MSNs to 171 m^2/g in hybrid-MSNs (Figure S3d). These data suggest that the external surface of the particles was

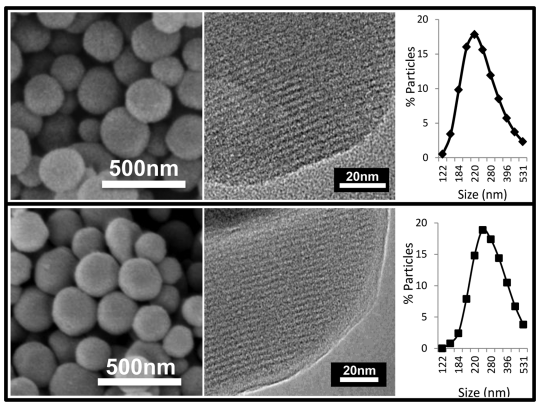

Figure 2. From left to right: SEM images, TEM micrographs and size distribution (measured by DLS) of MSNs (top) and hybrid-MSNs (bottom).

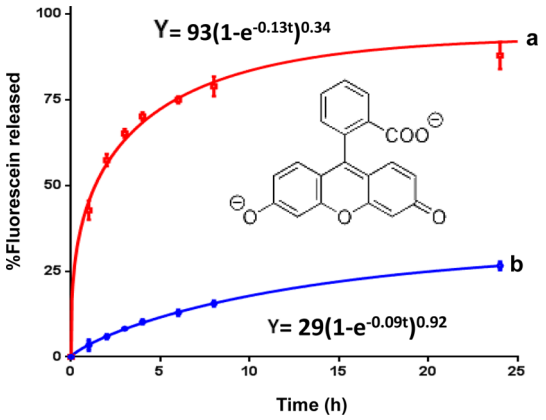

Figure 3. Release profiles of fluorescein from hybrid-MSNs in PBS solution *versus* time with US exposure (10 min and 1.3 MHz, 100 W) (a) and without US (b).

TABLE 1. Main Features Corresponding to MSNs and Hybrid-MSNs

sample	MSNs	hybrid-MSNs
Z potential	−21.1 mV	−31.6 mV
BET surface area	935 m^2/g	171 m^2/g
size mean (DLS)	220 nm	252 nm
organic matter (TGA)	5.1%	30.5%

covered with the copolymer blocking the mesopores entrances.

The morphology and size of MSNs and hybrid-MSNs are very similar, as can be seen in Figure 2. The spherical morphology of MSNs remained after the functionalization process as it can be observed in the SEM micrographs. The mean size was determined by dynamic light scattering (DLS), and found to be 220 nm (MSNs) and 252 nm (hybrid-MSNs). In both cases, well-ordered mesoporous silica particles can be appreciated in the corresponding TEM micrographs. Table 1 resumes some of the most important nanoparticle characteristics before and after functionalization with the US-sensitive copolymer.

Finally and since these nanoparticles will be used in a biological application, their degradation in PBS solution over time was evaluated (Figure S4). After 8 days under physiological conditions, the mesostructure and morphology of the hybrid-MSNs remained almost unaffected, while MSNs started to degrade after 5 days of experiment. In this sense, hybrid-MSNs showed slower degradation rate than naked MSNs. This observation is in agreement with other results reported in the literature.[31]

***In Vial* Cargo Release Experiments.** As mentioned above, one of the great advantages of thermoresponsive systems like the one here proposed relays on the loading process. Conventionally, functionalized MSNs must adsorb the cargo into the mesopores simultaneously to the grafting process, which leads to poor loading and functionalization yields and efficiency. However, our system allows opening the nanogates at 4 °C after the functionalization process has been completed, loading the cargo, and then, closing the pore entrances just increasing the temperature to 37 °C.

Fluorescein was used as a model molecule to evaluate the ultrasound-responsiveness of the copolymer-grafted MSNs. Hybrid-MSNs were dispersed into a solution of 20 mg/mL of fluorescein dissolved in PBS at 4 °C for 24 h. This temperature is lower than the LCST1, so the copolymer p(MEO_2MA-*co*-THPMA) shows a hydrophilic behavior with a coil-like conformation, which allows fluorescein molecules to be introduced into the pores of the nanocarrier. After this time, the bath temperature was increased at 37 °C (temperature higher than the LCST1), so the copolymer shows a hydrophobic behavior with a collapsed state, which blockes the outlets of the pores and impedes the release of fluorescein (see details in Materials and Methods section). The successful loading of cargo molecules inside the mesopores of the hybrid-MSNs was verified by the decrease in pore volume by Nitrogen adsorption porosimetry (data not shown).

Figure 3 shows the release profiles of US irradiated hybrid-MSNs and nonirradiated nanoparticles (control), in which a great difference on cargo release can be observed. At 37 °C (T > LCST1) the copolymer chains are collapsed, blocking the entrances of pores. As it has been showed above (Figure 1b), the application of ultrasounds induces the hydrolysis of THPMA groups present in the copolymer resulting onto hydrophilic methacrylic acid, MAA groups. This polarity change provokes the opening of the gates of the mesoporous channels resulting in a release of fluorescein to the medium. These data confirm that these hybrid-MSNs proposed can act as an effective system for US stimuli-responsive drug delivery.

Fluorescein release data showed in Figure 3 can be fitted to a first-order kinetic model with an empirical nonideality factor (δ) (eq 1).[32]

$$Y = A(1 - e^{-kt})^{\delta} \quad (1)$$

being Y the percentage of fluorescein released at time t, A the maximum amount of fluorescein released (in percentage), and k, the release rate constant. The values for δ are comprised between 1 for materials that follow first-order kinetics, and 0, for materials that release the loaded drug in the very initial time of analysis. The parameters of the kinetic fitting, shown in Figure 3 and Table S2, indicate that, while the maximum amount of fluorescein released is practically the totality of the loaded dye after US application, most of the cargo is retained without the stimulus. Also, the value of δ is much lower for the kinetic fitting of cargo release after ultrasound exposure (0.34 *vs* 0.92) which is indicative of a burst release of fluorescein at very short times after the stimulus is applied. That is, the system shows a fast response to the external stimulus, promptly releasing its cargo.

To ensure that the cargo release after US exposure is due to the mechanism above proposed and not merely because some mechanical/thermal effects caused by the US waves, similar release experiments were carried out with MSNs functionalized only with the temperature responsive polymer (MEO_2MA). Theoretically, that polymer should not be sensitive to US, so if there is any cargo release that should had to be caused by some mechanical or thermal effects from the US radiation. Certainly, most of the cargo in the MEO_2MA-MSNs was retained after US radiation, since similar release patterns are observed with and without US stimulus (Figure S5), which validates the release mechanism above proposed. Additionally, when those studies were carried out with MSNs with no polymeric nanogates (Figure S5), the release patterns were very similar to those of US-irradiated hybrid-MSNs (Figure 3), which confirms that the latter is behaving with totally opened gates.

When developing stimuli-responsive nanocarriers, it is very important that they could efficiently respond to the stimuli independently of the type of cargo molecules transported. The versatility of our nanocarrier system was evaluated using a fluorescent ruthenium complex $[Ru(bipy)_3]^{2+}$, which was loaded and released from the p(MEO_2MA-*co*-THPMA)-grafted MSNs. Figure 4 shows the release patterns with and without US irradiation, which are in total agreement with those obtained with fluorescein; a good response of the material to the external stimuli, with higher amount of dye released upon US exposure compared to the amount released without stimulus. However, a tiny difference might be found in both release patterns, with a slightly slower release in the case of ruthenium complex. The negatively charged surface of the silica walls might interact with the positively charged complex, slowing down the release. This would be in agreement with the smaller burst effect estimated in the δ value, close to 1, in the kinetic fitting of ruthenium complex release, which means that the pore wall-cargo

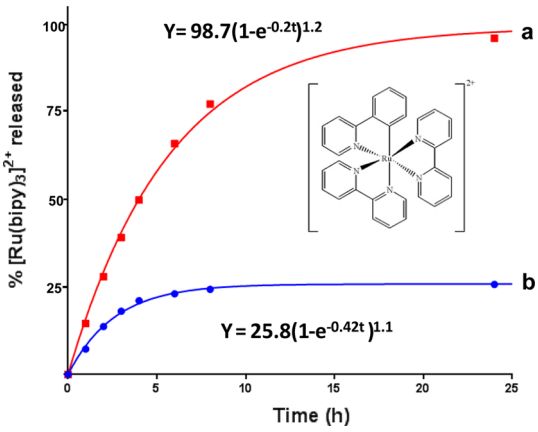

Figure 4. Release profiles of $[Ru(bipy)_3]^{2+}$ from hybrid-MSNs in PBS solution *versus* time with US exposure (10 min and 1.3 MHz, 100 W) (a) and without US (b).

molecule interaction is slowing down the release kinetics. However, the difference between the release from the control (no US) and the US-irradiated nanoparticles is still very significative (Figure 4), which confirms that our versatile responsive system can work efficiently independently of the type of cargo transported.

***In Vitro* Biological Evaluation.** Finally, to evaluate the biological compatibility of our hybrid-MSNs system, nanoparticles were incubated with tumor cells (LNCaP cells, from human prostate adenocarcinoma) for 2 h. The media were changed with fresh media and the cells were incubated overnight before measuring cell viability. In order to check that byproducts from US exposure (like THP-ol) were not cytotoxic either, hybrid-MSNs that had been exposed to 10 min US irradiation (1.3 MHz and 100 W) were also cultured with LNCaP cells under the same conditions. The hybrid-MSNs (with or without exposure to ultrasound) induced no toxicity at least up to 500 μg/mL in LNCaP cells as measured by MTS reduction assay (Figure 5).

Regarding the future application in living organisms of our hybrid system, a different US set up was investigated. In this sense, *in vitro* experiments were performed using a commercial US apparatus frequently used for physical therapy in humans, working at 1 MHz and 15 W. First, we checked the displacement of the LCST of the p(MEO_2MA-*co*-THPMA) after 5 min US irradiation using this equipment (Figure S6a). Also, we proved that under these US conditions no damage was produced in relevant biological molecules. Using catalase as a protein model, we did not find any change in the enzymatic activity after US application under the same conditions (catalase enzymatic activity was determined as described elsewhere[12]) (Figure S6b). After this test, the release of a cargo after internalization of the hybrid-MSNs in cells was studied. Rhodamine B-labeled MSNs with fluorescein loaded into their mesopores were incubated with the same LNCaP tumor cells and fluorescence microscopy was performed to

check the localization of green and red fluorescence (Figure 6). Before ultrasound exposure, green (from fluorescein loaded) and red (from rhodamine labeled) fluorescence match perfectly, which confirms that fluorescein is entrapped inside the polymer-grafted MSNs thanks to the closed polymer nanogates. Also, the perinuclear location of the nanoparticles seems to indicate that the hybrid-MSNs have been uptaken by the cells. After 5 min US irradiation of the cells with the equipment used in physical therapy, a significant part of fluorescein diffuses out of the material and stains the cell cytoplasm (fluorescence microscopy images taken 30 min after the US exposure was perfomed). Unequivocally, the green cytoplasm means that the nanogates of the pores were opened as a consequence of the US waves releasing the fluorescein loaded into the mesopores of the nanoparticles. This proves that our material retains its ultrasound-responsive capability even after being internalized in LNCaP cells.

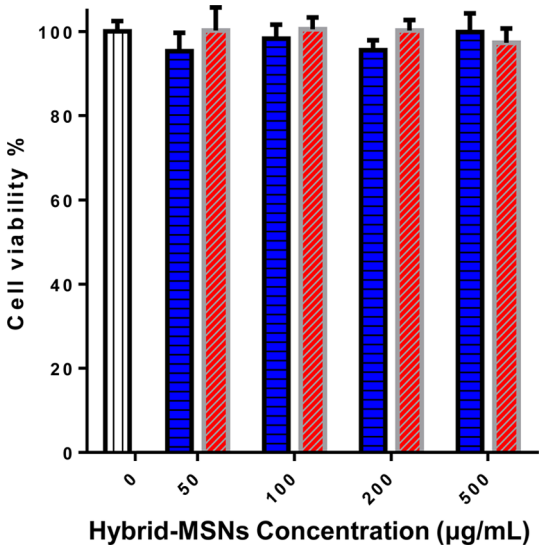

Figure 5. Cytotoxicity assay measured by MTS reduction in LNCaP cells with different concentrations of hybrid-MSNs (blue) without US exposure and (red) with US exposure (10 min and 1.3 MHz, 100 W).

Finally, to test the feasibility to use this material for future anticancer therapy, doxorubicin-loaded hybrid-MSNs were also cultured with LNCap cells under the same conditions as those used for the cytotoxicity study with unloaded-hybrid-MSNs (Figure 7). The results show that, while no toxicity was observed with nanoparticles not exposed to US, significant decrease in cell viability was observed at the three concentrations tested (10, 50, and 100 μg/mL) when the nanoparticles had been exposed to US (Figure 7a). Moreover, fluorescence microscopy images show that doxorubicin fluorescence was localized in the perinuclear region in the samples without stimulus (Figure 7b). On the other hand, doxorubicin fluorescence stained the cytoplasm of the cells with US stimulus (Figure 7c), indicating that the drug is being released from the nanoparticles only in that case.

CONCLUSIONS

In this work, we have successfully designed and prepared a new stimuli-responsive system that uses mesoporous silica nanoparticles as carriers and polymers as nanogates sensitive to ultrasounds. The combination of the advantageous structural properties of mesoporous silica particles with an ultrasound-responsive gatekeeper provides an efficient strategy for the preparation of stable and safe drug delivery system. US responsive copolymer with a LCST below 37 °C was successfully grafted to the surface of mesoporous silica nanoparticles to close the pore entrance avoiding premature release of the loaded cargo. Upon US irradiation, the hydrophobic tetrahydropyranyl groups in the polymer backbone were cleaved leading to hydrophilic methacrylate and increasing the LCST over 37 °C. Consequently, the copolymer changed its phase state at physiological temperature and the

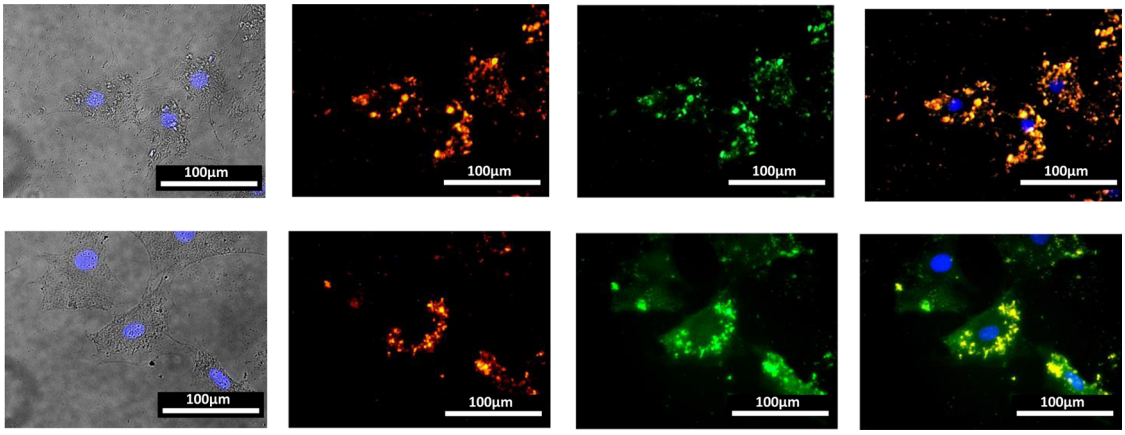

Figure 6. Fluorescence microscopy images of LNCaP cells incubated with Rhodamine B-labeled hybrid-MSNs with fluorescein loaded before (top) and after (bottom) ultrasound irradiation. From left to right: Blue fluorescence (nuclei) and transmission images, red fluorescence (Hybrid-MSNs), green fluorescence (fluorescein cargo), overlay images of the three fluorescence channels (fluorescence microscopy images taken 30 min after the US exposure was perfomed).

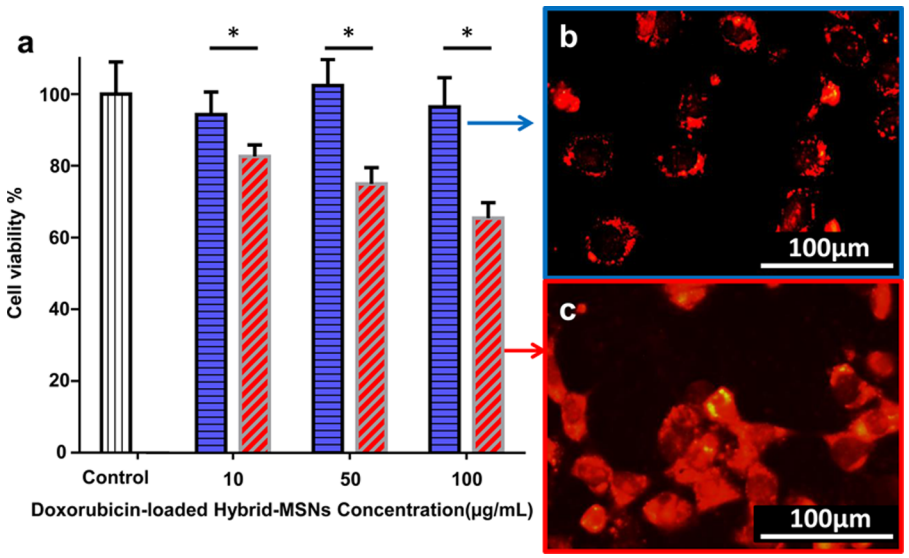

Figure 7. (a) Cytotoxicity assay measured by MTS reduction in LNCaP cells with different concentrations of doxorubicin-loaded hybrid-MSNs (blue) without US exposure and (red) with US exposure (10 min and 1.3 MHz, 100 W). (b) Fluorescence microscopy images of LNCaP cells incubated with doxorubicin-loaded hybrid-MSNs (showing doxorubicin fluorescence) without US and (c) with US irradiation. (Fluorescence microscopy images taken 24 h after the US exposure and nanoparticle incubation). *$p < 0.05$ (Student's *t*-test).

loaded molecules were released from the nanocarriers upon US irradiation. These hybrid nanoparticles are not cytotoxic and can also be endocyted by LNCaP cells retaining their ultrasound-responsible capability because they can release the cargo inside the cells upon US irradiation. Moreover, when loaded with doxorubicin, the hybrid-mesoporous silica nanoparticles only induced cell death when they had been exposed to ultrasound.

MATERIALS AND METHODS

Materials. Following compounds were purchased from Sigma-Aldrich Inc.: Aminopropyltriethoxysilane (APTES), ammonium nitrate, cetyltrimethylammonium bromide (CTAB), tetraethyl orthosilicate (TEOS), rhodamine B isothiocyanate (RBITC), methacrylic acid (MAA), pyridine, *p*-toluenesulfonic acid, toluene, dichloromethane (DCM), dihydropyran, dimethylformamide (DMF), 2-(2-methoxyethoxy) ethyl methacrylate (MEO_2MA), 4,4′-Azobis(4-cyanovaleric acid) (ABCVA), diethyl ether, *N*,*N*′-dicyclohexylcarbodiimide (DCC), *N*-hydroxysuccinimide (NHS), catalase, phosphate-buffered solution (PBS), fluorescein sodium salt and $[Ru(bipy)_3]Cl_2$. These compounds were used without further purification.

Characterization Techniques. The materials were analyzed by X-ray diffraction (XRD) in a Philips X-Pert MPD diffractometer equipped with Cu Kα radiation. Thermogravimetry and differential temperature analyses (TGA/DTA) were performed in a PerkinElmer Pyris Diamond TG/DTA analyzer, with 5 °C/min heating ramps, from room temperature to 600 °C. Fourier transform infrared (FTIR) spectra were obtained in a Nicolet (Thermo Fisher Scientific) Nexus spectrometer equipped with a Smart Golden Gate ATR accessory. Surface morphology was analyzed by scanning electron microscopy (SEM) in a JEOL 6400 Electron microscope. Transmission electron microscopy (TEM) was carried out with a JEOL JEM 2100 instrument operated at 200 kV, equipped with a CCD camera (KeenView Camera). N_2 adsorption was carried out on a Micromeritics ASAP 2010 instrument; surface area was obtained by applying the BET method to the isotherm and the pore size distribution was determined by the BJH method from the desorption branch of the isotherm. The mesopore diameter was determined from the maximum of the pore size distribution curve. The zeta potential and hydrodynamic size of nanoparticles were measured by means of a Zetasizer Nano ZS (Malvern Instruments) equipped with a 633 nm "red" laser. ^{1}H NMR experiments were carried out in a Bruker AV 250 MHz apparatus. To determine the molecular weight distribution of the copolymers, Gel permeation chromatography (GPC) was performed in a Waters Alliance automatic analysis system with a Model #2695 separations module coupled to a Model #2414 Refractive Index Detector. GPC measurements were carried out using polyethylene (Glycol/Oxide) standards and DMF with LiCl 10 mM as the eluent. Fluorescence spectrometry was used to determine cargo release by means of a Biotek Synergy 4 device. Fluorescence microscopy was performed with an Evos FL Cell Imaging System equipped with tree Led Lights Cubes (IEX (nm); IEM (nm)): DAPY (357/44; 447/60), GFP (470/22; 525/50), RFP (531/40; 593/40) from AMG (Advance Microscopy Group).

Synthesis of Mesoporous Silica Nanoparticles (MSNs). Mesoporous silica nanoparticles, MSNs, were synthesized by the modified Stöber method from TEOS in the presence of CTAB, as structure-directing agent: 1 g of CTAB, 480 mL of H_2O (Milli-Q) and 3.5 mL of NaOH (2 M) were added to a 1000 mL round-bottom flask. The mixture was heated to 80 °C and stirred at 600 rpm. Then, 5 mL of TEOS were added dropwise at 0.25 mL/min rate with a pump. The white suspension obtained was magnetically stirred for further 2h at 80 °C. Then, the reaction mixture was centrifuged and washed with water and ethanol. Finally, the surfactant was removed by ionic exchange using a solution of amonium nitrate (10 mg/mL) in ethanol (95%) at 70 °C overnight under magnetic stirring. The nanoparticles were collected by centrifugation, washed with ethanol three times and dried under a vacuum overnight.

Rhodamine B-labeled nanoparticles were synthesized by reacting 1 mg of Rhodamine-B isothiocyanate with 2.2 μL APTES in 100 μL ethanol for 2h. Then the reaction mixture was added with the 5 mL of TEOS as previously described.

Synthesis and Characterization of Ultrasound-Responsive Monomer, Tetrahydropyranyl Methacrylate (THPMA). THPMA was synthesized following a previously described method.[33] Briefly, methacrylic acid (8 g), pyridine (0.3 mL), and *p*-toluenesulfonic acid (0.7 g)

were dissolved in 80 mL of dichloromethane (Figure S7a). Dihydropyran (0.162 mol) was slowly added at room temperature. After stirring overnight, the solution was filtered by a short silica column. The solution was extracted by water and brine three times. Finally, the solvent was removed under a vacuum to yield THPMA. The obtained product was characterized by ^{1}H NMR (Figure S7b).

Synthesis and Characterization of the Temperature and Ultrasound-Responsive Copolymer p(MEO$_2$MA-*co*-THPMA). The copolymer, poly-(2-(2methoxyethoxy)ethyl methacrylate-*co*-2-tetrahydropyranyl methacrylate), p(MEO$_2$MA-*co*-THPMA), was synthesized by free radical polymerization from MEO$_2$MA (temperature-responsive monomer) and THPMA (ultrasound-responsive monomer) (Figure S8a). Briefly, MEO$_2$MA and THPMA at different molar ratios (0.01 mol in total) were placed in a seal vial and purged with nitrogen. Sixteen mL of DMF were added under inert atmosphere and the solution was placed at 80 °C under magnetic stirring. 1 mL of DMF with 0.003 mmol of initiator (ABCVA) was added. The reaction was carried out overnight. Then, the polymer was precipitated in cold diethyl ether, separated by centrifugation and washed 3 times with diethyl ether followed by evaporation of the solvent. The polymer was characterized by ^{1}H NMR (Figure S8b), FTIR spectroscopy (Figure S3) and GPC. The obtained copolymer has a number-average molecular weight, determined by GPC, of 27094 Da with a polydispersity of 1.83.

In order to check the changes in the polymer structure after US exposure, the aqueous solutions of the polymers after the application of the stimulus were freeze-dried. Then, the polymers were washed with diethyl ether and, after the evaporation of the ether, they were dissolved in $CDCl_3$ and ^{1}H NMR spectra were acquired.

Preparation of Polymer Grafted MSN Nanoparticles. 0.3 g of carboxylic acid-terminated poly(MEO$_2$MA-*co*-THPMA), 11 mg of DCC and 6 mg of NHS were added to a glass vial. The vial was purged with nitrogen and 2 mL of DMF were added. Then, under N_2 atmosphere and with magnetic stirring, DMF (1 mL) with 8 μL of APTES were added. The solution was stirred overnight (Solution 1, sililated copolymer solution). Then, 1 mL of Solution 1 was added dropwise to 20 mL of toluene containing 50 mg of MSNs under vigorous stirring. The reaction medium was heated under reflux. After 4 h, another mL of Solution 1 was added. Four h later, the remaining Solution 1 was added. The reaction was left under vigorous stirring for 24 h. Then, the hybrid MSNs were collected by centrifugation and washed with toluene, DMF (twice), cold water (twice) and ethanol. Afterward, the nanoparticles were dried under a vacuum for 16 h (Scheme 2).

Determination of Phase Transition Temperatures (LCST). The LCST was determined by Dynamic Light Scattering (DLS) by means of the drastic change in the scattering intensity obtained by the precipitation of the polymer at the LCST (determined as the temperature at which the scattering intensity is 50% of the maximum). Measurement of the LCST was performed using a Zetasizer Nano ZS (Malvern Instruments) equipped with a 633 nm "red" laser. To determine the transition temperature, the temperature dependence of the scattering intensity at 90° from 1 mL of solution in a glass cuvette was measured. The temperature was increased by discrete temperature increments in the range 10−45 °C, and the readings were taken after 2 min equilibration at each temperature.

Nanoparticles Degradation Studies. In order to study nanoparticle degradation in PBS, several aliquots of 1 mg of MSNs or hybrid-MSNs were dispersed in 1 mL of PBS each (10 mM pH = 7.4) in Eppendorf tubes. Every 24 h, the nanoparticles were centrifuged and redispersed in fresh PBS. At 5, 8, and 12 days, some of the samples were washed with deionized water and observed by transmission electron microscopy.

Cargo Loading and Release. *Cargo Loading.* Twenty mg of nanoparticles were placed in a glass vial with a septum and dried at 80 °C under a vacuum for 24 h. Then, the vial was placed at 4 °C with magnetic stirring and 5 mL of cargo solution (20 mg/mL, fluorescein or Ru(bipy)$_3^{2+}$ in PBS) were added and the suspension was stirred at 4 °C for 24 h. After that time, the sample was filtered and washed two times with previously hot PBS (50 °C) in order to remove the cargo absorbed on the external surface. Finally, the products were dried under a vacuum at 25 °C.

Cargo Release. Nine mg of cargo-loaded nanoparticles were suspended in 1.8 mL of fresh PBS pH 7.4 (10 mM). Then, 0.5 mL of nanoparticles suspension were placed on a Transwell permeable support with 0.4 μm of polycarbonate membrane (3 replicas were performed). The well was filled with 1.5 mL of PBS pH 7.4 (10 mM) and the suspension was stirred at 37 °C and 100 rpm during all the experiment. To study the US responsiveness of the cargo-loaded nanoparticles, the particles suspension was subjected to US exposure (10 min at 1.3 MHz and 100 W) before to place the 0.5 mL on a Transwell. At every time point studied, the solution outside the transwell insert was replaced with fresh medium and the amount of cargo released was determined by fluorescence spectrometry (Fluorescein: λexc 490, λem 514 nm; Ru(bipy)$_3^{2+}$: λexc 454, λem 593 nm).

Cytotoxicity Assays and Intracelular Fluorescein Release. LNCaP cells were plated 24 h before the start of the experiment in 12 well plates at a density of 10^4 cells per cm^2. The cytotoxicity of hybrid-MSNs was evaluated using the standard MTS assay protocol using a commercial assay and following the manufacturer protocol (CellTiter Aqueous One Solution Cell Proliferation Assay). Briefly, LNCaP cells were incubated with various concentrations of hybrid-MSNs for 2 h (n = 3). To study the toxicity induced by US-exposed hybrid-MSNs, the nanoparticles were exposed to ultrasound as described for the *in vial* cargo released studies before incubating them with the cells. The cells were then cultured for another 24 h. The medium was then replaced with 600 μL culture medium including MTS, and the incubation proceeded for 3 h. The medium was then removed, and its absorption at 490 nm was measured using a microplate reader. The same procedure was used to determine the cytotoxicity of doxorubicin-loaded MSNs. In this case, before measuring cell viability, the culture media was replaced with fresh media and fluorescence microscopy images were taken to determine the location of doxorubicin in the cells.

For the *in vitro* intracellular release experiments, rhodamine B-labeled hybrid-MSNs with fluorescein loaded were used. LNCaP cells were incubated with the nanoparticles for 2h in serum-free culture medium. Then, the medium was withdrawn and cells were washed with PBS three times. Cells were fixed with isopropanol for 2 min and stained with DAPI. Fluorescence microscopy images were taken to evaluate cargo localization before and after US exposure (5 min at 1 MHz and 15 W). Red channel was used to locate nanoparticles, green for cargo and blue for cell nucleus.

Ultrasonic Experiments. All the US experiments, except those related with the intracellular release studies, were performed in a commercial ultrasound apparatus, which generates an ultrasound beam of adjustable power (up to 100 W) at a frequency of 1.3 MHz. In the experiments, a power of 100 W was used. The tube reactor, a cylindrical glass vial (4.5 × 1 cm) with a latex cover, containing 1.5 mL of the polymer solution (5 mg/mL) or 1.8 mL of nanoparticles suspension (5 mg/mL) was immersed in a water tank (Figure S9a). The tube was positioned at the center of the ultrasound beam and at 3 cm of the acoustic lens transducer. The US beam can penetrate through the latex cover and act on the solution placed in the tube reactor. After the ultrasound irradiation, the tube reactor was removed from the tank and used.

In order to study if the US beam can penetrate trough the cells ant acts over loaded nanoparticles releasing the cargo, *in vitro* intracellular cargo release experiments, a commercial ultrasound apparatus for application in physical therapy was used (Pagani Sonoquartz Evo). The parameters selected were 1 MHz, 15 W, continuous application, 5 min. Ultrasounds were applied from the top of a filled culture well through a latex membrane (ultrasound transmission gel was placed between the transducer and the latex membrane) (Figure S9b).

Conflict of Interest: The authors declare no competing financial interest.

Acknowledgment. Financial support from *Ministerio de Economía y Competitividad,* Spain (Project MAT2012-35556 and Project CSO2010-11384-E, Ageing Network of Excellence) and CIBER-BBN are gratefully acknowledged. CIBER-BBN is an

initiative funded by the VI National R&D&i Plan 2008-2011, *Iniciativa Ingenio* 2010, Consolider Program, CIBER Actions and financed by the *Instituto de Salud Carlos III* with assistance from the European Regional Development Fund. The XRD measurements and ^{1}H NMR spectra were performed at C.A.I *Difracción de Rayos X* and *Resonancia Magnética Nuclear*, UCM (Spain), respectively. SEM and TEM were performed at ICTS National Centre for Electron Microscopy (Spain). JL Paris gratefully acknowledges *Ministerio de Economía y Competitividad*, Spain, for his PhD grant (BES-2013-064182).

Supporting Information Available: The Supporting Information is available free of charge on the ACS Publications website at DOI: 10.1021/acsnano.5b04378.

Temperature responsive monomer:US responsive monomer (MEO_2MA:THPMA) ratios tested for the dual p(MEO_2MA-*co*-THPMA) synthesis (Table S1), experimental conditions for the copolymer grafting to silica nanoparticles (Table S2) and cargo release kinetic parameters (Table S3). LSCT and ^{1}H NMR spectra of the p(MEO_2MA) before and after US (Figure S1), ^{1}H NMR spectra of p(MEO_2MA-*co*-THPMA) with different treatments and LCST before and after heating at 80 °C for 30 min (Figure S2), XRD, FTIR TGA and Nitrogen adsorption/desorption corresponding to MSNs and hybrid-MSNs (Figure S3), TEM micrographs of MSNs and hybrid-MSNs suspended in PBS for different periods of time (Figure S4), release experiments corresponding to MSNs and p(MEO_2MA)-MSNs (Figure S5), LCST of p(MEO_2MA-*co*-THPMA) and Catalase enzymatic activity before and after US exposure with a US physical therapy apparatus (Figure S6), synthesis scheme and ^{1}H NMR characterization of ultrasound monomer (THPMA) (Figure S7) and copolymer poly(MEO_2MA-*co*-THPMA) (Figure S8), schematic representation of the two ultrasound systems used in this work (Figure S9). (PDF)

REFERENCES AND NOTES

1. Farokhzad, O. C.; Langer, R. Impact of Nanotechnology on Drug\nDelivery. *ACS Nano* **2009**, *3*, 16–20.
2. Steichen, S. D.; Caldorera-Moore, M.; Peppas, N. a. A Review of Current Nanoparticle and Targeting Moieties for the Delivery of Cancer Therapeutics. *Eur. J. Pharm. Sci.* **2013**, *48*, 416–427.
3. Bogart, L. K.; Pourroy, G.; Murphy, C. J.; Puntes, V.; Pellegrino, T.; Rosenblum, D.; Peer, D.; Lévy, R. Nanoparticles for Imaging, Sensing, and Therapeutic Intervention. *ACS Nano* **2014**, *8*, 3107–3122.
4. Manzano, M.; Vallet-Regí, M. New Developments in Ordered Mesoporous Materials for Drug Delivery. *J. Mater. Chem.* **2010**, *20*, 5593.
5. Vivero-Escoto, J. L.; Slowing, I. I.; Trewyn, B. G.; Lin, V. S.-Y. Mesoporous Silica Nanoparticles for Intracellular Controlled Drug Delivery. *Small* **2010**, *6*, 1952–1967.
6. Li, Z.; Barnes, J. C.; Bosoy, A.; Stoddart, J. F.; Zink, J. I. Mesoporous Silica Nanoparticles in Biomedical Applications. *Chem. Soc. Rev.* **2012**, *41*, 2590.
7. Baeza, A.; Colilla, M.; Vallet-Regí, M. Advances in Mesoporous Silica Nanoparticles for Targeted Stimuli-Responsive Drug Delivery. *Expert Opin. Drug Delivery* **2015**, *12*, 319–337.
8. Vallet-Regi, M.; Rámila, a.; Del Real, R. P.; Pérez-Pariente, J. A New Property of MCM-41: Drug Delivery System. *Chem. Mater.* **2001**, *13*, 308–311.
9. Tarn, D.; Ashley, C. E.; Xue, M.; Carnes, E. C.; Zink, J. I.; Brinker, C. J. Mesoporous Silica Nanoparticle Nanocarriers: Biofunctionality and Biocompatibility. *Acc. Chem. Res.* **2013**, *46*, 792–801.
10. Argyo, C.; Weiss, V.; Bräuchle, C.; Bein, T. Multifunctional Mesoporous Silica Nanoparticles as a Universal Platform for Drug Delivery. *Chem. Mater.* **2014**, *26*, 435–451.
11. Mura, S.; Nicolas, J.; Couvreur, P. Stimuli-Responsive Nanocarriers for Drug Delivery. *Nat. Mater.* **2013**, *12*, 991–1003.
12. Baeza, A.; Guisasola, E.; Ruiz-Hernández, E.; Vallet-Regí, M. Magnetically Triggered Multidrug Release by Hybrid Mesoporous Silica Nanoparticles. *Chem. Mater.* **2012**, *24*, 517–524.
13. Lai, J.; Mu, X.; Xu, Y.; Wu, X.; Wu, C.; Li, C.; Chen, J.; Zhao, Y. Light-Responsive Nanogated Ensemble Based on Polymer Grafted Mesoporous Silica Hybrid Nanoparticles. *Chem. Commun. (Cambridge, U. K.)* **2010**, *46*, 7370–7372.
14. Martínez-Carmona, M.; Baeza, A.; Rodriguez-Milla, M. A.; García-Castro, J.; Vallet-Regí, M. Mesoporous Silica Nanoparticles Grafted with a Light-Responsive Protein Shell for Highly Cytotoxic Antitumoral Therapy. *J. Mater. Chem. B* **2015**, *3*, 5746–5752.
15. Ruiz-Hernández, E.; Baeza, A.; Vallet-Regí, M. Smart Drug Delivery through DNA/magnetic Nanoparticle Gates. *ACS Nano* **2011**, *5*, 1259–1266.
16. Sirsi, S. R.; Borden, M. A. State-of-the-Art Materials for Ultrasound-Triggered Drug Delivery. *Adv. Drug Delivery Rev.* **2014**, *72*, 3–14.
17. Rapoport, N.; Nam, K. H.; Gupta, R.; Gao, Z.; Mohan, P.; Payne, A.; Todd, N.; Liu, X.; Kim, T.; Shea, J.; *et al.* Ultrasound-Mediated Tumor Imaging and Nanotherapy Using Drug Loaded, Block Copolymer Stabilized Perfluorocarbon Nanoemulsions. *J. Controlled Release* **2011**, *153*, 4–15.
18. Wood, A. K. W.; Sehgal, C. M. A Review of Low-Intensity Ultrasound for Cancer Therapy. *Ultrasound Med. Biol.* **2015**, *41*, 905–928.
19. Cintas, P.; Tagliapietra, S.; Caporaso, M.; Tabasso, S.; Cravotto, G. Ultrasonics Sonochemistry Enabling Technologies Built on a Sonochemical Platform: Challenges and Opportunities. *Ultrason. Sonochem.* **2015**, *25*, 8–16.
20. Wang, J.; Pelletier, M.; Zhang, H.; Xia, H.; Zhao, Y. High-Frequency Ultrasound-Responsive Block Copolymer Micelle. *Langmuir* **2009**, *25*, 13201–13205.
21. Brantley, J. N.; Wiggins, K. M.; Bielawski, C. W. Unclicking the Click: Mechanically Facilitated 1,3-Dipolar Cycloreversions. *Science* **2011**, *333*, 1606–1609.
22. Xuan, J.; Boissière, O.; Zhao, Y.; Yan, B.; Tremblay, L.; Lacelle, S.; Xia, H.; Zhao, Y. Ultrasound-Responsive Block Copolymer Micelles Based on a New Amplification Mechanism. *Langmuir* **2012**, *28*, 16463–16468.
23. You, Y. Z.; Kalebaila, K. K.; Brock, S. L.; Oupický, D. Temperature-Controlled Uptake and Release in PNIPAM-Modified Porous Silica Nanoparticles. *Chem. Mater.* **2008**, *20*, 3354–3359.
24. Chen, J.; Liu, M.; Chen, C.; Gong, H.; Gao, C. Synthesis and Characterization of Silica Nanoparticles with Well-Defined Thermoresponsive PNIPAM *via* a Combination of RAFT and Click Chemistry. *ACS Appl. Mater. Interfaces* **2011**, *3*, 3215–3223.
25. Liu, R.; Zhang, Y.; Zhao, X.; Agarwal, A.; Mueller, L. J.; Feng, P. pH-Responsive Nanogated Ensemble Based on Gold-Capped Mesoporous Silica through an Acid-Labile Acetal Linker. *J. Am. Chem. Soc.* **2010**, *132*, 1500–1501.
26. Lutz, J.-F. J.-F.; Hoth, A.; Schade, K. Design of Oligo-(ethylene {glycol)-Based} Thermoresponsive Polymers: An Optimization Study. *Des. Monomers Polym.* **2009**, *12*, 343–353.
27. Jung, J.; Lee, I.-H.; Lee, E.; Park, J.; Jon, S. pH-Sensitive Polymer Nanospheres for Use as a Potential Drug Delivery Vehicle. *Biomacromolecules* **2007**, *8*, 3401–3407.
28. Lutz, J. F. Polymerization of Oligo(ethylene Glycol) (meth)acrylates: Toward New Generations of Smart Biocompatible Materials. *J. Polym. Sci., Part A: Polym. Chem.* **2008**, *46*, 3459–3470.
29. Kim, H. J.; Matsuda, H.; Zhou, H.; Honma, I. Ultrasound-Triggered Smart Drug Release from a Poly(dimethylsiloxane)-Mesoporous Silica Composite. *Adv. Mater.* **2006**, *18*, 3083–3088.
30. Kwon, E. J.; Lee, T. G. Surface-Modified Mesoporous Silica with Ferrocene Derivatives and Its Ultrasound-Triggered Functionality. *Appl. Surf. Sci.* **2008**, *254*, 4732–4737.
31. Cauda, V.; Schlossbauer, A.; Bein, T. Bio-Degradation Study of Colloidal Mesoporous Silica Nanoparticles: Effect of Surface Functionalization with Organo-Silanes and Poly(ethylene Glycol). *Microporous Mesoporous Mater.* **2010**, *132*, 60–71.

32. Nieto, A.; Balas, F.; Colilla, M.; Manzano, M.; Vallet-Regí, M. Functionalization Degree of SBA-15 as Key Factor to Modulate Sodium Alendronate Dosage. *Microporous Mesoporous Mater.* **2008**, *116*, 4–13.
33. Lee, J.-T.; George, M. C.; Moore, J. S.; Braun, P. V. Multiphoton Writing of Three-Dimensional Fluidic Channels within a Porous Matrix. *J. Am. Chem. Soc.* **2009**, *131*, 11294–11295.

Supporting Information

Polymer-Grafted Mesoporous Silica Nanoparticles as Ultrasound-Responsive Drug Carriers

Juan L. Paris, M. Victoria Cabañas, Miguel Manzano, and María Vallet-Regí.

Table S1. Temperature responsive monomer: US responsive monomer (MEO_2MA:THPMA) ratios tested for the dual p(MEO_2MA-THPMA) synthesis.

MEO_2MA:THPMA theoretical	MEO_2MA:THPMA experimental	Comment
100:0	100:0	Not US-responsive
90:10	93.5:6.5	$LCST_2$<37ºC
87.5:12.5	**90.9:9.1**	**Suitable**
75:25	77.5:22.5	Not soluble in aqueous solution
50:50	60.2:39.8	Not soluble in aqueous solution

Table S2. Experimental conditions for the preparation of polymer grafted MSN nanoparticles

Reaction conditions	Polymer/NPs ratio	Organic matter %	BET Surface area (m^2/g)	% Fluorescein released at 24h at 37ºC
1 step addition	2:1	18.38	648.3	65.38
1 step addition	4:1	20.61	183.2	55.67
1 step addition	6:1	14.89	714.4	81.81
3 steps addition	**6:1**	**30.45**	**170.86**	**26.57**

Table S3. Kinetic parameters corresponding to the different cargos released from the hybrid-MSNs before and after US irradiation.

Cargo	Conditions	A (%)	K (h^{-1})	δ	R^2
Fluorescein	Without Ultrasound	29 ± 1	0.09 ± 0.02	0.92 ± 0.05	0.997
	With Ultrasound	93 ± 2	0.13 ± 0.03	0.34 ± 0.04	0.988
$[Ru(bipy)_3]^{2+}$	Without Ultrasound	25.8 ± 0.2	0.42 ± 0.03	1.10 ± 0.05	0.998
	With Ultrasound	98.7 ± 0.7	0.20 ± 0.01	1.2 ± 0.1	0.999

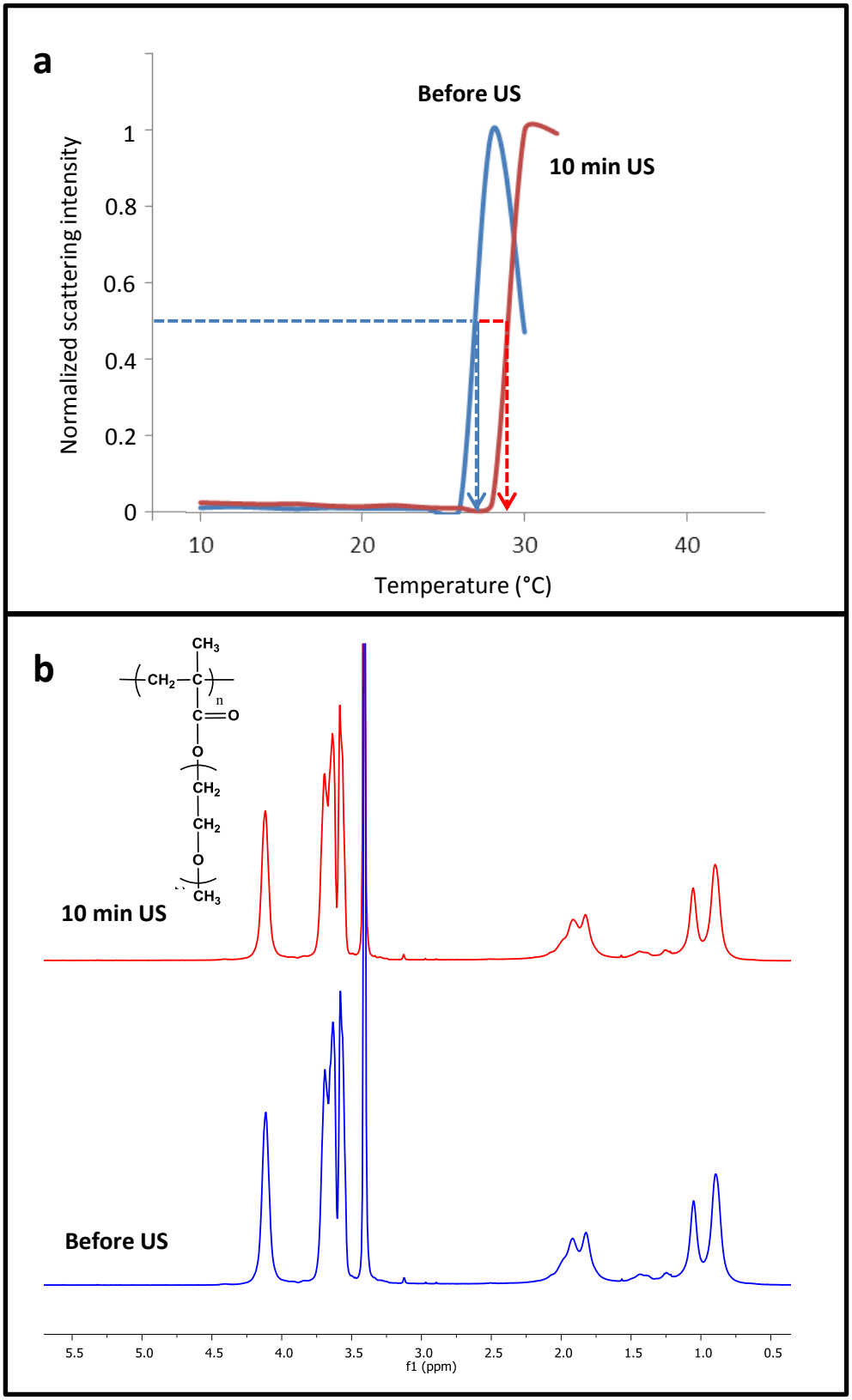

Figure S1. (a) Lower Critical Solution Temperature corresponding to p(MEO_2MA) before and after US exposure. (b) ^1H NMR spectra of p(MEO_2MA) before and after US exposure (in $CDCl_3$)

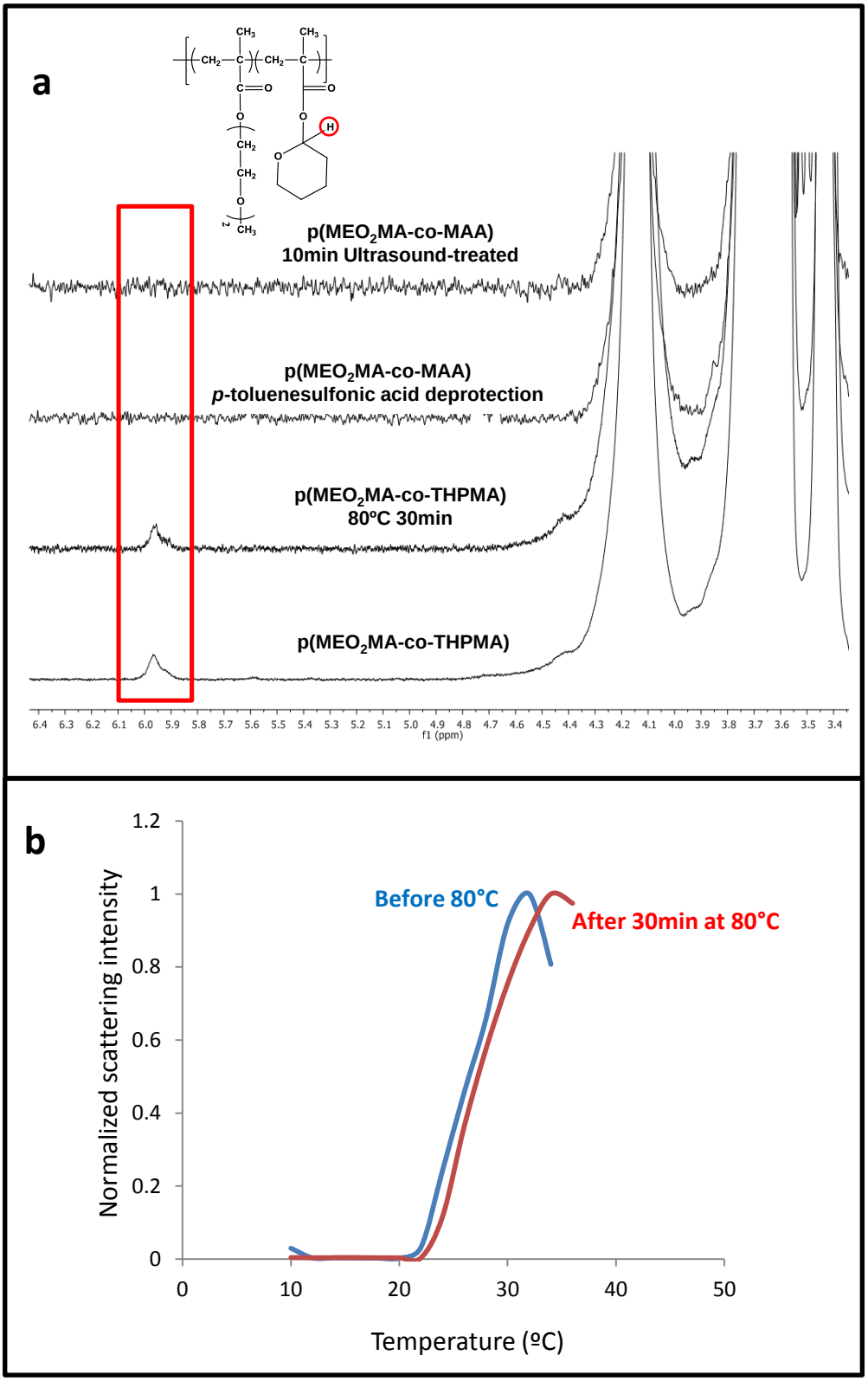

Figure S2. (a) ^{1}H NMR (in $CDCl_3$) spectra of p(MEO_2MA-co-THPMA) (from bottom to top) before and after several treatments: 80ºC 30 min; THP deprotection with *p*-toluensulfonic acid in methanol for 5 h; US-exposure for 10 min, 1.3 MHZ, 100 W, (b) LCST of p(MEO_2MA-co-THPMA) before and after treatment at 80ºC for 30 min (polymer in water at a concentration of 5 mg/mL).

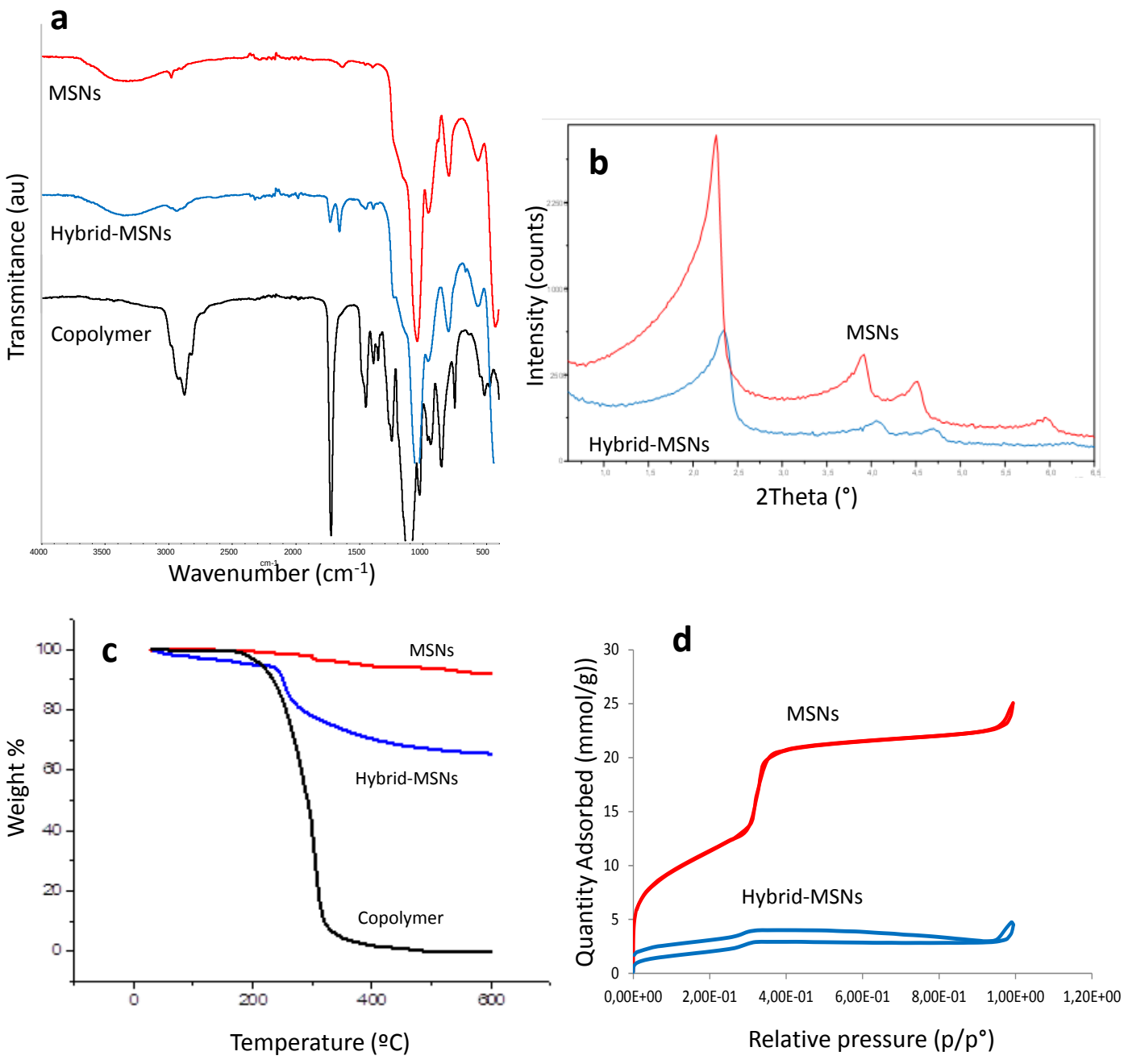

Figure S3. FTIR (a), XRD (b) TGA (c) and BET (d) corresponding to MSNs and hybrid-MSNs.

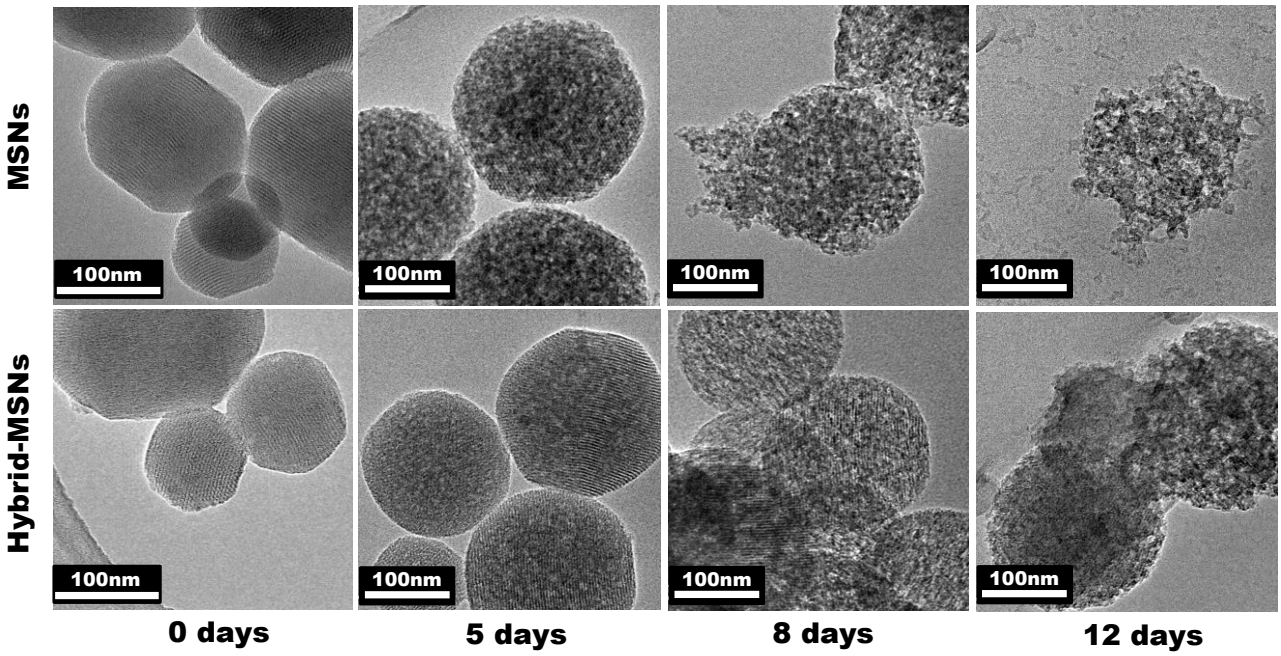

Figure S4. TEM micrographs of MSNs and hybrid-MSNs after dispersion in PBS for different periods of time.

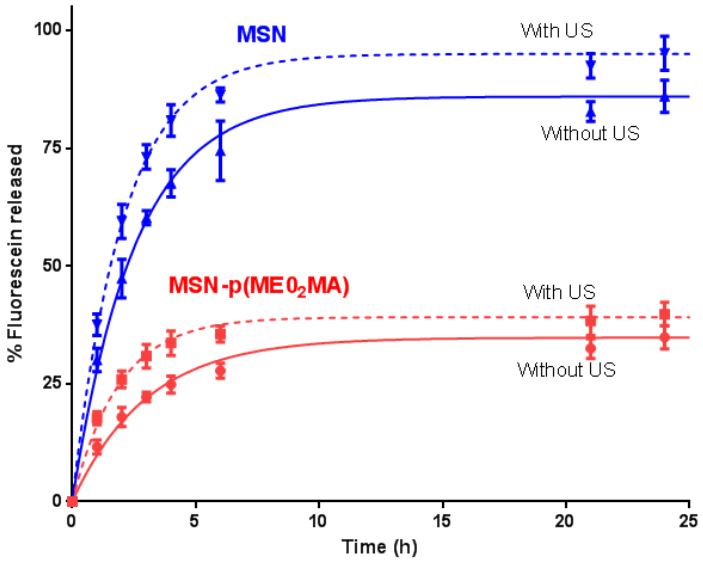

Figure S5. Release profiles of fluorescein from MSNs and p(MEO$_2$MA)-MSNs in PBS solution *versus* time with and without US exposure

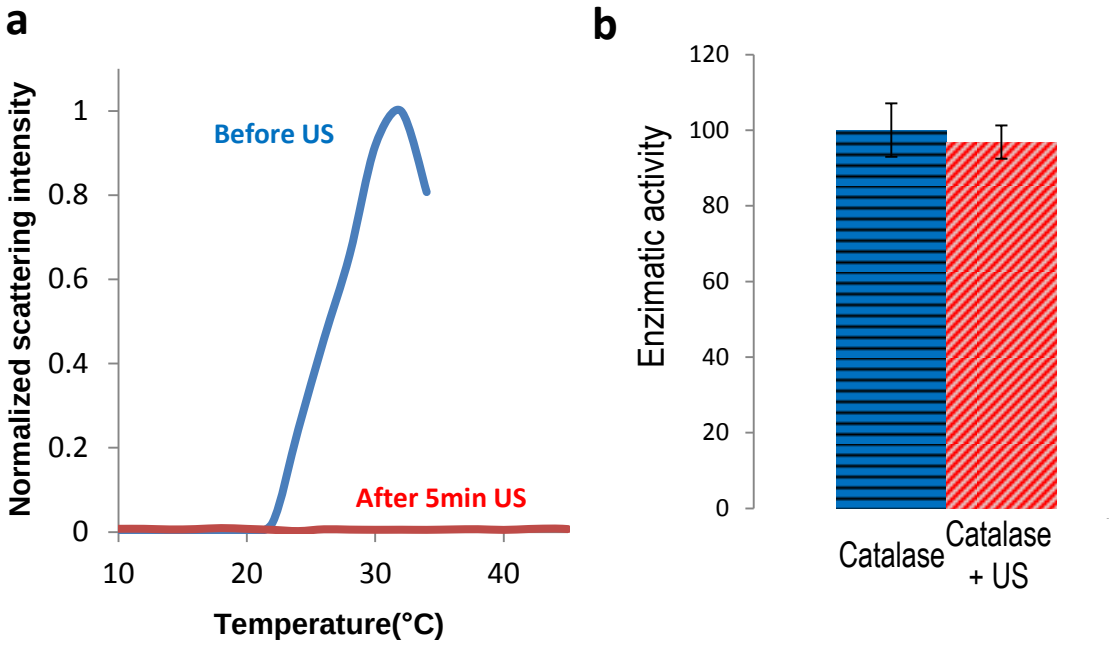

Figure S6. (a) LCST of p(MEO_2MA-co-THPMA) before and after US treatment (5 min, 1 MHz, 15 W), (b) Catalase enzimatic activity before and after US treatment (5 min, 1 MHz, 15 W).

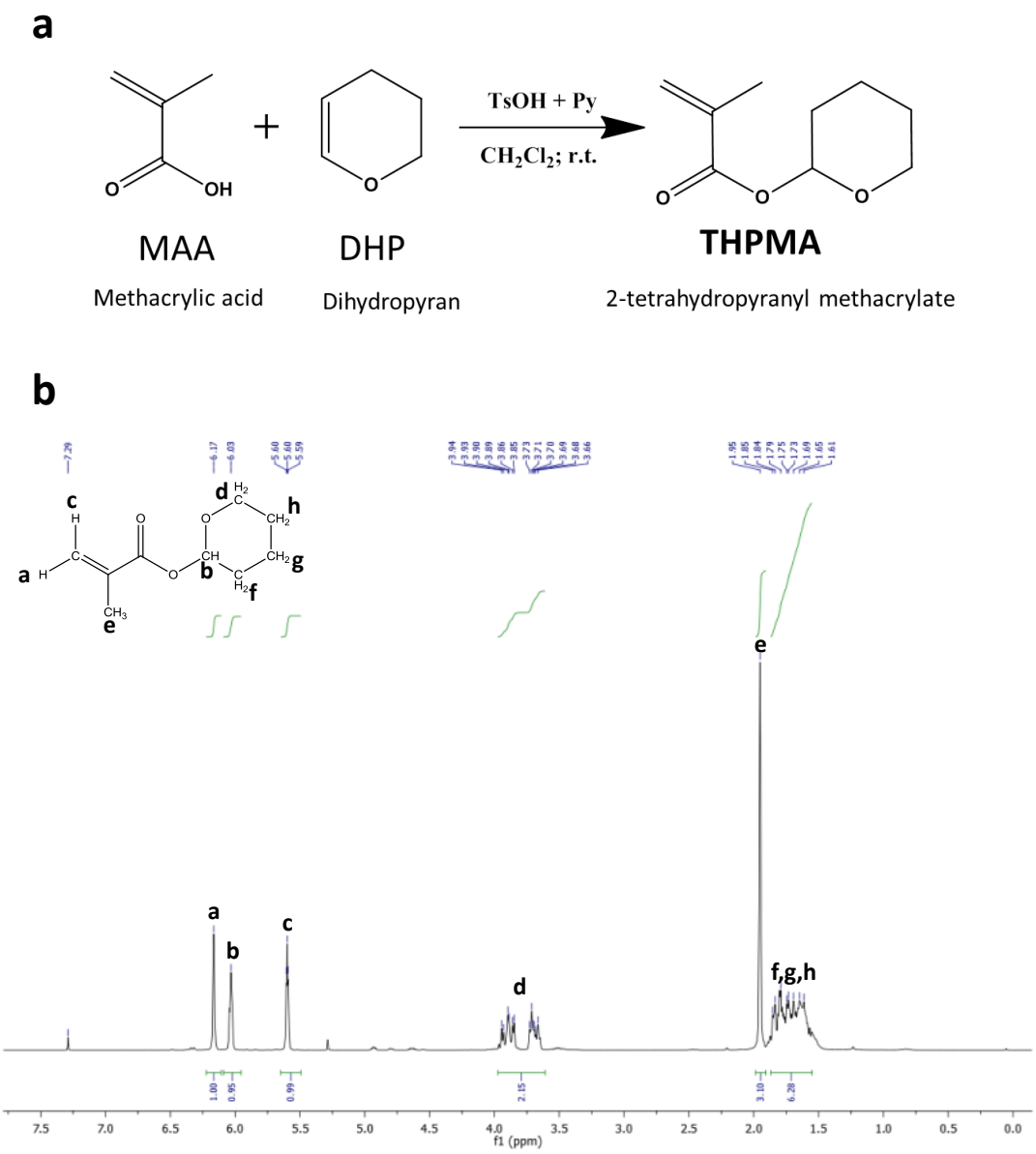

Figure S7. Synthesis scheme (a) and ^{1}H-NMR characterization of ultrasound monomer (THPMA)

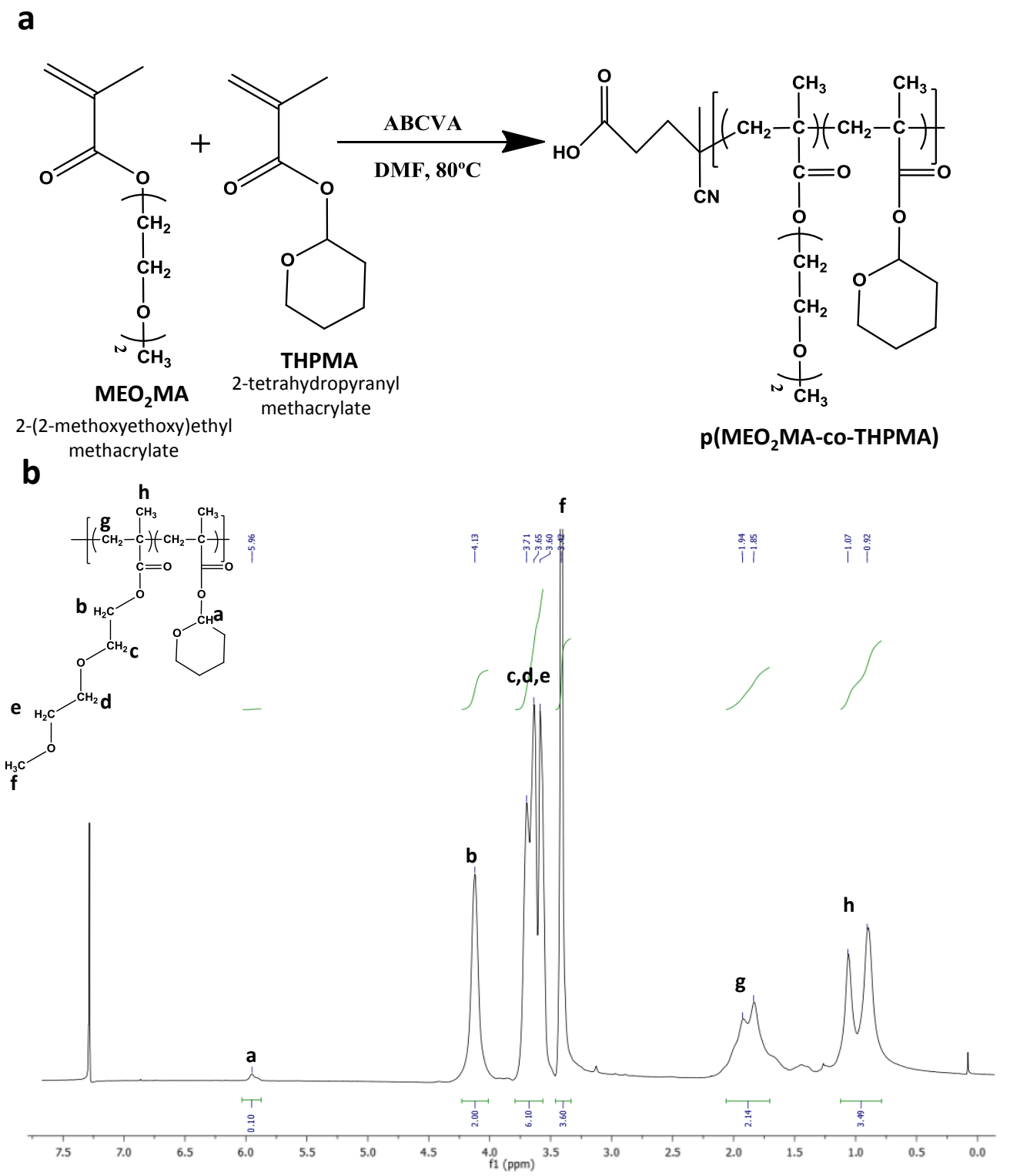

Figure S8. Synthesis scheme (a) and ^{1}H-NMR characterization of copolymer p-(MEO2MA-co-THPMA.

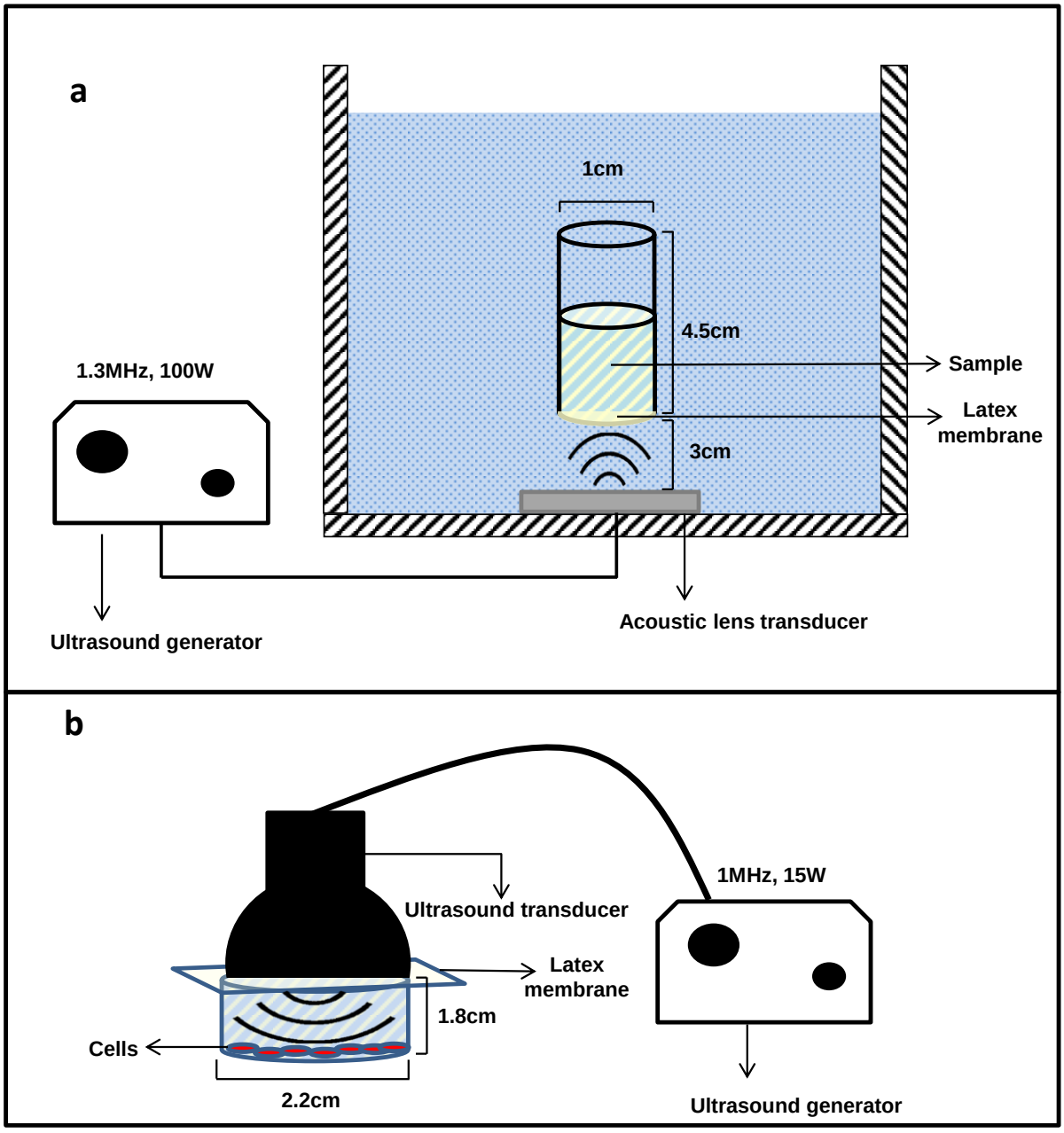

Figure S9. Schematic representation of the two ultrasound systems used in this work.

3.1.2 Mechanistic evaluation of cargo release from Ultrasound-Responsive Polymer-Grafted Mesoporous Silica Nanoparticles

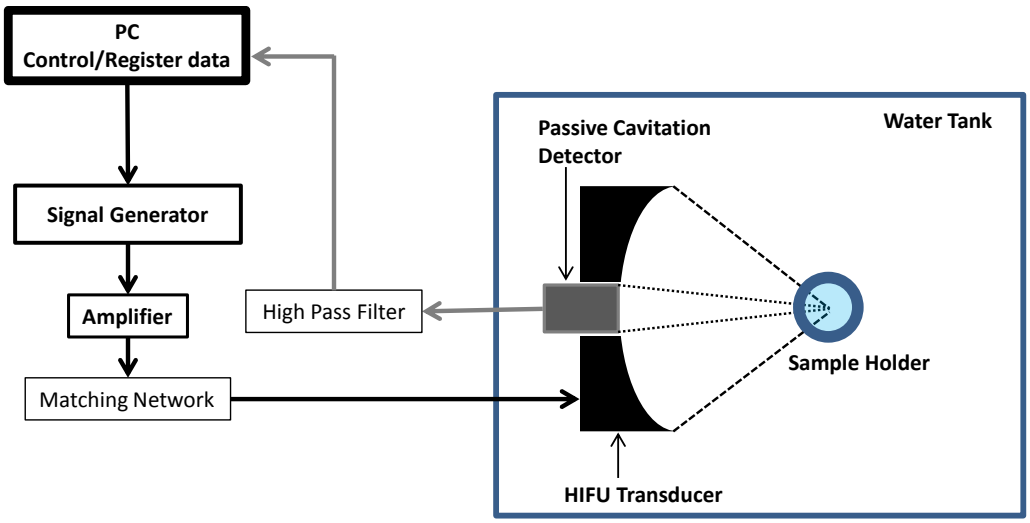

Mechanistic evaluation of cargo release from Ultrasound-Responsive Polymer-Grafted Mesoporous Silica Nanoparticles

In previous work we have successfully developed an ultrasound (US)-responsive hybrid material for drug delivery purposes by grafting a polymeric gate on the surface of Mesoporous Silica Nanoparticles (MSN).[1] That material had the ability of retaining the cargo within its mesoporosity under physiological conditions, releasing it only upon US exposure.

US is a versatile external stimulus that can penetrate deep into the human body in a non-invasive manner.[2] US can be used for many applications in biomedicine, either due to its thermal or mechanical bioeffects.[2]

The objective of the present work is to determine the main mechanism driving the cargo release from our previously reported hybrid nanoparticles by employing different US experimental configurations. In particular, the thermal effects were studied by measuring sample bulk heating through a thermocouple. On the other hand, the main mechanical effect evaluated was the presence of inertial cavitation during US exposure. Inertial cavitation can be defined as the rapid expansion and violent collapse of gas bubbles in a fluid being exposed to US.[3]

This work was performed during a short research stay at the Biomedical Ultrasonics, Biotherapy and Biopharmaceuticals Laboratory (BUBBL) at the University of Oxford, under the supervision of Prof. Constantin C. Coussios.

Experimental section

The material used in this work (hybrid MSNs) consisted in MCM-41 type mesoporous silica nanoparticles with an US-responsive polymeric gate on its surface (p(MEO_2MA-co-THPMA)). This material was synthesized, characterized and loaded with the dye fluorescein as described in our previous work.[1] This chapter will be focused on analyzing the cargo release mechanism from those hybrid MSNs. Fluorescein release was evaluated in this work by fluorimetry, measuring the fluorescence of the supernatants of hybrid MSNs suspensions after release for 2 h in phosphate buffered solution (PBS) at 37 ºC (Fluorescein: λexc 490, λem 514 nm).

All US exposure experiments were performed in a tank filled with degassed water that was temperature-controlled at 37 ºC. For this work, different High Intensity

Focused Ultrasound (HIFU) transducers were used. The sample holder was aligned with the HIFU transducer, which included within it another focused transducer used as a Passive Cavitation Detector (PCD). The signal received from the PCD enables monitoring the cavitation activity within the sample during HIFU exposure. That way, the onset of inertial cavitation will be detected as a broadband spectrum on the PCD data. A schematic representation of the described experimental setup can be seen in Scheme 1. More details about the US experimental setup used can be found below.

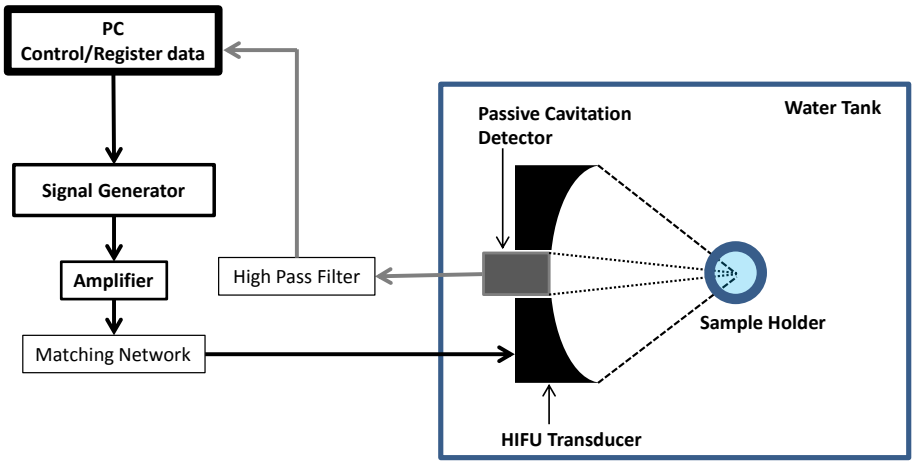

Scheme 1. Experimental setup used for the US exposures of the samples.

The HIFU and PCD transducers are controlled from custom-made software (LabVIEW, National Instruments, USA). An arbitrary waveform generator (33220A, Agilent, USA) was used to create the transmit signal which was amplified by a 300W RF power amplifier (A-300, ENI, Mountain View, USA) and sent to the focused transducer via a 50 Ohm matching network. Three frequencies were here used: 0.5, 1 and 3.3 MHz. To do that, three spherically-focused single-element HIFU transducers were here used, with a center frequency of 0.5, 1 and 1.1 MHz respectively (Sonic Concepts, USA). The third harmonic of the 1.1 MHz transducer was used for the 3.3 MHz experiments. All HIFU transducers used here were previously calibrated in water using a 0.4 mm diameter needle hydrophone (ONDA 1056, Onda Corporation). All acoustic pressures reported in this study are in MPa peak rarefactional pressures. Experimental conditions employed for US exposure at the three different frequencies used were: 0.5 MHz (3.6 MPa, 5 % duty cycle), 1 MHz (5 or 6 MPa, 95% duty cycle) and 3.3 MHz (8 MPa, 95% duty cycle). All US exposures lasted 500 s.

A 7.5 MHz single element and spherically focused PCD (V320, Panametrics, Olympus, USA) was aligned with the HIFU transducer via a central circular opening.

Acoustic emissions arising from cavitation were sensed by a PCD as described previously.[4] The acquired PCD signal was filtered using a 5 MHz high pass filter (FILT-HP5-A, Allen Avionics), amplified 5 times with a low noise amplifier (Stanford Research Systems, SR445A, USA) and recorded with a 14-bit PCI Oscilloscope device (PCI-5122, National Instruments, USA) at a rate of 100 MHz. The high-pass filter was used to reject strong reflections from the sample holder. An initial segment ('background') that was free of any signal was used to compare it with the rest of the signal received to determine if inertial cavitation had occurred (MATLAB program, Mathworks, USA).[5] All of the PCD traces collected were employed to calculate the probability of cavitation under each set of US settings. Inertial cavitation was identified due to broadband spectral elevation in the signal relative to the background.

The sample holder was designed specifically for this work (Figure 1). The sample holder consisted of a cylindrical container (1 cm diameter) that was sealed with two US-transparent Mylar® sheets. An orifice on its wall allowed us to introduce a thermocouple inside the holder to measure the temperature during the experiment. An opening on the side of the holder was used to introduce the sample and change it between experiments, closing it with a rubber lid afterwards.

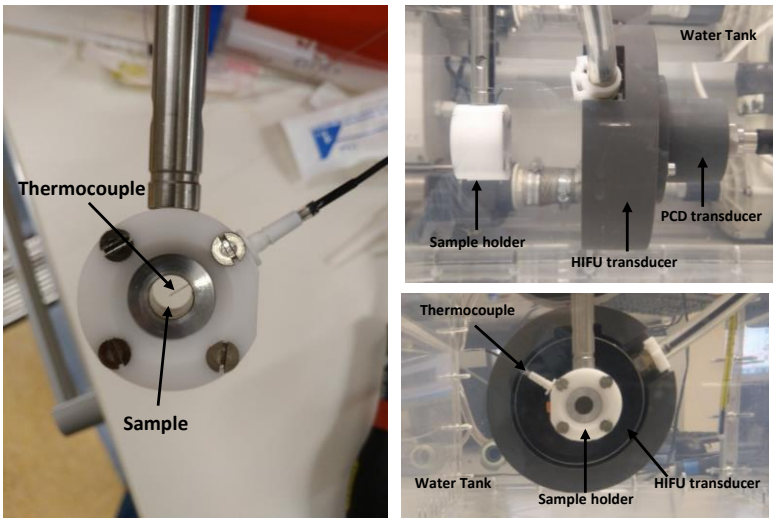

Figure 1. Sample holder used in this work with a thermocouple inside (left). Sample holder aligned with the transducers in a water tank as used for this work (right).

Samples were first exposed to the different experimental conditions, and then incubated in PBS at 37 ºC for 2 h before centrifugation and measurement of their supernatants to determine cargo release. Experiments were performed in triplicate.

Results and Discussion

First, a 1 MHz focused transducer was employed to replicate our previous cargo release experiments. Suspensions of the fluorescein-loaded US-responsive material were exposed to 1 MHz US for 500 seconds (95 % Duty Cycle), at two different peak rarefactional pressures: 5 and 6 MPa. Sample temperature and cavitation activity were monitored during the US exposure, and cargo release was measured with a fluorimeter after incubation at 37 ºC under orbital shaking for 2 h.

The results (Figure 2) show that 1 MHz US exposure induced a temperature increase of 6 ºC at 5 MPa and 14 ºC at 6 MPa. PCD data also shows broadband emissions under both conditions, indicating that inertial cavitation was happening in the sample holder. A control experiment performed with water in the sample holder and applying US at a low pressure showed no inertial cavitation (data not shown).The mean broadband power was larger at 6 MPa, implying higher cavitation intensity. Fluorescein release results (Figure 2) show that only at the 6 MPa US exposure there is a cargo release significantly increased compared to the sample not exposed to US. These results show that there is a threshold in the US intensity at which the sample has to be exposed to release its cargo. The existence of an intensity threshold is compatible with our hypothesis that cargo release is produced after the cleavage of one of the monomers in the polymeric gate.[1] No significant difference in cargo release should be observed until a sufficient amount of US-responsive monomers are cleaved.

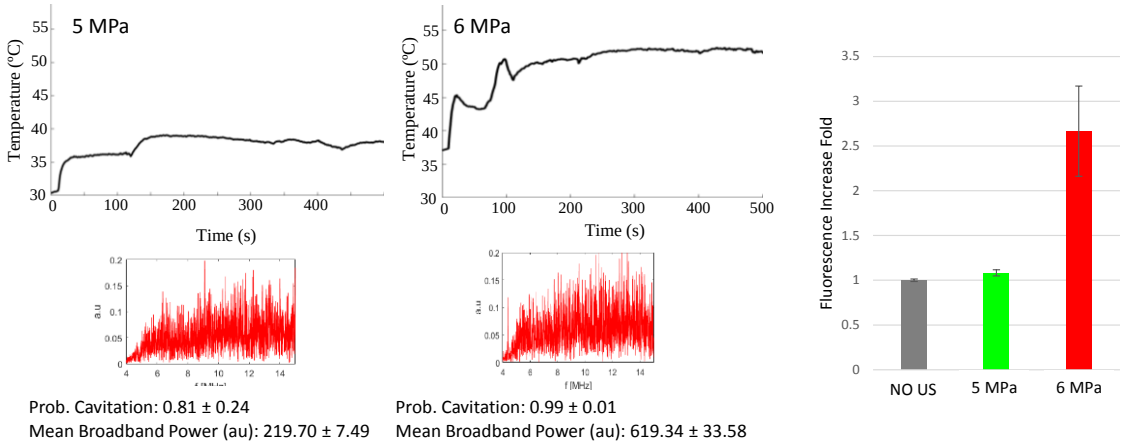

Figure 2. Temperature measurements obtained during 1 MHz US exposure at 5 and 6 MPa over time (left, top); PCD power spectra obtained during those same experiments (left, bottom). Fluorescence increase folds of the supernatants of the sample suspensions after exposure to 1 MHz US and stirring at 37 ºC for 2 h (compared to samples not exposed to the stimulus) (right).

The mechanical and thermal effects of US are related to the frequency of US being employed. Higher frequencies will provide a more intense thermal effect. On the other hand, at lower frequencies, the probability of inertial cavitation is usually much higher.[6] Experiments with different US frequencies were carried out to test what mechanism (thermal or mechanical) is most likely to be responsible for cargo release. We employed one transducer with a frequency lower than the one used in the above experiment (0.5 MHz) and another one working at a much higher frequency (3.3 MHz). At 0.5 MHz we would be able to obtain intense cavitation activity at lower pressures than those necessary at 1 MHz, and using a low duty cycle (5 %) could allow us to reach inertial cavitation without significantly heating up the sample. On the other hand, the inertial cavitation threshold at 3.3 MHz should be much higher, what could allow us to induce significant bulk heating to the sample without generating an intense cavitation activity. A control experiment was performed through a thermal treatment of the sample by introducing it in an oven at 55 ºC (maximum temperature reached under 1 MHz US at 6 MPa) for 500 s (duration of the US exposure).

Figure 3 shows that 0.5 MHz US application at 3.6 MPa of pressure, which provoked inertial cavitation but did not cause any significant heating of the sample, induced a greater cargo release than in samples which were not exposed to the stimulus. Furthermore, the fluorescence increase fold obtained at 0.5 MHz was in the same range as that obtained at 1 MHz under conditions that induced both thermal and intense cavitational effects. On the other hand, neither thermal treatment at 55 ºC nor exposure to 3.3 MHz US produced any significant increase in cargo release. These results indicate that, while cavitation activity seems to be indispensable to observe cargo release from our material, sample heating was not involved in the process. Therefore, the mechanism appears to be more closely related to the mechanical effect of US than to its thermal effects. However, we cannot rule out the effect of a thermal mechanism in the nanoscale, by close proximity of the sample to inertially cavitating bubbles, where the local temperatures can be much higher than those reached in the bulk suspension.[7]

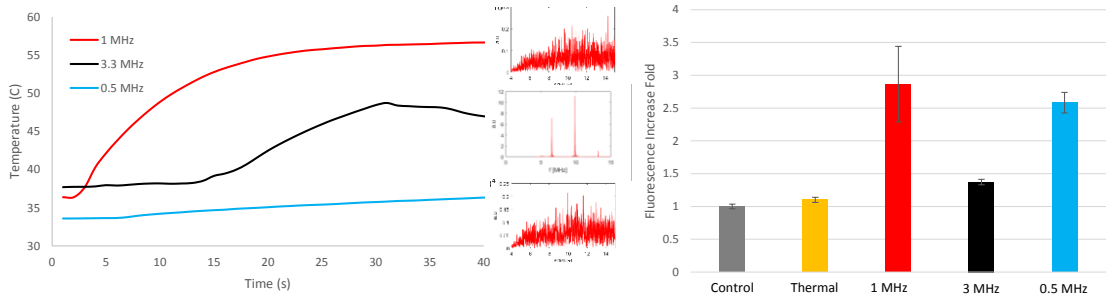

Figure 3. Temperature measurements in the sample holder carried out during US exposure until a maximum temperature is reached at three different frequencies (left) and associated representative PCD data (center). Fluorescence increase folds of the supernatants of the sample suspensions after exposure to thermal or US treatments and stirring at 37 ºC for 2 h (compared to samples not exposed to the stimulus).

Conclusion

The mechanism of ultrasound-induced cargo release from hybrid polymer-grafted mesoporous silica nanoparticles has been here evaluated. We have determined that inertial cavitation was necessary to induce cargo release from hybrid MSNs. Additionally, a thermal mechanism was discarded as the main cause of the US-responsive behavior of the material. The existence of a threshold in the intensity of cavitation needed to induce cargo release further supports the sonochemical mechanism previously hypothesized.

References

1. Paris, J. L., Cabañas, M. V., Manzano, M. & Vallet-Regí, M. Polymer-Grafted Mesoporous Silica Nanoparticles as Ultrasound-Responsive Drug Carriers. *ACS Nano* **9,** 11023–11033 (2015).
2. Wood, A. K. W. & Sehgal, C. M. A Review of Low-Intensity Ultrasound for Cancer Therapy. *Ultrasound Med. Biol.* **41,** 905–928 (2015).
3. Arvanitis, C. D., Bazan-Peregrino, M., Rifai, B., Seymour, L. W. & Coussios, C. C. Cavitation-Enhanced Extravasation for Drug Delivery. *Ultrasound Med. Biol.* **37,** 1838–1852 (2011).
4. Hockham, N., Coussios, C. C. & Arora, M. A real-time controller for sustaining thermally relevant acoustic cavitation during ultrasound therapy. *IEEE Trans. Ultrason. Ferroelectr. Freq. Control* **57,** 2685–2694 (2010).
5. Kwan, J. J., Graham, S., Myers, R., Carlisle, R., Stride, E. & Coussios, C. C. Ultrasound-induced inertial cavitation from gas-stabilizing nanoparticles. *Phys. Rev. E* **92,** 23019 (2015).
6. Gaertner, W. Frequency Dependence of Ultrasonic Cavitation. *J. Acoust. Soc. Am.* **26,** 977–980 (1954).
7. Costley, D., Mc Ewan, C., Fowley, C., McHale, A. P., Atchison, J., Nomikou, N. & Callan, J. F. Treating cancer with sonodynamic therapy: A review. *Int. J. Hyperth.* **31,** 107–117 (2015).

Bloque 3.2

Estrategias físico-químicas de vectorización de nanopartículas de sílice mesoporosa sensibles a ultrasonido

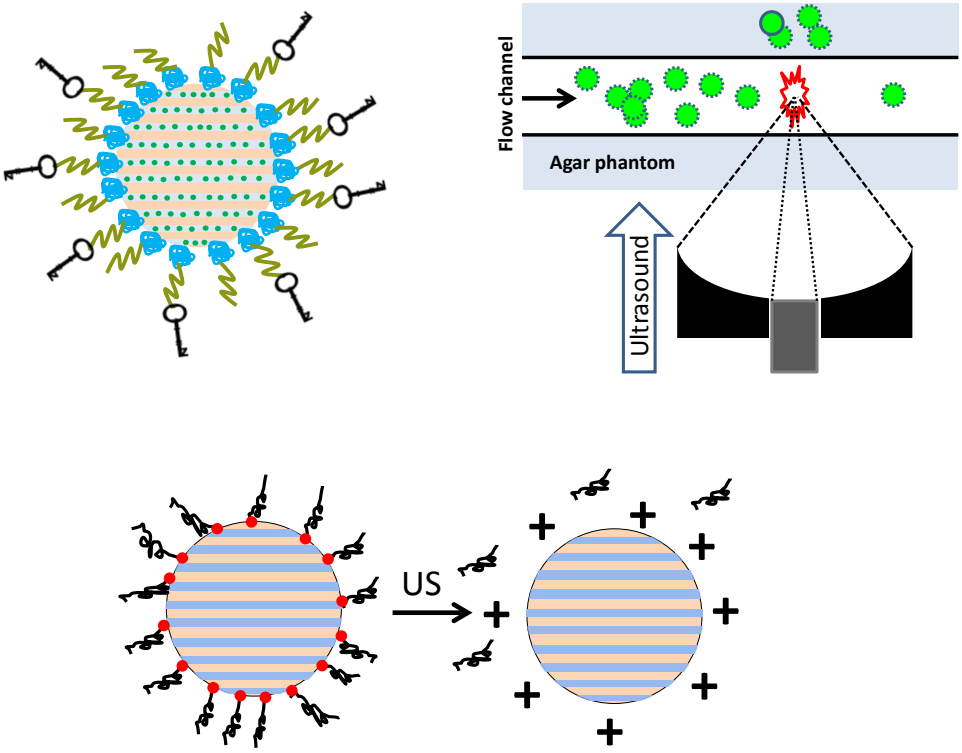

El segundo bloque de Resultados y Discusión versa sobre el uso de estrategias físico-químicas para lograr la vectorización hacia tumores de MSNs sensibles a US.

Como ya se ha mencionado anteriormente, la acumulación de nanopartículas en tumores sólidos se produce debido a las características patológicas de la vasculatura de dichos tumores. Su rápido crecimiento induce la formación de vasos sanguíneos imperfectos, que poseen poros o fenestraciones en la pared de los vasos por las cuales macromoléculas o partículas pequeñas (hasta varios cientos de nanómetros) pueden extravasarse al tejido tumoral. La elevada presión intersticial del tejido tumoral colapsa los vasos linfáticos, impidiendo la retirada de las partículas que se hayan extravasado. Este efecto de permeabilidad y retención aumentadas (EPR por sus siglas en inglés) es el principal motivo del uso de nanopartículas en oncología, y a menudo es denominado "vectorización pasiva".[1–3] Para que la acumulación de nanopartículas en tumores por medio del efecto EPR sea eficaz, las nanopartículas deben ser capaces de circular en el torrente sanguíneo durante suficiente tiempo. Como se ha visto en el capítulo 1.1, una estrategia comúnmente empleada para aumentar dicho tiempo de circulación es la modificación de su superficie con cadenas de polietilenglicol (PEG, proceso denominado PEGilación).[4–6] Las cadenas de PEG disminuyen la adsorción de proteínas en su superficie (Figura 1), ralentizando su retirada de la circulación por los órganos del sistema retículoendotelial (hígado y bazo, principalmente).[7]

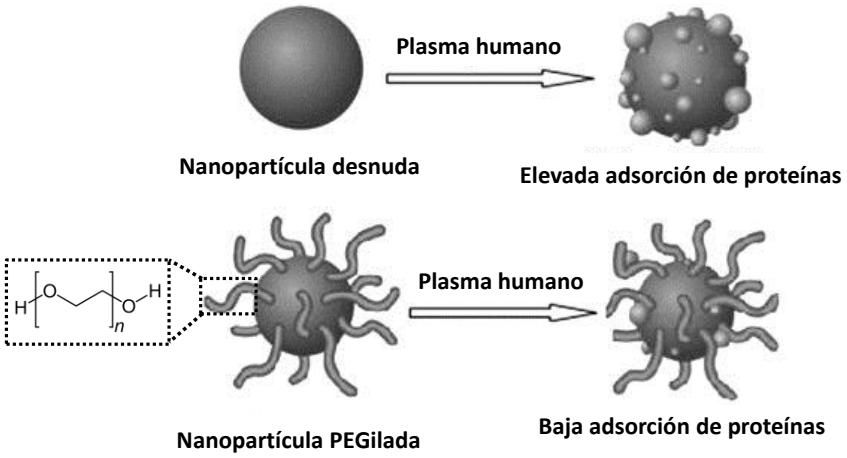

Figura 1. Efecto de la PEGilación en la adsorción de proteínas. Adaptado con permiso.[8]

Por otra parte, las estrategias de vectorización activa se han empleado con éxito para aumentar la eficacia de las terapias basadas en nanopartículas.[3,9–11] La vectorización activa consiste en decorar la superficie de las nanopartículas con moléculas que induzcan su internalización selectiva en células tumorales. Las moléculas

de vectorización activa suelen ser anticuerpos, proteínas o moléculas pequeñas,[3] y es especialmente habitual emplear nutrientes para los cuales las células tumorales sobreexpresan receptores en su membrana, tales como la transferrina o el ácido fólico.[11,12]

El Capítulo 3.2.1 abarca la obtención de un material híbrido con liberación inducida por US, PEGilado y con agentes de vectorización activa. Para ello, se llevó a cabo la modificación del método de síntesis del polímero descrito en el bloque 1 para permitir el anclaje de cadenas de PEG que porten además agentes de vectorización activa que induzcan su internalización en células tumorales. El método empleado en este capítulo para la obtención de la compuerta polimérica sensible a US es la polimerización por adición fragmentación y transferencia de cadena reversible (RAFT por sus siglas en inglés). La polimerización RAFT es también un tipo de polimerización radicalaria, en la cual se obtiene un control mucho mayor del proceso y con una distribución mucho más estrecha de pesos moleculares del polímero resultante.[13] Esta técnica permite, y es la razón por la que aquí la usamos, la obtención de polímeros con un grupo funcional distinto en cada uno de los dos extremos,[14,15] empleando posteriormente uno de los extremos para anclarlo a la nanopartícula y el otro para llevar a cabo la unión con una cadena de PEG. El nuevo polímero PEGilado obtenido por este método mantenía su capacidad de respuesta a ultrasonido. En la polimerización RAFT, además de los monómeros y el iniciador (que serán los mismos que los empleados para la polimerización FRP), se añade en el medio de reacción un agente de transferencia de cadena o agente RAFT. Éste controlará la velocidad de la reacción, al ir transfiriendo cada molécula de monómero a su estructura a medida que va creciendo la cadena de polímero.[13] El esquema 1 muestra el mecanismo de la polimerización tipo RAFT, en cinco etapas posibles diferenciadas: iniciación, transferencia de cadena reversible/propagación, reiniciación, equilibración de cadena/propagación y terminación.

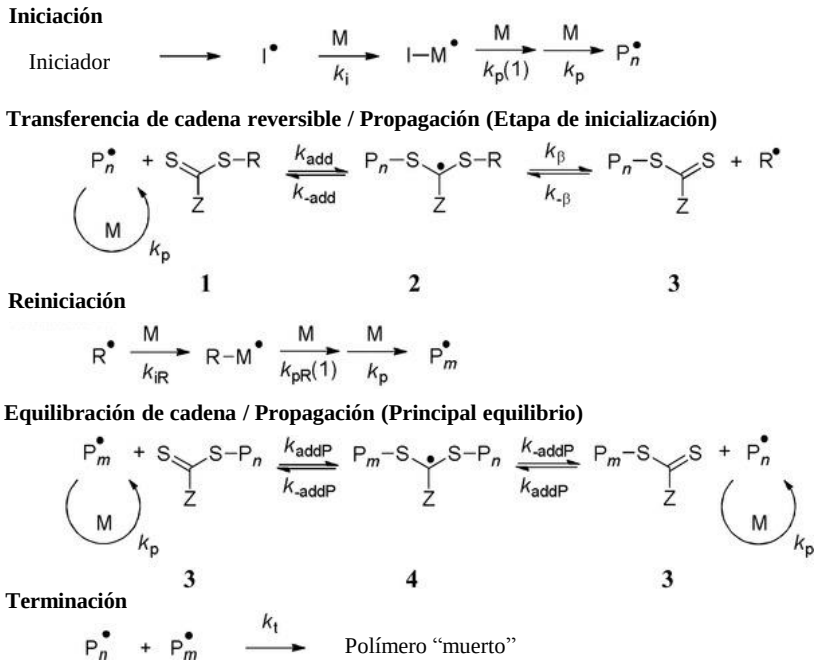

Esquema 1. Mecanismo de polimerización tipo RAFT. Adaptado con permiso.[13]

Como se verá en el capítulo 3.2.1, el polímero así obtenido fue anclado a las MSNs, dando lugar a un nuevo material PEGilado que mostró una mayor estabilidad en suspensión que el material no PEGilado. Además, se obtuvo un material PEGilado modular al que poder anclar diferentes agentes de vectorización activa utilizando la cicloadición 1,3-dipolar de Huisgen empleando un alquino tensionado.[16,17] Así, tras la conjugación de un péptido conteniendo la secuencia RGD (arginina-glicina-aspártico), se mostró la capacidad de vectorización activa *in vitro* de dicho material empleando células tumorales HeLa.[10,18,19] Finalmente, se observó un incremento en la toxicidad de las nanopartículas PEGiladas cargadas con doxorrubicina y con vectorización activa tras la aplicación de US, indicando la mayor liberación del fármaco en respuesta al estímulo.

A pesar del aumento en la eficacia terapéutica de nanosistemas con vectorización activa, se han descrito también varias desventajas de su uso.[20] Por ejemplo, las nanopartículas PEGiladas y con agentes de vectorización activa son retiradas más rápidamente de la circulación que nanopartículas PEGiladas sin vectorización activa.[21] Además, puede darse un efecto paradójico ya que la primera línea de células del tumor captará la gran mayoría de las nanopartículas que lleguen a la zona, impidiendo su penetración a capas más profundas del tumor. Este efecto se conoce como la barrera del sitio de unión, y ha sido ampliamente descrito para el uso de anticuerpos.[22] Con el objetivo de atacar éste y otros problemas, se han desarrollado una

serie de estrategias comúnmente denominadas de vectorización jerarquizada (Figura 2).[20,23] En muchas de estas estrategias, el agente de vectorización activa se encuentra oculto durante la circulación de las nanopartículas en el torrente sanguíneo, para luego ser expuesto una vez en el tumor debido a la presencia de un estímulo interno o externo.[24]

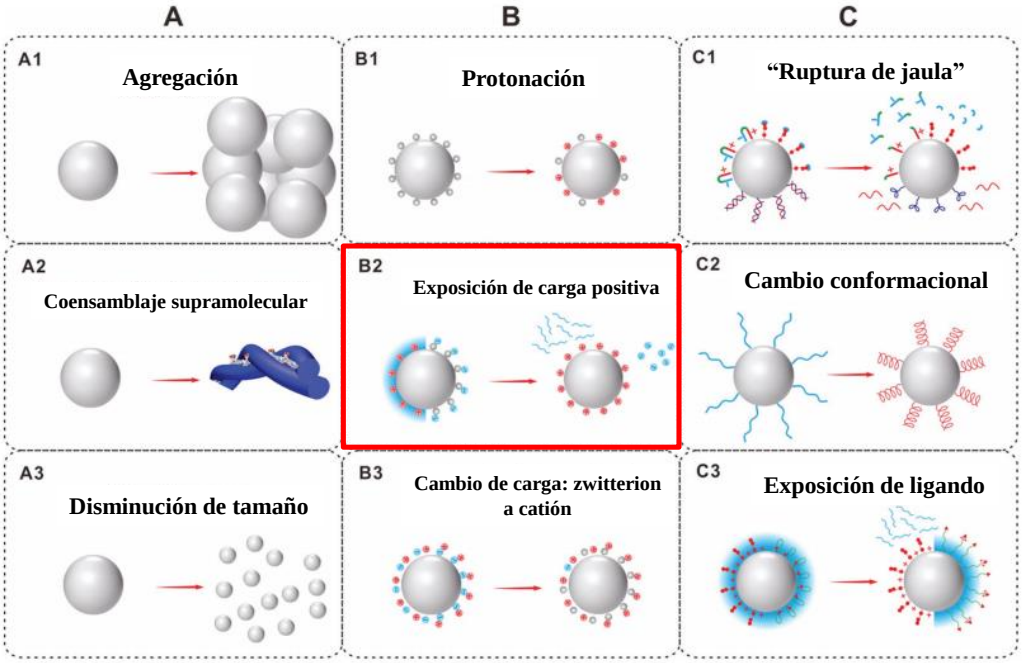

Figura 2. Principales estrategias de vectorización jerarquizada. Adaptado con permiso.[20]

El capítulo 3.2.2 trata sobre el desarrollo de una de estas estrategias de vectorización jerarquizada, concretamente MSNs PEGiladas capaces de eliminar la capa de PEG de su superficie cargada positivamente al ser expuestas a US. Las cadenas de PEG son ancladas al material mediante un enlace termosensible.[25,26] Los efectos térmicos del US inducen la separación de la capa de PEG, permitiendo la exposición de una carga superficial positiva. Entonces, las nanopartículas con su carga superficial positiva expuesta, interaccionan con los fosfolípidos cargados negativamente de la membrana celular, lo cual, en nuestro caso, aumentó su internalización en células de osteosarcoma (HOS).[27] Este incremento en la internalización de las nanopartículas condujo a una mayor toxicidad de nanopartículas cargadas con topotecan que habían sido expuestas a US.

Las estrategias mencionadas hasta ahora para mejorar la distribución de nanopartículas hacia tumores y aumentar su eficacia (PEGilación, vectorización activa, vectorización jerarquizada) dependen en primer lugar de la acumulación pasiva de nanopartículas en el tumor mediante el efecto EPR. Sin embargo, el efecto EPR no es

un fenómeno homogéneo a lo largo de toda la masa tumoral, ni es igual de intenso en todos los tipos de tumores.[21,28–30] De hecho, muchos tumores sólidos presentan un efecto EPR de poca magnitud, siendo difícil distinguir en el entorno clínico aquellos pacientes que podrían beneficiarse de él.[31] Por otra parte, la elevada presión intersticial presente en los tumores sólidos dificulta la penetración de nanopartículas a zonas profundas del mismo, dado que la única fuerza motriz que está actuando durante la extravasación de las nanopartículas es la difusión.[32,33] Por todo esto, es necesario desarrollar otras aproximaciones por las cuales asegurar el transporte de nanopartículas y otros agentes terapéuticos hacia tumores, así como su correcta distribución dentro de los mismos. Una posible estrategia para lograr ambos objetivos es la generación de fuerzas de convección en el interior de los vasos sanguíneos del tumor por los cuales estén pasando las nanopartículas. La generación de cavitación inercial ha sido empleada para inducir la extravasación y distribución más homogénea de distintos tipos de agentes terapéuticos para su uso en terapias oncológicas.[34–37] De esta manera, existiría otra fuerza motriz que indujese la extravasación y posterior penetración de las partículas en el tumor.

El Capítulo 3.2.3 se centra en la evaluación del uso de cavitación acústica mediada por US en un modelo *in vitro* de extravasación empleando MSNs. Este trabajo se realizó durante una estancia en la Universidad de Oxford, en el grupo de investigación dirigido por el Prof. Constantin C. Coussios. Para llevar a cabo este trabajo, se empleó un gel de agarosa como modelo del tejido tumoral. Una suspensión de las MSNs se hizo pasar con un flujo constante a través de canales creados en el gel. Empleando un transductor de US focalizado de 0.5 MHz y un detector de cavitación pasiva, se evaluó el efecto de diferentes condiciones de US en la extravasación de MSNs al gel de agarosa. Las condiciones óptimas para la extravasación fueron también evaluadas para MSNs cargadas con un fluoróforo como modelo de un fármaco cargado en los poros. Posteriormente, también se evaluó la combinación de las MSNs con núcleos de cavitation poliméricos submicrométricos,[38,39] que permitieron disminuir la presión necesaria para lograr extravasación de las MSNs. Los resultados obtenidos en este capítulo muestran que la combinación de MSNs y núcleos de cavitación poliméricos puede ayudar a inducir la extravasación de las MSNs en tumores al aplicar US focalizados en la zona tras la inyección combinada de ambos tipos de partículas. Posteriormente, las MSN embebidas en el tejido tumoral podrían actuar como reservorio de un fármaco, liberándolo lentamente en la zona de actuación.

Bibliografía

1. Maeda, H., Nakamura, H. & Fang, J. The EPR effect for macromolecular drug delivery to solid tumors: Improvement of tumor uptake, lowering of systemic toxicity, and distinct tumor imaging in vivo. *Adv. Drug Deliv. Rev.* **65,** 71–79 (2013).
2. Fang, J., Nakamura, H. & Maeda, H. The EPR effect: Unique features of tumor blood vessels for drug delivery, factors involved, and limitations and augmentation of the effect. *Adv. Drug Deliv. Rev.* **63,** 136–151 (2011).
3. Bertrand, N., Wu, J., Xu, X., Kamaly, N. & Farokhzad, O. C. Cancer nanotechnology: the impact of passive and active targeting in the era of modern cancer biology. *Adv. Drug Deliv. Rev.* **66,** 2–25 (2014).
4. Hatakeyama, H., Akita, H. & Harashima, H. The Polyethyleneglycol Dilemma: Advantage and Disadvantage of PEGylation of Liposomes for Systemic Genes and Nucleic Acids Delivery to Tumors. *Biol. Pharm. Bull.* **36,** 892–899 (2013).
5. He, Q., Zhang, J., Shi, J., Zhu, Z., Zhang, L., Bu, W., Guo, L. & Chen, Y. The effect of PEGylation of mesoporous silica nanoparticles on nonspecific binding of serum proteins and cellular responses. *Biomaterials* **31,** 1085–1092 (2010).
6. Chen, F., Hong, H., Zhang, Y., Valdovinos, H. F., Shi, S., Kwon, G. S., Theuer, C. P., Barnhart, T. E. & Cai, W. In Vivo Tumor Targeting and Image-Guided Drug Delivery with Antibody-Conjugated, Radiolabeled Mesoporous Silica Nanoparticles. *ACS Nano* **7,** 9027–9039 (2013).
7. Xu, X., Ho, W., Zhang, X., Bertrand, N. & Farokhzad, O. Cancer nanomedicine: from targeted delivery to combination therapy. *Trends Mol. Med.* **21,** 223–232 (2015).
8. Naahidi, S., Jafari, M., Edalat, F., Raymond, K., Khademhosseini, A. & Chen, P. Biocompatibility of engineered nanoparticles for drug delivery. *J. Control. Release* **166,** 182–194 (2013).
9. Baeza, A., Colilla, M. & Vallet-Regí, M. Advances in mesoporous silica nanoparticles for targeted stimuli-responsive drug delivery. *Expert Opin. Drug Deliv.* **12,** 319–337 (2015).
10. Yang, W., Cheng, Y., Xu, T., Wang, X. & Wen, L. P. Targeting cancer cells with biotin-dendrimer conjugates. *Eur. J. Med. Chem.* **44,** 862–868 (2009).
11. Stella, B., Arpicco, S., Peracchia, M. T., Desmaële, D., Hoebeke, J., Renoir, M., D'Angelo, J., Cattel, L. & Couvreur, P. Design of folic acid-conjugated nanoparticles for drug targeting. *J. Pharm. Sci.* **89,** 1452–1464 (2000).
12. Martínez-Carmona, M., Baeza, A., Rodriguez-Milla, M. A., García-Castro, J. & Vallet-Regí, M. Mesoporous silica nanoparticles grafted with a light-responsive protein shell for highly cytotoxic antitumoral therapy. *J. Mater. Chem. B* **3,** 5746–5752 (2015).
13. Moad, G. Mechanism and Kinetics of Dithiobenzoate-Mediated RAFT Polymerization - Status of the Dilemma. *Macromol. Chem. Phys.* **215,** 9–26 (2014).
14. Qiu, X. P. & Winnik, F. M. Facile and efficient one-pot transformation of RAFT polymer end groups via a mild aminolysis/michael addition sequence. *Macromol. Rapid Commun.* **27,** 1648–1653 (2006).
15. Boyer, C., Granville, A., Davis, T. P. & Bulmus, V. Modification of RAFT-polymers via thiol-ene reactions: A general route to functional polymers and new architectures. *J. Polym. Sci. Part A Polym. Chem.* **47,** 3773–3794 (2009).
16. Algar, W. R., Prasuhn, D. E., Stewart, M. H., Jennings, T. L., Blanco-Canosa, J.

B., Dawson, P. E. & Medintz, I. L. The controlled display of biomolecules on nanoparticles: A challenge suited to bioorthogonal chemistry. *Bioconjug. Chem.* **22,** 825–858 (2011).
17. Li, F., Xie, C., Cheng, Z. & Xia, H. Ultrasound responsive block copolymer micelle of poly(ethylene glycol)–poly(propylene glycol) obtained through click reaction. *Ultrason. Sonochem.* **30,** 9–17 (2016).
18. Fisichella, M., Dabboue, H., Bhattacharyya, S., Saboungi, M.-L., Salvetat, J.-P., Hevor, T. & Guerin, M. Mesoporous silica nanoparticles enhance MTT formazan exocytosis in HeLa cells and astrocytes. *Toxicol. In Vitro* **23,** 697–703 (2009).
19. Lin, C. Y., Javadi, M., Belnap, D. M., Barrow, J. R. & Pitt, W. G. Ultrasound sensitive eLiposomes containing doxorubicin for drug targeting therapy. *Nanomed.-Nanotechnol. Biol. Med.* **10,** 67–76 (2014).
20. Wang, S., Huang, P. & Chen, X. Hierarchical Targeting Strategy for Enhanced Tumor Tissue Accumulation/Retention and Cellular Internalization. *Adv. Mater.* **28,** 7340–7364 (2016).
21. Dawidczyk, C. M., Kim, C., Park, J. H., Russell, L. M., Lee, K. H., Pomper, M. G. & Searson, P. C. State-of-the-art in design rules for drug delivery platforms: Lessons learned from FDA-approved nanomedicines. *J. Control. Release* **187,** 133–144 (2014).
22. Goodman, T. T., Olive, P. L. & Pun, S. H. Increased nanoparticle penetration in collagenase-treated multicellular spheroids. *Int. J. Nanomedicine* **2,** 265–274 (2007).
23. Su, Y.-L., Yu, T.-W., Chiang, W.-H., Chiu, H.-C., Chang, C.-H., Chiang, C.-S. & Hu, S.-H. Hierarchically Targeted and Penetrated Delivery of Drugs to Tumors by Size-Changeable Graphene Quantum Dot Nanoaircrafts for Photolytic Therapy. *Adv. Funct. Mater.* **27,** 1700056 (2017).
24. Villaverde, G., Nairi, V., Baeza, A. & Vallet-Regí, M. Double Sequential Encrypted Targeting Sequence: A New Concept for Bone Cancer Treatment. *Chem. - A Eur. J.* **23,** 7174–7179 (2017).
25. Berkowski, K. L., Potisek, S. L., Hickenboth, C. R. & Moore, J. S. Ultrasound-Induced Site-Specific Cleavage of Azo-Functionalized Poly(ethylene glycol). *Macromolecules* **38,** 8975–8978 (2005).
26. Saint-Cricq, P., Deshayes, S., Zink, J. I. & Kasko, A. M. Magnetic field activated drug delivery using thermodegradable azo-functionalised PEG-coated core–shell mesoporous silica nanoparticles. *Nanoscale* **7,** 13168–13172 (2015).
27. Villegas, M. R., Baeza, A. & Vallet-Regí, M. Hybrid Collagenase Nanocapsules for Enhanced Nanocarrier Penetration in Tumoral Tissues. *ACS Appl. Mater. Interfaces* **7,** 24075–24081 (2015).
28. Nichols, J. W. & Bae, Y. H. EPR: Evidence and fallacy. *J. Control. Release* **190,** 451–464 (2014).
29. Kwon, I. K., Lee, S. C., Han, B. & Park, K. Analysis on the current status of targeted drug delivery to tumors. *J. Control. Release* **164,** 108–114 (2012).
30. van der Meel, R., Lammers, T. & Hennink, W. E. Cancer nanomedicines: oversold or underappreciated? *Expert Opin. Drug Deliv.* **14,** 1–5 (2017).
31. Wilhelm, S., Tavares, A. J., Dai, Q., Ohta, S., Audet, J., Dvorak, H. F. & Chan, W. C. W. Analysis of nanoparticle delivery to tumours. *Nat. Rev. Mater.* **1,** 16014 (2016).
32. Nichols, J. W. & Bae, Y. H. Odyssey of a cancer nanoparticle: From injection site to site of action. *Nano Today* **7,** 606–618 (2012).
33. Florence, A. T. 'Targeting' nanoparticles: The constraints of physical laws and

physical barriers. *J. Control. Release* **164,** 115–124 (2012).
34. Arvanitis, C. D., Bazan-Peregrino, M., Rifai, B., Seymour, L. W. & Coussios, C. C. Cavitation-Enhanced Extravasation for Drug Delivery. *Ultrasound Med. Biol.* **37,** 1838–1852 (2011).
35. Carlisle, R., Choi, J., Bazan-Peregrino, M., Laga, R., Subr, V., Kostka, L., Ulbrich, K., Coussios, C.-C. & Seymour, L. W. Enhanced Tumor Uptake and Penetration of Virotherapy Using Polymer Stealthing and Focused Ultrasound. *JNCI J. Natl. Cancer Inst.* **105,** 1701–1710 (2013).
36. Bazan-Peregrino, M., Arvanitis, C. D., Rifai, B., Seymour, L. W. & Coussios, C.-C. Ultrasound-induced cavitation enhances the delivery and therapeutic efficacy of an oncolytic virus in an in vitro model. *J. Control. Release* **157,** 235–242 (2012).
37. Theek, B., Baues, M., Ojha, T., Möckel, D., Veettil, S. K., Steitz, J., van Bloois, L., Storm, G., Kiessling, F. & Lammers, T. Sonoporation enhances liposome accumulation and penetration in tumors with low EPR. *J. Control. Release* **231,** 77–85 (2016).
38. Kwan, J. J., Graham, S., Myers, R., Carlisle, R., Stride, E. & Coussios, C. C. Ultrasound-induced inertial cavitation from gas-stabilizing nanoparticles. *Phys. Rev. E* **92,** 23019 (2015).
39. Kwan, J. J., Myers, R., Coviello, C. M., Graham, S. M., Shah, A. R., Stride, E., Carlisle, R. C. & Coussios, C. C. Ultrasound-Propelled Nanocups for Drug Delivery. *Small* **11,** 5305–5314 (2015).

3.2.1 From proof-of-concept material to PEGylated, modularly targeted ultrasound-responsive mesoporous silica nanoparticles

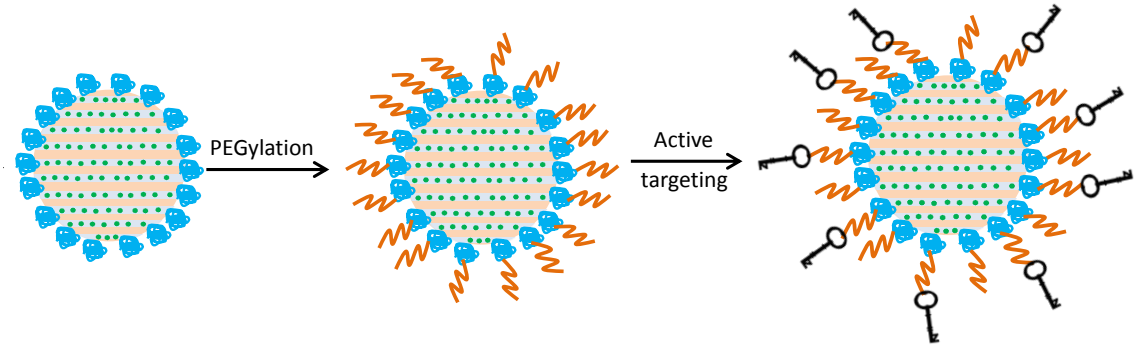

From proof-of-concept material to PEGylated, modularly targeted ultrasound-responsive mesoporous silica nanoparticles.

Abstract

In this work we present the synthesis and characterization of PEGylated and actively-targeted ultrasound-responsive hybrid mesoporous silica nanoparticles. This work covers the development of the chemical strategies necessary to afford this modular nanodevice starting from a proof-of concept material presented in previous work. We have developed a modular material by employing the strain-induced azide-alkyne Huisgen reaction. This modular US-responsive material could be adapted to different specific pathological conditions by carefully choosing the appropriate targeting moieties to be used. The new ultrasound responsive material was shown to be more stable in aqueous suspension than its non-PEGylated counterpart. This material was also able to target HeLa cells after conjugation with an RGD peptide. Ultrasound-responsive cytotoxicity of doxorubicin-loaded nanoparticles was observed in an *in vitro* cytotoxicity assay.

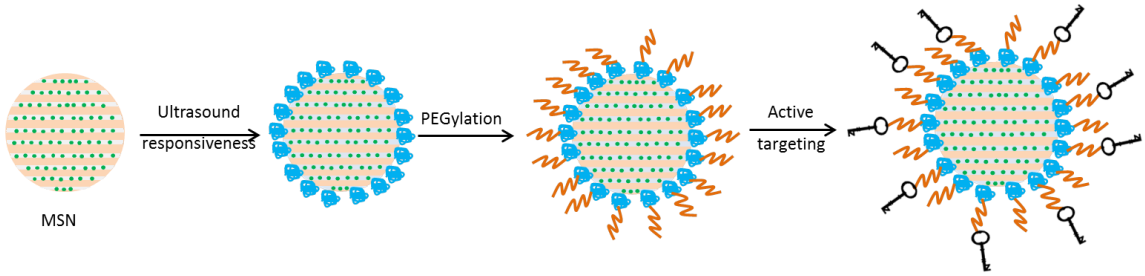

Graphical abstract. Conceptual representation of the work. Starting from naked mesoporous silica nanoparticles (MSNs), we can obtain a proof-of concept ultrasound-responsive hybrid nanomaterial.

1. Introduction

Nanomedicine, the use of nanotechnology to diagnose or treat different pathologies, holds great promise to improve patient care.[1] The main rationale behind the use of drug-loaded nanoparticles in medicine is their capacity to improve the pharmacokinetics of the drug. Nanocarriers can enhance the stability and circulation time of the drug, increasing the amount that reaches the target organ and therefore, decreasing the toxicity of chemotherapeutic drugs[1]. In the context of cancer, nanoparticles are able to reach tumor tissues due to the enhanced permeation and retention (EPR) effect.[2] The EPR effect is based on an increased extravasation of nanoparticles and macromolecules in the tumor due to leaky vasculature in

the area, coupled with a decreased withdrawal caused by the collapse of lymphatic vessels in solid tumors. Decorating the nanoparticle surface with polyethylene glycol (PEG) chains is known as PEGylation. PEGylation inhibits protein adsorption on the nanoparticle surface, which hinders its recognition by macrophages and increases their circulation time in the bloodstream. This allows more nanoparticles to reach the tumor site. Additionally, active targeting strategies have also been developed, by decorating the surface of nanocarriers with molecules that will induce their selective internalization in cancer cells.[3] This active targeting has been shown to increase the therapeutic efficacy of nanomedicines.[3]

Stimuli-responsive nanomaterials have attracted great attention in recent years in the context of cancer treatment.[4] The possibility of inducing drug release only in the diseased site could potentially improve the efficacy of nanotherapeutics while decreasing the side-effects of systemic administration of anticancer drugs. Both internal (like pH or redox)[5,6] and external (like light, magnetic field and ultrasound)[7–9] stimuli have been widely studied during last years. However, ultrasound (US) appears especially interesting due to its non-invasiveness and high penetration capacity in living tissues, together with the possibility to focus high frequency ultrasound deep into the body and the tumor mass, avoiding unnecessary exposure to surrounding healthy tissues.[9]

Mesoporous Silica Nanoparticles (MSNs) have also attracted much attention as drug carriers due to their high physicochemical stability and high surface area that would allow a high drug loading capacity.[10,11] In our group, we have recently reported an US-responsive MSN-based drug nanocarrier as an efficient proof of concept system for on-demand drug delivery.[12] However, the material presented in our previous work lacked some of the necessary characteristics for its use in therapeutic application. For example, the surface of the material at physiological temperature is highly hydrophobic and the particles tend to be aggregated. The lack of a PEG layer and active targeting moieties would also prevent them from reaching the desired target cancer cells.[13,14] The objective of this work is to synthesize a PEGylated and modularly targeted US-responsive nanomaterial. Consequently, a series of chemical strategies were here developed to adapt our previous proof-of-concept material to a more viable design that could be used *in vivo*.

2. Experimental section

2.1. Materials.

The following compounds were purchased from Sigma-Aldrich, and were used without further purification: (3-aminopropyl)triethoxysilane (APTES), cetyltrimethylammonium bromide (CTAB), ammonium nitrate, tetraethyl orthosilicate (TEOS), fluorescein isothiocyanate (FITC), methacrylic acid (MAA), pyridine, p-toluenesulfonic acid, toluene, dichloromethane (DCM), dihydropyran (DHP), dibenzocyclooctyne-amine (DBCO-amine), dimethylformamide (DMF), 2-(2-methoxyethoxy) ethyl methacrylate (MEO_2MA), 4,4'-azobis(4-cyanovaleric acid) (ABCVA), diethyl ether, hexylamine, 4-cyano-4-[(dodecylsulfanylthiocarbonyl)sulfanyl]pentanoic acid (CDTPA), triethylamine (TEA), N,N-diisopropylethylamine (DIPEA), N-hydroxysuccinimide (NHS), N,N'-dicyclohexylcarbodiimide (DCC), phosphate-buffered saline (PBS), methoxypolyethylene glycol maleimide (MAL-PEG-OMe), poly(ethylene glycol) [N-(2-maleimidoethyl)carbamoyl]ethyl ether 2-(biotinylamino)ethane average M_n 3800 Da (MAL-PEG-BIOTIN), poly(ethylene glycol) (N-hydroxysuccinimide 5-pentanoate) ether *N*′-(3-maleimidopropionyl)aminoethane average M_n 4000 Da (MAL-PEG-NHS), 4-hydroxyazobenzene-2-carboxylic acid (HABA)/avidin kit, doxorubicin and fluorescein sodium salt. Tetramethylrhodamine Azide (TAMRA-N_3) was purchased from Thermo Fisher Scientific, and used without further purification. Dulbecco's Modified Eagle's Medium (DMEM), penicillin–streptomycin, and trypsin–EDTA were purchased from Invitrogen (Fisher Scientific, Spain). Fetal bovine serum (FBS) was purchased from Biowest (Labclinics, Spain).

2.2.Characterization techniques.

Characterization of the materials used in this study was performed by the following techniques: thermogravimetry and differential thermal analysis (TGA/DTA) in a PerkinElmer Pyris Diamond TG/DTA analyzer, with 10 ºC/min heating ramps, from 25 ºC to 600 ºC. Fourier transform infrared (FTIR) spectra were obtained in a Nicolet Nexus spectrometer (Thermo Fisher Scientific) equipped with a Smart Golden Gate attenuated total reflectance (ATR) accessory. Transmission electron microscopy (TEM) was carried out in a JEOL JEM 2100 instrument operated at 200 kV, equipped with a CCD camera (KeenView Camera). Phosphotungstic acid (PTA) was used to stain organic matter in the hybrid materials. N_2 adsorption was carried out on a Micromeritics ASAP 2010 instrument; surface area was

obtained by applying the Brunauer–Emmett–Teller (BET) method to the isotherm and the pore size distribution was determined by the Barrett–Joyner–Halenda (BJH) method from the desorption branch of the isotherm. Mesopore diameter was obtained from the maximum of the pore size distribution curve. Z potential and hydrodynamic size of nanoparticles by Dynamic Light Scattering (DLS) were measured by means of a Zetasizer Nano ZS (Malvern Instruments) equipped with a 633 nm "red" laser. ^{1}H NMR experiments were carried out in a Bruker AV 250 MHz apparatus. Mass spectra were acquired with a Voyager DE-STR Biospectrometry Matrix-Assisted Laser Desorption/Ionization-Time Of Flight (MALDI-TOF) mass spectrometer. To determine the molecular weight distribution of the copolymers, Gel Permeation Chromatography (GPC) was performed in a Waters Alliance automatic analysis system with a Model #2695 separations module coupled to a Model #2414 Refractive Index Detector. GPC measurements were carried out using polyethylene (Glycol/ Oxide) standards and DMF with LiCl 10 mM as the eluent.

The Lower Critical Solution Temperature (LCST) of the polymers was determined by DLS by means of the drastic change in the scattering intensity obtained by the precipitation of the polymer at the LCST (determined as the temperature at which the scattering intensity is 50 % of the maximum). To determine the transition temperature, the temperature dependence of the scattering intensity of a polymer solution was measured. The temperature was increased by discrete temperature increments in the range 10-45 ºC.

Fluorescence spectrometry was used to determine cargo release by means of a Biotek Synergy 4 device. Fluorescence microscopy was performed in an Evos FL Cell Imaging System equipped with tree Led Lights Cubes (λ_{Ex} (nm); λ_{Em} (nm)): DAPI (357/44; 447/60), GFP (470/22; 525/50), RFP (531/40; 593/40) from AMG (Advance Microscopy Group). Quantitative analysis of cellular uptake was performed by flow cytometry in a BD FACSCalibur™ cytometer, and results were processed using Flowing Software.

2.3. Preparation of PEGylated ultrasound-responsive system.

2.3.1 Synthesis of Mesoporous Silica Nanoparticles.

MSNs were synthesized by a condensation reaction of TEOS in the presence of CTAB template under dilute, basic conditions, as described elsewhere.[12] FITC-labeled MSNs were synthesized by reacting 1 mg of FITC with 2.2 μL APTES in 100 μL ethanol for 2 h. Then, the reaction mixture was added with TEOS to obtain the FITC-labeled MSNs, following the same protocol as before.

2.3.2 Synthesis of Ultrasound-Responsive Copolymer.

The monomer tetrahydropyranyl methacrylate (THPMA) was synthesized and purified as previously described.[12,15]

The random copolymer poly(2-(2-methoxyethoxy) ethyl methacrylate-co-2-tetrahydropyranyl methacrylate), with two functional ends and a monomer ratio 90:10 (MEO_2MA:THPMA), was obtained by Reversible Addition-Fragmentation Chain Transfer (RAFT) polymerization, adding CDTPA, ABCVA, MEO_2MA and THPMA in a Schlenk flask. The flask was purged with N_2 and 8 mL dry DMF were added, with a catalytic amount of DIPEA to protect THPMA from degradation during the synthesis. Then, the flask was deoxygenated by three freeze-pump-thaw cycles. The reaction mixture was placed at 80 ºC under N_2 overnight with magnetic stirring. The obtained polymer was then precipitated and washed with diethyl ether. During synthesis optimization, different monomers/CDTPA ratios (Table S1) were used to obtain US-responsive polymers (PUS, Figure 1) with different molecular weights. Depending on the length of the polymers, each specific sample was named as follows: *ca.* 25000 Da (small, PUS_S), *ca.* 50000 Da (medium, PUS_M) and *ca.* 70000 Da (large, PUS_L).

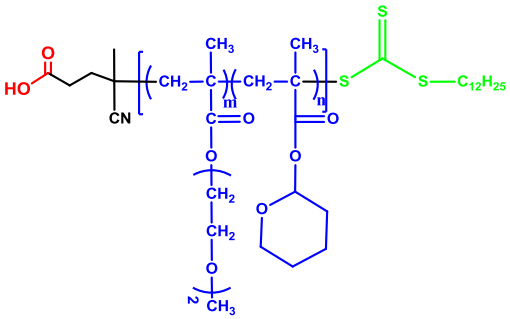

Figure 1. Structure of the obtained US-responsive polymer, PUS, obtained by RAFT polymerization.

2.3.3 Preparation of PEGylated Ultrasound-Responsive Copolymer.

PEGylation of the obtained RAFT random copolymers was carried out by reacting MAL-PEG-OMe with the copolymer after the aminolysis of the trithiocarbonate group from CDTPA, which gives rise to a thiol moiety that reacted with the maleimide through a thiol-ene click reaction. This was performed as a one-pot reaction, by adding the MAL-PEG-OMe to the solution where the aminolysis was going to take place. Three PUS-PEG samples were obtained, PUS_S-PEG, PUS_M-PEG and PUS_L-PEG, depending on the PUS used. The conditions to obtain PUS_L-PEG were: 500 mg of PUS_L and 100 mg of MAL-PEG-OMe were

dissolved in 14 mL of dry DMF under inert atmosphere. The solution was deoxygenated by bubbling N_2. Then, 500 µL of dry DMF containing 5 µL of hexylamine and 5 µL of TEA were added (to obtain PUS_M-PEG and PUS_S-PEG, the amount of MAL-PEG-OMe, hexylamine and TEA were adjusted to keep the same molar ratios as described above). The reaction took place overnight at room temperature, under N_2 and with magnetic stirring. Then, the polymers were precipitated in diethyl ether. After evaporating the ether, the solid was dissolved in ice-cold water. After heating the solution to 50 ºC, the precipitate formed was centrifuged and washed with preheated water. The purified polymer was then freeze-dried to obtain PUS-PEG.

2.3.4 Grafting PEGylated Ultrasound-Responsive Copolymer to MSNs.

Polymer grafting on the surface of MSNs to obtain HYBRID-PEG was performed as described previously.[12] Depending on the molecular weight of the polymeric gate being grafted, three different materials were obtained: $HYBRID_S$-PEG, $HYBRID_M$-PEG and $HYBRID_L$-PEG. To prepare $HYBRID_L$-PEG, 200 mg of PUS_L-PEG were conjugated with APTES (5 µL) using DCC (4 mg) and NHS (2 mg) under N_2 in 3 mL dry DMF at room temperature, overnight, under magnetic stirring. Then, this sililated copolymer was reacted with previously dispersed MSNs (35 mg) in toluene at 80 ºC, overnight. The addition of the polymer to the MSNs suspension in toluene was performed in three steps, leaving 4 h gaps between additions to prevent polymer-to-polymer condensation. The hybrid nanoparticles so obtained, $HYBRID_L$-PEG, were then collected by centrifugation and washed with toluene, DMF (3 times), cold water (3 times) and ethanol. Then, the nanoparticles were dried under vacuum. To obtain $HYBRID_M$-PEG and $HYBRID_S$-PEG, the amount of APTES, DCC and NHS were adjusted to keep the same molar ratios as used above.

2.4 Preparation of Actively-targeted PEGylated ultrasound-responsive system.

2.4.1 Synthesis of Biotin-targeted nanoparticles.

The polymer PUS_L-PEG-BIOTIN was synthesized in a similar way to the one described for PUS-PEG (section 2.3.3), grafting MAL-PEG-BIOTIN to the US-responsive copolymer PUS_L obtained by RAFT. Then, this polymer containing biotin was reacted with MSNs to obtain $HYBRID_L$-PEG-BIOTIN, in a similar way as described above (section 2.3.4). In this case, half of the polymer chains had the moiety of interest, while the other half were PUS-PEG chains without further modification.

2.4.2 Synthesis of RGD-targeted nanoparticles.

The synthesis of the material *HYBRID$_L$-PEG-RGD* was carried out in two steps: First, we prepared the hybrid containing DBCO moieties (HYBRID$_L$-PEG-DBCO), which was then reacted with an azide-functionalized peptide containing the RGD sequence: N_3-Lys-Cys-**Arg-Gly-Asp**-Arg (RGD-N_3).

(a) HYBRID$_L$-PEG-DBCO: The polymer dibenzocyclooctyne-polyethilenglicol-maleimide, MAL-PEG-DBCO, was synthesized as follows: 14 mg of DBCO-amine derivate were dissolved in the minimum amount possible of methylene chloride anhydrous. Under inert atmosphere, 10 µL of DIPEA were added and the mixture was stirred 30 minutes at room temperature (solution A). On the other hand, 40 mg of MAL-PEG-NHS were also dissolved in the minimum amount of dichloromethane under nitrogen atmosphere (solution B). Solution A was added dropwise over solution B and the resulted mixture was stirred overnight at 40 ºC (Scheme 1). The methylene chloride was removed under vacuum and the resulting crude was purified by silica flash column chromatography using DCM:MeOH (30:1) as eluent. The final product was characterized by ^{1}H NMR, and the spectrum can be found in Figure S1.

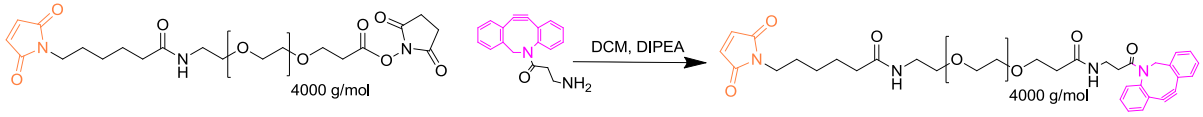

Scheme 1. Synthesis reaction employed to obtain MAL-PEG-DBCO.

Then, PUS$_L$-PEG-DBCO was synthesized in a similar way as described for PUS$_L$-PEG-BIOTIN (section 2.3.1), by grafting the synthesized MAL-PEG-DBCO to the US-responsive copolymer PUS$_L$ obtained by RAFT. This PUS$_L$-PEG-DBCO was reacted with MSNs to obtain the HYBRID$_L$-PEG-DBCO similarly as described for the preparation of the hybrid containing biotin (section 2.3.1).

(b) HYBRID$_L$-PEG-RGD: Initially, the peptide RGD-N_3 was synthetized following the standard solid-phase techniques using Fmoc-coupling chemistry (Scheme S1). Amino acids were added sequentially to build the peptide sequence on a solid resin. After the coupling of each amino acid, the solid resin was washed and deprotection of the last amino acid incorporated was performed to allow the coupling of the next one. The final functionalized Wang resin was treated with TFA/TIPS/H_2O cleavage cocktail in order to

afford a peptide crude that was purified by G-25 Sephadex column size exclusion chromatography. ^{1}H NMR spectrum can be found in Figure S2.

To obtain RGD-modified particles, HYBRID$_L$-PEG-RGD, 4 mg of HYBRID$_L$-PEG-DBCO nanoparticles were reacted with RGD-N_3 (2 mg) in water at 4 ºC under magnetic stirring overnight. Then, the nanoparticles were collected by centrifugation and washed once with cold water and twice with preheated PBS (37 ºC).

2.5 Cargo loading and release.

Fluorescein loading was performed by dispersing the HYBRID-PEG material (10 mg) in a solution of fluorescein (100 mg) in PBS (5 mL) and stirring overnight at 4 ºC, since the polymeric gate will be open at that temperature. The medium was then heated to 37 ºC and the particles were collected by centrifugation. The loaded nanoparticles were extensively washed with PBS at 37 ºC.

Doxorubicin loading was performed in a similar way using RGD-targeted nanoparticles: 4 mg of HYBRID$_L$-PEG-RGD were loaded with doxorubicin in 2.5 mL of PBS containing 1 mg/mL of the drug at 4 ºC overnight.

Release experiments were performed as follows: Fluorescein-loaded materials dispersed in PBS were exposed to a commercial laboratory ultrasound device before starting the experiment (1.3 MHz, 100 W, 10 min, continuous wave (CW), conditions used in our previous work).[12] The experiment was carried out placing aliquots of suspensions of the loaded material in 12 well plate Transwell inserts (0.5 mL per insert), and adding 1.5 mL PBS to the outer volume of the well. At each time point, the external volume was collected and analyzed, and the well was filled with 1.5 mL of fresh PBS (to ensure sink conditions). The samples were measured by fluorimetry to determine the amount of fluorescein released (λ_{Ex}: 490 nm; λ_{Em}: 514 nm). Same procedure was carried out with samples without US exposure.

2.6 Cell culture experiments.

Cell culture experiments with HeLa cells were carried out to evaluate nanoparticle uptake by the cells, as well as cell viability when incubated with drug-loaded nanoparticles. HeLa cells were seeded in 24 well plates at a density of 20,000 cells per cm^2 24 h before the experiments were performed.

For the nanoparticle uptake experiments, cells were incubated with 200 µg/mL suspension of the nanoparticles (with or without the targeting moiety) in complete culture

medium (DMEM with 10% FBS). The particles were incubated with the cells overnight, and then they were removed and the cells were washed with PBS to remove non-internalized nanoparticles. Cellular uptake was evaluated by fluorescence microscopy and flow cytometry.

For the cytotoxicity experiment, RGD-targeted nanoparticles ($HYBRID_L$-PEG-RGD), loaded with doxorubicin were incubated with the cells overnight (100 µg/mL suspension). Then, the cells were rinsed with PBS, and half of the wells were exposed to ultrasound (using a physiotherapy device, New Pocket Sonovit, New Age Italia Srl, Italy) from the top of the well totally filled with culture medium (1 MHz, 3 W/cm^2, 5 min, CW). The cells were then further incubated with 1 mL of complete culture medium per well. At different time points, cell viability was evaluated by Alamar Blue assay (Promega, Spain) following the manufacturer's instructions.

3. Results and Discussion

3.1 PEGylated ultrasound-responsive system

We have recently developed an ultrasound-responsive hybrid Mesoporous Silica Nanocarrier (HYBRID) capable of inducing cargo release when exposed to High Frequency Ultrasound.[12] That material was obtained by grafting a thermo-and ultrasound-responsive random copolymer, p(MEO_2MA-co-THPMA) to the surface of MCM 41-type MSNs. Before ultrasound exposure, the copolymer shows a Lower Critical Solution Temperature (LCST) lower than 37 ºC, so the polymer will be collapsed on the nanoparticle surface, capping its pores. After US exposure, the US-sensitive monomer THPMA will be cleaved, inducing an increase in the LCST behavior of the polymer, which will change to a coil-like conformation, inducing cargo release at physiological temperature.[12,16]

However, that proof-of-concept material presents several problems when considering an *in vivo* scenario. For example, the polymeric gate closes the pores of the material when collapsing on its surface due to the thermoresponsive behavior of the polymer.[12] This implies that, when the material is closed, the surface is highly hydrophobic and the particles would therefore be likely to aggregate. Furthermore, this material also lacks of any type of active targeting moieties, which are thought to be of great importance for the efficacy of nanotherapeutics.[3] Both problems could be potentially addressed by the attachment of PEG chains with a targeting agent to the exposed end of the polymer. The aim of this work is to adapt the proof-of-concept material previously reported to a more useful one, PEGylated and

actively targeted. However, the chemical strategies employed in our previous work would not enable to carry out this modification in an easy fashion.

In order to attach a PEG molecule to the US-responsive copolymer, a bifunctional polymer must be obtained first. That way, one functional end will be used to graft a PEG chain while the other one will be attached to the nanoparticle surface. The polymer presented in our previous work,[12] which was obtained by Free Radical Polymerization (FRP), only possessed one functional end, with a carboxylic acid provided by the initiator ABCVA. An US responsive copolymer with two different functional ends has been here obtained by changing the synthetic procedure from FRP to RAFT polymerization by using a trithiocarbonate RAFT agent (CDTPA) that also presents a carboxylic acid. The monomer ratio was kept at 90:10 (MEO_2MA:THPMA) according to our previous results.[12] ^{1}H NMR spectra confirmed the correct synthesis of the desired copolymers (Figure S3). US-Responsive copolymers, PUS, with different molecular weights were obtained (PUS_S, PUS_M and PUS_L) by modifying the monomers/RAFT agent ratio,[17] as shown in Table 1. This allowed us to evaluate the effect of the molecular weight of the polymeric gate on the behavior of the final material. The molecular weight of the polymers was successfully controlled by modifying the monomer:CDTPA ratio, obtaining longer chains when more monomer molecules were available for each RAFT agent molecule. The polymers had yellow color due to the presence of the trithiocarbonate group from the RAFT agent, which confirmed the integrity of CDTPA through the polymerization reaction.[18,19]

Table 1. GPC data of the different PUS obtained in this work before and after coupling with MAL-PEG-OMe (PUS-PEG)

PUS sample	M_n (Da)	PDI	PUS-PEG sample	M_n (Da)	PDI	PEG M_n (Da)
PUS_S	25624	1.19	**PUS_S-PEG**	26599	1.22	2000
PUS_M	46776	1.56	**PUS_M-PEG**	51880	1.68	5000
PUS_L	67030	1.63	**PUS_L-PEG**	73061	1.78	5000

The aminolysis of the trithiocarbonate was carried out in the presence of a maleimide-modified PEG to graft it to the above RAFT copolymers. A one-pot thiol-ene click reaction took place, coupling the PEG chain to our US-responsive copolymers,[19] obtaining PUS-PEG polymers (Scheme 2) with different molecular weights (Table 1). After purification, the ^{1}H NMR spectra of the obtained copolymers confirms the PEG grafting (signal between 3.6 and 3.7 ppm) (Figure S3). Table 1 shows an increase in the molecular weight of the copolymers after the PEGylation process in the same range as the molecular weights of the PEG chains being grafted. Furthermore, the absence of smaller polymer chains in the GPC

chromatograms (data not shown) confirms the purification of the PEGylated copolymers from unreacted PEG chains.

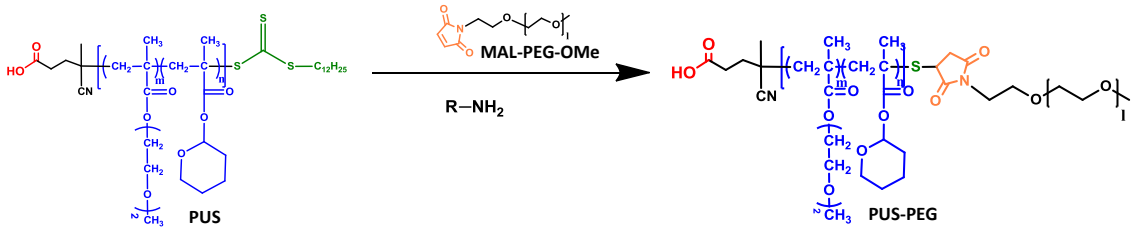

Scheme 2. Representation of the synthetic procedure employed to obtain PUS-PEG.

The US-responsiveness of the copolymer after conjugation with PEG was checked by monitoring the LCST behavior before and after ultrasound exposure. The results show that our PUS-PEG presents a LCST below 37 ºC in water before the application of US (Figure 2). This behavior implies that at physiological temperature the polymer will be collapsed on the nanoparticle surface, effectively capping the pores and preventing the premature release of the drug. After US application, the LCST is shifted to values above 45 ºC. This change is due to the cleavage of the hydrophobic THPMA and its conversion to hydrophilic MAA, which induces a change in the overall hydrophilicity of the p(MEO_2MA-co-THPMA) block, displacing the LCST to a higher temperature.[12] The US-responsiveness of PUS-PEG was independent of its molecular weight (data not shown). This US-responsive behavior will provide the induced release capability in the final hybrid material.

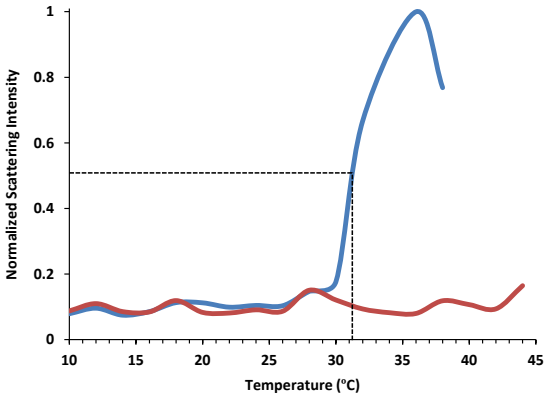

Figure 2. Lower critical solution temperature (LCST) of PUS_L-PEG before (blue) and after 10 min (red) of ultrasound application (1.3MHz, 100 W, CW). A 1 mg/mL solution in water was used.

Once the US-responsiveness of PUS-PEG had been shown, it was then conjugated with APTES through its carboxylic acid (*via* DCC/NHS chemistry) and grafted to the surface of MSNs by condensation with the silanol groups of the silica particle,[12] as shown in Scheme 3.

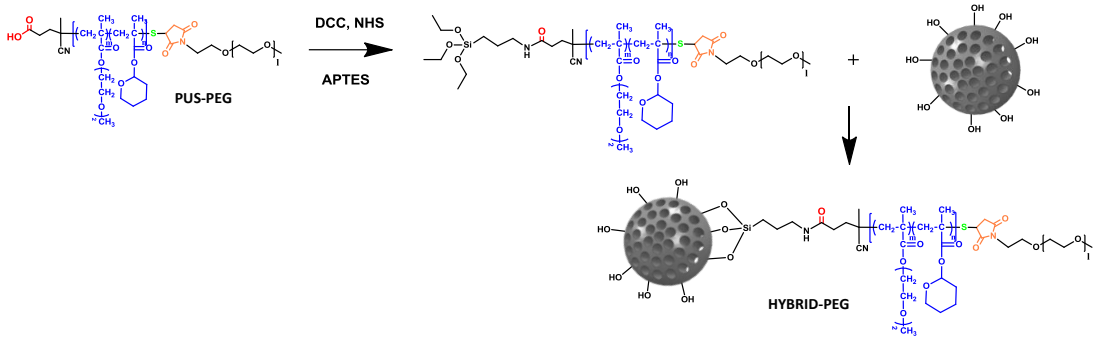

Scheme 3. Synthetic procedure employed to obtain the PEGylated Ultrasound-responsive material, HYBRID-PEG.

The different PEGylated US-responsive copolymers presented in Table 1 were grafted to MSNs to obtain the PEGylated hybrid materials, HYBRID-PEG, which can be seen in Table 2. The organic matter percentage (determined by TGA) is similar (24-29 %) regardless of the molecular weight of the grafted polymer. This data indicate a successful grafting of the polymers to the silica nanoparticles. However, significant differences can be found in the BET surface area, with decreasing values being obtained as the molecular weight of the polymers increased (Table 2).

Table 2. Effect of molecular weight of the grafted copolymer on the organic matter %, BET surface area and % of dye released from HYBRID-PEG samples.

Samples	Organic matter % (TGA)	BET surface area (m^2/g)	Pore volume (cm^3/g)	% Fluorescein released after 20 h
$HYBRID_S$-PEG	24.93	634	0.55	80
$HYBRID_M$-PEG	24.04	585	0.39	45
$HYBRID_L$-PEG	28.82	188	0.13	23

The different PEGylated hybrid materials prepared were loaded with fluorescein. The percentage of dye released in PBS at 37 ºC was measured after 20 h to test if the PEGylated US-responsive polymers effectively block the pore entrances of the nanoparticles. Data collected in Table 2 indicates that the molecular weight of the RAFT polymer was found to be crucial on capping the pores to block premature cargo release. Thus, higher molecular weight (M_n) led to less release of fluorescein. This result is in good agreement with previous work reported in the literature, showing that the molecular weight of polymers used as capping agents of MSNs drastically affects their efficiency.[20] Longer polymer chains form larger aggregates when they collapse on the surface of the silica particle, acting as a more effective capping agent (Table 2). This is also in consonance with BET surface areas mentioned above for those same materials.

It is worth noting that the M_n needed to effectively cap the pores in this work is significantly higher than what we had seen in our preceding paper (around 28000 Da).[12] This different behavior can be explained by the change in the polymer synthetic method. RAFT polymerization allows a much better control over the polymerization reaction compared to FRP.[21] By employing RAFT polymerization, the molecular weight distribution of the obtained copolymers is narrower than that obtained by FRP (PDI values around 2). Therefore, for the same M_n, the polymers obtained by FRP will present a significant percentage of polymer chains with a much larger size than the mean, which could have contributed to a better seal at the pore ends. According to these results, the hybrid material with the largest polymeric gate, HYBRID$_L$-PEG, was selected for all further experiments.

Once HYBRID$_L$-PEG had been selected, a more extensive characterization of the material further confirmed the successful grafting of PUS$_L$-PEG on the material surface. Figure 3 shows the TEM micrographs of MSN and HYBRID$_L$-PEG, where the highly ordered mesoporous structure of the nanoparticles can be observed. Those same TEM micrographs of HYBRID$_L$-PEG (Figure 3) show a PTA-stained layer on the nanoparticle surface not present on MSN, corresponding to the polymeric gate, and confirming the successful grafting of the polymer to the nanoparticle surface. The FTIR spectrum of HYBRID$_L$-PEG (Figure 3) shows the typical bands of the polymer, between 1400 and 1800 cm^{-1}. The hydrodynamic diameter obtained by DLS indicates a peak size of 250 nm, with Z potential values of -45 mV. Hydrodynamic diameter of MSN was 220 nm with a Z potential value of -21 mV. These data confirm the correct grafting of a PEGylated polymeric gate capable of blocking premature cargo release from the mesopores of the material at physiological temperature.

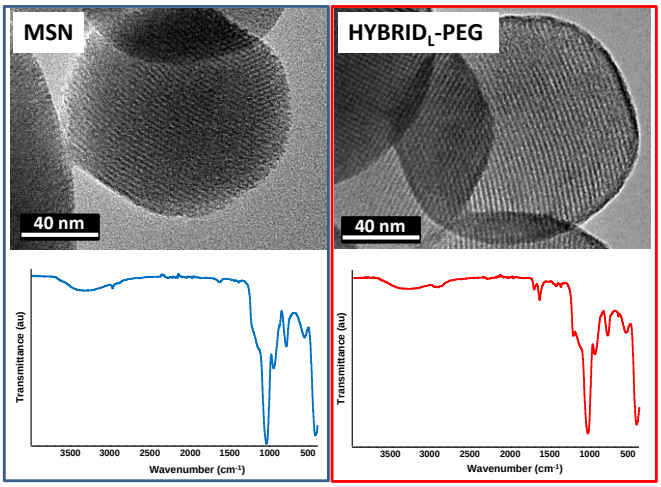

Figure 3. Characterization of MSN (left) and HYBRID$_L$-PEG (right). TEM micrographs showing polymeric coating stained with PTA (top), FTIR spectra of the materials (bottom).

The stability of this new PEGylated hybrid material ($HYBRID_L$-PEG) was compared with our previously reported non-PEGylated hybrid material (HYBRID),[12] using FITC-labeled nanoparticles (Figure 4). The particles were dispersed in PBS (1 mg/mL of nanoparticles) and a photograph of the suspensions was taken. The suspensions were then kept at 37 ºC for 1 h without stirring, and they were then re-evaluated under visible and ultraviolet (UV) light. HYBRID nanoparticles can be clearly observed at the bottom of the cuvette (better assessed by the fluorescence of nanoparticles under UV light), while $HYBRID_L$-PEG nanoparticles remain much better dispersed. This result indicates that the stability of the nanoparticle suspension was greatly improved in the PEGylated system, which was one of the main aims of our approach. Besides, PEGylation is known to extend circulation time after injection *in vivo*,[13,22] due to a slow withdrawal from the circulation by organs from the Mononuclear phagocyte system (MPS).

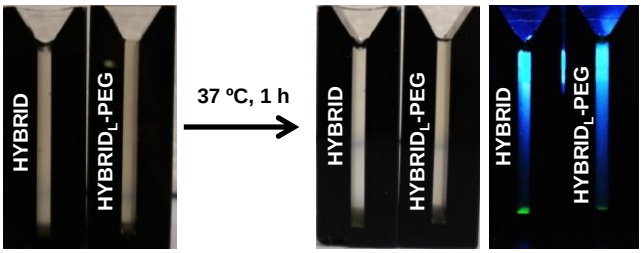

Figure 4. Suspension stability of HYBRID and $HYBRID_L$-PEG. Photographs taken under visible (left, center) or UV light (right).

Finally, the US-responsiveness of $HYBRID_L$-PEG was evaluated performing fluorescein release experiments. The material should be capable of retaining the cargo at 37 ºC, and releasing it in response to the application of US as an external stimulus. Figure 5 shows that fluorescein release was greatly enhanced when US is applied on a loaded $HYBRID_L$-PEG suspension.

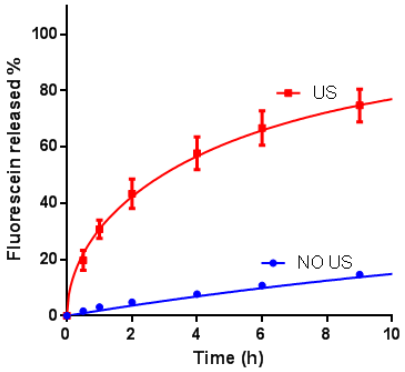

Figure 5. *In vitro* fluorescein release from $HYBRID_L$-PEG without or with US exposure (10 min, 1.3 MHz, 100 W, CW).

These results indicate that the US-induced cargo release capability is retained in this PEGylated material, and its behavior is comparable to that obtained in our previous work.[12] This US-responsive behavior would enable the cargo to be released mostly in the tumor environment, improving the safety and efficacy profile of the system.

3.2 Targeted PEGylated ultrasound-responsive system

Heretofore, we have successfully obtained a PEGylated material that can trigger the release of its cargo when exposed to US. However, no active targeting strategy had been implemented to enhance the specificity of this material. To address the need for active targeting molecules, a different hybrid material was obtained by a similar process, but employing biotin-conjugated PEG, MAL-PEG-BIOTIN (Scheme 4). Consequently, the biotin moiety will be present on the end of the PEG chain attached to the polymeric gate on the nanoparticle surface. Biotin, also known as vitamin B7, can be employed as an active targeting agent due to the overexpression of biotin receptors by a variety of cancer cells.[23] The amount of biotin molecules present in HYBRID$_L$-PEG-BIOTIN was quantified by the HABA/Avidin test, and the value obtained (2.13 nmol biotin/mg of nanoparticles) was in close agreement with the value expected from the TGA and the M_n of the attached polymer.

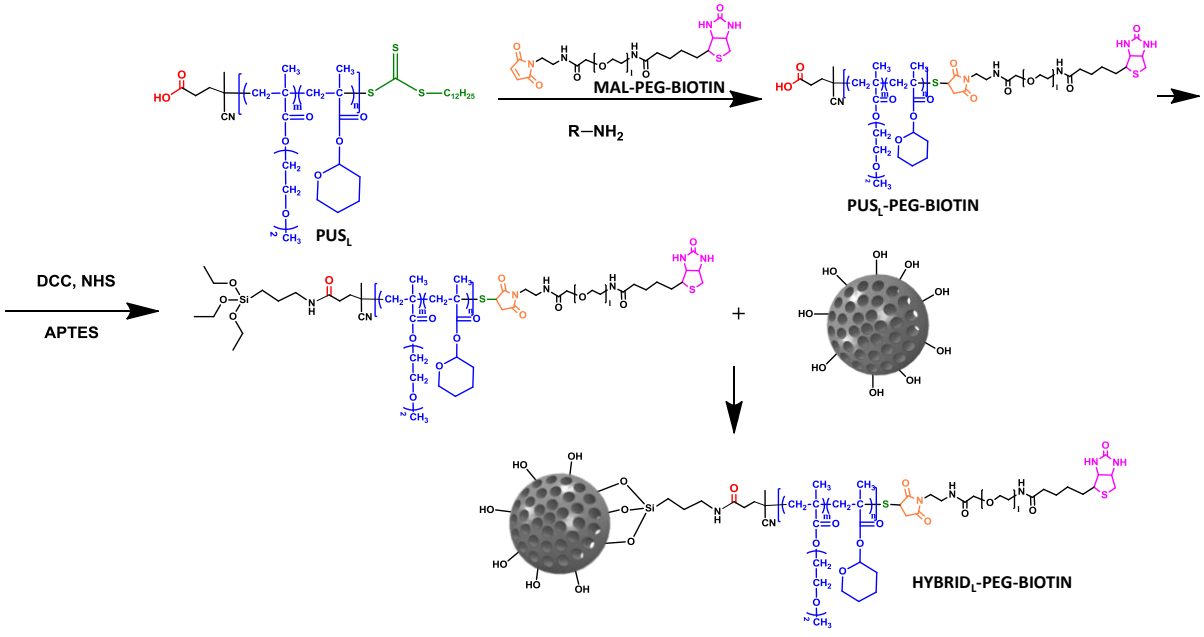

Scheme 4. Synthetic procedure employed to obtain the PEGylated, biotin-targeted ultrasound-responsive material, HYBRID$_L$-PEG-BIOTIN.

An *in vitro* cellular uptake experiment was performed to test the efficacy of the biotin molecules exposed by our nanoparticles as active targeting agents. Incubation of non-targeted

and targeted PEGylated nanoparticles ($HYBRID_L$-PEG and $HYBRID_L$-PEG-BIOTIN) with HeLa cells, which have been reported to overexpress biotin receptors,[24] shows a significantly increased cellular uptake of biotin-modified nanoparticles, as can be seen from fluorescence microscopy and flow cytometry data (Figure 6).

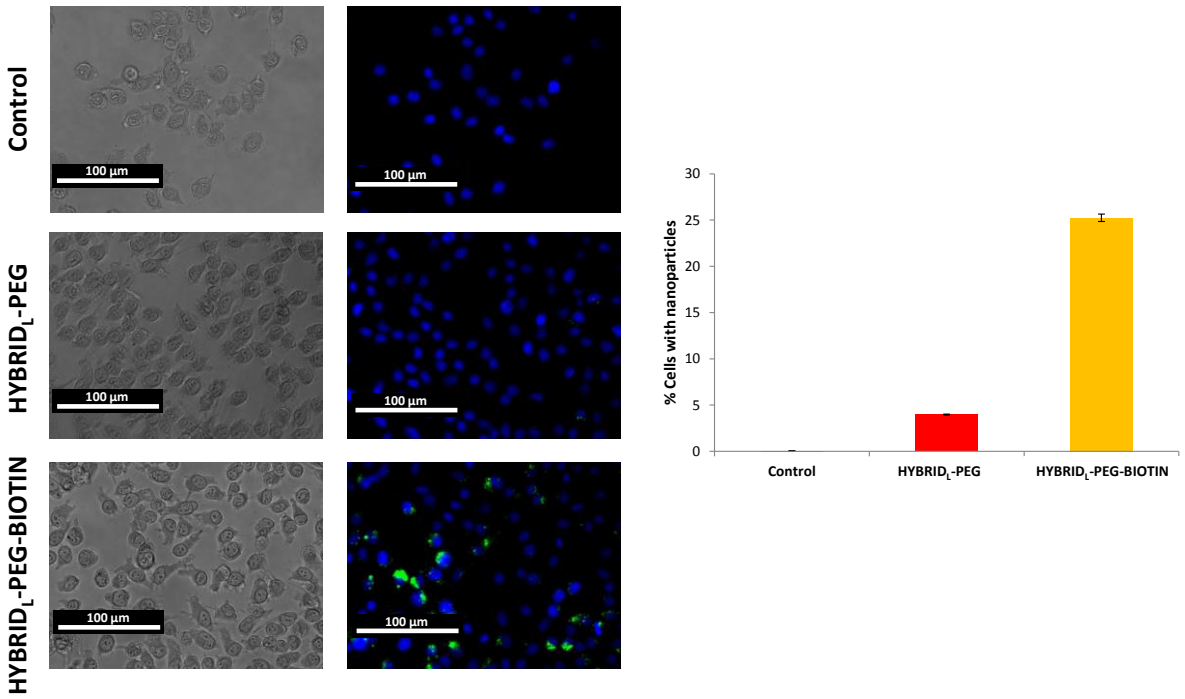

Figure 6. Uptake experiments in HeLa cells comparing $HYBRID_L$-PEG and $HYBRID_L$-PEGBIOTIN by fluorescence microscopy (left, showing cell nuclei in blue and nanoparticles in green) and flow cytometry (right).

These results confirm the possibility to attach a targeting moiety to the external surface of our US-responsive nanocarrier, allowing a selective delivery to specific types of cancer cells. Taking into account the chemical strategies employed to obtain our final system, there is a very limited amount of targeting agents that can be conjugated to the PEG chain before it is coupled with the polymeric gate and then grafted to the particles. Any molecule possessing free amines, carboxylic acids, thiols or maleimides can interfere with the subsequent reactions, giving rise to undesired side-products.

A modular device was designed to provide more versatility to our US-responsive system. Our approach consisted on conjugating a strained alkyne (the DBCO moiety) to a PEG molecule, which also presents a maleimide group in the other end, MAL-PEG-DBCO (Scheme 1). This would allow carrying out the grafting process as already described (Scheme 5), and then coupling the desired targeting agent to the already prepared hybrid system,

HYBRID$_L$-PEG-DBCO, by using a copper-free alkyne-azide cycloaddition. The DBCO moiety will react with azide-functionalized molecules to yield a stable triazole linkage.

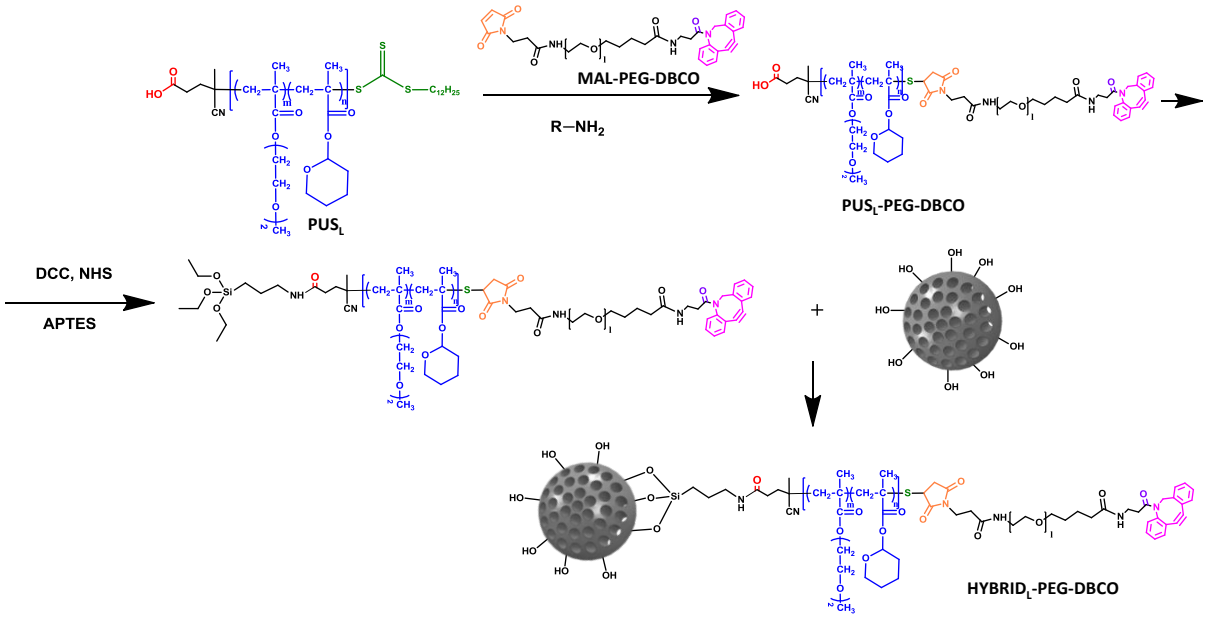

Scheme 5. Synthetic procedure employed to obtain the PEGylated, DBCO-modified ultrasound-responsive material, HYBRID$_L$-PEG-DBCO.

Before grafting any targeting molecules, a coupling reaction with an azide-dye (TAMRA-N_3) was performed to ensure the presence and availability of the DBCO moiety in the material (Supporting Information). That way, sample color and/or fluorescence could be used to test if the click reaction has taken place. After reaction of HYBRID-PEG-DBCO with TAMRA-N_3, sample fluorescence indicates a successful reaction with the dye (Figure S4). Same results were obtained with the intermediate products (MAL-PEG-DBCO, PUS$_L$-PEG-DBCO). This demonstrates the correct coupling of DBCO and that it is available to react through click chemistry. On the other hand, no reaction with the dye takes place in the materials not carrying DBCO. All of these results indicate that it is possible to graft an azide-modified molecule to our HYBRID$_L$-PEG-DBCO. These results open the gate for endless easy modifications of the material, fine-tuning the targeting capacity of the system towards specific cell lines, once the US-responsive material has already been prepared.

The versatility of this methodology has been tested by attaching a targeting agent to HYBRID$_L$-PEG-DBCO and evaluating its cellular uptake. A peptide containing the RGD (Arg-Gly-Asp) sequence was used as the active targeting agent to be anchored to HYBRID$_L$-PEG-DBCO. This sequence is selectively recognized by αvβ3 integrin receptor, and has been extensively studied as an active targeting agent for anticancer therapies.[25] Several functional

groups present in this molecule (like amines and carboxylic acids) would not allow us to include this peptide in the PEGylated polymeric gate, due to incompatibility issues with the polymer grafting methodology above described. For this reason, the RGD sequence was attached to HYBRID$_L$-PEG-DBCO by copper-free azide-alkyne cycloaddition using an azide-functionalized peptide, RGD-N_3 (Scheme S1) to obtain HYBRID$_L$-PEG-RGD (Figure 7).

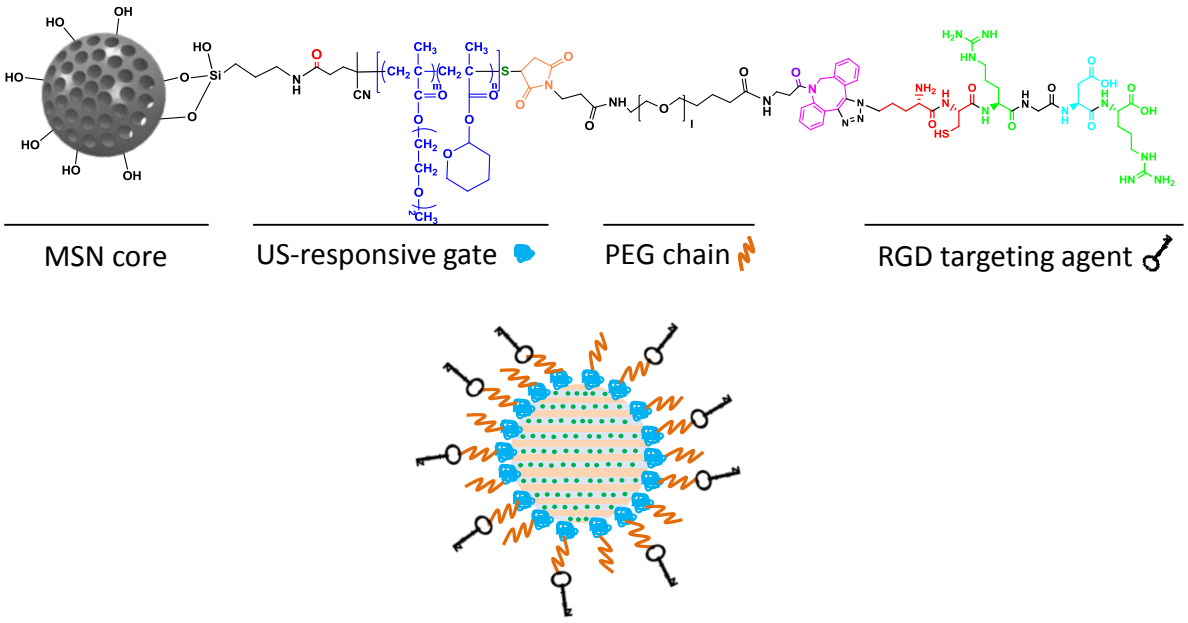

Figure 7. Structure of the obtained PEGylated RGD-targeted US-responsive hybrid mesoporous silica nanoparticles, HYBRID$_L$-PEG-RGD.

Cellular uptake studies were carried out with HeLa cells, which also overexpress integrins capable of interacting with the RGD sequence.[26] Figure 8 shows a significantly increased uptake in RGD-containing nanoparticles (HYBRID$_L$-PEG-RGD). This result highlights the successful development of our modular strategy to obtain an actively-targeted material. Further, a competition assay with the addition of free RGD in the medium shows a decrease in the internalization of HYBRID$_L$-PEG-RGD, indicating a receptor-mediated uptake mechanism.

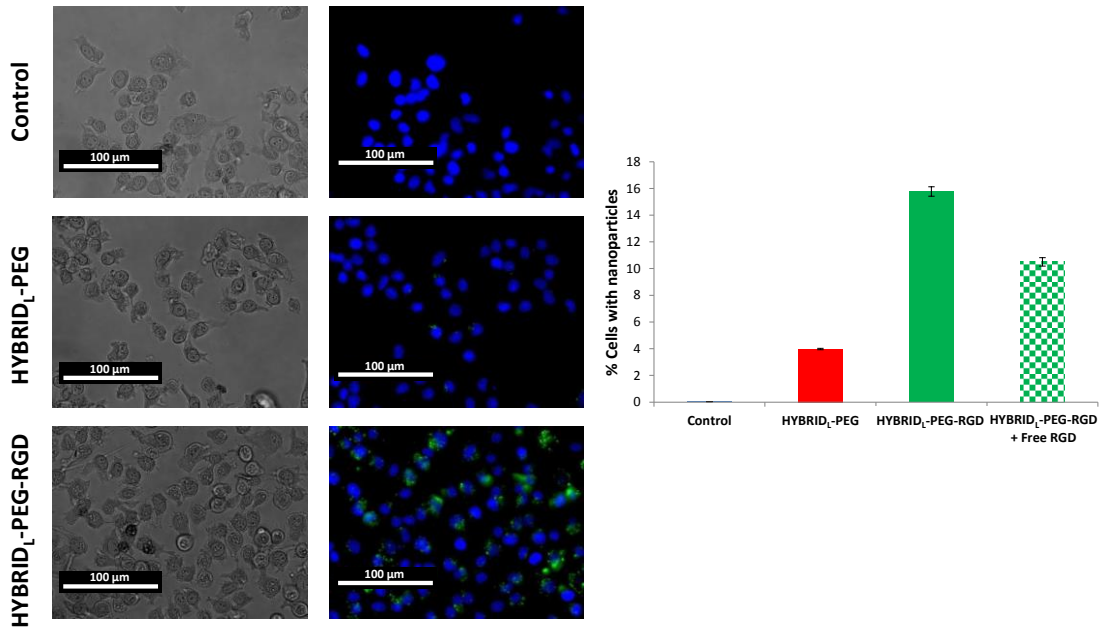

Figure 8. Uptake experiments in HeLa cells comparing HYBRID$_L$-PEG and HYBRID$_L$-PEG-RGD by fluorescence microscopy (left, showing cell nuclei in blue and nanoparticles in green) and flow cytometry (right).

Finally, and since the material presented in this work is aimed for anticancer therapy, these actively-targeted nanoparticles must be able to kill cancer cells upon US exposure when loaded with a cytotoxic drug. According to the cellular uptake results, the targeted system (HYBRID$_L$-PEG-RGD) was selected for our cytotoxicity experiment with drug-loaded nanoparticles. Doxorubicin-loaded HYBRID$_L$-PEG-RGD nanoparticles were incubated with HeLa cells overnight. Some of the cells were then exposed to ultrasound using a physiotherapy device, and cell viability was evaluated by Alamar Blue test over the next three days (Figure 9). Ultrasound itself was shown not to have any significant effect on cell viability. Ultrasound-exposed nanoparticles showed significantly higher cytotoxicity on HeLa cells than the ones not exposed to the stimulus, denoting the greater doxorubicin release upon US application. This further indicates that we have obtained a PEGylated, modularly-targeted, ultrasound responsive drug carrier that could be applied for further studies in the field of cancer nanomedicine. Nanoparticle uptake by the target cancer cells will be enhanced by the addition of an active targeting molecule, and the external application of ultrasound in the tumor area will induce the release of the cytotoxic drug loaded in the nanoparticle, killing the cancer cells while decreasing the undesired side effects of chemotherapy.

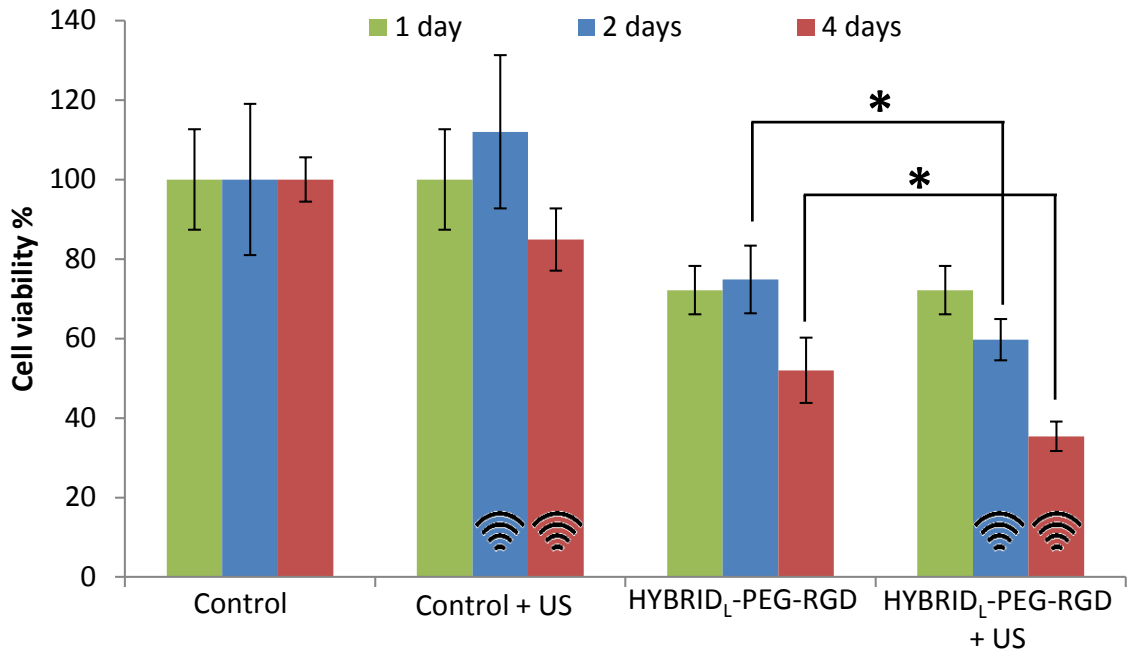

Figure 9. Cytotoxicity assay measured by Alamar Blue test in HeLa cells at different time points (1, 2 and 4 days) after incubation with doxorubicin-loaded HYBRID$_L$-PEG-RGD. Samples without US exposure and with US exposure (1 MHz, 3 W/cm^2, 5 min, CW) were evaluated (US was applied after measuring the 1 day time point). *$p < 0.05$ (Student's *t*-test).

Conclusions

A PEGylated and targeted modular ultrasound-responsive nanocarrier based on Mesoporous Silica Nanoparticles has been successfully obtained by modifying the chemical strategies employed previously to obtain a proof-of-concept stimulus-responsive material.

First, a non-targeted PEGylated material possessing US-promoted cargo release was obtained and characterized. That PEGylated material showed increased stability in aqueous suspension when compared to its non-PEGylated control, which is of great interest for its biomedical application.

By further modifying the material, a modular nanocarrier was obtained, in which any targeting agent could be easily attached to the final system through click chemistry. By taking advantage of that modularity of the material, RGD-decorated nanoparticles were obtained and demonstrated to induce enhanced cellular uptake. Drug-loaded RGD-targeted PEGylated nanoparticles were shown to produce significantly increased cancer cell killing when exposed to ultrasound.

References

1. Wicki, A., Witzigmann, D., Balasubramanian, V. & Huwyler, J. Nanomedicine in cancer therapy: Challenges, opportunities, and clinical applications. *J. Control. Release* **200,** 138–157 (2015).
2. Fang, J., Nakamura, H. & Maeda, H. The EPR effect: Unique features of tumor blood vessels for drug delivery, factors involved, and limitations and augmentation of the effect. *Adv. Drug Deliv. Rev.* **63,** 136–151 (2011).
3. Bertrand, N., Wu, J., Xu, X., Kamaly, N. & Farokhzad, O. C. Cancer nanotechnology: the impact of passive and active targeting in the era of modern cancer biology. *Adv. Drug Deliv. Rev.* **66,** 2–25 (2014).
4. Mura, S., Nicolas, J. & Couvreur, P. Stimuli-responsive nanocarriers for drug delivery. *Nat. Mater.* **12,** 991–1003 (2013).
5. Chen, Y., Ai, K., Liu, J., Sun, G., Yin, Q. & Lu, L. Multifunctional envelope-type mesoporous silica nanoparticles for pH-responsive drug delivery and magnetic resonance imaging. *Biomaterials* **60,** 111–120 (2015).
6. Song, N., Liu, W., Tu, Q., Liu, R., Zhang, Y. & Wang, J. Preparation and in vitro properties of redox-responsive polymeric nanoparticles for paclitaxel delivery. *Colloid Surf. B-Biointerfaces* **87,** 454–63 (2011).
7. Lai, J., Mu, X., Xu, Y., Wu, X., Wu, C., Li, C., Chen, J. & Zhao, Y. Light-responsive nanogated ensemble based on polymer grafted mesoporous silica hybrid nanoparticles. *Chem. Commun.* **46,** 7370–7372 (2010).
8. Guisasola, E., Baeza, A., Talelli, M., Arcos, D., Moros, M., de la Fuente, J. M. & Vallet-Regí, M. Magnetic-Responsive Release Controlled by Hot Spot Effect. *Langmuir* **31,** 12777–12782 (2015).
9. Sirsi, S. R. & Borden, M. A. State-of-the-art materials for ultrasound-triggered drug delivery. *Adv. Drug Deliv. Rev.* **72,** 3–14 (2014).
10. Vallet-Regí, M., Rámila, A., del Real, R. P. & Pérez-Pariente, J. A New Property of MCM-41: Drug Delivery System. *Chem. Mater.* **13,** 308–311 (2001).
11. Argyo, C., Weiss, V., Bräuchle, C. & Bein, T. Multifunctional Mesoporous Silica Nanoparticles as a Universal Platform for Drug Delivery. *Chem. Mater.* **26,** 435–451 (2014).
12. Paris, J. L., Cabañas, M. V., Manzano, M. & Vallet-Regí, M. Polymer-Grafted Mesoporous Silica Nanoparticles as Ultrasound-Responsive Drug Carriers. *ACS Nano* **9,** 11023–11033 (2015).
13. Cauda, V., Argyo, C. & Bein, T. Impact of different PEGylation patterns on the long-term bio-stability of colloidal mesoporous silica nanoparticles. *J. Mater. Chem.* **20,** 8693–8699 (2010).
14. Baeza, A., Manzano, M., Colilla, M. & Vallet-Regí, M. Recent advances in mesoporous silica nanoparticles for antitumor therapy: our contribution. *Biomater. Sci.* **4,** 803–813 (2016).
15. Lee, J.-T., George, M. C., Moore, J. S. & Braun, P. V. Multiphoton Writing of Three-Dimensional Fluidic Channels within a Porous Matrix. *J. Am. Chem. Soc.* **131,** 11294–11295 (2009).
16. Xuan, J., Boissière, O., Zhao, Y., Yan, B., Tremblay, L., Lacelle, S., Xia, H. & Zhao, Y. Ultrasound-Responsive Block Copolymer Micelles Based on a New Amplification Mechanism. *Langmuir* **28,** 16463–16468 (2012).
17. Chen, J., Liu, M., Chen, C., Gong, H. & Gao, C. Synthesis and Characterization of Silica Nanoparticles with Well-Defined Thermoresponsive PNIPAM via a Combination of RAFT and Click Chemistry. *ACS Appl. Mater. Interfaces* **3,** 3215–

3223 (2011).
18. Boyer, C., Granville, A., Davis, T. P. & Bulmus, V. Modification of RAFT-polymers via thiol-ene reactions: A general route to functional polymers and new architectures. *J. Polym. Sci. Part A Polym. Chem.* **47,** 3773–3794 (2009).
19. Qiu, X. P. & Winnik, F. M. Facile and efficient one-pot transformation of RAFT polymer end groups via a mild aminolysis/michael addition sequence. *Macromol. Rapid Commun.* **27,** 1648–1653 (2006).
20. Popat, A., Liu, J., Lu, G. Q. & Qiao, S. Z. A pH-responsive drug delivery system based on chitosan coated mesoporous silica nanoparticles. *J. Mater. Chem.* **22,** 11173–11178 (2012).
21. Liu, R., Fraylich, M. & Saunders, B. R. Thermoresponsive copolymers: from fundamental studies to applications. *Colloid Polym. Sci.* **287,** 627–643 (2009).
22. He, Q., Zhang, J., Shi, J., Zhu, Z., Zhang, L., Bu, W., Guo, L. & Chen, Y. The effect of PEGylation of mesoporous silica nanoparticles on nonspecific binding of serum proteins and cellular responses. *Biomaterials* **31,** 1085–1092 (2010).
23. Ren, W. X., Han, J., Uhm, S., Jang, Y. J., Kang, C., Kim, J.-H. & Kim, J. S. Recent development of biotin conjugation in biological imaging, sensing, and target delivery. *Chem. Commun.* **51,** 10403–10418 (2015).
24. Yang, W., Cheng, Y., Xu, T., Wang, X. & Wen, L. P. Targeting cancer cells with biotin-dendrimer conjugates. *Eur. J. Med. Chem.* **44,** 862–868 (2009).
25. Accardo, A., Tesauro, D. & Morelli, G. Peptide-based targeting strategies for simultaneous imaging and therapy with nanovectors. *Polym. J.* **45,** 481–493 (2013).
26. Oba, M., Aoyagi, K., Miyata, K., Matsumoto, Y., Itaka, K., Nishiyama, N., Yamasaki, Y., Koyama, H. & Kataoka, K. Polyplex Micelles with Cyclic RGD Peptide Ligands and Disulfide Cross-Links Directing to the Enhanced Transfection via Controlled Intracellular Trafficking. *Mol. Pharm.* **5,** 1080–1092 (2008).

Supporting Information

From proof-of-concept material to PEGylated, modularly targeted ultrasound-responsive mesoporous silica nanoparticles.

Table S1. Amount of different reagents employed to obtain PUS samples with different molecular weights.

PUS sample	CDTPA (mg)	ABCVA (mg)	MEO_2MA (mL)	THPMA (mL)
PUS_S	15	4	1.8	0.2
PUS_M	8	3	1.8	0.2
PUS_L	5	2	1.8	0.2

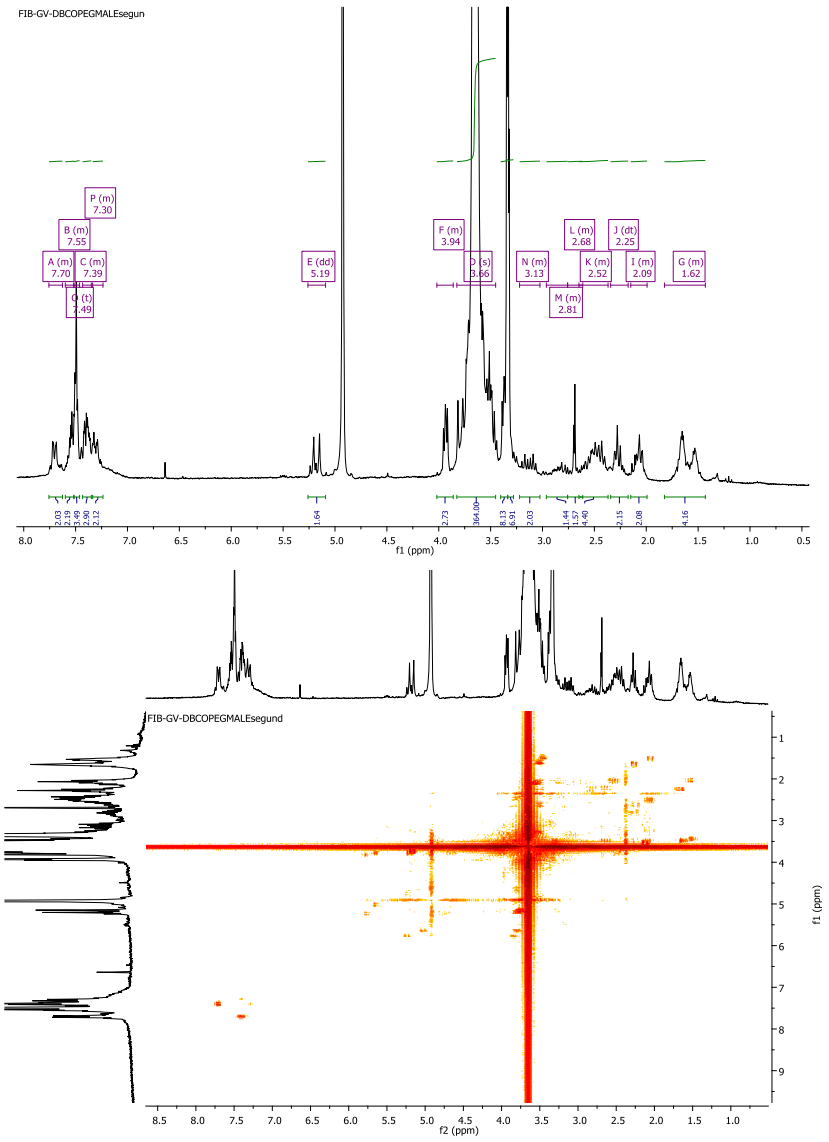

Figure S1. ^{1}H NMR spectrum and ^{1}H NMR COSY of MAL-PEG-DBCO in MeOD.

^{1}H NMR (250 MHz, MeOD) δ 7.69 (ddd, *J* = 14.0, 10.2, 3.8 Hz,2H, 2xCHAr, DBCO), 7.60 – 7.51 (m, 2H, 2xCHAr, DBCO), 7.49 (m, 4H, 2xCH, maleimide, 2xCHAr, DBCO), 7.39 (ddd, *J* = 8.9, 3.7, 2.2 Hz, 2H, 2xCHAr, DBCO), 7.30 (dt, *J* = 8.7, 5.1 Hz, 2H, , 2xCHAr, DBCO), 5.20 (s, *J* = 8.6 Hz, 1H, CH_2, DBCO), 5.15 (s, 1H, CH_2, DBCO), 4.02 – 3.86 (m, 2H, CH_2-N, maleimide), 3.66 (s, broad, 364 H, 90x(CH_2-CH_2-O), PEG), 3.22 – 3.02 (m, 2H, CH_2-NHCO), 2.96 – 2.76 (m, 2H, CH_2-NHCO), 2.65 – 2.37 (m, 4H, 2xCH_2-CONH), 2.26 (dd, *J* = 13.0, 5.8 Hz, 2H, CH_2, maleimide chain), 2.08 (dd, *J* = 12.5, 5.4 Hz, 2H, CH_2, maleimide chain), , 1.82 – 1.57 (m, 2H, CH_2, maleimide chain), 1.58 – 1.46 (m, 2H, CH_2, maleimide chain).

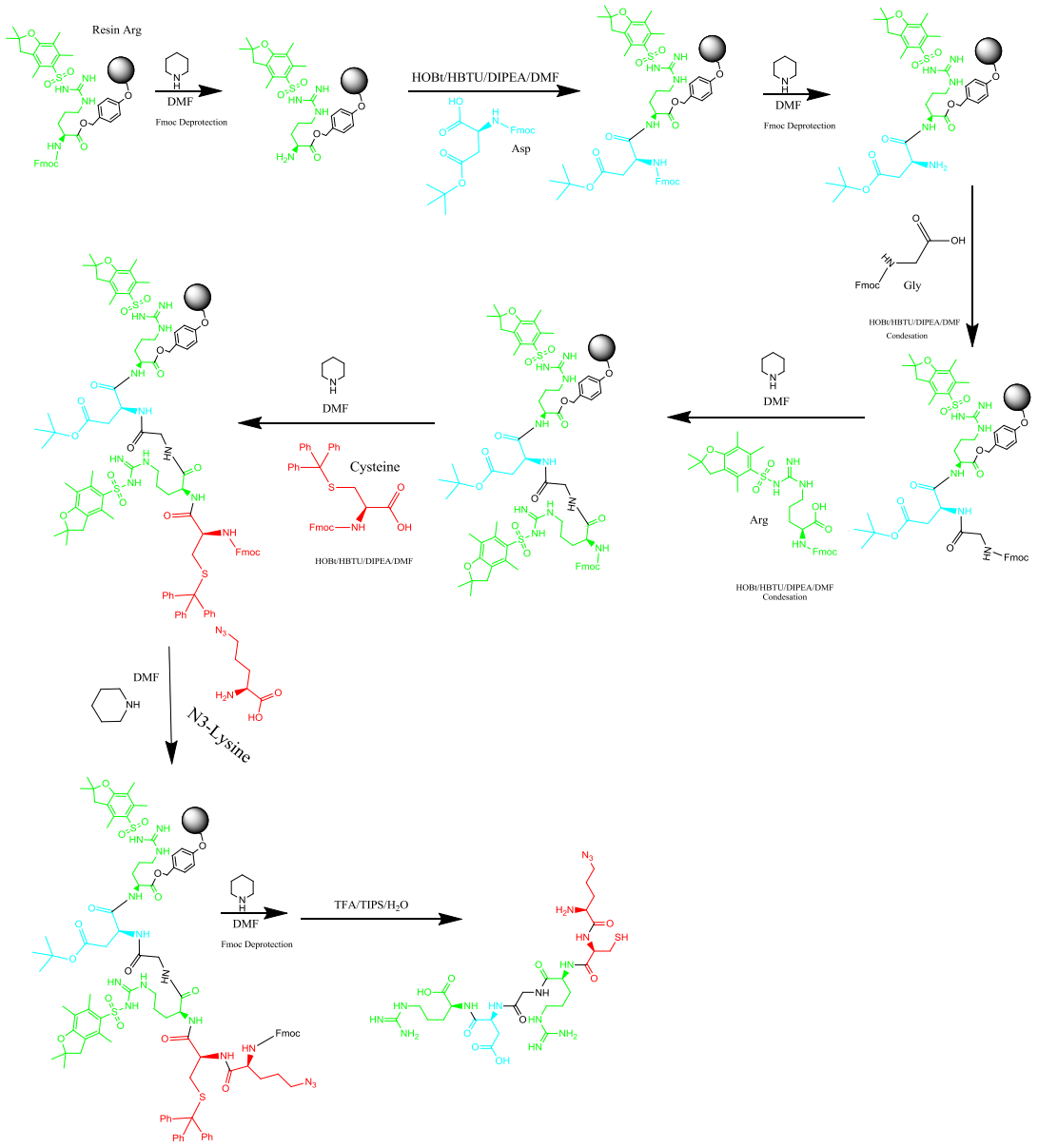

Scheme S1. Synthesis scheme employed to obtain RGD-N_3 by standard solid-phase techniques using Fmoc-coupling chemistry.

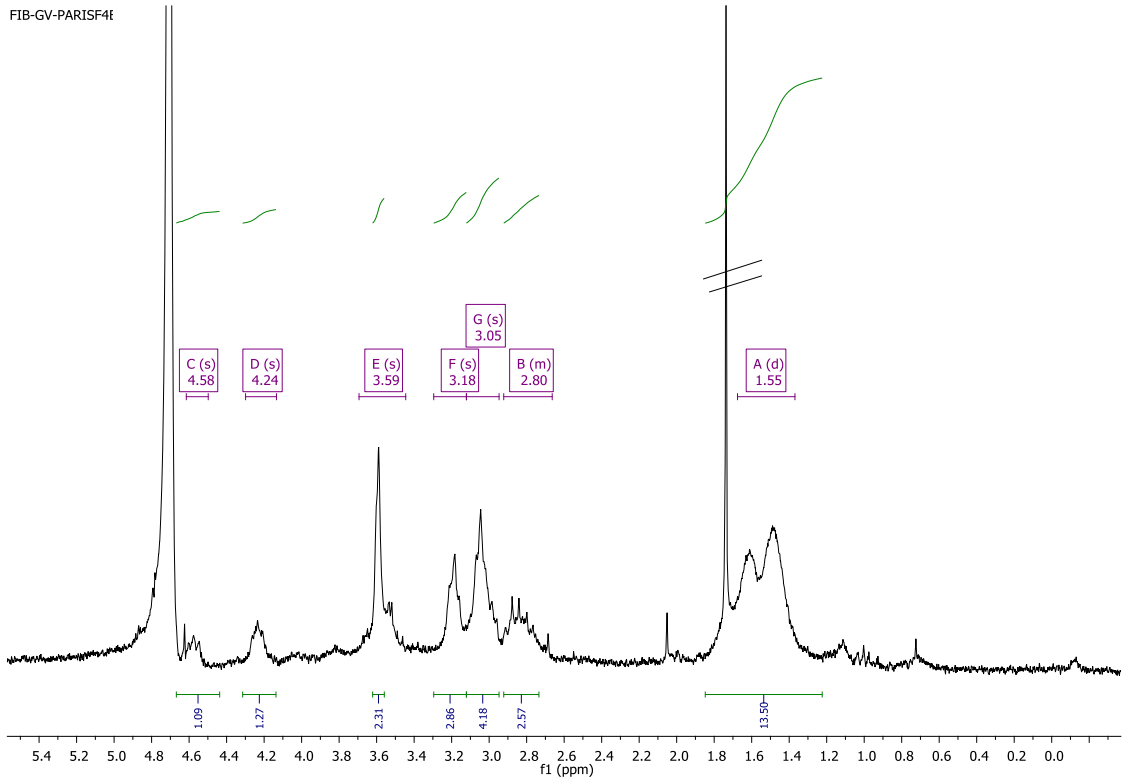

Figure S2. ^{1}H NMR spectrum of RGD-N_3 in D_2O.

^{1}H NMR (250 MHz, D_2O) δ 4.58 (1H, CH, Cys); 4.35 – 4.10 (2H, 2xCH, Arg), 3.60 (s, broad, 2H, CH_2, Gly), 3.33 – 3.13 (m, 3H, CH_2, Cys, CH Lys-N_3), 2.85 (s, broad, 4H, 2xCH_2, Arg), 2.83 – 2.64 (m, 2H, CH_2, Asp), 1.60 (s, broad, 6H, 2xCH_2, 2xArg, CH_2, Lys-N_3), 1.50 (s, broad, 8H, 2xCH_2, Lys-N_3, 2xCH_2, 2xArg).

MALDI/TOF/TOF= 713.080 m/z [M^+-SH] (100%);

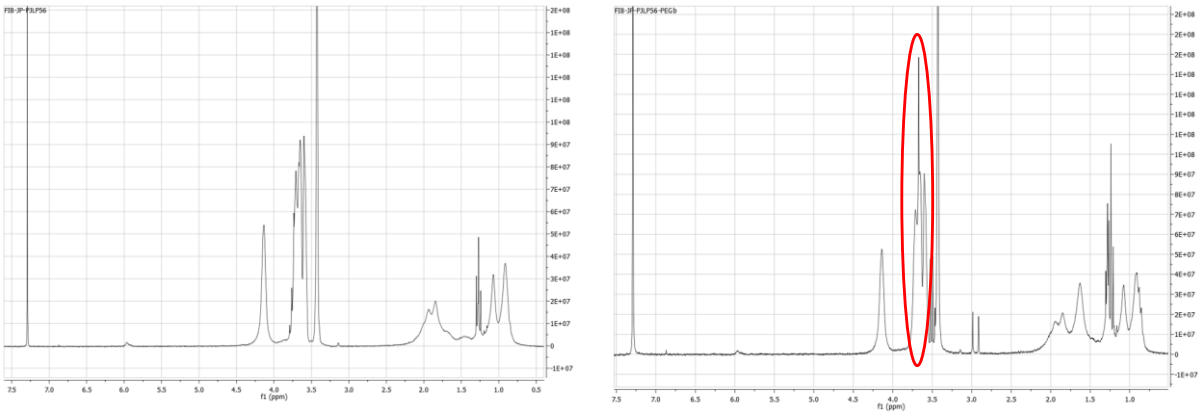

Figure S3. ^{1}H NMR spectra of PUS_L (left) and PUS_L-PEG (right) in $CDCl_3$.

Copper-Free Azide–Alkyne Cycloaddition with TAMRA-N_3

To react TAMRA-N_3 with MAL-PEG-DBCO, 2 mg of MAL-PEG-DBCO were dissolved in 300 µL of PBS and 2 µL of the stock TAMRA-N_3 solution were added (1 mg/mL in DMSO). The mixture was stirred at 37 ºC for 1 h. Then, the polymer was purified by G-25 Sephadex column size exclusion chromatography.

For the reaction of TAMRA-N_3 with PUS_L-PEG-DBCO, 10 mg of PUS_L-PEG-DBCO were dissolved in 1 mL of cold deionized (DI) water, and 2 µL of the stock TAMRA-N_3 solution were added. The mixture was stirred at 4 ºC overnight, and the polymer was then precipitated in diethyl ether and centrifuged.

To conjugate TAMRA-N_3 with DBCO-modified hybrid, 3 mg of $HYBRID_L$-PEG-DBCO were dispersed in 500 µL of DI water, and 6 µL of the stock TAMRA-N_3 solution were added. The mixture was stirred at 4 ºC overnight. The material was then collected by centrifugation and thoroughly washed with ethanol and cold water.

TAMRA fluorescence emission was then checked in DI water (Ex: 555 nm; Em: 575 nm) (Figure S4).

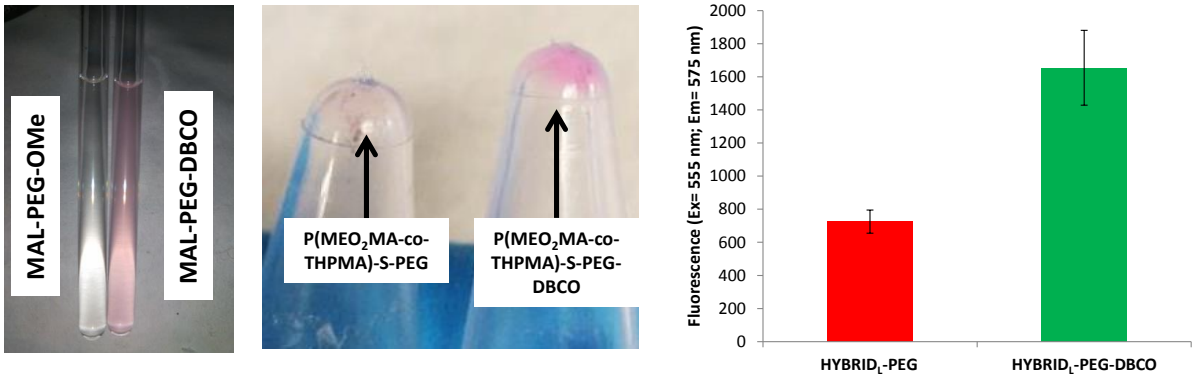

Figure S4. Reaction with TAMRA-N_3 of MAL-PEG-DBCO (left), PUS_L-PEG-DBCO (center) and $HYBRID_L$-PEG-DBCO (right). Control experiments were performed using MAL-PEG-OMe, PUS_L-PEG and $HYBRID_L$-PEG.

3.2.2 Mesoporous silica nanoparticles with ultrasound-induced uptake by cancer cells

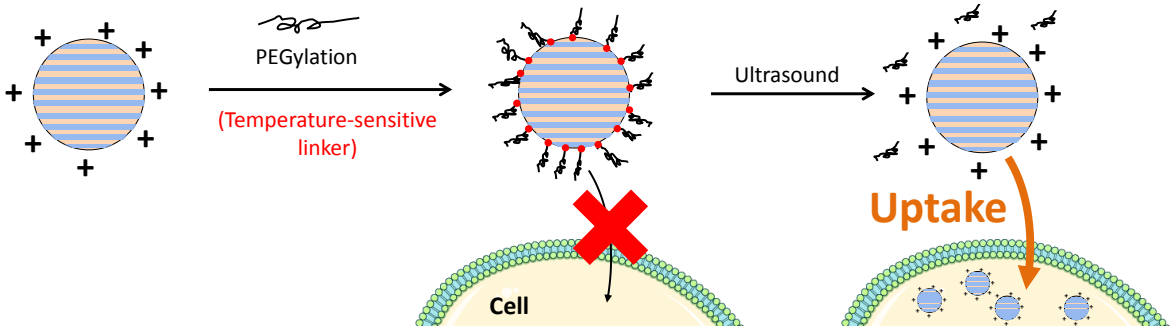

Mesoporous silica nanoparticles with ultrasound-induced uptake by cancer cells

Abstract

A novel smart hierarchical ultrasound-responsive mesoporous silica nanocarrier for cancer therapy is here presented. This dynamic nanosystem has been designed to display different surface characteristics during its journey towards tumor cells. Initially, the nanocarriers are shielded with a polyethylene glycol layer. Upon exposure to high frequency ultrasound, the polymer shell detaches from the nanoparticles, exposing a positively-charged surface. That favors the internalization in human osteosarcoma cells, where release of topotecan takes place, drastically enhancing the cytotoxic effect.

Introduction

The use of nanoparticles in medicine, in the so-called nanomedicine, has the potential of drastically improving cancer diagnostics and therapy.[1] In this sense, the selective accumulation of nanoparticles in tumor tissues due to the Enhanced Permeation and Retention (EPR) effect has been used as the main rationale to develop nanoparticle-based drug delivery devices as therapeutic agents for cancer treatment,[2,3] some of which have already reached the market.[4] Grafting polyethylene glycol (PEG) chains on the surface of nanoparticles, a process known as PEGylation, has been proven as an effective way of increasing the circulation time of nanoparticles in the bloodstream, thereby allowing a higher dose of the nanocarrier to reach the tumour.[5] However, nanoparticle uptake by cells is hindered after PEGylation.[5] Besides the passive accumulation of nanoparticles in tumor tissues due to the EPR effect, active targeting strategies have been extensively studied to improve the efficacy of nanomedicines.[2] However, active targeting is often accompanied by a series of disadvantages of its own. For example, PEGylated nanoparticles exposing targeting agents are withdrawn faster from systemic circulation than PEGylated nanoparticles without further modification.[6] This decrease in nanoparticle circulation time can indeed diminish the therapeutic efficacy of these nanocarriers. Additionally, the presence of targeting agents with a very high affinity for the target cells can also induce a paradoxical effect: cancer cells in the first line of the tumor tissue will interact with the nanoparticles in a very strong manner,

retaining the particles in the periphery of the tumor and effectively preventing their distribution to deeper areas.[7] This effect has been called the "binding site barrier".

Hierarchical targeting strategies have been developed to overcome the above limitations of targeted nanomedicines.[6] In these approaches, a targeting moiety is included in the formulation in a way that it remains hidden during nanoparticles transport along the bloodstream and it is later exposed once they reach the target tissue by passive accumulation. Cellular uptake of these materials can be triggered by a stimulus, either internal (such as pH or redox conditions)[8] or external (such as light).[9] In this context, pathological changes in internal conditions, like pH, are not very exacerbated.[10] Additionally, clinicians do not hold any control over the behavior of nanoparticles sensitive to internal stimuli. Nanoparticles sensitive to external stimuli can be more selective in their response, since they will only be activated by the voluntary application of the stimulus. However, the level of penetration in the tissue and potential damage to surrounding healthy tissues could be limitations for external stimuli. For example, light is known to penetrate poorly in solid tissues, even though Near Infrared light can be employed to improve this parameter.[10]

High frequency ultrasound can non-invasively penetrate very deep into tissues and is well tolerated by the body.[10] When an ultrasound (US) wave propagates through living tissues in the body, several thermal and mechanical effects occur, including pressure variation, acoustic fluid streaming, cavitation and local hyperthermia, and these effects can be used for different medical applications.[11] In these sense, we recently employed US to successfully trigger doxorubicin release from Mesoporous Silica Nanoparticles (MSNs) in cancer cells.[12] However, the use of ultrasound to trigger hierarchical targeting materials remains largely unexplored. The objective of the present work is to develop a nanoparticle that can undergo ultrasound-promoted uptake by cancer cells, by means of an ultrasound-induced temperature increase.

As a model nanoparticle we have selected MSNs due to their facile synthesis and functionalization and their high physicochemical stability.[13,14] Additionally, the textural properties of MSNs, such as their high surface area and pore volume, will provide high loading capacity of different drugs.

Nanoparticle uptake by cells is generally enhanced by employing internalization ligands (targeting agents) or positively charged moieties on the surface of the nanoparticles.[6] Due to the simplicity and broad applicability of this charge-dependent approach, we chose the exposure of a positively charged surface as the mechanism to

induce cell internalization by using amine functionalized MSNs.[15] The positive charge on the nanoparticle surface will be hidden by grafting PEG chains on the nanoparticle surface through a thermosensitive linker. These PEG chains will be disengaged from the nanoparticles by subjecting the material to an ultrasound-induced temperature increase, exposing the positive charges of the particles. The concept of the material designed in this work is shown in Scheme 1.

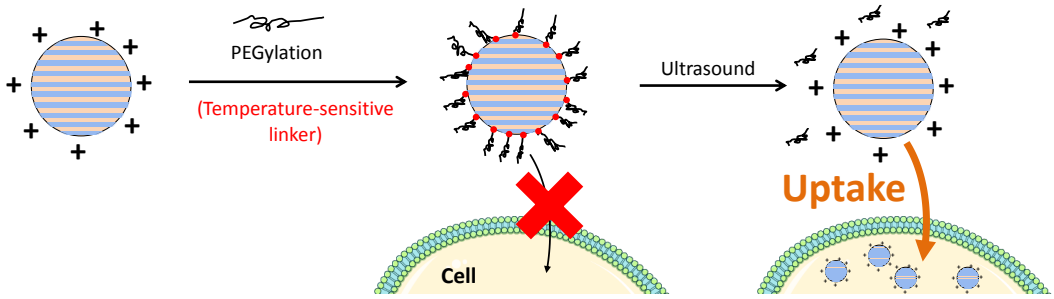

Scheme 1. Schematic representation of nanoparticle uptake by cells promoted by ultrasound-induced detachment of PEG shell from positively-charged MSNs.

Experimental section

Materials

The following compounds were purchased from Sigma-Aldrich Inc. (Spain): Ammonium nitrate, cetyltrimethylammonium bromide (CTAB), tetraethyl orthosilicate (TEOS), (3-aminopropyl)triethoxysilane (APTES), 9-Fluorenylmethoxycarbonyl (Fmoc) chloride, piperidine, poly(ethylene glycol) bis(amine) average M_n 3400 Da (NH_2-PEG-NH_2), dimethylformamide (DMF), N-hydroxysuccinimide (NHS), succinic anhydride, 4,4'-azobis(4-cyanovaleric acid) (ABCVA), N,N'-dicyclohexylcarbodiimide (DCC), phosphate-buffered saline (PBS), rhodamine-B isothyocianate (RBITC), fluorescein isothyocianate (FITC) and topotecan hydrochloride hydrate (TOP). Dulbecco's Modified Eagle's Medium (DMEM), penicillin-streptomycin, non-essential aminoacids, trypsin-EDTA were purchased from Invitrogen (Fisher Scientific, Spain). Fetal bovine serum is from Biowest (Labclinics, Spain). These compounds were used without further purification.

Characterization Techniques.

The materials were analyzed by small angle X-ray diffraction (XRD) in a Philips X'Pert Multipurpose Diffractometer (MPD) equipped with Cu Kα radiation. Fourier transformed infrared (FTIR) spectra were obtained in a Nicolet Nexus spectrometer

(Thermo Fisher Scientific) equipped with a Smart Golden Gate attenuated total reflectance (ATR) accessory. Thermogravimetry and differential thermal analysis (TGA/DTA) were performed in a PerkinElmer Pyris Diamond TG/DTA analyzer, with 10 ºC/min heating ramps, from room temperature to 600 ºC. ^{1}H NMR experiments were carried out in a Bruker AV 250 MHz apparatus. Surface morphology was analyzed by scanning electron microscopy (SEM) in a JEOL 6400 electron microscope. Z potential was measured in deionized water by means of a Zetasizer Nano ZS (Malvern Instruments) equipped with a 633 nm "red" laser. Fluorescence spectrometry was used to determine PEG detachment by means of a Biotek Synergy 4 device. Fluorescence microscopy was performed with an Evos FL Cell Imaging System equipped with three Led Lights Cubes (λ_{EX} (nm); λ_{EM} (nm)): DAPI (357/44; 447/60), GFP (470/22; 525/50), RFP (531/40; 593/40) from AMG (Advance Microscopy Group). Quantitative analysis of cellular uptake was performed by flow cytometry (FACS) in a BD FACSCalibur™ cytometer, and results were processed using Flowing Software. Ultrasound experiments were performed in a commercial laboratory ultrasound apparatus (RBI, France), working at 1.3 MHz and 100 W for 20 min, following similar conditions as those described in our previous work.[12]

Synthesis of PEGylated Mesoporous Silica Nanoparticles

Amino-functionalized mesoporous silica nanoparticles (MSN-NH_2) were obtained by a modified Stöber method from a mixture of TEOS and APTES (90:10 molar ratio) in the presence of CTAB as structure-directing agent under basic and very dilute conditions, as described elsewhere.[15] MSN-NH_2 labeled with FITC were also obtained by reacting 1 mg of FITC with 2.2 μL APTES in 100 μL ethanol for 2 h. Then, the reaction mixture was added with the TEOS and APTES solution as already described.

The quantification of amino groups available on MSN-NH_2 was performed by a Fmoc UV assay,[16] based on the reaction of Fmoc chloride with the amino groups to be quantified. Briefly, 50 mg of MSN-NH_2 were mixed with 125 mg of Fmoc chloride (excess), purged with nitrogen and dissolved in 3 mL of dry DMF under inert atmosphere. That solution was magnetically stirred overnight at room temperature. Then, the material was collected by centrifugation and washed with DMF, water (3 times) and ethanol (twice) to get rid of unbounded Fmoc. That material was dried under vacuum. Different portions were weighted and dispersed in 1 mL of a solution of 20 % piperidine in DMF to deprotect the amino groups and release the Fmoc from the

material. That reaction was performed under sonication for 20 min. After centrifugation, the absorbance of the supernatant at 301.5 nm was measured, and the amount of Fmoc released from the amines was measured. Once the amount of Fmoc released was known, the amount of amino groups per mg of material was extrapolated (molar ratio 1:1).

Before the PEGylation process, commercial NH_2-PEG-NH_2 was labeled with FITC (F-PEG-NH_2) or RBITC (R-PEG-NH_2) in order to be detected by green and red fluorescence, respectively. F-PEG-NH_2 was obtained by reacting 100 mg of NH_2-PEG-NH_2 with 11 mg of FITC (1:1 molar ratio) in 5 mL of dry DMF under inert atmosphere (N_2). The reaction was carried out at room temperature under magnetic stirring overnight (under inert atmosphere). Then, the reaction products were precipitated in diethyl ether and dried at room temperature. The products were dissolved in water and F-PEG-NH_2 was purified by size exclusion chromatography (Sephadex® G-25). ^{1}H NMR spectra of different fractions after liophylization were performed to select the desired product. R-PEG-NH_2 was obtained in a similar way, but using 16 mg of RBITC instead of FITC (to maintain the 1:1 molar ratio).

MSN-NH_2 functionalization with PEG was carried out through DCC/NHS chemistry using a thermosensitive linker such as ABCVA to obtain thermosensitive PEGylated nanoparticles (MSN-NH_2-T-PEG). Similar protocol was followed with succinic anhydride as a linker to prepare non-thermosensitive PEGylated nanoparticles (MSN-NH_2-PEG) to be used as control.

To obtain MSN-NH_2-T-PEG, 1.6 mg of ABCVA were activated with 3.4 mg of DCC and 1.9 mg of NHS in 2 mL of dry DMF under inert atmosphere with magnetic stirring at room temperature for 30 min. Then, 20 mg of F-PEG-NH_2 (or R-PEG-NH_2) dissolved in 1 mL of dry DMF were added and stirred for 2 h at room temperature (molar ratio of 1:1 with ABCVA). Finally, 20 mg of MSN-NH_2 nanoparticles dispersed in 1 mL of dry DMF were added. The reaction medium was stirred overnight and the product was collected by centrifugation and washed with DMF twice and with water 3 times. The material was then dried under vacuum.

To obtain MSN-NH_2-PEG, 20 mg of F-PEG-NH_2 (or R -PEG-NH_2) and 0.6 mg of succinic anhydride were dissolved in 2 mL of dry DMF under inert atmosphere, and the mixture was magnetically stirred at room temperature for 1.5 h. Then, 1.8 mg DCC and 1 mg of NHS dissolved in 1 mL of dry DMF were added and stirred for other 2 h. Then, 20 mg of MSN-NH_2 nanoparticles dispersed in 1 mL of dry DMF were added and reacted overnight. The material was purified as described above for MSN-NH_2-T-PEG.

Evaluation of stimuli-responsive PEG detachment from the material

To evaluate the detachment of PEG chains from MSN-NH_2-PEG or MSN-NH_2-T-PEG, nanoparticles with FITC-labeled PEG chains were employed. Several 1 mL aliquots of suspensions of those materials in PBS (1 mg/mL) were placed in an oven and subjected to two different thermal treatments: 37 ºC or 70 ºC overnight (samples were sealed to prevent any solvent evaporation). Additionally, suspensions of both nanoparticle types were exposed to US by using a commercial laboratory ultrasound apparatus working at 1.3 MHz and 100 W for 20 min. A thermocouple was introduced in the experimental setup during the ultrasound application experiments to evaluate the temperature rise induced by the stimulus.

After the different treatments, the suspensions were centrifuged (10000 rpm, 10 min). The supernatants were analyzed by fluorimetry to determine the presence of F-PEG-NH_2 detached from the materials. The materials were washed 3 times with PBS, dried and stored until further analysis. Z potential from those materials was performed in aqueous suspension to evaluate any changes on the surface charge of the materials after the different treatments.

In vitro nanoparticle uptake and cancer cell killing

Human Osteosarcoma (HOS) cells were seeded in 24 well plates at a density of around 20,000 cells/cm^2 24 h before the experiments were carried out. Cells were grown in DMEM supplemented with 2mM of glutamine, 1 % penicillin/streptomycin and 10 % fetal bovine serum, at 37 ºC, 5 % CO_2 and 95 % humidity.

Nanoparticle uptake by HOS cells was evaluated by fluorescence microscopy employing nanoparticles prepared with RBITC-labeled PEG and FITC-labeled MSN-NH_2. Thus, the location of both MSN-NH_2 and PEG could be traced with the microscope. HOS cells were exposed to a suspension of MSN-NH_2-T-PEG or MSN-NH_2-PEG (without or with ultrasound treatment in both cases) in DMEM culture medium (200 µg/mL) for 2 h. Then, the cells were washed with PBS twice and then fixed with a solution of DAPI in methanol. That medium was changed with PBS to perform fluorescence microscopy.

Quantitative analysis of cellular uptake was performed by flow cytometry. HOS cells were incubated with the nanoparticles in complete culture medium (200 µg/mL) for 2 h, and after washing out non-internalized nanoparticles with PBS, the cells were

trypsinised, collected by centrifugation and redispersed in PBS solution with trypan blue (0.5 %) to remove extracellular fluorescence. The fluorescence intensity of 10,000 cells was quantified by flow cytometry. Statistical analysis for differences between groups was carried out by the Student's *t* test.

Nanoparticles were loaded with topotecan, an anticancer drug, to carry out cytotoxicity experiments. Drug loading was performed by dispersing MSN-NH_2-PEG, or MSN-NH_2-T-PEG, in a solution of topotecan (2 mg/mL in PBS), and magnetically stirring them overnight at room temperature. Those nanoparticles containing topotecan, TOP-MSN-NH_2-PEG and TOP-MSN-NH_2-T-PEG, were collected by centrifugation and washed with PBS 3 times. Incubation of HOS cells with these nanoparticles was performed in complete culture media as described above for the internalization experiments. After washing out non-internalized nanoparticles with PBS, cell viability was evaluated at different time points (2 and 24 h) by a commercial Alamar Blue test (Invitrogen, Spain), following the manufacturer's instructions. Statistical analysis was carried out using the Student´s *t* test.

Results and Discussion

It is well known that nanoparticle surface characteristics have a great importance in their interactions with biological environments. For example, PEGylation is known to increase the circulation time of nanoparticles.[5] However, cellular uptake in PEGylated nanoparticles is hindered.[5] On the other hand, nanoparticles with positively charged surfaces are generally internalized efficiently by cells (due to an electrostatic interaction with negatively-charged phospholipids in the cell membrane),[6,15] but their circulation time is much shorter. Therefore, the design of a nanosystem with different surface characteristics in the different delivery stages is here approached.

Mesoporous silica nanoparticles decorated with amino groups, MSN-NH_2, were used in our experiments. These positive nanoparticles were shielded, by decorating them with PEG, using ABCVA as linker (MSN-NH_2-T-PEG nanoparticles). ABCVA acts here as a thermosensitive linker, although it is commonly used as a radical initiator in polymer synthesis because it is cleaved when heated above 69 ºC[17] forming radical species that can start the polymerization.[12] In our case, the temperature increase by using US would induce the cleavage of the ABCVA linker,[18,19] separating PEG chains from the nanoparticle surface. PEGylated nanoparticles that are not thermosensitive

(MSN-NH_2-PEG) were used as control and prepared by using succinic anhydride as a linker (Scheme 2).

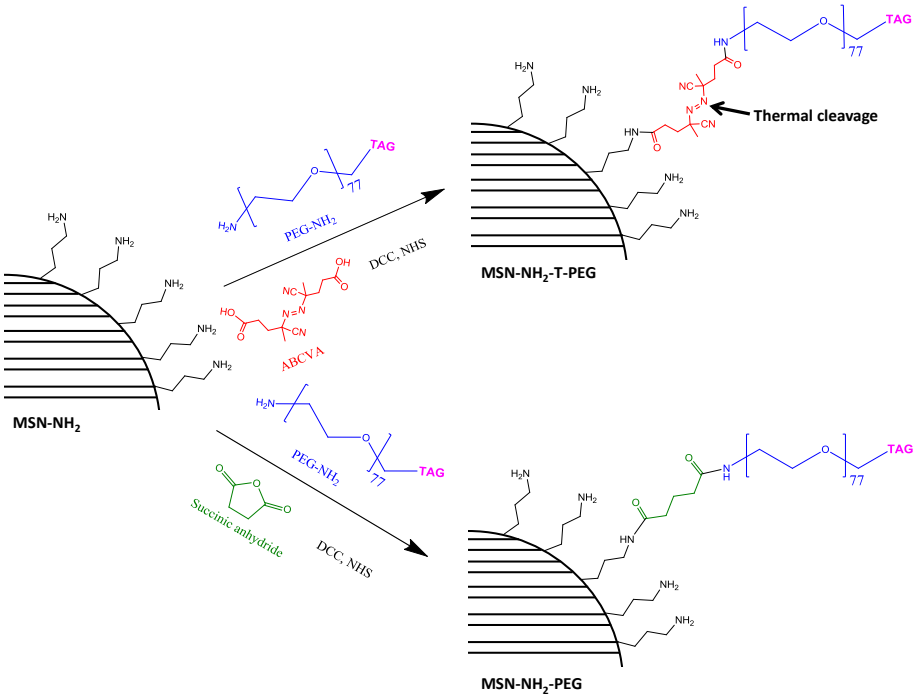

Scheme 2. Schematic representation of the preparation of MSN-NH_2-T-PEG and MSN-NH_2-PEG.

Samples were characterized before and after PEGylation (Figure 1). The SEM micrographs show that particle morphology (round-shaped) is maintained after PEG grafting. Small angle XRD patterns show that the ordered porous structure is maintained, although the intensity of the diffraction maxima decreases after PEG grafting, which is in agreement with previous results.[12] The FTIR spectra of MSN-NH_2-PEG and MSN-NH_2-T-PEG show the presence of amide bonds in the material (*ca.* 1650 cm^{-1}), confirming the successful PEG grafting through amide bond formation to the nanoparticles. TGA data indicate a percentage of organic matter due to PEG chains in the material of around 5.60 % and 5.18 % for MSN-NH_2-T-PEG and MSN-NH_2-PEG, respectively (after substracting the residual organic matter percentage present in MSN-NH_2 before PEG grafting). The amount of amino groups in MSN-NH_2 was $8.35x10^{-5}$ moles/g (as quantified by Fmoc UV assay). From the TGA data and knowing the molecular weight of the grafted PEG, the percentage of those amino groups occupied by PEG was estimated to be 18.2 % and 19.2 % for MSN-NH_2-PEG and MSN-NH_2-T-PEG, respectively. Z potential is modified from positive to negative values after PEGylation: +33.8 mV (MSN-NH_2), -32.1 mV (MSN-NH_2-PEG) and -30.2 mV (MSN-NH_2-T-PEG), indicating that the positive charge of the surface is hidden after the

PEGylation process. Since most of the amino groups on the nanoparticle are not involved in the linkage to PEG, the drastic changes in the Z potential values must be attributed to a physical masking of the nanoparticle surface by the PEG chains.

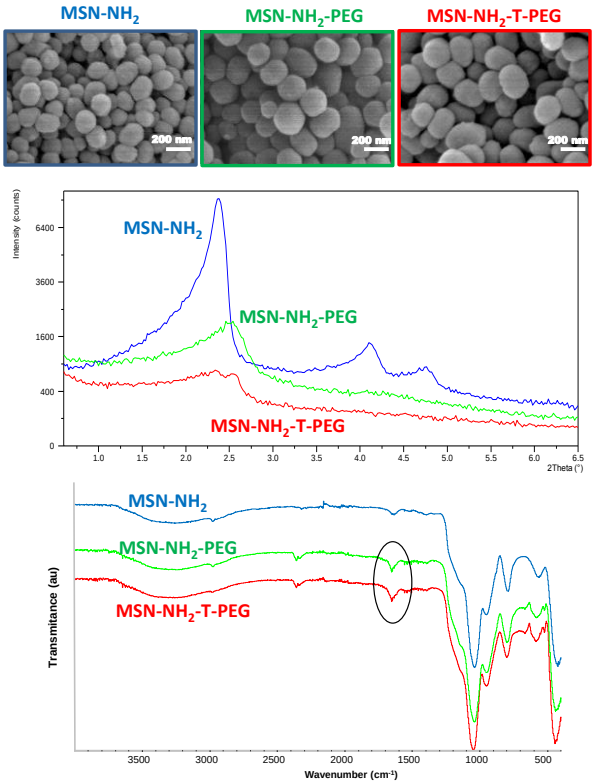

Figure 1. Characterization of MSN-NH_2, MSN-NH_2-PEG and MSN-NH_2-T-PEG. SEM micrographs (top), small angle XRD patterns (center) and FTIR spectra (bottom).

All of the above results confirm the successful masking of the nanoparticle surface by the PEGylation process. The system capacity to change its surface characteristics in response to stimuli was then evaluated step by step. First, we studied the PEG detachment after thermal and US treatments, then, the US-induced cellular uptake and finally, the cytotoxicity when the system was loaded with the anticancer drug topotecan.

The temperature responsiveness of the linker in our nanoparticles was evaluated through PEG chain detachment after thermal treatment. The PEG here employed (F-PEG-NH_2) was labeled with fluorescein to evaluate the fluorescence of the supernatant after treatment, which allowed the quantification of the PEG detached from our nanoparticles. According to the literature, the cleavage of the ABCVA linker is produced at *ca.* 69 ºC (10 h)[17]. Accordingly, suspensions of MSN-NH_2-T-PEG and MSN-NH_2-PEG particles in PBS (1 mg/mL) were treated at 37 and 70 ºC overnight, and

the supernatants obtained after centrifugation were analyzed by fluorimetry. Figure 2 shows that fluorescence intensity was only detectable in the aqueous medium after MSN-NH_2-T-PEG suspension treatment at 70 ºC while no significant fluorescence was found in the supernatant of sample at 37 ºC. As expected, no fluorescence was observed in the samples with no thermosensitive linker (MSN-NH_2-PEG) independently of the temperature. These results show the thermoresponsive capacity of MSN-NH_2-T-PEG particles thanks to the presence of the selected linker which promotes the PEG detachment.

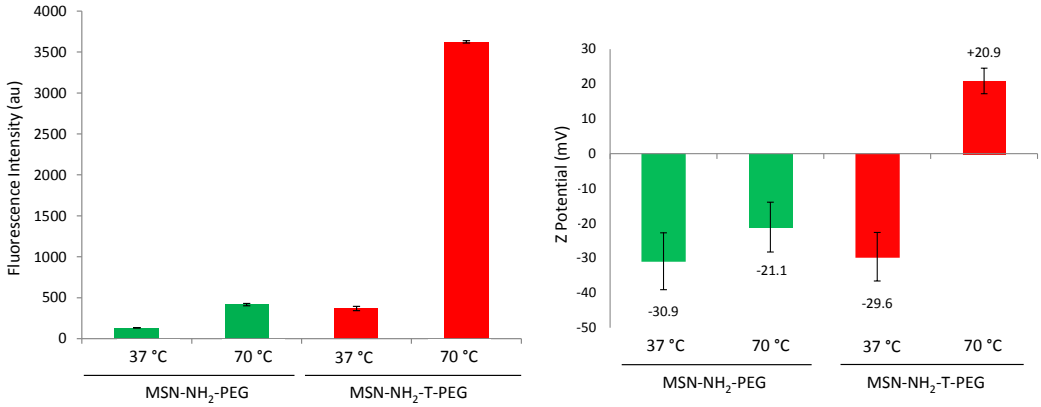

Figure 2. Fluorescence intensity of the supernatant of suspensions of MSN-NH_2-PEG and MSN-NH_2-T-PEG (obtained with FITC-labeled PEG) after different thermal treatments (left); Z potential measurements in water of the materials exposed to those same conditions (right).

After PEG detachment had been observed, the exposure of the positively-charged nanoparticle surface was evaluated by Z potential. Z potential measurements after thermal treatment are in consonance with the fluorescence experiments, since only MSN-NH_2-T-PEG particles treated at 70 ºC presented positive Z potential values (Figure 2).

Once the ability of this system to dissociate the PEG chains from its surface in response to temperature was confirmed, these materials were subjected to US as an external stimulus, to evaluate if a US-induced temperature increase could trigger that same behavior. Figure 3 shows the fluorescence of the supernatant of MSN-NH_2-T-PEG and MSN-NH_2-PEG suspensions after US exposure for 20 min. Again, PEG fluorescence is only observed in the nanoparticles containing the thermosensitive linker, which means that the azo moiety in the ABCVA linker between PEG and MSN-NH_2 (Scheme 2) was cleaved in response to the temperature increase induced by US. These results show that we have successfully developed a thermosensitive material that can

release its PEG coating when exposed to an external energy source, such as 1.3 MHz ultrasound. It is worth mentioning that under the US conditions used, the macroscopic temperature of the solution was determined to be 48 ± 1 ºC (by a thermocouple placed in the setup during the experiments). This temperature was much lower than the bulk temperature needed to induce the cleavage (70 ºC). This difference could be ascribed to a more intense localized heating in the nanoscale related to the occurrence of acoustic cavitation.[20] Even though the temperature reached is still high for the direct biological application of this material, this proof-of-concept strategy could be adapted to other thermosensitive linkers that can respond to a lower temperature (in the range of hyperthermia).

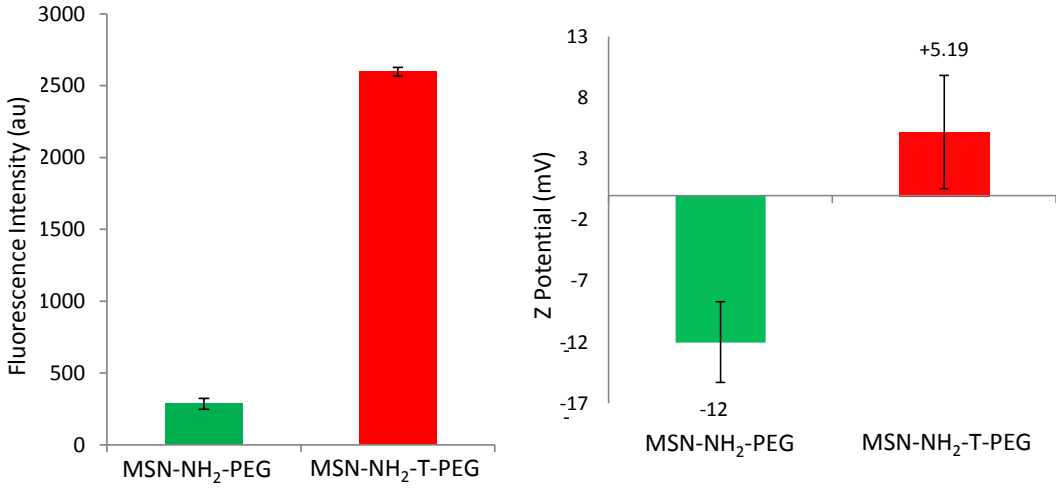

Figure 3. Fluorescence intensity of the supernatant of suspensions of MSN-NH_2-PEG and MSN-NH_2-T-PEG (obtained with FITC-labeled PEG) after US exposure (1.3 MHz, 100 W, 20 min) (left); Z potential measurements in water of the materials exposed to those same conditions (right).

Once that PEG detachment by US-induced temperature rise was demonstrated, the next step was to evaluate if it would be sufficient to provide a positively-charged surface. Thus, Z potential measurements of the nanoparticles after US treatment were carried out (Figure 3). Positive values were only obtained after the US treatment of MSN-NH_2-T-PEG, while a negative charge was found in MSN-NH_2-PEG, in agreement with the absence of PEG detachment.

The results obtained by fluorimetry and Z potential measurements show that the application of an external stimulus as US provokes the detachment of the PEG chains from MSN-NH_2, inducing the exposure of protonated amino groups and, therefore, conferring a positively-charged surface to the nanoparticles.

The next step was to study if PEG detachment favors nanoparticle uptake. To evaluate that, MSN-NH_2-T-PEG and MSN-NH_2-PEG were exposed to US and then they were incubated with HOS cells for 2 h and non-internalized nanoparticles were washed with PBS before performing fluorescence microscopy (Figure 4). In this experiment, we employed FITC labeled MSN-NH_2 and RBITC-labeled PEG chains. The results indicate a higher cellular uptake of MSN-NH_2-T-PEG nanoparticles that had been exposed to ultrasound than in any of the other experimental groups, in agreement with the surface charge reversion of the nanoparticles after the US-induced temperature increase. Moreover, a partial lack of co-localization between red and green fluorescence in the ultrasound-exposed MSN-NH_2-T-PEG sample indicates the detachment of PEG chains from the nanoparticles (Insert in Figure 4), in agreement with previous *in vial* experiments above shown. For ultrasound-exposed MSN-NH_2-PEG under the same conditions, red and green fluorescence overlap, indicating that PEG chains are still attached to the nanoparticles (Insert in Figure 4). Normalized fluorescence intensity of the cells determined by flow cytometry (Figure 4) shows a significant increase in MSN-NH_2-T-PEG uptake after US exposure, while no significant differences were found by ultrasound application for MSN-NH_2-PEG.

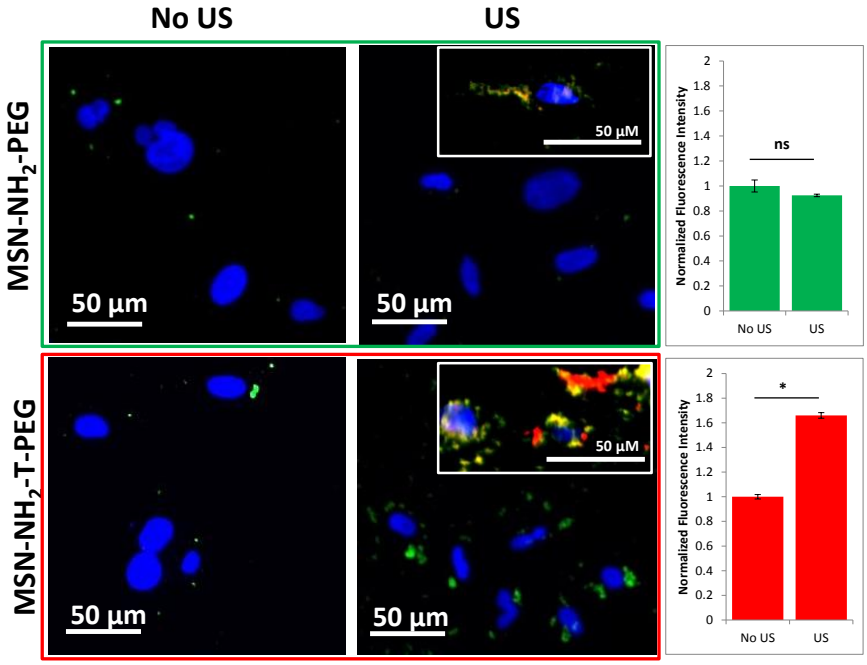

Figure 4. Fluorescence microscopy images (left) and flow cytometry data (right) of osteosarcoma cells (HOS) incubated with MSN-NH_2-PEG and MSN-NH_2-T-PEG exposed or not to ultrasound. Blue fluorescence shows stained nuclei with DAPI, green fluorescence shows MSN core and red fluorescence (inserts in right images) shows PEG chains. ns= no significant differences; *$p<0.05$.

Once the nanoparticles are internalized by the tumor cells after US stimulus, they should be able to induce their death. The therapeutic potential of our system was therefore evaluated with a cytotoxicity study. In this sense, we employed topotecan-loaded nanoparticles incubated with HOS cells. Topotecan is a water-soluble cytotoxic drug (classified as a topoisomerase 1 inhibitor, an analog of camptothecin). The use of nanocarriers that can release the drug in the intracellular compartment leads to very high concentrations of the drug, increasing the efficacy of the platform. Therefore, relative levels of cell death obtained with different nanocarrier formulations in the same cell line could also be an indicator of the degree of internalization of the different materials studied. The results of this cell viability study (Figure 5) show that significant cell death is only observable with US-exposed TOP-MSN-NH_2-T-PEG, while under all of the other conditions, the cells remained viable. These data are in agreement with the nanoparticle uptake experiments, since the nanoparticle uptake was much less efficient in absence of thermolinker and/or US application.

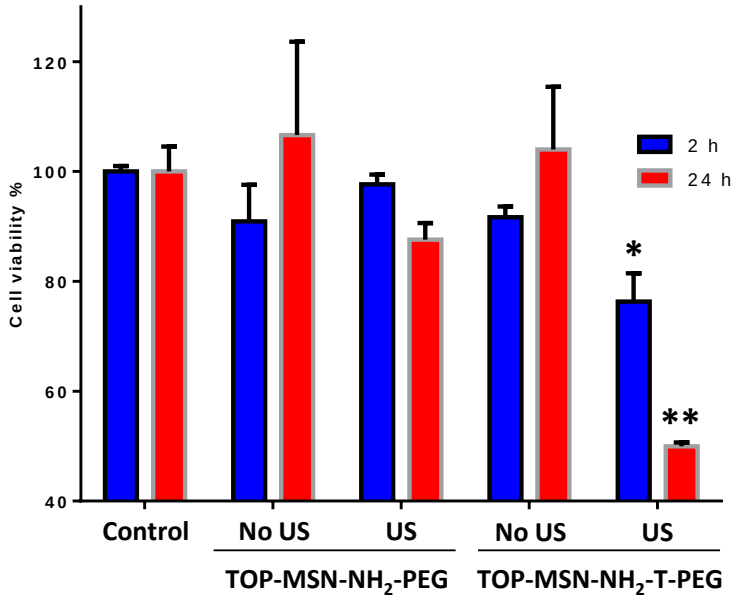

Figure 5. Cell viability of HOS cells (evaluated by Alamar Blue test) incubated with TOP-MSN-NH_2-PEG and TOP-MSN-NH_2-T-PEG with or without prior US application. *p<0.05; **p<0.001 (compared to control).

All of the results here presented confirm the fabrication of a smart hierarchical nanoparticle. Initially, the material presents a PEGylated surface, which allows it to circulate in the bloodstream until it is accumulated in the tumor tissue by the EPR effect. Once the tumor is reached, the nanosystem would change its surface properties in

response to the application of an external stimulus, enabling a more effective interaction with the cancer cells that would lead to nanoparticle uptake.

The results obtained in this work highlight a great potential for ultrasound-induced nanoparticle uptake. Further work is needed to adapt this approach to thermosensitive linkers that can trigger changes in the nanoparticle surface at a physiologically relevant temperature interval. Shielding active targeting molecules on the nanoparticle surface and exposing them only after the application of external stimuli by analogous strategies could also improve the specificity of this kind of approaches.

Conclusions

We have successfully synthesized a smart hierarchical system by developing a PEGylated Mesoporous Silica Nanoparticle capable of undergoing detachment of the PEG chains under thermal or US treatment. The application of an external stimulus such as US is also capable of displaying positively-charged surface of the nanoparticle.

The exposure of the positively-charged surface induced by ultrasound treatment enhanced the cellular uptake of the nanoparticles, while the application of ultrasound in a control material did not induce any changes in its uptake. Finally, US-promoted nanoparticle uptake greatly increased the toxicity of topotecan-loaded nanoparticles in human osteosarcoma cells.

References

1. Chen, G., Roy, I., Yang, C. & Prasad, P. N. Nanochemistry and Nanomedicine for Nanoparticle-based Diagnostics and Therapy. *Chem. Rev.* **116,** 2826–2885 (2016).
2. Maeda, H., Nakamura, H. & Fang, J. The EPR effect for macromolecular drug delivery to solid tumors: Improvement of tumor uptake, lowering of systemic toxicity, and distinct tumor imaging in vivo. *Adv. Drug Deliv. Rev.* **65,** 71–79 (2013).
3. Bertrand, N., Wu, J., Xu, X., Kamaly, N. & Farokhzad, O. C. Cancer nanotechnology: the impact of passive and active targeting in the era of modern cancer biology. *Adv. Drug Deliv. Rev.* **66,** 2–25 (2014).
4. Dawidczyk, C. M., Kim, C., Park, J. H., Russell, L. M., Lee, K. H., Pomper, M. G. & Searson, P. C. State-of-the-art in design rules for drug delivery platforms: Lessons learned from FDA-approved nanomedicines. *J. Control. Release* **187,** 133–144 (2014).
5. Hatakeyama, H., Akita, H. & Harashima, H. The Polyethyleneglycol Dilemma: Advantage and Disadvantage of PEGylation of Liposomes for Systemic Genes and Nucleic Acids Delivery to Tumors. *Biol. Pharm. Bull.* **36,** 892–899 (2013).
6. Wang, S., Huang, P. & Chen, X. Hierarchical Targeting Strategy for Enhanced Tumor Tissue Accumulation/Retention and Cellular Internalization. *Adv. Mater.* **28,** 7340–7364 (2016).

7. Chauhan, V. P. & Jain, R. K. Strategies for advancing cancer nanomedicine. *Nat. Mater.* **12,** 958–962 (2013).
8. Bandekar, A., Zhu, C., Gomez, A., Menzenski, M. Z., Sempkowski, M. & Sofou, S. Masking and Triggered Unmasking of Targeting Ligands on Liposomal Chemotherapy Selectively Suppress Tumor Growth in Vivo. *Mol. Pharm.* **10,** 152–160 (2013).
9. Barhoumi, A., Wang, W., Zurakowski, D., Langer, R. S. & Kohane, D. S. Photothermally Targeted Thermosensitive Polymer-Masked Nanoparticles. *Nano Lett.* **14,** 3697–3701 (2014).
10. Mura, S., Nicolas, J. & Couvreur, P. Stimuli-responsive nanocarriers for drug delivery. *Nat. Mater.* **12,** 991–1003 (2013).
11. Wood, A. K. W. & Sehgal, C. M. A Review of Low-Intensity Ultrasound for Cancer Therapy. *Ultrasound Med. Biol.* **41,** 905–928 (2015).
12. Paris, J. L., Cabañas, M. V., Manzano, M. & Vallet-Regí, M. Polymer-Grafted Mesoporous Silica Nanoparticles as Ultrasound-Responsive Drug Carriers. *ACS Nano* **9,** 11023–11033 (2015).
13. Baeza, A., Manzano, M., Colilla, M. & Vallet-Regí, M. Recent advances in mesoporous silica nanoparticles for antitumor therapy: our contribution. *Biomater. Sci.* **4,** 803–813 (2016).
14. Manzano, M., Colilla, M. & Vallet-Regí, M. Drug delivery from ordered mesoporous matrices. *Expert Opin. Drug Deliv.* **6,** 1383–1400 (2009).
15. Paris, J. L., de la Torre, P., Manzano, M., Cabañas, M. V., Flores, A. I. & Vallet-Regí, M. Decidua-derived mesenchymal stem cells as carriers of mesoporous silica nanoparticles. In vitro and in vivo evaluation on mammary tumors. *Acta Biomater.* **33,** 275–282 (2016).
16. Kay, C., Lorthioir, O. E., Parr, N. J., Congreve, M., McKeown, S. C., Scicinski, J. J. & Ley, S. V. Solid-phase reaction monitoring—Chemical derivatization and off-bead analysis. *Biotechnol. Bioeng.* **71,** 110–118 (2000).
17. Yorimitsu, H., Wakabayashi, K., Shinokubo, H. & Oshima, K. Radical Addition of 2-Iodoalkanamide or 2-Iodoalkanoic Acid to Alkenes with a Water-Soluble Radical Initiator in Aqueous Media: Facile Synthesis of γ -Lactones. *Bull. Chem. Soc. Jpn.* **74,** 1963–1970 (2001).
18. Saint-Cricq, P., Deshayes, S., Zink, J. I. & Kasko, A. M. Magnetic field activated drug delivery using thermodegradable azo-functionalised PEG-coated core–shell mesoporous silica nanoparticles. *Nanoscale* **7,** 13168–13172 (2015).
19. Berkowski, K. L., Potisek, S. L., Hickenboth, C. R. & Moore, J. S. Ultrasound-Induced Site-Specific Cleavage of Azo-Functionalized Poly(ethylene glycol). *Macromolecules* **38,** 8975–8978 (2005).
20. Rosenthal, I., Sostaric, J. Z. & Riesz, P. Sonodynamic therapy--a review of the synergistic effects of drugs and ultrasound. *Ultrason. Sonochem.* **11,** 349–63 (2004).

3.2.3 Ultrasound-Mediated Cavitation-Enhanced Extravasation of Mesoporous Silica Nanoparticles for Controlled-Release Drug Delivery

Paris, J. L.[1], Mannaris, C.[1], Cabañas, M. V., Carlisle, R., Manzano, M., Vallet-Regí, M., Coussios, C. C. Chemical Engineering Journal. 2017. *Enviado.*

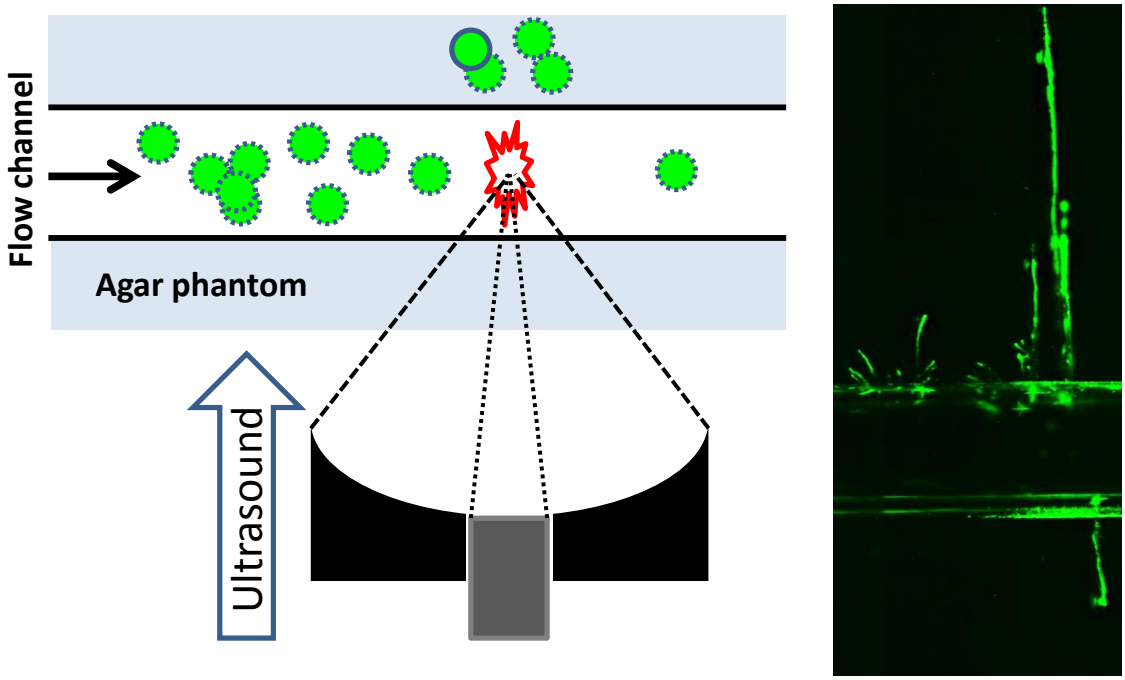

Ultrasound-Mediated Cavitation-Enhanced Extravasation of Mesoporous Silica Nanoparticles for Controlled-Release Drug Delivery

Juan L. Paris[1,2,+], Christophoros Mannaris[3,+], M. Victoria Cabañas[1], Robert Carlisle[3], Miguel Manzano[1,2], María Vallet-Regí[1,2], Constantin C. Coussios[3,*].

1. Dpto. Química Inorgánica y Bioinorgánica, Facultad de Farmacia, UCM, Instituto de Investigación Sanitaria Hospital, 12 de Octubre i+12, 28040-Madrid, Spain.

2. Centro de Investigación Biomédica en Red de Bioingeniería, Biomateriales y Nanomedicina (CIBER-BBN), Spain.

3. Institute of Biomedical Engineering, University of Oxford, Old Road Campus Research Building, Oxford OX3 7DQ, UK.

[+]Authors contributed equally to the work

*Corresponding author: constantin.coussios@eng.ox.ac.uk

Abstract

Mesoporous silica nanoparticles have been reported as suitable drug carriers, but their successful delivery to target tissues following systemic administration remains a challenge. In the present work, ultrasound-induced inertial cavitation was evaluated as a mechanism to promote their extravasation in a flow-through tissue-mimicking agarose phantom. Two different ultrasound frequencies, 0.5 or 1.6 MHz, with pressures in the range 0.5-4 MPa were used to drive cavitation activity which was detected in real time. The optimal ultrasound conditions identified were employed to deliver dye-loaded nanoparticles as a model for drug-loaded nanocarriers, with the level of extravasation evaluated by fluorescence microscopy. The same nanoparticles were then co-injected with submicrometric polymeric cavitation nuclei as a means to promote cavitation activity and decrease the required in-situ acoustic pressure required to attain extravasation. The overall cavitation energy and penetration of the combination was compared to mesoporous silica nanoparticles alone. The results of the present work suggest that combining mesoporous silica nanocarriers and submcrometric cavitation nuclei may help enhance the extravasation of the nanocarrier, thus enabling subsequent sustained drug release to happen from those particles already embedded in the tumour tissue.

Keywords: Extravasation, Nanoparticle Delivery, Cavitation, Mesoporous Silica Nanoparticles.

Introduction

Cancer remains one of the leading causes of death in the world.[1] The poor delivery and inadequate distribution of cancer therapeutics in tumours is considered to be one of the major hurdles yet to be overcome.[2] The use of nanocarriers to transport anticancer drugs has been extensively studied in recent years as a promising strategy to address this challenge.[3] Drug nanocarriers can provide many advantages, such as improving the pharmacokinetic profile of drugs, increasing their circulation times and improving their safety profile.[4] Mesoporous Silica Nanoparticles (MSNs) are one of the most promising types of nanoparticles for drug delivery, due to their high drug-loading capacity derived from their textural properties, such as their high surface area and pore volume, their physicochemical robustness and their ease of functionalization with different moieties through silanol chemistry, making them a versatile tool that can be easily adapted to different specific applications.[5,6]

The main rationale behind the vast amount of work in nanomedicine is the selective accumulation of nanostructures in solid tumours due to their anomalous vasculature related to their rapid growth, which constitutes the enhanced permeation and retention effect, often referred to as “passive targeting”.[7] Despite all the efforts spent in developing the field of nanomedicine, only a few nano-sized drugs have reached clinical application.[8] Furthermore, while these clinically available nano-drugs have significantly improved the safety profile compared to previous formulations with the same active components, mainly due to preventing the use of toxic excipients, the improvement in their efficacy has been modest at best.[9] A recent analysis on the accumulation of nanoparticles in tumours has shown that only a small percentage of the injected nanocarriers actually reach the target tumour tissue (*ca.* 0.7 %).[10] Besides, there has been no significant improvement in that parameter over the last decades.[10] Moreover, the heterogeneity of tumours in different patients, or even on different areas of the tumours from the same patient, implies that even the nanoparticles that reach them will not be distributed homogeneously. Furthermore, the elevated interstitial pressure of solid tumours also limits the penetration of nanoparticles into the tissue.[11] Consequently, a more controlled method to deliver cancer nanotherapeutics is necessary, while also ensuring a deeper penetration of the nanoformulations to allow them to achieve their full therapeutic potential.

Ultrasound (US) has emerged as a remarkable tool in biomedicine, being used to induce drug release from drug carriers,[12–16] to perform thermal ablation therapies[17] and to induce reversible opening of the blood-brain barrier,[18] among many other applications.[19–21] Ultrasound can be focused in the region of interest deep within the body, reducing the intensity of the stimulus applied to surrounding, non-target areas. The biological effects of ultrasound can be divided into thermal and mechanical.[17] Among those mechanical effects, cavitation is highlighted as one of the most useful ultrasound-related phenomena for biomedicine. It can be defined as the formation and linear or non-linear oscillation of gas bubbles in a fluid.[22,23] Sustained linear or non-linear oscillations about an equilibrium bubble radius for many acoustic cycles is termed non-inertial cavitation. However, at more elevated pressures for a given ultrasound frequency and bubble size, the bubble grows unstably during ultrasonic rarefaction, subsequently collapsing violently during compression under the inertia of the surrounding fluid.

This phenomenon, termed inertial cavitation (IC), has been used to enhance the delivery of different therapeutics for cancer therapy.[22,24–26] In this sense, the main strategy employed here consists on using cavitation nuclei that reduce the acoustic pressure required to induce IC, which implies violent collapse of gas bubbles.[27] Examples of such nuclei include micrometric shelled gas bubbles,[22] droplets [28] or gas-stabilizing solid nanoparticles.[29,30] Microstreaming, shockwaves and microjets, associated with IC within blood vessels, can propel the therapeutic into the tumour, increasing the delivered dosage and favouring a more homogeneous distribution.[31]
The main objective of the present work is to evaluate in an *in vitro* tissue mimicking flow model the possibility of MSNs to be used both as drug carriers and as nuclei for the generation of IC to improve their delivery and penetration. Additionally, the combination of MSNs with sub-micron polymeric cup-shaped gas-stabilizing sonosensitive particles (SSP)[29,30] to reduce the acoustic pressures required to initiate IC is also investigated.

Experimental section

Materials. Following compounds were purchased from Sigma-Aldrich Inc.: Aminopropyltriethoxysilane (APTES), ammonium nitrate, cetyltrimethylammonium bromide (CTAB), sodium hydroxide, tetraethyl orthosilicate (TEOS), fluorescein isothiocyanate (FITC), phosphate-buffered solution (PBS), rhodamine B. These

compounds were used without further purification. UltraPure™ Agarose-1000 (Invitrogen, Paisley, UK) was also used without further purification. Ultrapure deionized water was obtained using a Millipore Milli-Q plus system (Millipore S.A.S., France).

Characterisation Techniques. The materials were analysed by small angle X-ray diffraction (XRD) in a Philips X'Pert MPD diffractometer equipped with Cu Kα radiation. Fourier transform infrared (FTIR) spectra were obtained in a Nicolet (Thermo Fisher Scientific) Nexus spectrometer equipped with a Smart Golden Gate Attenuated Total Reflectance accessory. Transmission electron microscopy (TEM) was carried out in a JEOL JEM 2100 instrument operated at 200 kV, equipped with a CCD camera (KeenView Camera). The zeta potential and hydrodynamic size of nanoparticles determined by dynamic light scattering (DLS) were measured by means of a Zetasizer Nano ZS (Malvern Instruments) equipped with a 633 nm "red" laser. N_2 adsorption was carried out in a Micromeritics ASAP 2010 instrument; surface area was obtained by applying the Brunauer–Emmett–Teller (BET) method to the isotherm and the pore size distribution was determined by the Barrett–Joyner–Halenda (BJH) method from the desorption branch of the isotherm. Mesopore diameter was obtained from the maximum of the pore size distribution curve.

Fluorescence spectrometry was used to determine cargo release by means of a Biotek Synergy 4 device (λ_{exc} 540 nm, λ_{em} 625 nm). Fluorescence microscopy was performed in a Nikon Super Inverted Research Microscope (Ti-E). Individual images were taken using a 4x objective. 3D image stitching was performed using the software NIS-Elements Advanced Research (Nikon UK Limited). Nikon filter cubes were used to image FITC (filter cube for FITC, Exciter 465–495, Dichroic 505, Emitter 515–555) and rhodamine B (filter cube for TRITC, Exciter HQ545/30×, Dichroic Q570LP, Emitter HQ620/60 m).

Synthesis of Mesoporous Silica Nanoparticles: MSNs were prepared by a modified Stöber method, as previously described.[32] Briefly, 1 g of the surfactant CTAB was dissolved in 480 mL of deionised (DI) water with 3.5 mL of NaOH 2M in a 1 L round-bottom flask. The solution was heated up to 80 ºC under magnetic stirring, and the temperature was allowed to stabilize for 30 min. 5 mL of TEOS were added at 0.25 mL/min and the solution was vigorously stirred at 80 ºC for 2 h. The particles were then collected by centrifugation and washed with water and ethanol. The surfactant was then extracted by ionic exchange by dispersing the particles in 500 mL of NH_4NO_3 solution

in 95% ethanol (10 mg/mL) and magnetically stirring them under reflux overnight. The nanoparticles were then collected by centrifugation and washed twice with ethanol. The resulting solid was dried under vacuum at room temperature.

FITC-labelled MSNs (FMSNs) were prepared in a similar manner, by conjugating 1 mg of FITC with 2.2 µL of APTES in 100 µL of ethanol with magnetic stirring for 2 h. That solution was mixed with 5 mL of TEOS and added onto the CTAB solution under basic conditions, following the same protocol as described above.

Loading and release of Rhodamine B in FMSNs: 2 mg of Rhodamine B were dissolved in 20 mL of deionised (DI) water. 20 mg of FMSNs were then dispersed in the dye solution with the help of an ultrasound bath and the suspension was magnetically stirred at room temperature overnight. The dye-loaded particles (FMSN-RhB) were then collected by centrifugation and thoroughly washed with DI water before being dried and stored at room temperature until further use.

Rhodamine B release experiments were carried out as follows. A 1 mg/mL suspension of FMSN-RhB in water was prepared and 0.5 mL of such suspension were introduced in a Transwell® insert (polycarbonate membrane with a pore size of 0.4 µm) placed in a 12 well plate. 1.5 mL of DI water were placed in the well outside the insert. At predetermined time points, the release media outside the inserts were collected and replaced with fresh DI water. The samples were analysed by fluorimetry using a plate reader. Release experiments were performed in triplicate.

Sonosensitive Particles (SSPs): Submicrometric polymeric cups were obtained from OxSonics Ltd (Oxford, UK).[30] Degassed DI water was used to dilute a stock solution of 25 mg/mL of SSPs to a final concentration of 0.5 mg/mL. The SSPs had a mean diameter of 500 nm, with a cavity diameter between 230 and 340 nm.[30] Suspensions of both SSPs and FMSNs combined (final concentration of 0.5 mg/mL and 0.2mg/mL, respectively) were also prepared employing degassed DI water (FMSN-SSP suspension).

Experimental setup: The experimental setup used in this work had four main components: a focused therapeutic ultrasound transducer (FUS), a passive cavitation detector (PCD) that is used to passively record the acoustic emissions produced from cavitation, the *in vitro* tissue-mimicking agarose phantom model (with an embedded 1 mm channel through which the sample can flow) and a conventional ultrasound imaging device. The FUS and PCD are fully controlled from custom-made software using graphical programming language (LabVIEW, National Instruments, USA). An arbitrary

waveform generator (33220A, Agilent, USA) was used to create the transmit signal which was amplified by a 300W RF power amplifier (A-300, ENI, USA) and sent to the FUS via a 50 ohm matching network.

1. Focused therapeutic ultrasound: A spherically-focused single-element FUS transducer with a centre frequency of 0.5 MHz was used (H107, Sonic Concepts, USA). The same transducer driven at its third harmonic through a customized matching network was used for the 1.6 MHz experiments. The aperture and the geometric focus of the transducer were 64 mm and 60 mm, respectively. The FUS used was previously calibrated in water using a 0.4 mm diameter needle hydrophone (ONDA 1056, Onda Corporation, USA). All acoustic pressures reported in this study are in MPa peak rarefactional pressures (PRP). For all extravasation experiments, 600 pulses with a pulse repetition time (PRT) of 100 ms were employed. Duty cycle was kept at 5 % in all cases.

2. Passive Cavitation Detector: A single element PCD (V320, Panametrics, USA) was coaxially and confocally aligned with the FUS transducer via a central circular opening in the FUS. Acoustic emissions arising from cavitation were sensed by the PCD as described previously.[33] Here, a 7.5 MHz spherically focused PCD of element diameter 12.5 mm and focal length 75 mm was used. The acquired PCD signal was filtered using a 5 MHz high pass filter (FILT-HP5-A, Allen Avionics), amplified 5 times with a low noise amplifier (Stanford Research Systems, SR445A) and recorded with a 14-bit PCI Oscilloscope device (PCI-5122, National Instruments, USA) at a rate of 100 MHz. The high-pass filter was used to reject strong reflections from the agarose phantom at the fundamental frequency (and harmonics due to non-linear propagation of the incident beam). The pressure threshold required to initiate cavitation activity was determined by 50-cycle FUS excitation pulses that were ramped at small pressure increments under constant flow. A typical PCD data trace consisted of an initial ~85μs segment (‘background’) that was free of any signal content in the filter pass band, followed by scattering and cavitation emissions (‘signal’) whose durations varied with drive pulse length. The background and signal segments of each trace were analysed in MATLAB (Mathworks, USA) to determine if IC had occurred and the full ensemble of PCD traces were reviewed to calculate a probability of cavitation at the prescribed ultrasound settings. For this analysis, any harmonic components were removed by post-processing with a digital comb filter. The identification of IC was based upon broadband spectral elevation in the signal relative to the background. The harmonic-

suppressed traces were deemed to exhibit IC when the mean-squared signal was at least 10 times larger than the background signal.

3. Tissue-mimicking agarose phantom: A degassed biocompatible hydrogel composed of 1.25 % (w/v) low melting point ultrapure agarose gel with an embedded 1 mm channel was created by heating and cooling process.[22] The phantom contained three 50 mm long channels which allowed multiple conditions to be tested in the same gel, thus minimising variability. A clear and acoustically transparent Mylar film was used to isolate the gel from the surrounding water and allow free propagation of ultrasound. A low-pulsatility peristaltic pump (Minipulse Evolution, Gilson, USA) was used to flow the FMSNs or FMSN-SSP suspension at a constant flow rate of 0.2 mL/min. The flow rate was chosen to avoid channel rupture and leakage while still in agreement with previously published data of tumour perfusion.[34]

4. Ultrasound imaging: A Philips iU-22 ultrasound scanner was used to provide real-time imaging of the flow phantom during the experiment. A linear L12-5 probe was placed at an angle of 60° to the FUS and PCD propagation axis and imaging was done at a low mechanical index (MI < 0.05), in order to minimise interference with the experiment. The imaging allowed monitoring of the channel and its contents during the experiments and provided real-time feedback of the therapeutic process.

Experimental Procedure: All experiments were carried out in a large tank filled with DI water that was degassed overnight prior to each experiment. With the channel filled with air, the FUS was driven in pulse-echo mode using a pulser-receiver (DPR300, JSR Ultrasonics, USA) in order to ensure that the FUS and PCD were aligned with the middle of the flow channel. The sample was then introduced at a constant flow rate and was kept flowing during FUS exposures. Figure 1A shows a schematic representation of the experimental setup. The input voltages to the FUS matching network were also recorded and converted to peak negative pressures using previous hydrophone calibrations. Focused ultrasound was applied at different positions within the channel, while monitoring both the passive cavitation detector data (to detect cavitation during the ultrasound exposure) and performing B-mode imaging simultaneously. A photograph of the agarose phantom holder and examples of B-mode images taken during the experiments can be seen in Figure 1B and 1C, respectively.

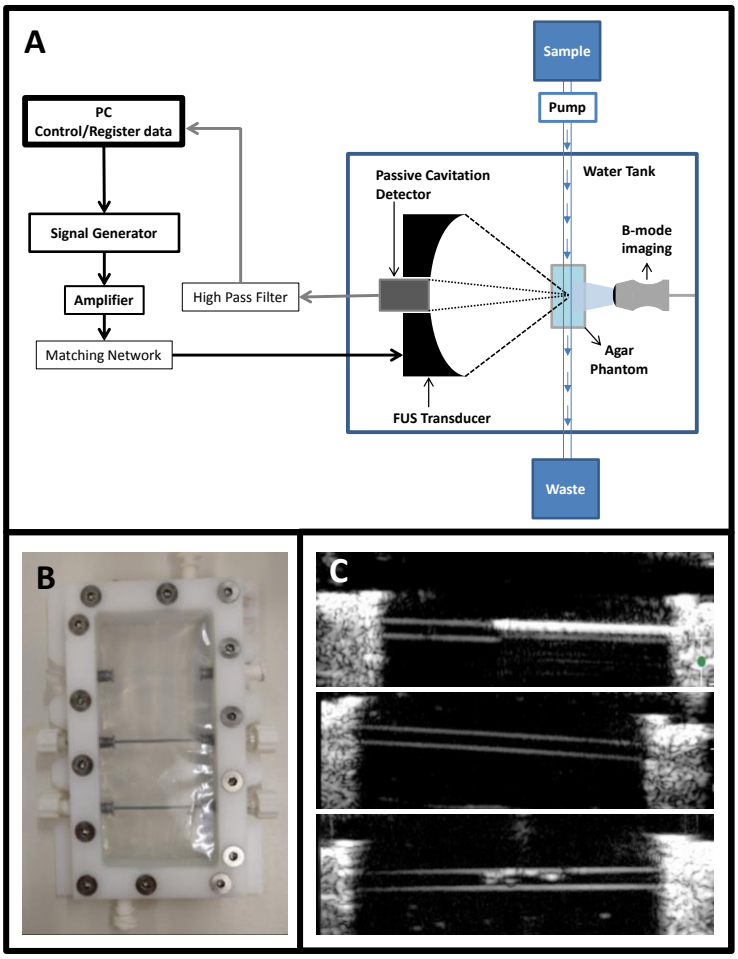

Figure 1. Schematic diagram of the experimental setup and the apparatus, containing the focussed ultrasound (FUS) transducer, passive cavitation detection (PCD) transducer, tissue-mimicking agarose phantom and diagnostic ultrasound imaging device (A), Photograph of the agarose phantom holder showing the gel with one of the three flow channels prepared (B) and B-mode images during experiment (C) showing displacement of air by incoming sample (top), channel with sample flowing (center) and inertial cavitation happening within the channel (bottom).

Flow channels were flushed with DI water following ultrasound exposure to remove any remaining fluorescent particles. A rectangular prism containing the flow channel, approximately 40 mm long, was then excised and placed on a glass microscope slide to evaluate nanoparticle extravasation through microscopy (extravasation is here defined as any particle fluorescence detected outside the flow channel).

Results and Discussion

Nanoparticle delivery experiments were carried out in an *in vitro* agarose phantom model. The agarose gel acts as tumour tissue mimicking material, having a porosity in the same range (*ca.* 500 nm pore size) as the endothelial gaps of the "leaky" tumour tissue.[35]

Cavitation has been previously used to induce the extravasation of nanoparticles to tumour tissues.[22,24–26] The main objective of this work is to evaluate *in vitro* the extravasation of MSNs in the presence of acoustic cavitation with or without SSPs. Previously dried FITC-labelled MSNs (FMSNs) were dispersed in degassed water at a concentration of 200 µg/mL. The cavitation threshold of the FMSNs suspension under flow through the agarose phantom was evaluated at two different frequencies (0.5 and 1.6 MHz) (Figure 2). The duty cycle (DC) in both cases was limited to 5 % in order to minimise ultrasound-induced hyperthermia. IC could be detected at both frequencies with those FMSN suspensions (and no cavitation could be detected under the applied pressures at any frequency with just degassed water). At 0.5 MHz, cavitation was observed at pressures as low as 0.6 MPa, and a threshold was observed at 2 MPa where sustained cavitation (probability > 0.7) is achieved. At 1.6 MHz, cavitation was first observed at 1.5 MPa and linearly increased to a probability of 0.71 at 4.3 MPa.

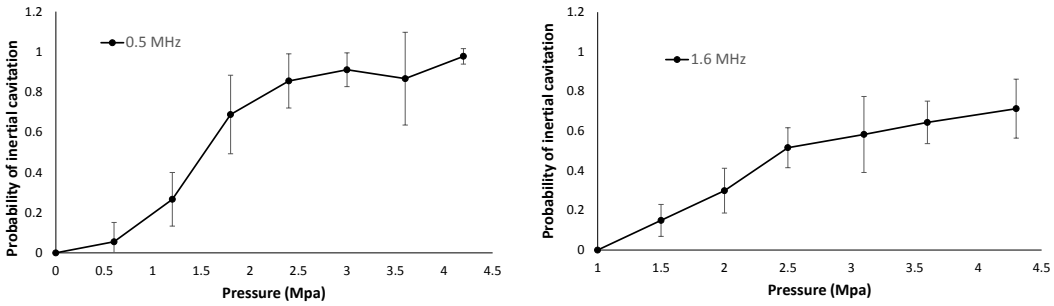

Figure 2. Probability of IC curves of FMSN in degassed water (200 µg/mL) exposed to ultrasound at 0.5 or 1.6 MHz. Data are Means ± SD, N=3.

The IC detected with FMSN suspensions could be attributed to air trapped during drying process which could be on the surface or inside nanoparticle aggregates.[36] FMSN suspensions were evaluated by Dynamic Light Scattering (DLS) to check for nanoparticle aggregates (Figure S1). While no significant percentage of nanoparticle aggregates could be observed in the number percentage, some aggregates of several microns were detected in the intensity percentage (where larger particulates give more intense signals).

Having confirmed the onset of IC when exposing FMSN suspensions to focused US, the extravasation and delivery of those FMSNs in the agarose flow phantom model was evaluated next. FMSN suspensions flowing through the agarose phantom were exposed to focused ultrasound at 0.5 and 1.6 MHz, at two different PRP for each frequency (1 and 2 MPa or 2 and 4 MPa, respectively). The agarose phantoms were then

cut and observed under the fluorescence microscope. Figure 3 shows a schematic representation of the nanoparticle delivery experiments and representative images of the results. Extravasated nanoparticles can be seen as green fluorescent spots in the agarose gel, outside the flow channel. As expected, the extravasation of FMSNs was more successful at higher pressures for each frequency, particularly once the cavitation threshold identified in Figure 2 was crossed. Differences were observed in the extravasation profiles, with 1.6 MHz achieving higher penetration depths but a more directional extravasation profile compared to 0.5 MHz, presumably due to the greater effect of acoustic radiation force at the higher frequency.

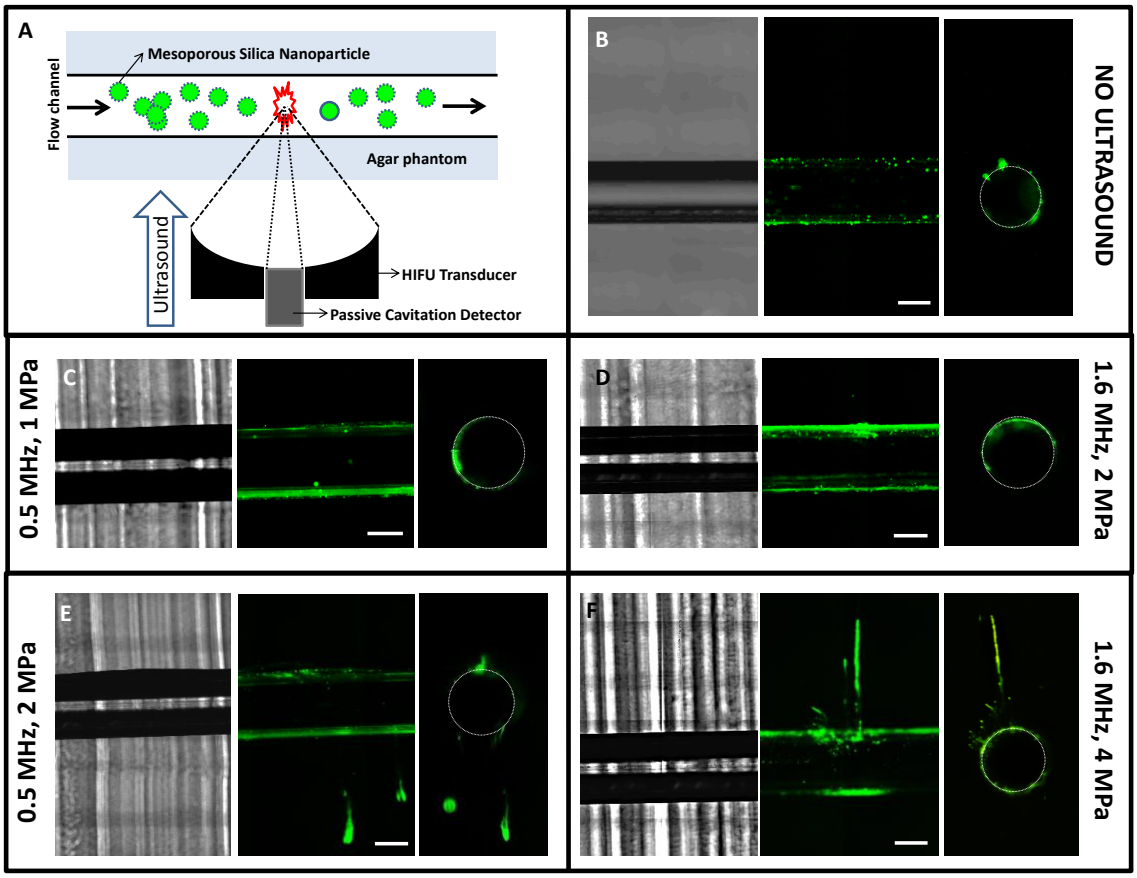

Figure 3. Scheme of FMSN delivery experiments in the agarose phantom model (A). Representative microscopy images of Nanoparticle delivery in the agarose phantom model under different different frequency (0.5 or 1.6 MHz) and pressure (1-4 MPa) conditions at the same duty cycle (5%) (N=3), showing bright field (left), green fluorescence (center) and green fluorescence in a cross section of the flow channel (right) (B-F). Scale bars represent 500 µm.

The main rationale behind the use of MSNs in nanomedicine is the possibility of including drugs and other small molecules inside their pores to be then released in a controlled manner. Our next experiment consisted on evaluating nanoparticle delivery

in the same model, but using loaded nanoparticles, to see if they could act as drug carriers while still being capable of propelling themselves into the tumour when insonified. FMSNs were therefore loaded with rhodamine B (FMSN-RhB). The successful loading can be observed by the colour change in the material, as well as by the FTIR spectrum and small angle XRD patterns (Figure S2). The drastic changes in BET surface area (from 1050 m^2/g to 560 m^2/g) and pore volume further confirm that the mesopores of the material have been occupied by rhodamine B. TEM micrographs also show that the ordered porosity is maintained after cargo loading and nanoparticle washing. Release experiments of the dye from FMSN-RhB show a sustained release of the cargo into the aqueous medium (Figure S3). Rhodamine B release followed first order kinetics, with a faster initial release followed by a slower release that can last for several days, as previously observed for mesoporous drug release matrices.[12,37]

The cavitation activity of a suspension of FMSN-RhB exposed to 1.6 MHz focused ultrasound was also evaluated following the same procedure as had been performed for FMSN and is shown in Figure S4. Results are very similar to FMSN indicating that the loading of the dye did not affect the cavitation activity of the particle suspensions. The size distribution of FMSN-RhB evaluated by DLS was similar to FMSN, with some aggregates being detected only in the intensity percentage distribution (Figure S5). 1.6 MHz, 4 MPa was chosen for the FMSN-RhB delivery experiments, as the extravasation profiles observed at these settings were easier to detect under the microscope. Figure 4 shows the successful extravasation of the nanoparticles into the agarose gel (green fluorescence). The fluorescence of the cargo (red channel) can also be observed, both inside the nanoparticles (fluorescent spots colocalizing with the nanoparticles, in the green channel), and partially released from the material. This could be explained because the gels were cut and imaged shortly after delivery, so the model drug did not have enough time to be released and diffuse in the surrounding tissue, as would be the case in an *in vivo* scenario. Dye fluorescence can also be observed around the channel, due to the diffusion of fluorophore released during nanoparticle flow through the channel.

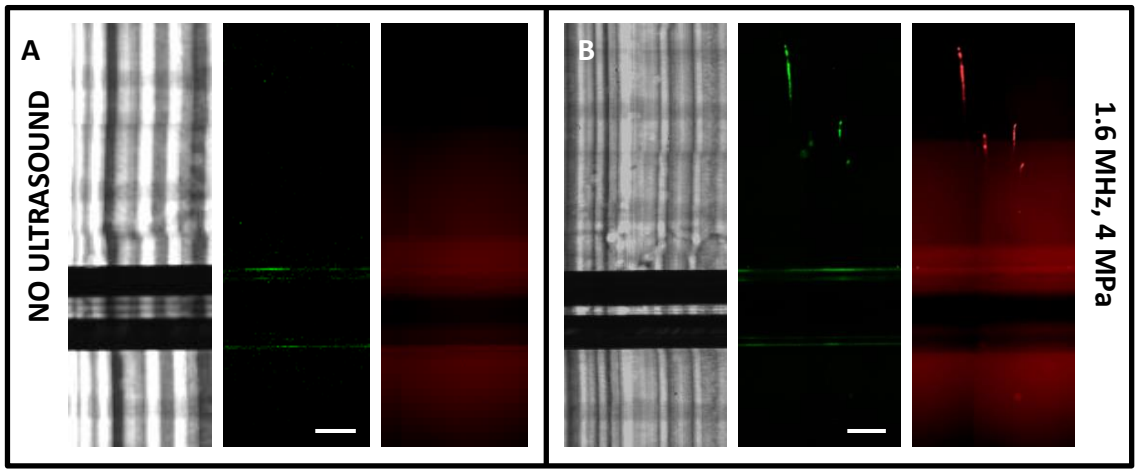

Figure 4. Representative microscopy images of FMSN-RhB delivery in the agarose phantom model without ultrasound (A) or with FUS exposure at 1.6 MHz and 4 MPa (B), showing bright field (left), green fluorescence (center) and red fluorescence (right) (N=3). Scale bars represent 500 µm.

These results show the feasibility of using MSNs as carriers of small molecules that could be propelled by the application of focused ultrasound through the onset of IC. However, the pressures required to induce MSN extravasation and delivery with FUS might be too high for the clinical application of this strategy. The use of cavitation nuclei has gathered a lot of attention in recent years, since their usage can greatly decrease the pressure threshold needed to generate cavitation.[27,38] Among the different cavitation nuclei that have been used to enhance drug delivery, submicrometer sized particles hold great promise due to their capacity of extravasating along with the therapeutic, and further propelling the drug into the tissue of interest. Microbubbles on the other hand would be restrained in the vascular compartment and unable to extravasate along with the therapeutic being employed.[30] However, combining cavitation nuclei directly with an anticancer drug would only provide an initial dose of the drug, without establishing a stable concentration of the drug over time. For these reasons, we studied the combination of mesoporous silica nanoparticles with submicrometric polymeric cups. In this manner, a lower ultrasound pressure could be applied to extravasate MSNs, which would then act as a reservoir of the drug that would be released in the tumour area. Figure 5 shows the successful delivery of FMSNs into the agarose gel using 1.6 MHz FUS at just 2 MPa of pressure, a pressure which is readily achievable clinically without significant bioeffects and at which no extravasation had been previously observed in the absence of cavitation nuclei (Figure 3). The cavitation energy measured with the combination of FMSNs and SSPs greatly

exceeded the energy reached at double the pressure without SSPs (Figure S6). Temperature elevation measurements were also performed with a fine wire thermocouple during FUS exposure (1.6 MHz, 4 MPa, 300 pulses, PRT of 100 ms) using both water or a SSPs suspension. The temperature increase produced under those conditions was negligible, below 1 ºC, indicating that thermal effects were unlikely to be the driving cause of any of the observed results (Figure S7). All of these results highlight the great potential of the combination of both types of particles for therapeutic application in drug delivery.

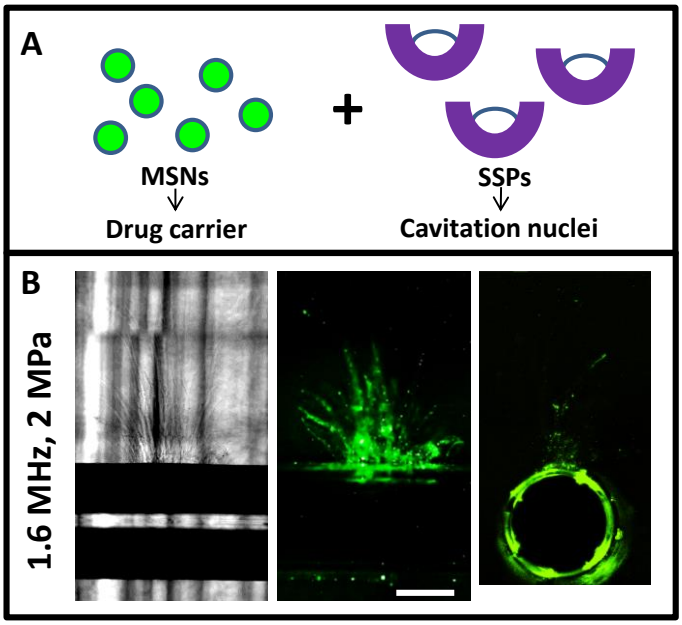

Figure 5. Schematic of combining MSNs with SSPs (A). Representative microscopy images of nanoparticle delivery in the agarose phantom model (FMSN in combination with SSPs), showing bright field (left), green fluorescence (center) and green fluorescence in a cross section of the flow channel (right) (B) (N=3). Scale bar represents 500 µm.

Finally, the combination of SSPs and FMSN-RhB shows significant delivery of FMSN-RhB to the agar gel, using 1.6 MHz US driven at 2 MPa PRP (Figure 6). Rhodamine B can be observed both still inside MSN and partially released into the surrounding gel. These results can be interpreted as a proof of concept of our approach, co-injecting SSPs with loaded MSN. A combination of both materials could be injected in a patient and US could be applied in the tumour area, activating SSPs and inducing IC in the area, propelling the particles towards the tumour tissue. Thus, drug-loaded MSN would be embedded in the tissue, which would then slowly release an anticancer drug close to its target cancer cells.

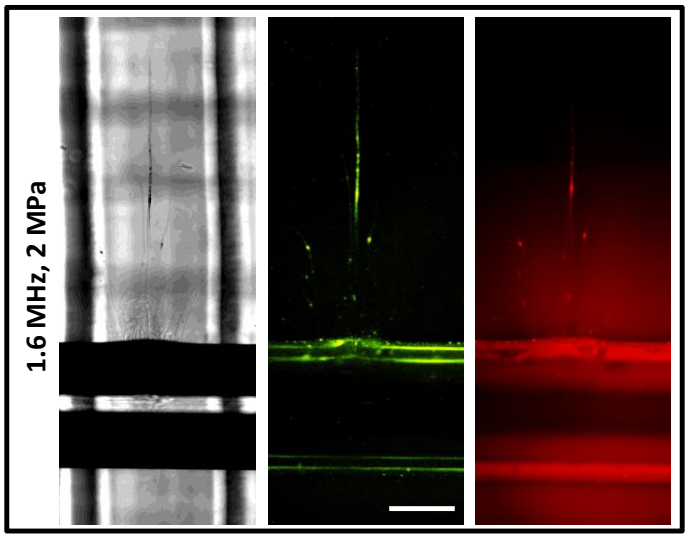

Figure 6. Representative microscopy images of dye-loaded nanoparticle delivery in the agarose phantom model (FMSN-RhB in combination with SSPs), showing bright field (left), green fluorescence (center) and red fluorescence (right) (B) (N=3). Scale bar represents 500 µm.

Conclusions

Ultrasound-induced inertial cavitation (IC) has been shown here to enable enhanced extravasation of mesoporous silica nanoparticles in an *in vitro* flow-through agarose tissue phantom. Both empty and dye-loaded nanoparticles were shown to extravasate into the agarose gel at ultrasound pressures beyond the IC threshold. The combination of those nanoparticles with submicrometric cavitation nuclei was demonstrated as a much more efficient way of inducing nanoparticle extravasation, decreasing the pressure needed to observe the desired extravasation effect by half. A two-stage strategy for the combination of both agents therefore emerges: in the initial step, the cavitation nuclei will drive nanoparticle extravasation and distribution throughout the tumour tissue when activated by focused ultrasound; mesoporous silica nanoparticles embedded in the target tissue then slowly release the drug of interest directly in the tumour mass.

Acknowledgements

The authors thank the funding from the European Research Council through the Advanced Grant VERDI (ERC-2015 AdG proposal no. 694160), Ministerio de Economía y Competitividad, (MEC), Spain (Project MAT2015- 64831-R), and the Oxford Centre for Drug Delivery Devices under programme grant EP/L024012/1 by the UK's Engineering and Physical Sciences Research Council.. JL Paris gratefully

acknowledges MEC, Spain, for his PhD grants (BES-2013- 064182, EEBB-I-17-12352).

References

[1] S.D. Steichen, M. Caldorera-Moore, N.A. Peppas, A review of current nanoparticle and targeting moieties for the delivery of cancer therapeutics., Eur. J. Pharm. Sci. 48 (2013) 416–27.

[2] C. von Roemeling, W. Jiang, C.K. Chan, I.L. Weissman, B.Y.S. Kim, Breaking Down the Barriers to Precision Cancer Nanomedicine, Trends Biotechnol. 35 (2017) 159–171.

[3] J. Shi, P.W. Kantoff, R. Wooster, O.C. Farokhzad, Cancer nanomedicine: progress, challenges and opportunities, Nat. Rev. Cancer. 17 (2016) 20–37.

[4] A. Wicki, D. Witzigmann, V. Balasubramanian, J. Huwyler, Nanomedicine in cancer therapy: Challenges, opportunities, and clinical applications, J. Control. Release. 200 (2015) 138–157.

[5] M. Vallet-Regí, A. Rámila, R.P. del Real, J. Pérez-Pariente, A New Property of MCM-41: Drug Delivery System, Chem. Mater. 13 (2001) 308–311.

[6] Z. Li, J.C. Barnes, a Bosoy, J.F. Stoddart, J.I. Zink, Mesoporous silica nanoparticles in biomedical applications, Chem. Soc. Rev. 41 (2012) 2590–2605.

[7] H. Maeda, H. Nakamura, J. Fang, The EPR effect for macromolecular drug delivery to solid tumors: Improvement of tumor uptake, lowering of systemic toxicity, and distinct tumor imaging in vivo, Adv. Drug Deliv. Rev. 65 (2013) 71–79.

[8] C.M. Dawidczyk, C. Kim, J.H. Park, L.M. Russell, K.H. Lee, M.G. Pomper, et al., State-of-the-art in design rules for drug delivery platforms: Lessons learned from FDA-approved nanomedicines, J. Control. Release. 187 (2014) 133–144.

[9] T.J. Anchordoquy, Y. Barenholz, D. Boraschi, M. Chorny, P. Decuzzi, M.A. Dobrovolskaia, et al., Mechanisms and Barriers in Cancer Nanomedicine: Addressing Challenges, Looking for Solutions, ACS Nano. 11 (2017) 12–18.

[10] S. Wilhelm, A.J. Tavares, Q. Dai, S. Ohta, J. Audet, H.F. Dvorak, et al., Analysis of nanoparticle delivery to tumours, Nat. Rev. Mater. 1 (2016) 16014.

[11] J.W. Nichols, Y.H. Bae, EPR: Evidence and fallacy, J. Control. Release. 190 (2014) 451–464.

[12] J.L. Paris, M.V. Cabañas, M. Manzano, M. Vallet-Regí, Polymer-Grafted Mesoporous Silica Nanoparticles as Ultrasound-Responsive Drug Carriers, ACS Nano. 9 (2015) 11023–11033.

[13] A. Schroeder, R. Honen, K. Turjeman, A. Gabizon, J. Kost, Y. Barenholz, Ultrasound triggered release of cisplatin from liposomes in murine tumors, J. Control. Release. 137 (2009) 63–68.

[14] M.J. Ernsting, A. Worthington, J.P. May, T. Tagami, M.C. Kolios, S.-D. Li, Ultrasound drug targeting to tumors with thermosensitive liposomes, in: 2011 IEEE Int. Ultrason. Symp., IEEE, 2011: pp. 1–4.

[15] H. Grüll, S. Langereis, Hyperthermia-triggered drug delivery from temperature-sensitive liposomes using MRI-guided high intensity focused ultrasound, J. Control. Release. 161 (2012) 317–327.

[16] J.-M. Escoffre, C. Mannaris, B. Geers, A. Novell, I. Lentacker, M. Averkiou, et al., Doxorubicin liposome-loaded microbubbles for contrast imaging and ultrasound-triggered drug delivery, IEEE Trans. Ultrason. Ferroelectr. Freq. Control. 60 (2013) 78–87.

[17] R.J.E. van den Bijgaart, D.C. Eikelenboom, M. Hoogenboom, J.J. Fütterer, M.H. den Brok, G.J. Adema, Thermal and mechanical high-intensity focused ultrasound: perspectives on tumor ablation, immune effects and combination strategies, Cancer Immunol. Immunother. 66 (2017) 247–258.

[18] K. Hynynen, N. McDannold, N.A. Sheikov, F.A. Jolesz, N. Vykhodtseva, Local and reversible blood–brain barrier disruption by noninvasive focused ultrasound at frequencies suitable for trans-skull sonications, Neuroimage. 24 (2005) 12–20.

[19] J. Unga, M. Hashida, Ultrasound induced cancer immunotherapy, Adv. Drug Deliv. Rev. 72 (2014) 144–153.

[20] A.K.W. Wood, C.M. Sehgal, A Review of Low-Intensity Ultrasound for Cancer Therapy, Ultrasound Med. Biol. 41 (2015) 905–928.

[21] X. Xue, X. Hong, Z. Li, C.X. Deng, J. Fu, Acoustic tweezing cytometry enhances osteogenesis of human mesenchymal stem cells through cytoskeletal contractility and YAP activation, Biomaterials. 134 (2017) 22–30.

[22] C.D. Arvanitis, M. Bazan-Peregrino, B. Rifai, L.W. Seymour, C.C. Coussios, Cavitation-Enhanced Extravasation for Drug Delivery, Ultrasound Med. Biol. 37 (2011) 1838–1852.

[23] C.C. Coussios, R.A. Roy, Applications of Acoustics and Cavitation to Noninvasive Therapy and Drug Delivery, Annu. Rev. Fluid Mech. 40 (2008) 395–420.

[24] M. Bazan-Peregrino, C.D. Arvanitis, B. Rifai, L.W. Seymour, C.-C. Coussios, Ultrasound-induced cavitation enhances the delivery and therapeutic efficacy of an oncolytic virus in an in vitro model, J. Control. Release. 157 (2012) 235–242.

[25] R. Carlisle, J. Choi, M. Bazan-Peregrino, R. Laga, V. Subr, L. Kostka, et al., Enhanced Tumor Uptake and Penetration of Virotherapy Using Polymer Stealthing and Focused Ultrasound, JNCI J. Natl. Cancer Inst. 105 (2013) 1701–1710.

[26] S.R. Sirsi, M.A. Borden, State-of-the-art materials for ultrasound-triggered drug delivery., Adv. Drug Deliv. Rev. 72 (2014) 3–14.

[27] C.K. Holland, R.E. Apfel, Thresholds for transient cavitation produced by pulsed ultrasound in a controlled nuclei environment, J. Acoust. Soc. Am. 88 (1990) 2059–2069.

[28] J.M. Correas, S.D. Quay, EchoGen emulsion: a new ultrasound contrast agent based on phase shift colloids, Clin. Radiol. 51 Suppl 1 (1996) 11–14.

[29] J.J. Kwan, S. Graham, R. Myers, R. Carlisle, E. Stride, C.C. Coussios, Ultrasound-induced inertial cavitation from gas-stabilizing nanoparticles, Phys. Rev. E. 92 (2015) 23019.

[30] J.J. Kwan, R. Myers, C.M. Coviello, S.M. Graham, A.R. Shah, E. Stride, et al., Ultrasound-Propelled Nanocups for Drug Delivery, Small. 11 (2015) 5305–5314.

[31] S. Mitragotri, Healing sound: the use of ultrasound in drug delivery and other therapeutic applications, Nat. Rev. Drug Discov. 4 (2005) 255–260.

[32] J.L. Paris, P.D. La Torre, M. Manzano, M.V. Cabañas, A.I. Flores, M. Vallet-Regí, Decidua-derived mesenchymal stem cells as carriers of mesoporous silica nanoparticles. In vitro and in vivo evaluation on mammary tumors, Acta Biomater. 33 (2016) 275–282.

[33] N. Hockham, C.C. Coussios, M. Arora, A real-time controller for sustaining thermally relevant acoustic cavitation during ultrasound therapy, IEEE Trans. Ultrason. Ferroelectr. Freq. Control. 57 (2010) 2685–2694.

[34] F. Kallinowski, K.H. Schlenger, S. Runkel, M. Kloes, M. Stohrer, P. Okunieff, et al., Blood Flow, Metabolism, Cellular Microenvironment, and Growth Rate of Human Tumor Xenografts, Cancer Res. 49 (1989) 3759–3764.

[35] M. Maaloum, N. Pernodet, B. Tinland, Agarose gel structure using atomic force microscopy: Gel concentration and ionic strength effects, Electrophoresis. 19 (1998) 1606–1610.

[36] A. Yildirim, R. Chattaraj, N.T. Blum, A.P. Goodwin, Understanding Acoustic Cavitation Initiation by Porous Nanoparticles: Toward Nanoscale Agents for Ultrasound Imaging and Therapy, Chem. Mater. 28 (2016) 5962–5972.

[37] A. Nieto, F. Balas, M. Colilla, M. Manzano, M. Vallet-Regí, Functionalization degree of SBA-15 as key factor to modulate sodium alendronate dosage, Microporous Mesoporous Mater. 116 (2008) 4–13.

[38] S. Datta, C.-C. Coussios, L.E. McAdory, J. Tan, T. Porter, G. De Courten-Myers, et al., Correlation of cavitation with ultrasound enhancement of thrombolysis, Ultrasound Med. Biol. 32 (2006) 1257–1267.

Supporting Information

Ultrasound-Mediated Cavitation-Enhanced Extravasation of Mesoporous Silica Nanoparticles for Controlled-Release Drug Delivery.

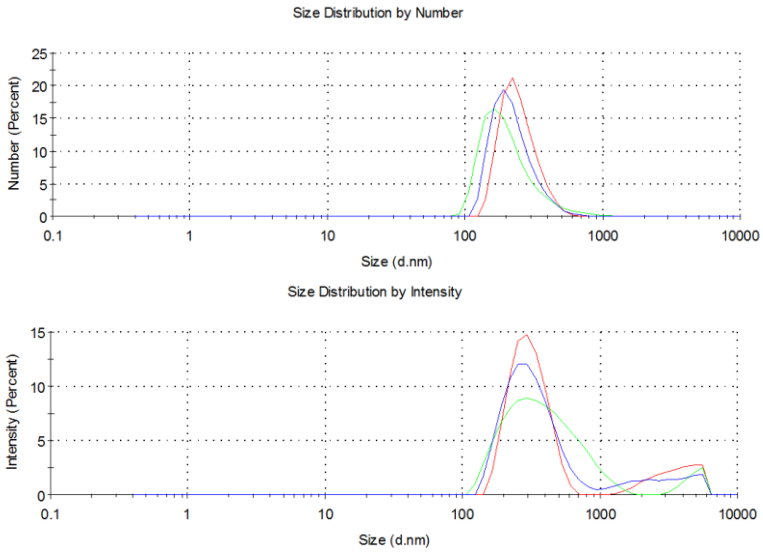

Figure S1. FMSN size distribution in water (200 µg/mL) by DLS in Number (top) or Intensity percentage (bottom).

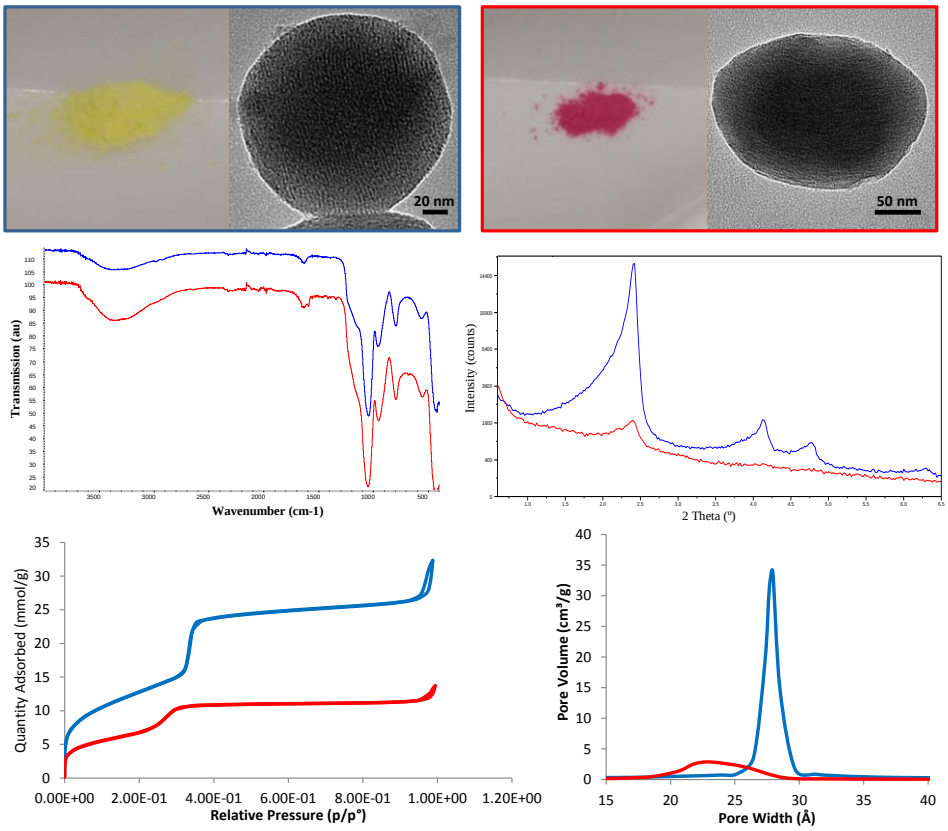

Figure S2. Characterization of FMSN (blue) and FMSN-RhB (red). Photograph of the materials (upper, left), TEM micrographs (upper, right), FTIR spectra (center, left) and Small Angle X-Ray Diffraction patterns (center, right), N_2 adsorption porosimetry data (bottom).

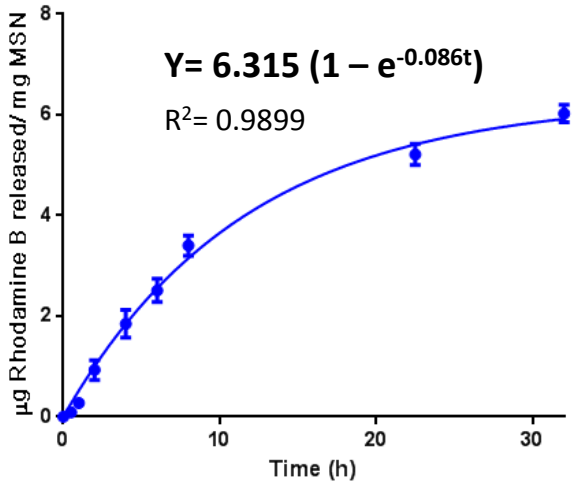

Figure S3. Release profile of Rhodamine B from FMSN-RhB in water at 37 ºC *versus* time. Dots represent data points, curve corresponds to kinetic fitting to first order kinetic model (equation and coefficient of determination shown in the figure). N=3.

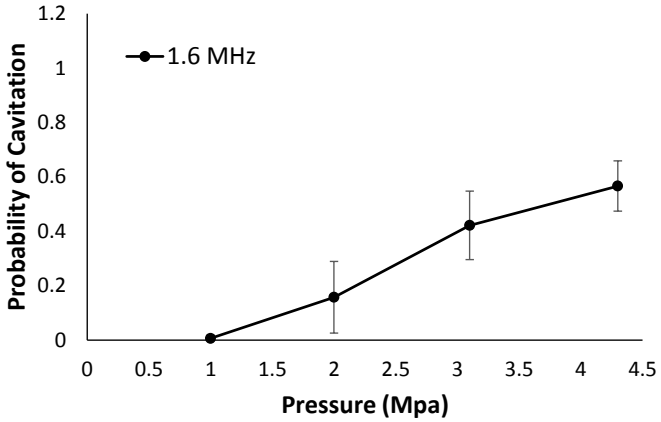

Figure S4. Probability of inertial cavitation curves of FMSN-RhB in degassed water (200 µg/mL) exposed to ultrasound at 1.6 MHz.

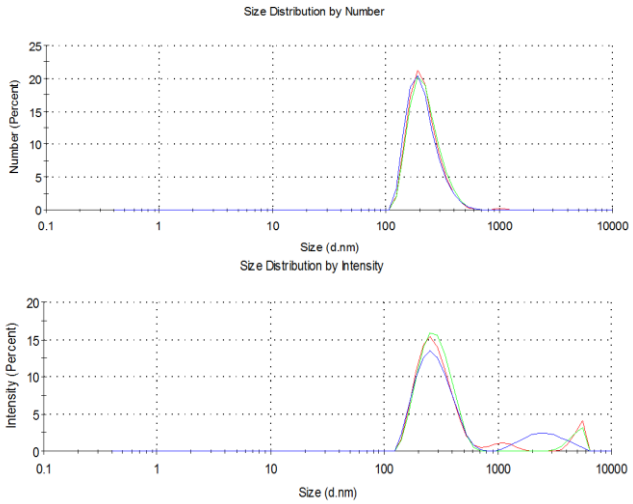

Figure S5. FMSN-RhB size distribution in water (200 µg/mL) by DLS in Number (top) or Intensity percentage (bottom).

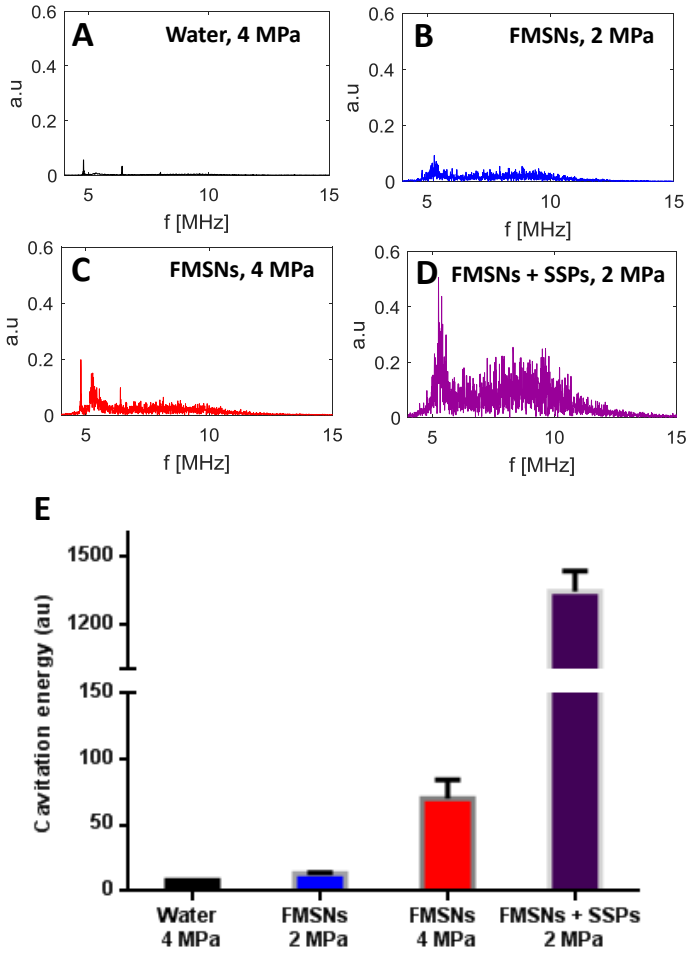

Figure S6. Power spectra of the PCD data during agar phantom experiments with different samples and pressures with 1.6 MHz HIFU (broadband signals indicate inertial cavitation happening within the flow channel) (A-D), Cavitation energy plots comparing the different experimental conditions (E).

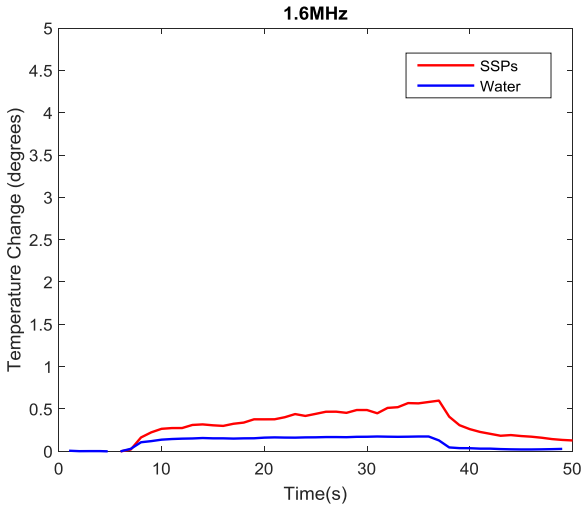

Figure S7. Temperature measurements performed with a thermocouple inserted within the agar phantom holder during FUS application (1.6 MHz, 4 MPa, 300 pulses, PRT of 100 ms).

Bloque 3.3

Vehiculización celular de nanopartículas de sílice mesoporosa sensibles a ultrasonido

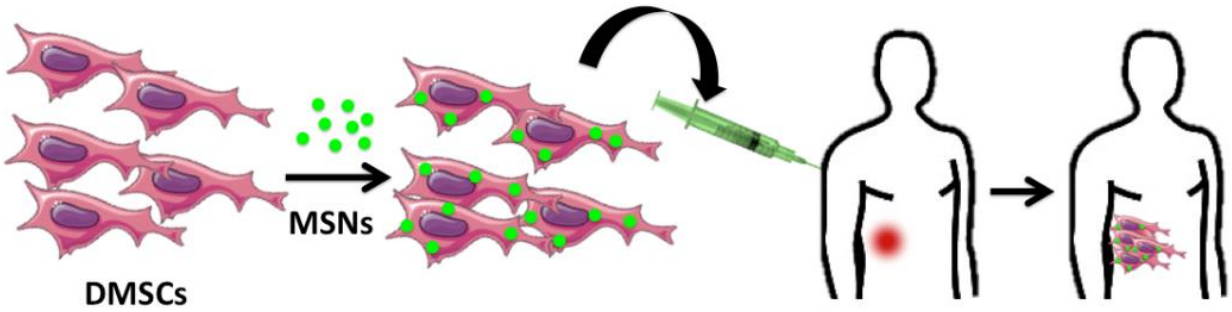

El tercer bloque de Resultados y Discusión de la presente tesis doctoral versa sobre el uso de vehiculización celular para lograr el transporte hacia tumores de MSNs sensibles a US.

A pesar de los prometedores resultados iniciales, la nanomedicina aún no ha sido capaz de satisfacer las expectativas sobre su eficacia en el tratamiento oncológico.[1] Una de las principales barreras que impiden el desarrollo de terapias eficaces basadas en nanopartículas es la distribución de las mismas, debido a la amplia variabilidad del efecto EPR. Esto conduce a que, en términos de porcentaje, menos del 1 % de la dosis inyectada de nanopartículas sea capaz de alcanzar el tumor.[2–4] Una estrategia alternativa a la dependencia de la vectorización pasiva (EPR) y activa de nanopartículas es la utilización de vehículos celulares.[5,6] Ciertos tipos de células con capacidad migratoria hacia tumores y otros tejidos patológicos pueden emplearse como vehículos para transportar las nanopartículas hasta el tejido diana. Por ejemplo, se han propuesto para ello macrófagos, bacterias, linfocitos y células madre mesenquimales.[7–13] Las células madre mesenquimales (MSCs) son células adherentes de proliferación rápida capaces de diferenciarse en distintos tipos celulares (multipotentes).[14] Además, pueden secretar distintas hormonas y factores de crecimiento, y poseen propiedades inmunomoduladoras. Pueden obtenerse de distintas fuentes, tales como tejido adiposo, médula ósea o placenta (Figura 1).

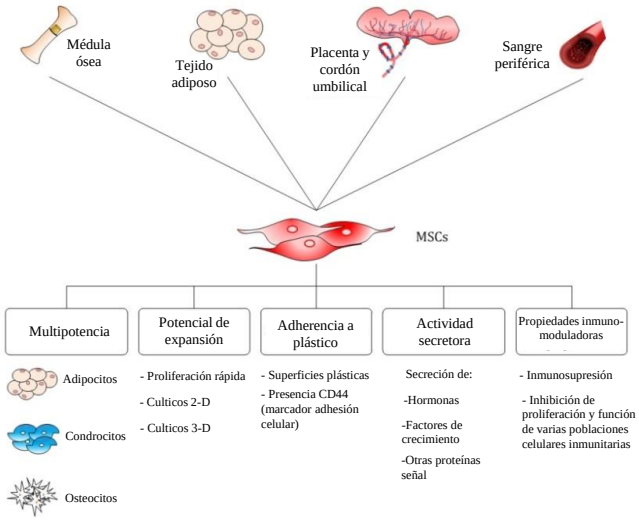

Figura 1. Fuentes que pueden emplearse para obtener MSCs, así como algunas de sus principales características. Reproducido con permiso.[15]

Distintos tipos de células mesenquimales han demostrado capacidad migratoria hacia tumores.[10,12] Las células madre mesenquimales procedentes de la decidua de

placenta humana (DMSCs por sus siglas en inglés) son especialmente prometedoras, debido a su facilidad de obtención y su gran homogeneidad.[16] Al ser células adultas, carecen de los inconvenientes éticos que presentan las células madre embrionarias. Las DMSCs migran hacia tumores tanto *in vitro* como *in vivo*.[17] Además, son capaces de disminuir el crecimiento de tumores primarios así como de tumores secundarios.[17] Por todas estas características, las DMSCs se presentan como una opción prometedora para actuar como vehículos de nanopartículas.

En el Capítulo 3.3.1 se evalúa la capacidad de las DMSCs para internalizar y transportar MSNs hacia tumores, tanto *in vitro* como *in vivo*. Los contenidos de dicho capítulo se encuentran recogidos en un artícuo publicado en la revista Acta Biomaterialia, que puede encontrarse más adelante.[18] Las MSNs mostraron no ser tóxicas para las DMSCs, y fueron internalizadas rápidamente por las células, quedando retenidas en su interior durante al menos 5 días. Las MSNs con carga superficial positiva fueron internalizadas de forma más eficiente que las MSNs con carga negativa. La capacidad migratoria tanto *in vitro* como *in vivo* de las DMSCs se mantuvo tras la incorporación de nanopartículas en su interior. Finalmente, en un co-cultivo de DMSCs con células tumorales de mama (NMU)[19] se observó la muerte de las NMU cuando se habían introducido MSNs cargadas con doxorrubicina en las DMSCs.

Después de demostrar la capacidad de las DMSCs para captar las MSNs y transportarlas hacia tumores, nos encontramos con la necesidad de asegurar la supervivencia de las células transportadoras durante el trayecto hasta el tumor. Si las DMSCs están transportando nanopartículas cargadas con un fármaco citotóxico, la liberación prematura del mismo podría comprometer la viabilidad y capacidad migratoria de las DMSCs antes de que estas sean capaces de llegar al tejido diana.[13] Para atacar este problema, y para tener un control real de cuándo y dónde se produce la liberación, en el capítulo 3.3.2 se evalúa la capacidad de las DMSCs para transportar MSNs con liberación sensible a US. Para ello, se tuvo que llevar a cabo una modificación de la superficie de las nanopartículas sensibles a US, mediante el recubrimiento con el policatión polietilenimina (PEI), con objeto de aumentar su internalización en las DMSCs.[20,21] Este capítulo se encuentra recogido en un artículo publicado en la revista Nanoscale, que puede encontrarse más adelante.[22] El recubrimiento de las nanopartículas híbridas con PEI para dotarlas de carga positiva aumentó de forma drástica su internalización por parte de las DMSCs, tal y como se esperaba. Este resultado se encuentra en consonancia con los resultados obtenidos en el

Capítulo 3.3.1 con respecto al efecto de la carga superficial de las MSNs en su interacción con las DMSCs. La capacidad de respuesta a US de las nanopartículas híbridas tras el recubrimiento con PEI fue comprobada *in vitro* e *in vivo*. Tanto la capacidad de respuesta de las nanopartículas como la capacidad migratoria *in vitro* de las DMSCs se mantuvieron tras la internalización de las nanopartículas por parte de las células transportadoras. Finalmente, se evaluó el potencial terapéutico de esta estrategia mediante un co-cultivo con células NMU, observando toxicidad de la doxorrubicina liberada desde las nanopartículas sólo tras la aplicación de US, demostrando así el control de la liberación de fármacos en un escenario *in vitro*.

Las células madre mesenquimales como agentes terapéuticos también se han estudiado ampliamente en el contexto de la terapia génica mediante la expresión de genes suicidas.[23] Los genes suicidas codifican proteínas que, directa o indirectamente, conducen a la muerte de la célula que expresa el gen, y también pueden afectar a células circundantes. Esta muerte de células tumorales próximas a la célula que expresa el gen suicida se denomina "efecto espectador" (*bystander effect* en inglés).[24–26] La expresión de un gen suicida por las células mesenquimales nos permitirá provocar la muerte de células tumorales circundantes tras la migración al tejido tumoral. El Capítulo 3.3.3 comprende la utilización de las MSNs sensibles a US con el recubrimiento de PEI como agentes de transfección para inducir la expresión de un gen suicida en las DMSCs, evaluando la muerte de células tumorales co-cultivadas con ellas como consecuencia del efecto espectador. El gen suicida seleccionado, que se inserta en el recubrimiento de PEI de las nanopartículas, permitirá la conversión de un profármaco no tóxico, la 5-fluorocitosina que puede inyectarse por vía intravenosa, en una especie altamente tóxica. Esta estrategia podría combinarse con la ya desarrollada introducción de un fármaco antitumoral en las MSNs cuya liberación sería promovida por la aplicación de US, logrando un efecto combinado de las dos estrategias terapéuticas de forma simultánea.

Bibliografía

1. Wicki, A., Witzigmann, D., Balasubramanian, V. & Huwyler, J. Nanomedicine in cancer therapy: Challenges, opportunities, and clinical applications. *J. Control. Release* **200,** 138–157 (2015).
2. Wilhelm, S., Tavares, A. J., Dai, Q., Ohta, S., Audet, J., Dvorak, H. F. & Chan, W. C. W. Analysis of nanoparticle delivery to tumours. *Nat. Rev. Mater.* **1,** 16014 (2016).
3. Lammers, T., Kiessling, F., Ashford, M., Hennink, W., Crommelin, D. & Strom, G. Cancer nanomedicine: is targeting our target? *Nat. Rev. Mater.* **1,** 16069 (2016).
4. Nichols, J. W., Sakurai, Y., Harashima, H. & Bae, Y. H. Nano-sized drug carriers: Extravasation, intratumoral distribution, and their modeling. *J. Control. Release* (2017). doi:10.1016/j.jconrel.2017.08.003
5. Tang, C., Russell, P. J., Martiniello-Wilks, R., Rasko, J. E. J. & Khatri, A. Concise review: Nanoparticles and cellular carriers-allies in cancer imaging and cellular gene therapy? *Stem Cells* **28,** 1686–1702 (2010).
6. Hosoya, H., Dobroff, A. S., Driessen, W. H. P., Cristini, V., Brinker, L. M., Staquicini, F. I., Cardó-Vila, M., D'Angelo, S., Ferrara, F., Proneth, B., Lin, Y.-S., Dunphy, D. R., Dogra, P., Melancon, M. P., Stafford, R. J., Miyazono, K., Gelovani, J. G., Kataoka, K., Brinker, C. J., Sidman, R. L., Arap, W. & Pasqualini, R. Integrated nanotechnology platform for tumor-targeted multimodal imaging and therapeutic cargo release. *Proc. Natl. Acad. Sci.* **113,** 1877–1882 (2016).
7. Harrington, K., Alvarez-Vallina, L., Crittenden, M., Gough, M., Chong, H., Diaz, R. M., Vassaux, G., Lemoine, N. & Vile, R. Cells as Vehicles for Cancer Gene Therapy: The Missing Link Between Targeted Vectors and Systemic Delivery? *Hum. Gene Ther.* **13,** 1263–1280 (2002).
8. Pawelek, J. M., Low, K. B. & Bermudes, D. Bacteria as tumour-targeting vectors. *Lancet Oncol.* **4,** 548–556 (2003).
9. Roger, M., Clavreul, A., Venier-Julienne, M.-C., Passirani, C., Sindji, L., Schiller, P., Montero-Menei, C. & Menei, P. Mesenchymal stem cells as cellular vehicles for delivery of nanoparticles to brain tumors. *Biomaterials* **31,** 8393–8401 (2010).
10. Gao, Z., Zhang, L., Hu, J. & Sun, Y. Mesenchymal stem cells: A potential targeted-delivery vehicle for anti-cancer drug, loaded nanoparticles. *Nanomedicine Nanotechnology, Biol. Med.* **9,** 174–184 (2013).
11. Kidd, S., Spaeth, E., Dembinski, J. L., Dietrich, M., Watson, K., Klopp, A., Battula, V. L., Weil, M., Andreeff, M. & Marini, F. C. Direct Evidence of Mesenchymal Stem Cell Tropism for Tumor and Wounding Microenvironments Using In Vivo Bioluminescent Imaging. *Stem Cells* **27,** 2614–2623 (2009).
12. Karp, J. M. & Leng Teo, G. S. Mesenchymal Stem Cell Homing: The Devil Is in the Details. *Cell Stem Cell* **4,** 206–216 (2009).
13. Hu, Y.-L., Fu, Y.-H., Tabata, Y. & Gao, J.-Q. Mesenchymal stem cells: A promising targeted-delivery vehicle in cancer gene therapy. *J. Control. Release* **147,** 154–162 (2010).
14. Pittenger, M. F., Mackay, A. M., Beck, S. C., Jaiswal, R. K., Douglas, R., Mosca, J. D., Moorman, M. A., Simonetti, D. W., Craig, S. & Marshak, D. R. Multilineage potential of adult human mesenchymal stem cells. *Science* **284,**

143–147 (1999).
15. Jossen, V., Pörtner, R., Kaiser, S. C., Kraume, M., Eibl, D. & Eibl, R. Mass Production of Mesenchymal Stem Cells — Impact of Bioreactor Design and Flow Conditions on Proliferation and Differentiation, in *Cells and Biomaterials in Regenerative Medicine.* (InTech, 2014).
16. Macias, M. I., Grande, J., Moreno, A., Domínguez, I., Bornstein, R. & Flores, A. I. Isolation and characterization of true mesenchymal stem cells derived from human term decidua capable of multilineage differentiation into all 3 embryonic layers. *Am. J. Obstet. Gynecol.* **203,** 495.e9-495.e23 (2010).
17. Vegh, I., Grau, M., Gracia, M., Grande, J., de la Torre, P. & Flores, A. I. Decidua mesenchymal stem cells migrated toward mammary tumors in vitro and in vivo affecting tumor growth and tumor development. *Cancer Gene Ther.* **20,** 8–16 (2013).
18. Paris, J. L., de la Torre, P., Manzano, M., Cabañas, M. V., Flores, A. I. & Vallet-Regí, M. Decidua-derived mesenchymal stem cells as carriers of mesoporous silica nanoparticles. In vitro and in vivo evaluation on mammary tumors. *Acta Biomater.* **33,** 275–282 (2016).
19. Vegh, I. & de Salamanca, R. E. Prolactin, TNF alpha and nitric oxide expression in nitroso-N-methylurea-induced-mammary tumours. *J. Carcinog.* **6,** 18 (2007).
20. Xia, T., Kovochich, M., Liong, M., Meng, H., Kabehie, S., George, S., Zink, J. I. & Nel, A. E. Polyethyleneimine Coating Enhances the Cellular Uptake of Mesoporous Silica Nanoparticles and Allows Safe Delivery of siRNA and DNA Constructs. *ACS Nano* **3,** 3273–3286 (2009).
21. Gosselin, M. A., Guo, W. & Lee, R. J. Efficient gene transfer using reversibly cross-linked low molecular weight polyethylenimine. *Bioconjug. Chem.* **12,** 989–994 (2001).
22. Paris, J. L., de la Torre, P., Cabañas, M. V., Manzano, M., Grau, M., Flores, A. I. & Vallet-Regí, M. Vectorization of ultrasound-responsive nanoparticles in placental mesenchymal stem cells for cancer therapy. *Nanoscale* **9,** 5528–5537 (2017).
23. You, M.-H., Kim, W.-J., Shim, W., Lee, S.-R., Lee, G., Choi, S., Kim, D.-Y., Kim, Y. M., Kim, H. & Han, S.-U. Cytosine deaminase-producing human mesenchymal stem cells mediate an antitumor effect in a mouse xenograft model. *J. Gastroenterol. Hepatol.* **24,** 1393–1400 (2009).
24. Springer, C. J. & Niculescu-Duvaz, I. Prodrug-activating systems in suicide gene therapy. *J. Clin. Invest.* **105,** 1161–1167 (2000).
25. Kucerova, L., Matuskova, M., Pastorakova, A., Tyciakova, S., Jakubikova, J., Bohovic, R., Altanerova, V. & Altaner, C. Cytosine deaminase expressing human mesenchymal stem cells mediated tumour regression in melanoma bearing mice. *J. Gene Med.* **10,** 1071–1082 (2008).
26. Bourbeau, D., Lavoie, G., Nalbantoglu, J. & Massie, B. Suicide gene therapy with an adenovirus expressing the fusion gene CD::UPRT in human glioblastomas: different sensitivities correlate with p53 status. *J. Gene Med.* **6,** 1320–1332 (2004).

3.3.1 Decidua-derived mesenchymal stem cells as carriers of mesoporous silica nanoparticles. In vitro and in vivo evaluation on mammary tumors

Paris, J. L., de la Torre, P., Manzano, M., Cabañas, M. V., Flores, A. I. & Vallet-Regí, M. Acta Biomater. 33, 275–282 (2016).
DOI: 10.1016/j.actbio.2016.01.017

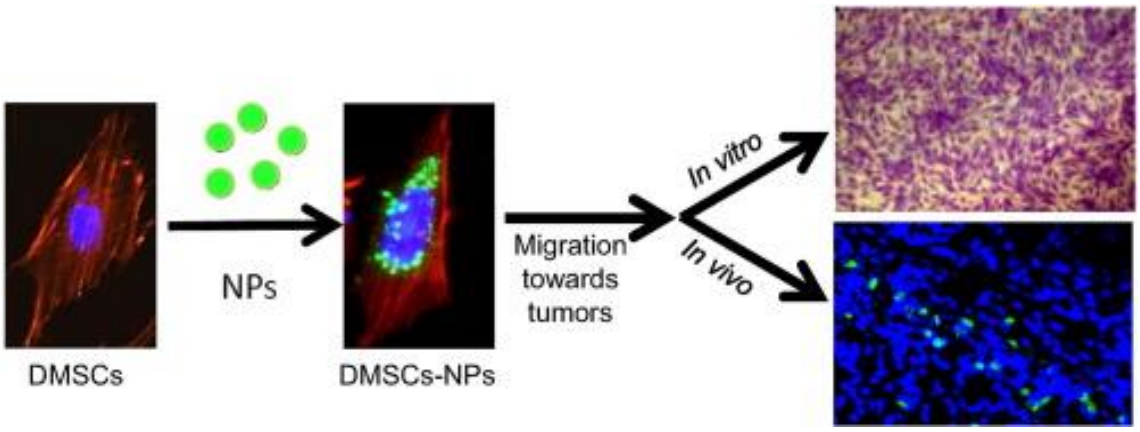

Acta Biomaterialia 33 (2016) 275–282

Contents lists available at ScienceDirect

Acta Biomaterialia

journal homepage: www.elsevier.com/locate/actabiomat

Full length article

Decidua-derived mesenchymal stem cells as carriers of mesoporous silica nanoparticles. *In vitro* and *in vivo* evaluation on mammary tumors

Juan L. Paris [a,b], Paz de la Torre [c], Miguel Manzano [a,b], M. Victoria Cabañas [a], Ana I. Flores [c,*], María Vallet-Regí [a,b,*]

[a] Dpto. Química Inorgánica y Bioinorgánica, Facultad de Farmacia, UCM, Instituto de Investigación Sanitaria Hospital 12 de Octubre i+12, Madrid, Spain
[b] CIBER de Bioingeniería, Biomateriales y Nanomedicina (CIBER-BBN), Spain
[c] Grupo de Medicina Regenerativa, Centro de Investigación, Instituto de Investigación Hospital 12 de Octubre i+12, Madrid, Spain

ARTICLE INFO

Article history:
Received 8 September 2015
Received in revised form 8 January 2016
Accepted 16 January 2016
Available online 18 January 2016

Keywords:
Nanoparticles
Mesoporous silica
Nanomedicine
Human Decidua-derived mesenchymal stem cells

ABSTRACT

The potential use of human Decidua-derived mesenchymal stem cells (DMSCs) as a platform to carry mesoporous silica nanoparticles in cancer therapy has been investigated. Two types of nanoparticles were evaluated. The nanoparticles showed negligible toxicity to the cells, a fast uptake and a long retention inside them. Nanoparticle location in the cell was studied by colocalization with the lysosomes. Moreover, the *in vitro* and *in vivo* migration of DMSCs towards tumors was not modified by the evaluated nanoparticles. Finally, DMSCs transporting doxorubicin-loaded nanoparticles were capable of inducing cancer cell death *in vitro*.

Statement of Significance

The use of nanotechnology for anticancer drug delivery has recently attracted great interest. Nanoparticles such as mesoporous silica nanoparticles (MSNs) can reach tumors, either by passive targeting, through the enhanced permeability and retention (EPR) effect, or active targeting, through the functionalization of nanoparticle surface. However, nanotechnology has not yet achieved the expected results in improving drug targeting, highlighting the need for a better localization of the nanoparticles in the tumors. Human mesenchymal stem cells from the decidua of the human placenta (DMSCs) have been observed to migrate towards tumors in a preclinical model of breast cancer. Moreover, they have been shown to inhibit growth of primary tumors and development of new tumors. In this work, combining MSNs and DMSCs, we have studied for the first time whether placental stem cells could be employed as a platform to load nanoparticles and carry them towards tumors for future anticancer therapies.

1. Introduction

The use of nanotechnology for drug delivery is nowadays changing the fields of biotechnology and biomedicine, allowing the incorporation of multiple therapeutic, sensing and targeting agents into nanoparticles (NPs) [1,2]. Those NPs can be manufactured with a great variety of compositions and/or structures [3]. Among the different types of NPs, mesoporous silica NPs offer superior structural properties compared to other NPs, such as, large surface area and pore volume, tunable pore sizes, colloidal stability and robustness that allows straightforward functionalization of the silica walls [4–6]. NPs have been widely investigated as carriers for targeted drug delivery to cancer cells because they can overcome several inconveniences of systemic drug administration, such as poor solubility and limited stability of several drugs and side-effects due to non-specific uptake of the cytotoxic drugs by healthy cells [7–9]. In this sense, a key aspect of this technology is that NPs can be targeted and delivered into the tumors, which can be achieved by either passive targeting, through the enhanced permeability and retention (EPR) effect [10,11], or active targeting, through the functionalization of nanoparticle surface with certain affinity ligands that would be specifically recognized by the targeted diseased cells [12]. However, the recent progress in

* Corresponding authors at: Grupo de Medicina Regenerativa, Centro de Investigación, Instituto de Investigación Sanitaria Hospital 12 de Octubre i+12, Madrid, Spain (A.I. Flores); Dpto. Química Inorgánica y Bioinorgánica, Facultad de Farmacia, UCM, Instituto de Investigación Sanitaria Hospital 12 de Octubre i+12, Madrid, Spain (M. Vallet-Regí).
E-mail addresses: anaisabel.flores@salud.madrid.org (A.I. Flores), vallet@ucm.es (M. Vallet-Regí).

http://dx.doi.org/10.1016/j.actbio.2016.01.017
1742-7061/

nanotechnology has not achieved the expected results in improving drug targeting [13,14], highlighting the need of a better localization of the nanoparticles towards the tumor sites.

Human mesenchymal stem cells (MSCs), which are multipotent progenitors cells that maintain and regenerate connective tissues [15], present migratory properties towards tumors. Those inherent tumor tropism and migratory properties suggest their possible use as carriers of NPs to isolated tumors and metastatic diseases [16,17]. A particular type of MSCs, those from the decidua of human placenta, have shown migratory capacity towards tumors *in vitro*, as well as in a preclinical model of breast tumors [18]. Although the driving force for DMSCs to migrate into tumor sites is unknown, it is already well known that human MSCs have high tropism towards tumors [19]. The inflammatory tumor microenvironment enables human MSCs to specifically home to tumor tissues. Several factors such as cytokines, growth factors, receptors, extracellular matrix and inflammation factors appear to be involved in this migration capacity [20,21]. More interestingly, DMSCs have been observed to inhibit the growth of primary tumors and the development of new tumors [18]. These observations, together with the facts that DMSCs are easy to obtain and constitute a homogeneous population, inspired the idea of using them as therapeutic agents and as cellular vehicles of nanoparticles towards tumors.

The aim of the present work is to exploit the benefits of the chemistry and biology of both systems. On one hand, NPs can be loaded with different chemical molecules and their surface can be easily modified with diverse chemical groups. On the other hand, the biological abilities of DMSCs, including the migration features towards tumors and the inherent inhibition of the growth of certain tumors, motivated the use of those cells as carriers of NPs towards tumor cells. Although the idea of introducing NPs in MSCs has been already reported for actively targeted delivery [22], this article investigates for the first time whether human DMSCs could be employed as a platform to load NPs and carry them to tumors for future anticancer therapies.

DMSCs, like other MSCs, are adult stem cells without the ethical concerns of embryonic cells, they present a low risk of viral infection and have low or non-immune response, and also show genomic stability under extended culture periods. Further, DMSCs present additional advantages respect to other MSCs sources, such us, the cells are easy to obtain, in a greater number and without invasive procedures. Moreover, the capacities of proliferation and differentiation of MSCs from other sources such as bone marrow or adipose tissue, are variable and dependent of the donor age while DMSCs present a high proliferation and differentiation capacity. All these characteristics of DMSCs suggest that they could be considered a good and safe product for future clinical applications.

This work explores the internalization of two different types of NPs into DMSCs, the cellular retention capacity of the NPs, their effect on DMSCs survival and, the *in vitro* and *in vivo* migration capacity towards mammary tumor tissue. Also, the capacity of DMSCs carrying drug-loaded NPs to induce cancer cell death was evaluated. The integration of NPs with DMSCs would allow the design of a multifunctional platform for effective treatment of diseases such as cancer.

2. Experimental section

2.1. Fabrication and characterization of dye-doped NPs

NPs were synthesized by modifying previous methods [23]. Briefly, APTES-dyes were synthesized by labeling 3-aminopropyl triethoxysilane (APTES) with active groups of dyes. For example, APTES (2.2 μL) was labeled with 1 mg of fluorescein isothiocyanate (FITC) in 100 μL of ethanol solution. The reaction mixture was stirred at room temperature for 2 h. Separately, cetyltrimethylammonium bromide (CTAB) (1 g) was dissolved in 480 mL of deionized water and 3.5 mL of 2 M NaOH were added with magnetic stirring. The mixture was heated to 80 °C and left for 30 min. Then, 5 mL of tetraethyl orthosilicate (TEOS) for negatively-charged NPs (neg-NPs), or a mixture of TEOS and APTES (4.5 and 0.5 mL, respectively), for positively-charged NPs (pos-NPs), was added slowly during 20 min, then the particles were left at 80 °C under stirring for 2 h. The resulting particles were collected by centrifugation and then washed three times with deionized water and ethanol, respectively. The surfactant template was removed by ion exchange using an extracting solution of NH_4NO_3 (10 mg/mL) in EtOH (95%). The particles were suspended in that medium and magnetically stirred at 75 °C overnight. The particles were centrifuged and washed three times with deionized water and ethanol. Surfactant removal was confirmed by thermogravimetric analysis.

All the reagents used for the synthesis of NPs were commercial products (Sigma–Aldrich, Spain) and were used without further purification.

The materials were analyzed by X-ray diffraction (XRD) in a Philips X-Pert MPD diffractometer equipped with Cu Kα radiation. Thermogravimetry and Differential Temperature Analysis (TGA/DTA) were performed in a Perkin Elmer Pyris Diamond TG/DTA analyser, with 5 °C/min heating ramps, from room temperature to 600 °C. Fourier Transformed Infrared (FTIR) spectra were obtained in a Nicolet (Thermo Fisher Scientific) Nexus spectrometer equipped with a Smart Golden Gate Attenuated Total Reflectance (ATR) accessory. Surface morphology was analysed by Scanning Electron Microscopy (SEM) in a JEOL 6400 Electron microscope. Transmission Electron Microscopy (TEM) was carried out with a JEOL JEM 2100 instrument operated at 200 kV, equipped with a CCD camera (KeenView Camera). N_2 adsorption was carried out on a Micromeritics ASAP 2010 instrument; surface area was obtained by applying the Brunauer, Emmet & Teller (BET) method to the isotherm and the pore size distribution was determined by the Barrett, Joyner & Halenda (BJH) method from the desorption branch of the isotherm. The mesopore size was determined from the maximum of the pore size distribution curve. The Z-potential and hydrodynamic size of nanoparticles were measured in deionized water by means of a Zetasizer Nano ZS (Malvern Instruments) equipped with a 633 nm "red" laser.

2.2. Isolation and culture of DMSCs

Human placentas from healthy mothers were obtained from the Department of Obstetrics and Gynecology under written informed consent approved by the Ethics Committee from *Hospital Universitario* 12 *de Octubre*. Processing of placental membranes and culture of primary cells was done as previously described [18,24]. Briefly, extra- embryonic membranes (amnion, chorion [fetal origin] and decidua [maternal origin]) were processed by enzymatic digestion with trypsin–EDTA (Lonza, Spain). Isolated cells were grown in Dulbecco's modified Eagle's medium (DMEM) supplemented with 2 mM of glutamine, 0.1 mM of sodium pyruvate, 55 mM β-mercaptoethanol, 1% non-essential amino acids, 1% penicillin/streptomycin, 10% fetal bovine serum and 10 ng/mL of EGF (epidermal growth factor), at 37 °C, 5% CO_2 and 95% humidity. Non-adherent cells were discarded after 5 days. In our preceding study, we reported the morphology, phenotype, maternal origin and MSCs characteristics of DMSCs [24]. At confluence, adherent cells were passaged and seeded at a density of 10^4 cells per cm^2.

2.3. Cellular uptake of particles by DMSCs

DMSCs were plated 24 h before the start of the experiment in culture multiwell plates at a density of 10^4 cells per cm^2. After incubation with 200 μg/mL particles for 2 h, the media were replaced by fresh media and cells were incubated for one additional hour. The cells were fixed with Z-fix solution (Anatech, USA) for 15 min, permeabilized with 0.1% Triton X-100 in phosphate buffer saline (PBS) solution, at room temperature, for 5 min and, subsequently incubated for 20 min with Alexa Fluor®568 phalloidin (Invitrogen, Spain) for staining F-actin. DAPI (40, 60 diamidino-2-phenylindole) at 1 μg/mL was used to stain and visualize the nuclei. Fluorescence microscopy was performed with an Evos® FL Cell Imaging System equipped with tree Led Lights Cubes (lEX (nm); lEM (nm)): DAPI (357/44; 447/60), GFP (470/22; 525/50), RFP (531/40; 593/40) from AMG (Advance Microscopy Group). Quantitative analysis of cellular uptake was performed by flow cytometry (FACS). 200 μg/mL particles were incubated with the DMSCs for the indicated time points, and then removed by washing three times and cells were incubated for one additional hour. Subsequently, the cells were trypsinised, collected by centrifugation and redispersed in PBS solution with trypan blue (0.5%) to remove extracellular fluorescence. The fluorescence intensity of 10,000 cells was quantified by FACS. Statistical analysis for differences between groups was carried out by the Student's t test.

Quantitative analysis of retention ability of particles was performed by FACS. Particles at a concentration of 200 μg/mL were incubated with the MSCs for 2 h, and then removed by washing three times. The cells were then cultured in fresh medium for indicated time points. Subsequently, the cells were collected by trypsinization and centrifugation, and redispersed in PBS solution with trypan blue (0.5%). The fluorescence intensity of 10,000 cells was quantified by FACS. The fluorescence intensities obtained after the first day were corrected by the cell dilution folds due to cell division.

2.4. Intracellular fate of NPs

For the co-localization of NPs and lysosomes, the cells were incubated with 200 μg/mL particles for 2 h. The cells were washed twice with PBS solution. Then, lysosomes were stained with the Cell Tracker® Lysosome staining kit following the manufacturer protocol (AAT Bioquest, Inc, USA). The cells were washed twice with PBS, and then fresh medium was added. The cells were fixed and stained with DAPI as previously described. Fluorescence microscopy was performed with an Evos® FL Cell Imaging System.

2.5. Cytotoxicity of NPs

The cytotoxicity of NPs was evaluated using the following standard protocols:

Lactate dehydrogenase (LDH) activity test: extracellular LDH activity was measured in the media using the kit for quantitative determination of LDH (Spinreact, Spain). DMSCs were incubated with NPs for 24 h at different concentrations. Then, the culture medium was collected for measuring the extracellular LDH activity. The LDH activity was directly measured by spectrophotometer at 340 nm in the culture medium following the manufacturer protocol.

MTS (3-(4,5-dimethylthiazol-2-yl)-5-(3-carboxymethoxyphenyl)-2-(4-sulfophenyl)-2H-tetrazolium) assay: the MTS reduction assay was performed using a commercial assay and following the manufacturer's protocol (CellTiter® Aqueous One Solution Cell Proliferation Assay). Briefly, DMSCs were incubated with various concentrations of NPs for 2 h ($n = 3$). The medium was replaced with 600 μL culture medium including MTS, and the incubation proceeded for 3 h. The medium was then removed, and its absorption at 490 nm was measured using a microplate reader.

2.6. Tissue homogenates from NMU-induced mammary tumors

N-nitroso-N-methylurea (NMU) tumors were induced in 45-day-old Sprague–Dawley female rats according to our previously published protocol [25]. Concisely, NMU (Sigma–Aldrich, Spain) was administered once a week during two weeks by intraperitoneal injection at a concentration of 5 mg/100 g rat body weight. As well, metoclopramide (0.125 mg/L) was administered in the drinking water. Animals were palpated weekly for the detection of mammary tumors. The tumors were disected out from the animals, immediately frozen in liquid nitrogen and subsequently stored at −80 °C until use.

Homogenates were performed at 4 °C as we previously described [18]. The protein concentration was measured using the Lowry protein assay kit (Biorad, Spain) following the manufacturer's instructions.

2.7. Transwell assay

The *in vitro* effect of mammary tumor homogenate on DMSCs migration capacity was determined using Millicell culture plate inserts with 8 μm pore polycarbonate membranes (Merk Millipore, Spain) in 24-well plates. Briefly, 1.5×10^5 DMSCs in 300 μL of serum-free DMEM were seeded in the insert. Tumor homogenate (5 mg/mL of protein concentration was added in the well below). Migration medium (serum-free DMEM) without tissue was used as a negative control. Migration was assessed at 24 h by the CytoSelect 24-Well Cell Migration Assay (8 μm, Colorimetric, Cell Biolabs, Bionova Cientifica, S.L., Spain). Non-migratory cells were removed from the top of the membrane and migratory cells on the bottom of the polycarbonate membrane were stained with the cell stain solution. Migratory cells were visualized (three individual fields per insert) using a light microscope under ×40 magnification objective. Color of stained cells was subsequently extracted with the extraction solution, and quantified by absorbance at 560 nm using the multimodal plate reader Enspire (Perkin Elmer). All experiments were done as a minimum in triplicate.

2.8. In vivo migration

To evaluate the *in vivo* migration capacity of NP loaded DMSCs, cells were incubated with pos-NPs as previously described. After washing non-internalized NPs, 10^6 cells were injected into the circulation through the tail-vein of Spraw-Dawley rats with NMU-mammary tumors. Seventy-two hours later, rats were anesthetized, and mammary tumors were removed and stored at −80 °C until use. Frozen tissue was sectioned in the cryostat, fixed and treated with Sudan Black (Sigma–Aldrich, Spain) to remove self-fluorescence following the manufacturer's instructions. The nuclei were stained with DAPI for 1 min and sections were mounted with Vectashield and the tissue sections were visualized by fluorescence microscopy.

2.9. In vitro experiments with doxorubicin-loaded NPs

Doxorubicin was loaded in neg- and pos-NPs by stirring 10 mg of NPs in 5 mL of a 1 mg/mL solution of doxorubicin in PBS for 24 h. Doxorubicin-loaded NPs (DOX-NPs) were washed by centrifugation and redispersion in PBS several times.

DMSCs were incubated with 200 μg/mL DOX-NPs for 2 h and washed with PBS to remove non-internalized nanoparticles. Cell viability was evaluated after 2 h, 1 day and 2 days by Alamar Blue

assay (Promega, Spain), following the manufacturer's instructions. Briefly, 10% of the reagent was added to the culture medium with the DMSCs and incubated at 37 °C for 1 h. Then, fluorescence at 560EX nm/590EM nm was measured in a microplate reader. Cell viability was then analyzed as a percentage of the control wells (DMSCs not exposed to DOX-NPs).

In order to determine the feasibility of using DOX-NPs inside DMSCs as a platform for future anticancer therapies, DMSCs with DOX-pos-NPs were co-cultured with NMU rat mammary cancer cells (ATCC, LGC Standards S.L.U., Spain). NMU cells were cultured in 24 well plates at a density of 20,000 cells per well. Twenty-four hours later, three wells were trypsinized and cells were counted. Then, DMSCs with DOX-pos-NPs (incubated as described previously) were seeded in Transwell® culture inserts (0.4 μm pore, polycarbonate membranes, tissue cultured treated, Costar®) in two different DMSCs:NMU ratios (1:2 and 1:5). After 4 days, the inserts were removed and NMU cells were trypsinized and stained with BD Pharmingen™ FITC Annexin V Apoptosis Detection Kit I, following the manufacturer's instructions. Then, the cells were analyzed by FACS. Statistical analysis was performed by the Student's t test.

3. Results and discussion

In order to evaluate DMSCs as potential carriers of NPs, mesoporous silica NPs (neg-NPs and pos-NPs) were synthesized according to a modified Stöber method [23]. Both types of NPs were covalently labeled with fluorescein by co-condensation during nanoparticle synthesis in order to be able to follow the fate of the NPs in contact with cells by fluorescence microscopy. Regarding particle morphology, SEM micrographs showed NPs, neg-NPs and pos-NPs, with spherical shape. Additionally, well-ordered mesoporous channels could be appreciated in the corresponding TEM micrographs (Fig. 1). In fact, typical XRD patterns of MCM-41 type materials were observed in all cases, with the three characteristic maxima (100), (110) and (200), confirming the 2D hexagonal order of the mesopores arrangement (Fig. S1). N_2 adsorption isotherms observed in all cases were type IV, with typical surface areas (1051 and 1109 m^2/g) and pore diameter (2.8 and 2.5 nm) for this type of negatively and positively-charged NPs, respectively. The NPs show a hydrodynamic particle diameter of *ca.* 190 nm. The charge of the NPs was confirmed through Z-potential (−31.5 mV and +23.3 mV, respectively), and the organic functionality through FTIR spectroscopy (Si-OH and $-NH_2$ groups, respectively) (Fig. S1).

With respect to the interaction of the particles with the cells, in addition to size and shape, the NP surface is also a very important feature. The mechanism of NP internalization into the cell is generally via endocytosis [26], a process in which extracellular materials are intracellularly incorporated into a membranous vesicle. The chemical groups attached to the surface of the NPs strongly influence their interaction with biological entities and, therefore, their internalization. In this sense, the surface of NPs can be easily modified through a functionalization process with a great variety of organic groups [27]. In an effort to evaluate the contribution of surface chemistry, the effect of both charge and functionality on the cellular uptake, neg-NPs and pos-NPs was tested.

First, we incubated NPs with DMSCs to evaluate the toxicity of the nanoparticles on these cells in culture. Both negatively and positively-charged NPs were dispersed in serum-free medium at different concentrations and incubated with DMSCs for 2 h. Then, the nanoparticles were withdrawn and the cells were cultured in complete medium for 24 h. Cell viability was examined by LDH release and MTS reduction assay (Fig. 2).

We observed that there was no increase in LDH released in the culture medium of DMSCs incubated with the NPs. This indicates that, at 24 h, the NPs did not induce cell death in DMSCs. Furthermore we looked to confirm these results using an assay that estimates the number of viable cells. The results of the MTS reduction assay (Fig. 2) show that NPs did not induce significant toxicity over a very wide range of NP concentrations (at least up to 1 mg/mL). This is of great value for subsequent experiments because it is very important to have as much NPs as possible incorporated into cells.

Once toxicity was found not to be an issue, the next step was to evaluate the endocytosis process, studying how long the NPs remain inside the cells (retention time) and describing their location within the cells, whether lysosomal or cytoplasmic. To evaluate the endocytosis process, both types of NPs (negatively and positively-charged) were dispersed in serum-free DMEM and incubated with DMSCs for different periods of time. The concentrations of NPs, 100 and 200 μg/mL, were selected to avoid nanoparticle aggregates outside the cells (Fig. S2). The NP suspension was then withdrawn and the cells were rinsed three times with PBS. Fluorescence microscopy images of DMSCs incubated with neg-NPs and pos-NPs can be seen in Fig. 3a. After staining cytoplasmatic actin with AlexaFluor®568 Phalloidin (red) and nuclei with DAPI (blue), NPs with a fluorescent dye attached are observed internalized into the cytoplasm of the DMSCs, with most cells carrying NPs when

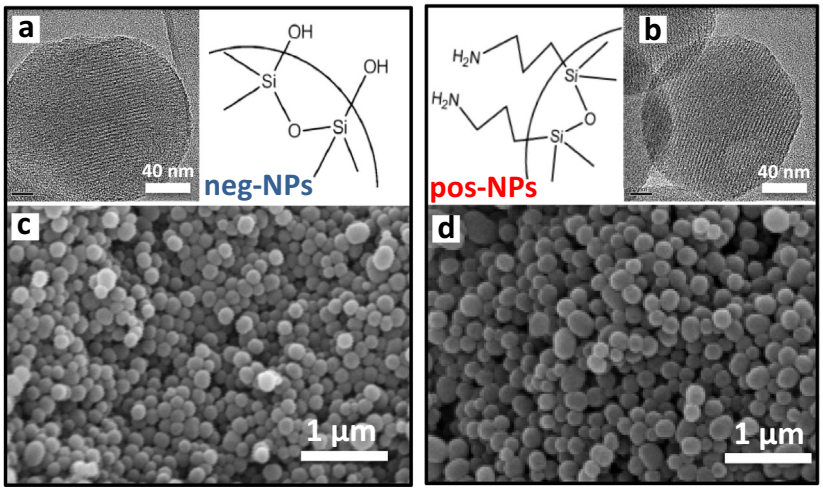

Fig. 1. TEM (a, b) and SEM (c, d) micrographs of neg-NPs (left) and pos-NPs (right).

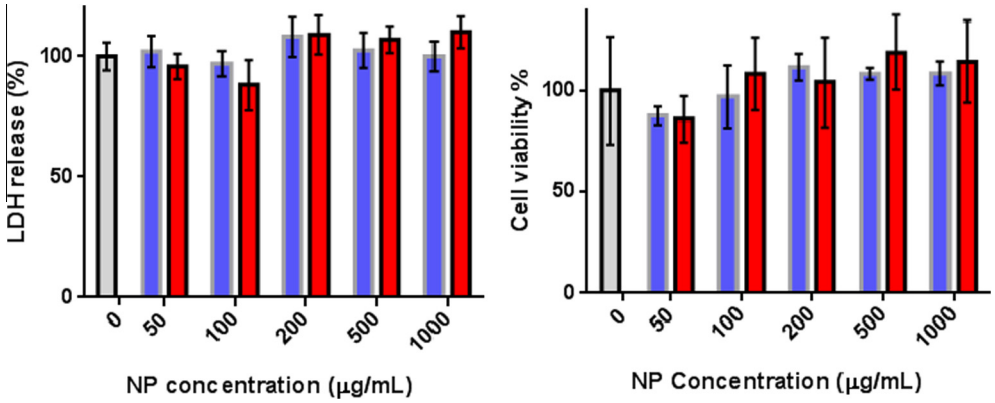

Fig. 2. LDH release by DMSCs with internalized neg-NPs (blue) and pos-NPs (red) for 24 h (left); cytotoxicity assay measured by MTS reduction of neg-NPs (blue) and pos-NPs (red) in DMSCs at 24 h after endocytosis (right). No significant differences were found at any of the evaluated concentrations (Data presented as Mean ± SD, $N = 3$). (For interpretation of the references to color in this figure legend, the reader is referred to the web version of this article.)

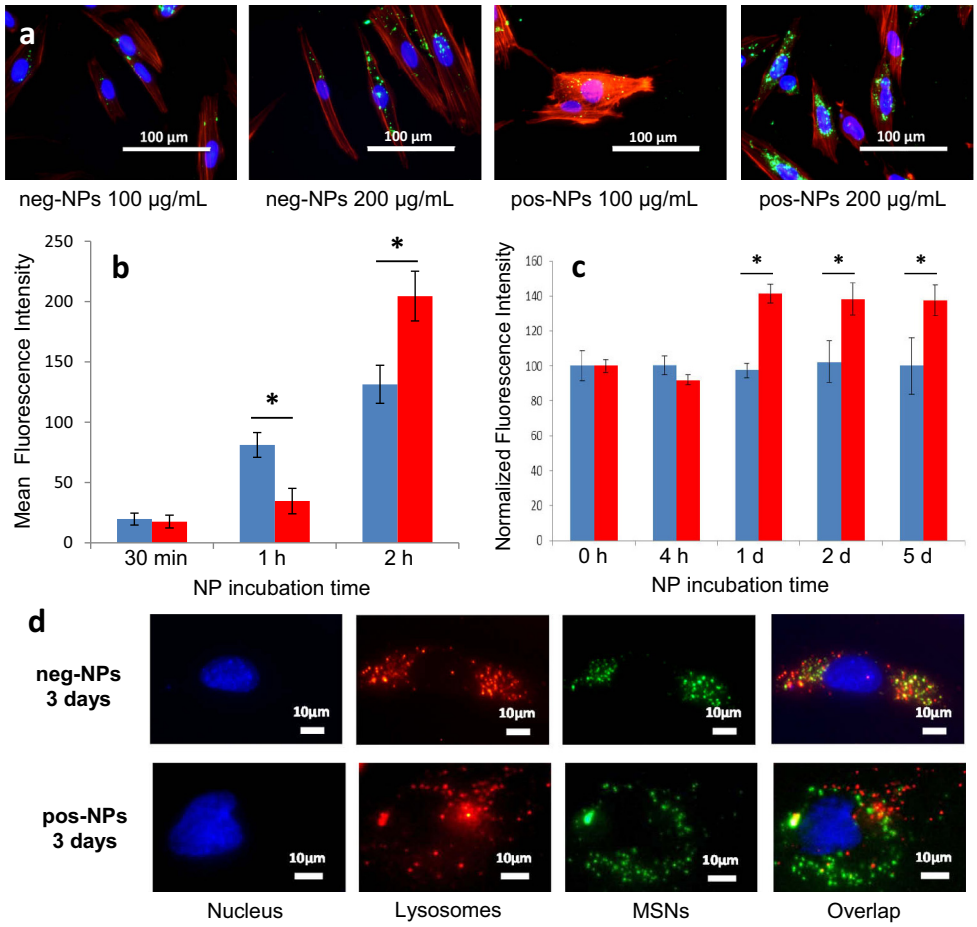

Fig. 3. Fluorescence images of NP-loaded DMSCs; blue (nucleus), red (cytoplasm), green (NPs) (a), flow-cytometry data regarding neg-NPs (blue) and pos-NPs (red) uptake (b) and retention (c) (Mean ± SD, $N = 3$, $^{*}p < 0.05$), Colocalization study of NPs (green), nucleus (blue) and lysosomes (red) in DMSCs after 3 days (d). (For interpretation of the references to color in this figure legend, the reader is referred to the web version of this article.)

incubated at 200 µg/mL. The morphology of the cells remained unmodified after NP internalization (Fig. S3).

When incubating NPs (green) with a concentration of 100 µg/mL, pos-NPs were observed to be internalized more efficiently than neg-NPs. The same trend was observed with higher concentrations (200 µg/mL). Thus, we found that 200 µg/mL and 2 h were the optimal concentration and incubation time parameters for the best internalization results. Besides, pos-NPs were internalized better in DMSCs than neg-NPs, with many particles localized around the nucleus after 2 h of incubation (Fig. 3a).

The uptake of NPs was quantified using flow cytometry at different times of internalization (Fig. 3b). The cells were dispersed in trypan blue solution in order to remove extracellular fluorescence and quantify only internalized nanoparticles. The results showed that, at shorter periods of time, the amount of endocytosed NPs was higher for those negatively charged, probably due to an

electrostatic interaction of the positively-charged particles with the cell surface, delaying their internalization. However, after two hours, both types of NPs were effectively endocytosed, with percentages of cells with internalized NPs close to 85% in all cases (Fig. S4).

Fluorescence intensity of internalized particles followed the same trend, with more neg-NPs internalized after 1 h than pos-NPs (Fig. 3b). However, after 2 h of incubation, the intensity of the pos-NPs was higher than the neg-NPs, which indicates that the former NPs are better internalized than the later. All of these results are in agreement with previous results in the literature [28], and could be explained by the stronger interaction of pos-NPs with negatively-charged phospholipids in the cell membrane. In order to check that interaction, the same cells dispersed in PBS were analyzed by flow-cytometry and intracellular and membrane-adhered NPs were measured. The fluorescence of membrane-adhered NPs was estimated as the difference of cell fluorescence in PBS and cell fluorescence in trypan blue solution. This extracellular fluorescence was 2.5 times higher for pos-NPs than for neg-NPs (data not shown). In any case, the necessary time to complete the internalization process was found to be 2 h, so this was the incubation time of NPs with cells for the subsequent experiments.

Once the NPs have been internalized, the next important parameter to consider is the retention time of the particles in the cells. According to previous studies by our group [18], it was found that 3 days is the necessary time for the DMSCs to reach the tumor tissues in an *in vivo* model, so the particles should remain in the cells a minimum of 3 days. The procedure to evaluate the retention capacity of the particles in DMSCs was similar to the uptake

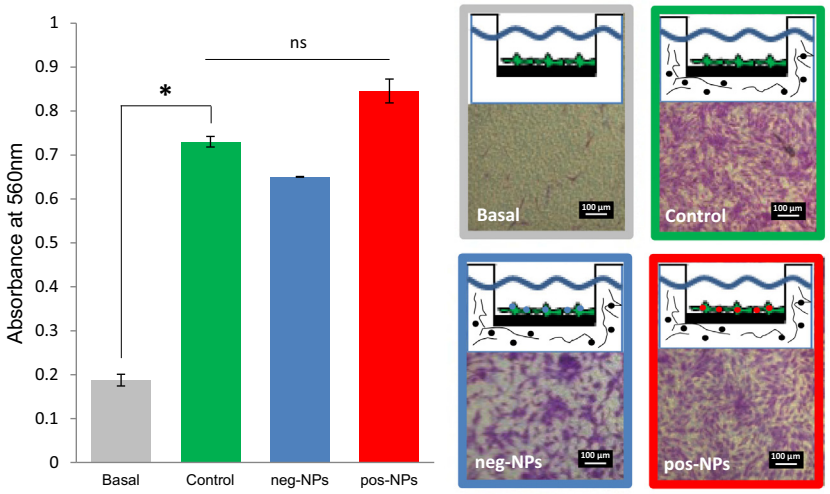

Fig. 4. *In vitro* Transwell migration assay of DMSCs against culture medium (basal), tumor homogenate (control) and migration of NP-loaded DMSCs against tumor homogenate. (Mean ± SD, $N = 3$, $^{*}p < 0.05$).

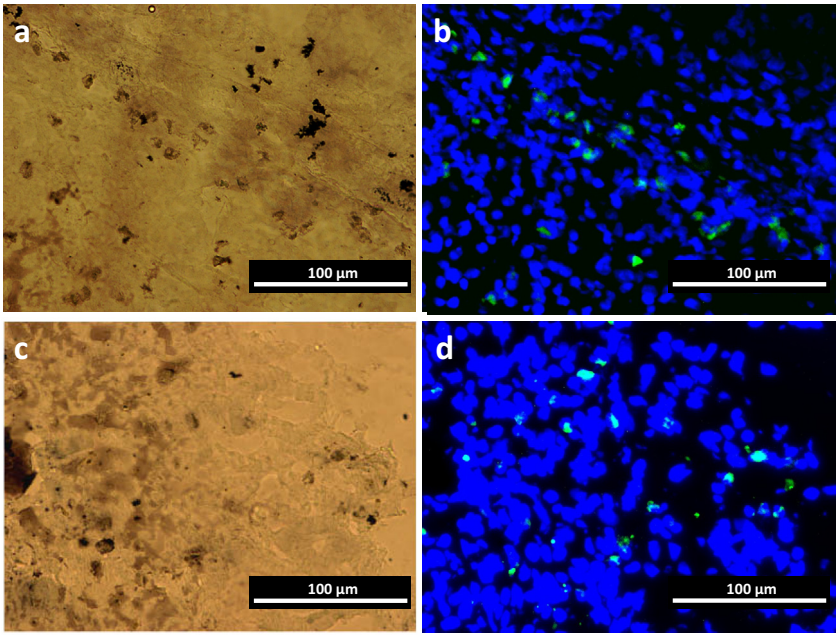

Fig. 5. Fluorescence microscopy images of sections of NMU-induced rat adenocarcinomas after *in vivo* migration of DMSCs (images were taken 72 h after tail-vein injection of 10^6 DMSCs). Bright field images (a, c) of the tumor sections and Fluorescence images (b, d) of the same sections showing blue fluorescence of cell nuclei stained with DAPI and green fluorescence of the pos-NPs, indicating the *in vivo* migration towards tumors of DMSCs carrying pos-NPs. (For interpretation of the references to color in this figure legend, the reader is referred to the web version of this article.)

experiment, that is, cells were incubated with 200 μg/mL of both neg- and pos-NPs for 2 h, then washed and cultured for up to 5 days. Fig. 3c shows the normalized fluorescence intensity percentage of the cells at different culturing times, being almost constant for the neg-NPs, which means that those NPs were retained in the cytoplasm. Pos-NPs fluorescence was kept unchanged at the initial stages, but after 1 day the intensity increased up to *ca.* 140%. This could be explained by a slow uptake of membrane-adhered nanoparticles due to interactions between pos-NPs and negatively-charged phospholipids at the cell membrane [28]. This means that in terms of retention capacity, a greater amount of particles were observed in the group of pos-NPs than in the neg-NPs. Most importantly, in all cases, NPs were still retained in the cells at day 5. Taking into account that it takes around 3 days for the cells to reach the tumor in the *in vivo* model previously evaluated [18], those results guarantee that our NPs will be still in the cells when reaching the tumor tissue, validating our initial hypothesis of using DMSCs as carriers of nanoparticles.

Once internalization and retention of NPs into living mesenchymal cells were validated, the next step was exploring the location of internalized NPs in the cells. NPs are normally transported to the endo-lysosomal system after internalization, and the ability of the NPs to escape from the lysosomes is an important parameter regarding the stability of the NPs [17].

A co-localization study was performed in DMSCs with internalized NPs by staining the cell lysosomes (Cell Navigator® Lysosome staining kit) and comparing the location within the cells of lysosomal red fluorescence and NP-associated green fluorescence. We observed that NPs were located inside lysosomes just after internalization (Fig. S5), independently of their surface charge. However, after 3 days, the location of NPs inside the cells was different for pos-NPs and neg-NPs (Fig. 3d). In neg-NPs, the fluorescence due to NPs was co-localized within the lysosomes, which indicates that neg-NPs were not able to escape the lysosomes in that time. On the other hand, fluorescence from pos-NPs does not match the fluorescence of the cell lysosomes at day 3, which shows that these NPs had escaped the lysosomes, probably by a charge-dependent mechanism previously described in the literature [17]. This result indicates that pos-NPs could be a better option to be transported by DMSCs, as the lysosomal escape would ensure a less aggressive environment both for the NPs and its cargo.

All the above results show the stability of NPs in DMSCs, which is a necessary requirement to combine both elements. The internalization of the NPs into the cells and their persistence has been shown so far, so we next evaluated the migration capacity of NP-loaded DMSCs towards tumors. The *in vitro* and *in vivo* migrating capability of DMSCs towards tumors has been previously observed by our research group [18]. Here we evaluated if DMSCs with uptaken NPs retained those tumor tropism properties in an *in vitro* migration study. Thus, their *in vitro* migration capability was analyzed in the presence and absence of tumor human breast homogeneate using a standardized Transwell migration assay (Fig. 4). DMSCs without particles (control) and with both types of NPs were tested.

Compared to the migration in the absence of tumor homogenate, DMSCs migration capacity was almost 4 times higher when the tumor homogenate was present. Interestingly, the presence of any of the types of NPs (pos- and neg-) in the cells, did not appreciably affect the migration capacity of DMSCs toward tumor homogenate. Thus, combining these migration results together with cellular uptake, retention time and lysosomal leakage, it is clear that pos-NPs inside DMSCs is the best combination for the design of an efficient construct for drug delivery technologies. Therefore, pos-NPs were chosen to study the *in vivo* migration of DMSCs towards mammary tumors. DMSCs were cultured with pos-NPs and injected into the tail vein of NMU-induced tumor rats. After 3 days, the tumors were surgically removed, and the presence of green-fluorescent NPs was examined by fluorescence microscopy. The results presented in Fig. 5 show the presence of NPs inside the tumors, located around of some nuclei in the tissue. This indicates that the DMSCs retain their *in vivo* homing capacity towards the tumors when carrying NPs. These results show the ability of the cells to transport the NPs to the diseased site.

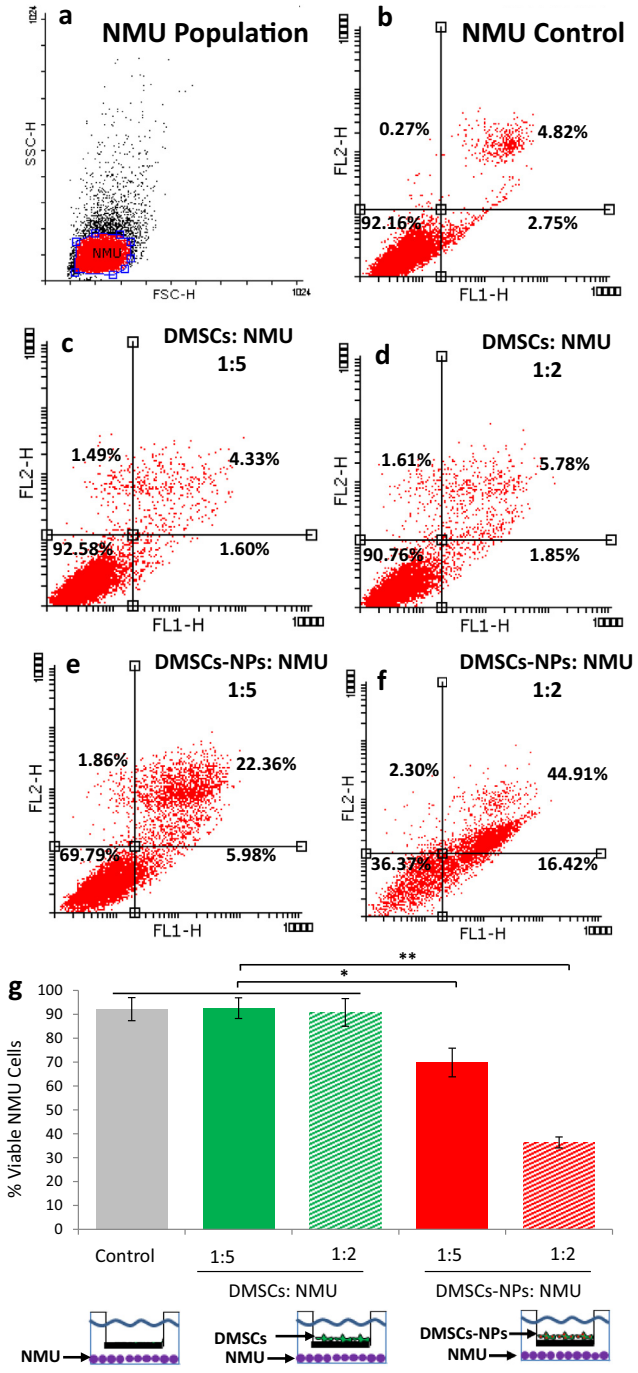

Fig. 6. Flow cytometry results of NMU cells after co-culture in different ratios with DMSCs or with DMSCs with internalized doxorubicin-loaded pos-NPs (DMSCs-NPs). NMU population analyzed (a), apoptosis/necrosis evaluation of NMU cells showing viable cells (lower left quadrant), early apoptotic cells (lower right quadrant) and late apoptotic/necrotic cells (upper right quadrant) (b–f), percentage of viable NMU cells after co-culture (g). (Mean ± SD, $N = 3$, $^{*}p < 0.05$, $^{**}p < 0.01$).

Regarding the antitumor application of this platform, NPs were loaded with doxorubicin, an anticancer drug. DOX-NPs were then incubated with DMSCs and cell viability was evaluated by Alamar Blue assay at different time points (Fig. S6). DOX-neg-NPs induced significantly higher toxicity in DMSCs than DOX-pos-NPs after 2 days. This effect could be due to the higher doxorubicin loading capacity of neg-NPs previously reported in the literature [29], which leads to higher toxicity. As a consequence, DOX-pos-NPs were chosen for the subsequent experiments.

The therapeutic potential of this approach was evaluated through an *in vitro* co-culture assay, using DMSCs with DOX-pos-NPs and NMU mammary cancer cells. DMSCs with or without drug-loaded NPs were seeded in the Transwell culture insert and the insert placed on top of a well that contains the NMU cells. Two different DMSC:NMU ratios (1:2 and 1:5) were tested. After 4 days, the Transwell inserts were removed and the NMU cells were evaluated by FACS using an apoptosis/necrosis detection kit (BD Pharmingen™ FITC Annexin V Apoptosis Detection Kit I). The Fig. 6 shows that a significant fraction of the cancer cells became apoptotic/necrotic (cells appear in the right quadrants of the dot plots FL1-H *vs* FL2-H) only when the DMSCs were carrying DOX-NPs. Furthermore, this effect also appears to be dose-dependent, observing lower cancer cell viability when larger amounts of DMSCs transporting DOX-NPs were present.

4. Conclusions

Mesoporous silica nanoparticles (NPs) show negligible toxicity after being incubated with human Decidua-derived mesenchymal stem cells (DMSCs). NP uptake by DMSCs is fast (2 h) and the particles are retained inside the cells for a long period of time (at least 5 days), more than enough for DMSCs to accumulate in the tumor environment. The presence of NPs inside DMSCs does not inhibit their tumor-tropic behavior *in vitro* and *in vivo*. DMSCs transporting doxorubicin-loaded NPs were capable of inducing cell death in NMU cancer cells when co-cultured *in vitro*. All of these results indicate that DMSCs could be a promising platform for cancer therapy as carriers of anticancer drug-loaded NPs.

Acknowledgments

Financial support from Ministerio de Economía y Competitividad, Spain (Project MAT2012-35556 and Project CSO2010-11384-E, Ageing Network of Excellence) and CIBER-BBN are gratefully acknowledged. CIBER-BBN is an initiative funded by the VI National R&D&i Plan 2008-2011, *Iniciativa Ingenio* 2010, Consolider Program, CIBER Actions and financed by the Instituto de Salud Carlos III with assistance from the European Regional Development Fund. The XRD measurements were performed at *C.A.I Difracción de Rayos X*, *Universidad Complutense de Madrid* (Spain). SEM and TEM were performed at ICTS National Centre for Electron Microscopy (Spain). JL Paris gratefully acknowledges *Ministerio de Economía y Competitividad*, Spain, for his PhD grant (BES-2013-064182). This work was sponsored by Grants from Acción Estratégica en Salud (FIS PI080137; PI11/00581; PI13/00045); the Comunidad Autónoma de Madrid (S 2013/MIT-2862-MULTIMAT-CHALLENGE); the MMA Foundation (FMMA 2008-108), and the Neurosciences and Aging Foundation, the Francisco Soria Melguizo Foundation, Octopharma and Parkinson Madrid (PI2012/0032). The authors are very grateful to M. Grau and D. de la Fuente for their assistance in the *in vivo* experiments.

Appendix A. Supplementary data

Supplementary data associated with this article can be found, in the online version, at http://dx.doi.org/10.1016/j.actbio.2016.01.017.

References

[1] O.C. Farokhzad, R. Langer, Impact of nanotechnology on drug delivery, ACS Nano 3 (2009) 16–20.
[2] C. Minelli, S.B. Lowe, M.M. Stevens, Engineering nanocomposite materials for cancer therapy, Small 6 (2010) 2336–2357.
[3] S.D. Steichen, M. Caldorera-Moore, N.A. Peppas, A review of current nanoparticle and targeting moieties for the delivery of cancer therapeutics, Eur. J. Pharm. Sci. 48 (2013) 416–427.
[4] C. Argyo, V. Weiss, C. Bräuchle, T. Bein, Multifunctional mesoporous silica nanoparticles as a universal platform for drug delivery, Chem. Mater. 26 (2014) 435–451.
[5] M. Manzano, M. Colilla, M. Vallet-Regí, Drug delivery from ordered mesoporous matrices, Expert Opin. Drug Deliv. 6 (2009) 1383–1400.
[6] M. Manzano, M. Vallet-Regí, New developments in ordered mesoporous materials for drug delivery, J. Mater. Chem. 20 (2010) 5593.
[7] J. Lu, M. Liong, J.I. Zink, F. Tamanoi, Mesoporous silica nanoparticles as a delivery system for hydrophobic anticancer drugs, Small 3 (2007) 1341–1346.
[8] Z. Li, J.C. Barnes, A. Bosoy, J.F. Stoddart, J.I. Zink, Mesoporous silica nanoparticles in biomedical applications, Chem. Soc. Rev. 41 (2012) 2590–2605.
[9] J. Lu, M. Liong, Z. Li, J.I. Zink, F. Tamanoi, Biocompatibility, biodistribution, and drug-delivery efficiency of mesoporous silica nanoparticles for cancer therapy in animals, Small 6 (2010) 1794–1805.
[10] J. Fang, H. Nakamura, H. Maeda, The EPR effect: unique features of tumor blood vessels for drug delivery, factors involved, and limitations and augmentation of the effect, Adv. Drug Deliv. Rev. 63 (2011) 136–151.
[11] H. Maeda, H. Nakamura, J. Fang, The EPR effect for macromolecular drug delivery to solid tumors: improvement of tumor uptake, lowering of systemic toxicity, and distinct tumor imaging in vivo, Adv. Drug Deliv. Rev. 65 (2013) 71–79.
[12] N. Bertrand, J. Wu, X. Xu, N. Kamaly, O.C. Farokhzad, Cancer nanotechnology: the impact of passive and active targeting in the era of modern cancer biology, Adv. Drug Deliv. Rev. 66 (2014) 2–25.
[13] I.K. Kwon, S.C. Lee, B. Han, K. Park, Analysis on the current status of targeted drug delivery to tumors, J. Control Rel. 164 (2012) 108–114.
[14] V.J. Venditto, F.C. Szoka, Cancer nanomedicines: so many papers and so few drugs!, Adv Drug Deliv. Rev. 65 (2013) 80–88.
[15] M.F. Pittenger, A.M. Mackay, S.C. Beck, R.K. Jaiswal, R. Douglas, J.D. Mosca, et al., Multilineage potential of adult human mesenchymal stem cells, Science 284 (1999) 143–147.
[16] Y.-L. Hu, Y.-H. Fu, Y. Tabata, J.-Q. Gao, Mesenchymal stem cells: a promising targeted-delivery vehicle in cancer gene therapy, J. Control Rel. 147 (2010) 154–162.
[17] Z. Gao, L. Zhang, J. Hu, Y. Sun, Mesenchymal stem cells: a potential targeted-delivery vehicle for anti-cancer drug, loaded nanoparticles, Nanomed. Nanotechnol. Biol. Med. 9 (2013) 174–184.
[18] I. Vegh, M. Grau, M. Gracia, J. Grande, P. de la Torre, A.I. Flores, Decidua mesenchymal stem cells migrated toward mammary tumors in vitro and in vivo affecting tumor growth and tumor development, Cancer Gene Therapy 20 (2013) 8–16.
[19] S. Kidd, E. Spaeth, J.L. Dembinski, M. Dietrich, K. Watson, A. Klopp, et al., Direct evidence of mesenchymal stem cell tropism for tumor and wounding microenvironments using in vivo bioluminescent imaging, Stem Cells 27 (2009) 2614–2623.
[20] E. Spaeth, A. Klopp, J. Dembinski, M. Andreeff, F. Marini, Inflammation and tumor microenvironments: defining the migratory itinerary of mesenchymal stem cells, Gene Therapy 15 (2008) 730–738.
[21] D. Bexell, S. Scheding, J. Bengzon, Toward brain tumor gene therapy using multipotent mesenchymal stromal cell vectors, Mol. Ther. 18 (2010) 1067–1075.
[22] X. Huang, F. Zhang, H. Wang, G. Niu, K.Y. Choi, M. Swierczewska, et al., Mesenchymal stem cell-based cell engineering with multifunctional mesoporous silica nanoparticles for tumor delivery, Biomaterials 34 (2013) 1772–1780.
[23] A. Baeza, E. Guisasola, A. Torres-Pardo, J.M. González-Calbet, G.J. Melen, M. Ramirez, et al., Hybrid enzyme-polymeric capsules/mesoporous silica nanodevice for in situ cytotoxic agent generation, Adv. Funct. Mater. 24 (2014) 4625–4633.
[24] M.I. Macias, J. Grande, A. Moreno, I. Domínguez, R. Bornstein, A.I. Flores, Isolation and characterization of true mesenchymal stem cells derived from human term decidua capable of multilineage differentiation into all 3 embryonic layers, Am. J. Obstet. Gynecol. 203 (2010) 495.e9–495.e23.
[25] I. Vegh, R.E. de Salamanca, Prolactin, TNF alpha and nitric oxide expression in nitroso-N-methylurea-induced-mammary tumours, J. Carcinog. 6 (2007) 18.
[26] J.L. Vivero-Escoto, I.I. Slowing, B.G. Trewyn, V.S.-Y. Lin, Mesoporous silica nanoparticles for intracellular controlled drug delivery, Small 6 (2010) 1952–1967.
[27] F. Hoffmann, M. Cornelius, J. Morell, M. Fröba, Silica-based mesoporous organic–inorganic hybrid materials, Angew. Chem. Int. Ed. Engl. 45 (2006) 3216–3251.
[28] T. Yu, A. Malugin, H. Ghandehari, Impact of silica nanoparticle design on cellular toxicity and hemolytic activity, in: ACS Nano, 2011: pp. 5717–5728.
[29] H. Meng, M. Xue, T. Xia, Y.-L. Zhao, F. Tamanoi, J.F. Stoddart, et al., Autonomous in vitro anticancer drug release from mesoporous silica nanoparticles by pH-sensitive nanovalves, J. Am. Chem. Soc. 132 (2010) 12690–12697.

Supplementary data

Decidua-derived Mesenchymal Stem Cells as carriers of Mesoporous Silica Nanoparticles. *In vitro* and *in vivo* evaluation on mammary tumors.

J.L. Paris, P. de la Torre, M. Manzano, M.V. Cabañas, A.I. Flores and M. Vallet-Regí**

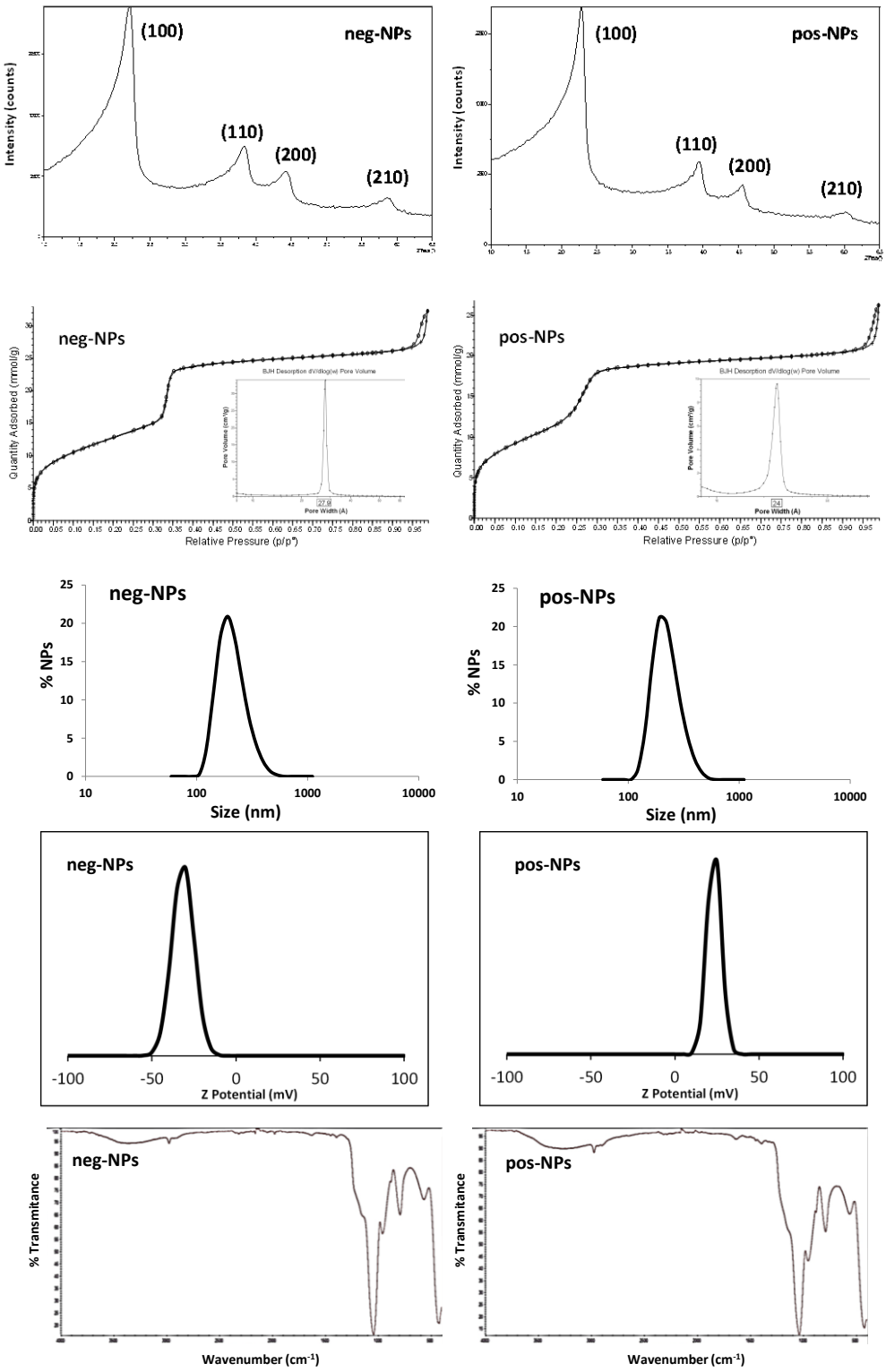

Figure S1. Characterization of Mesoporous Silica Nanoparticles (neg-NPs and pos-NPs) (from top to bottom): Small Angle XRD pattern, N_2 adsorption-desorption isotherms and mesopore size distribution, Hydrodynamic size distribution by Dynamic Light Scattering, Z potential distribution, FTIR spectra.

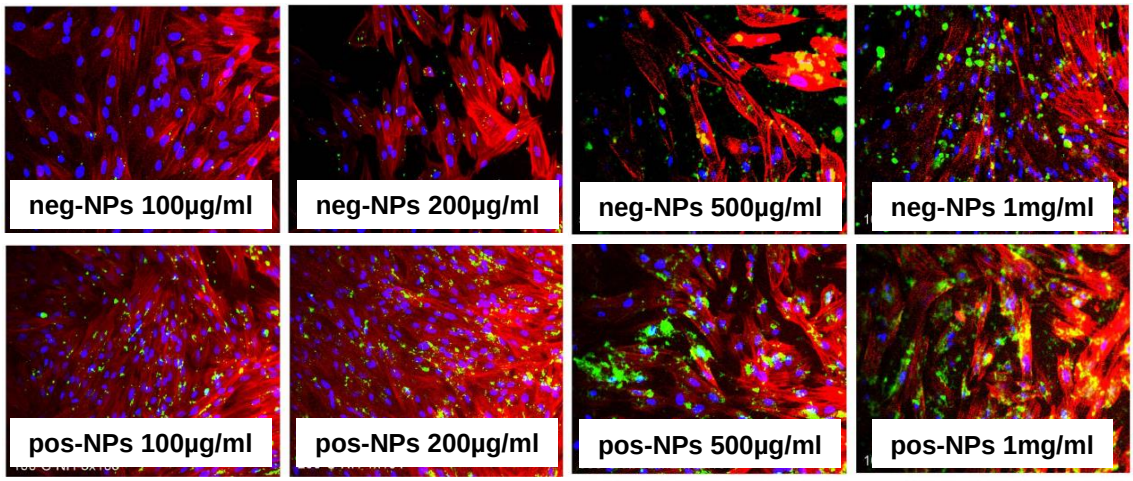

Figure S2. Fluorescence images of DMSCs incubated with neg-NPs and pos-NPs at 100, 200, 500 and 1000 µg/mL.

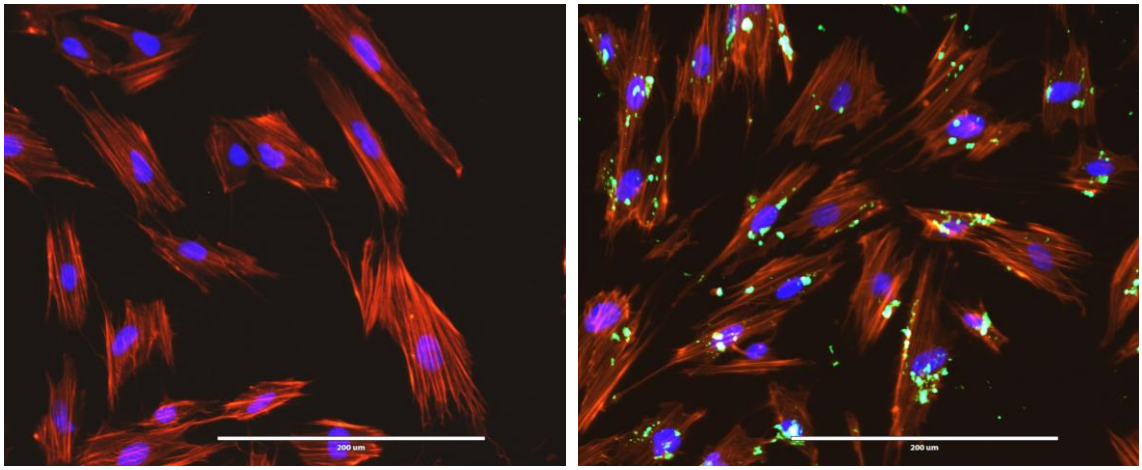

Figure S3. Fluorescence microscopy images of DMSCs without NPs (left) and incubated with pos-NPs (200 µg/mL). The morphology of the cells remains unmodified after NP internalization.

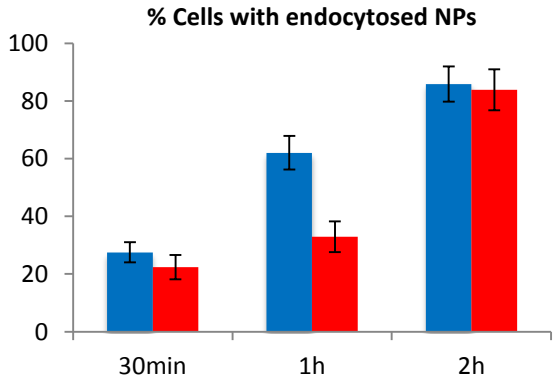

Figure S4. Percentage of DMSCs with internalized neg-NPs (blue) and pos-NPs (red) measured by flow cytometry. (Mean ± SD, N=3)

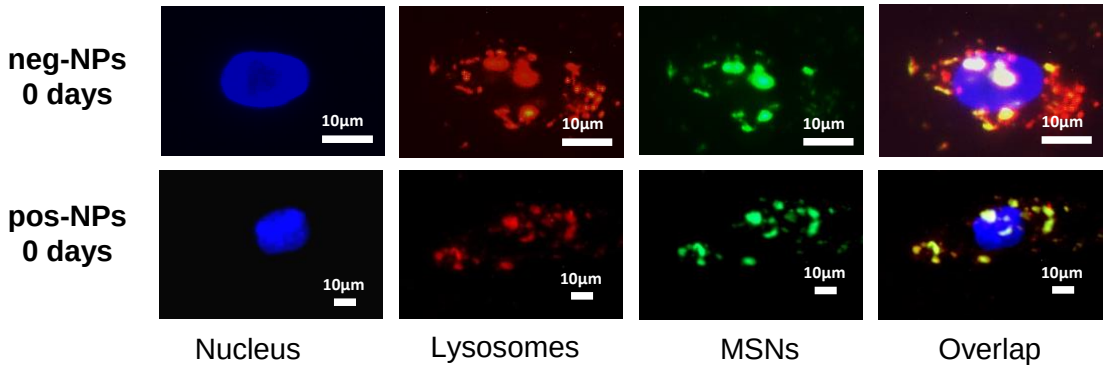

Figure S5. Colocalization study of NPs (green) and lysosomes (red) in DMSCs right after internalization.

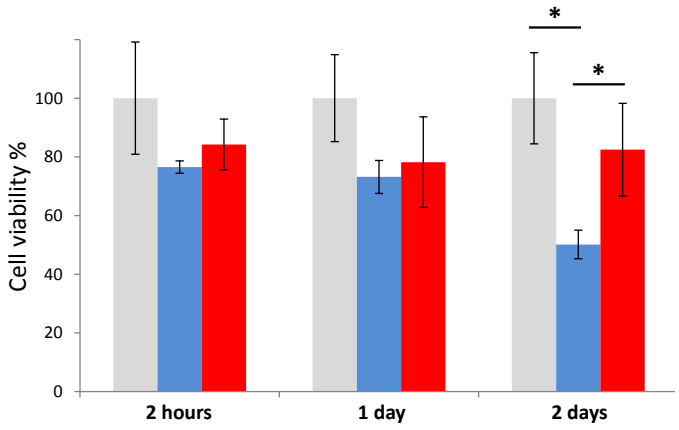

Figure S6. Cell viability percentage of DMSCs determined by Alamar Blue assay at different periods of time after incubation for 2 h with DOX-neg-NPs (blue) and DOX-pos-NPs (red). (Mean ± SD, N=3, *p<0,05)

3.3.2 Vectorization of ultrasound-responsive nanoparticles in placental mesenchymal stem cells for cancer therapy

Paris, J. L., de la Torre, P., Cabañas, M. V., Manzano, M., Grau, M., Flores, A. I. & Vallet-Regí, M. Nanoscale 9, 5528–5537 (2017).
DOI: 10.1039/C7NR01070B

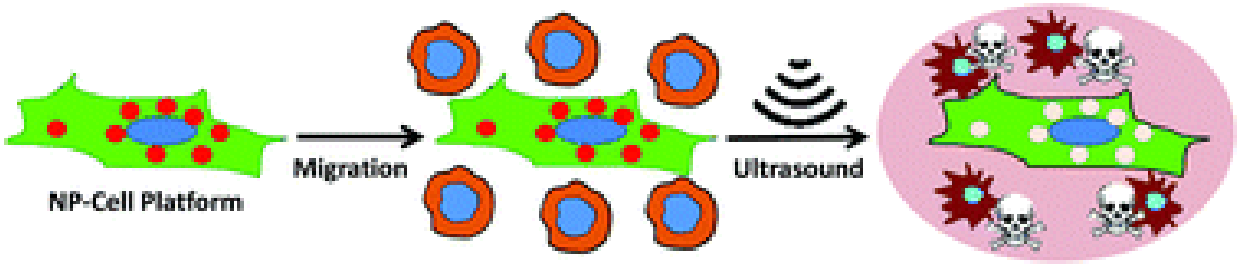

Nanoscale

PAPER

View Article Online
View Journal

Cite this: DOI: 10.1039/c7nr01070b

Vectorization of ultrasound-responsive nanoparticles in placental mesenchymal stem cells for cancer therapy†

Juan L. Paris,[a,b] Paz de la Torre,[c] M. Victoria Cabañas,[a] Miguel Manzano,[a,b] Montserrat Grau,[d] Ana I. Flores*[c] and María Vallet-Regí*[a,b]

Received 13th February 2017,
Accepted 23rd March 2017

DOI: 10.1039/c7nr01070b

rsc.li/nanoscale

A new platform constituted by engineered responsive nanoparticles transported by human mesenchymal stem cells is here presented as a proof of concept. Ultrasound-responsive mesoporous silica nanoparticles are coated with polyethylenimine to favor their effective uptake by decidua-derived mesenchymal stem cells. The responsive-release ability of the designed nanoparticles is confirmed, both *in vial* and *in vivo*. In addition, this capability is maintained inside the cells used as carriers. The migration capacity of the nanoparticle–cell platform towards mammary tumors is assessed *in vitro*. The efficacy of this platform for anticancer therapy is shown against mammary tumor cells by inducing the release of doxorubicin only when the cell vehicles are exposed to ultrasound.

Introduction

In the last few years research in nanomedicine has been focusing on developing nanocarriers for targeted drug delivery combined with on-demand release behavior.[1,2] In this sense, porous nanoparticles with great loading capacity and tunable surface properties have become a promising alternative for certain biomedical applications such as cancer therapy. Among these materials, mesoporous silica nanoparticles present high drug adsorption capacity because of their available pores and high robustness, which allows further chemical modification of their surface.[3–5] The release of the transported drugs can be controlled through a stimuli-responsive release that can be achieved through different trigger mechanisms, which can be endogenous, such as changes in pH,[6] redox potential,[7] and the presence of specific enzymes or analytes;[8] or exogenous, such as temperature,[9] light,[10,11] magnetic fields,[12,13] electronic fields or ultrasound.[14,15]

An ideal nanocarrier for drug delivery in cancer therapy should be capable of specifically targeting tumor tissue avoiding premature release of the payload, and releasing high concentrations of the cargo only at the diseased tissues.[16–18] Targeted nanoparticles towards tumors can be accomplished by either passive or active targeting, or by a combination of both.[19] Passive targeting is based on the combination of two features of tumor tissues: high permeability and enhanced retention, in what is called the Enhanced Permeation and Retention (EPR) effect.[20,21] Nanoparticles tend to accumulate in tumor zones due to the abnormal architecture and permeability of the tumor blood vessels. Additionally, there is a poor drainage which results in the retention of the nanoparticles within the tissue.[20] On the other hand, active targeting is based on grafting affinity ligands on the surface of nanoparticles able to interact with specific membrane receptors overexpressed by tumor cells, leading to specific retention and uptake by the targeted cancer cells.[2,19]

However, despite the recent advances in nanoparticles' research for biomedicine, the translation of targeted nanocarriers (both passive and active targeting) to the clinic remains to be a challenge.[22–24] In a totally different approach, cell-based therapies have been investigated as transporters of nanoparticles for cancer treatment.[25,26] In this sense, human mesenchymal stem cells are multipotent cells that maintain and regenerate connective tissues, with inherent migratory properties, in response to inflammation and/or injury.[27–29] This migratory and homing capacities have suggested their use as drug delivery agents for the treatment of isolated and metastatic tumors.[26,30–32] Conventionally, bone marrow and

[a]Dpto. Química Inorgánica y Bioinorgánica, Facultad de Farmacia, UCM, Instituto de Investigación Sanitaria Hospital, 12 de Octubre i+12, 28040-Madrid, Spain. E-mail: vallet@ucm.es
[b]Centro de Investigación Biomédica en Red de Bioingeniería, Biomateriales y Nanomedicina (CIBER-BBN), Spain
[c]Grupo de Medicina Regenerativa, Instituto de Investigación Hospital, 12 de Octubre i+12, Madrid, Spain. E-mail: anaisabel.flores@salud.madrid.org
[d]Animal Core Facility, Research Center, Instituto de Investigación Hospital, 12 de Octubre i+12, Madrid, Spain

†Electronic supplementary information (ESI) available: Characterization of mesoporous silica nanoparticles, *in vivo* fluorescence, cytotoxicity assays. See DOI: 10.1039/c7nr01070b

adipose tissue are the common sources of adult MSCs, although the isolation techniques are invasive and not very efficient in terms of isolated cell quantities.[33] Besides, the donor age strongly influences the number, proliferation and differentiation capabilities, which decline with the donor age.[34] In the last few years our research group has been investigating an additional source of MSCs from the human decidua of the placenta, which are isolated avoiding invasive procedures.[33] Decidua Mesenchymal Stem Cells (DMSCs) present a number of advantages over conventional MSCs, such as: they are very easy to obtain without invasive techniques; they constitute a homogeneous population with high proliferation and differentiation capacities; they are adult stem cells from the maternal part of the placenta, with low or non-immune response and genetically stable during expansion.[33] Additionally, DMSCs present migratory properties towards tumors, both *in vitro* and *in vivo*, and, additionally, they inhibit the growth of primary tumors and the development of new tumors.[34] Consequently, DMSCs seem to be excellent carriers of pharmaceutical agents towards tumor tissues. However, if the cells are carrying cytotoxic agents, some strategy should be developed to ensure DMSCs' survival during transport. An interesting approach would consist of loading the cytotoxic cargo on stimuli-responsive nanoparticles for drug delivery. These smart nanocarriers would be introduced into the DMSCs, which would transport them to the targeted tissue. The application of an external stimulus would trigger the release of the cytotoxic drug. As a consequence, the drug would have to be released from the DMSCs to the surrounding tissue.[26,35] The process by which hydrophobic cytotoxic molecules (like doxorubicin)[36,37] can diffuse out of a transporting cell to kill the surrounding cancer cells has been called the "bystander effect".[38–40]

In this manuscript we have developed a proof of concept cell-platform constituted by engineered ultrasound-responsive nanoparticles which are vectorized to tumor tissues by using DMSCs. The nanocarrier provides a controlled release, triggering the payload release on demand when a penetrating stimulus such as ultrasound would be applied. To the best of our knowledge this is the first time that human mesenchymal stem cells are employed as transporters that can release a therapeutic molecule on-demand.

Results and discussion

Engineered ultrasound-responsive nanoparticles

Ultrasound-Responsive Nanoparticles (UR-NPs) are composed of an ultrasound (US) responsive copolymer (poly(2-(2-methoxyethoxy)ethylmethacrylate-*co*-2-tetrahydropyranyl methacrylate), p(MEO_2MA-*co*-THPMA)), covalently grafted to the surface of MCM-41 type mesoporous silica nanoparticles. The synthesis, characterization and behavior of these hybrid nanoparticles have been previously reported.[15] The material presents a negatively charged surface at the pore walls, due to the silanol groups, which permits loading of a high amount of the cytotoxic drug doxorubicin within the pores.[35,41] Then, the pores are closed with a responsive polymeric gate to avoid premature release. The application of an exogenous stimulus, such as ultrasound, enables the delivery of the maximum amount of drug possible.

We have developed a cell-platform to transport the UR-NPs selectively to tumor tissues. Once in the tumor, the cytotoxic agent would be released, damaging the cancer cells without affecting healthy tissues. In this combined approach, the NPs will provide the responsive drug release, while the biological component (DMSCs) will act as a specific vehicle to carry the NPs to the tumor. To obtain this goal, the nanoparticles must be internalized into the cell vehicles. Cellular uptake is generally enhanced employing internalization ligands or positively charged moieties on the surface of NPs.[42] In this sense, polyethylenimine (PEI) is a synthetic cationic polymer that has been widely used to deliver oligonucleotides, siRNA and plasmid DNA to cells.[43,44] An interesting approach for effective NP internalization into cells consists of decorating the NP surface with PEI. Cellular uptake of PEI-coated nanoparticles relies on the electrostatic interaction between the positively charged polymer and the negatively charged cell membrane, in a charge-dependent mechanism that is not selective on the cell type.[43] The above synthesized UR-NPs were coated with 1800 Da PEI (UR-NPs@PEI), which is known to present low cytotoxicity, to confer a positive charge on their external surface that will increase the amount of NPs internalized in DMSCs.[35]

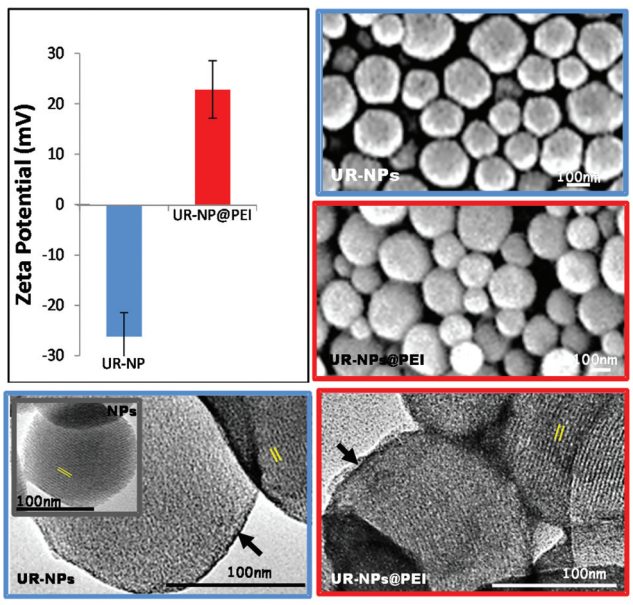

Fig. 1 Characterization of ultrasound-responsive nanoparticles with or without PEI coating: zeta potential values (top, left), scanning electron microscopy micrographs of UR-NPs and UR-NPs@PEI (top, right), transmission electron microscopy micrographs of phosphotungstic acid-stained non-ultrasound responsive NPs, UR-NPs and UR-NPs@PEI (bottom). Arrows indicate the presence of a polymeric coating, parallel segments indicate the ordered mesochannels.

The presence of PEI in the particles was confirmed by different techniques: the zeta potential changed from negative to positive values after PEI coating (Fig. 1). Thermogravimetric Analysis (TGA) data showed an organic matter percentage for the UR-NPs of 25%, and 40% for UR-NPs@PEI, what indicated an estimate of 15% of PEI in the final material. The BET surface area decreased from 180 m^2 g^{-1} for UR-NPs to 70 m^2 g^{-1} for UR-NPs@PEI. Small angle X-ray diffraction patterns show that the hexagonal pore order of the mesoporous silica nanoparticles was maintained (see Fig. S1†). The diameter and morphology of the NPs remains unmodified after the PEI coating, as it can be seen in the scanning electron microscopy images (Fig. 1). The mesoporous order can be appreciated in the transmission electron microscopy micrographs which also showed the presence of the US-responsive copolymer, or the copolymer plus the PEI, on the external surface of the mesoporous ordered NPs when the materials were stained with phosphotungstic acid (Fig. 1). As it will be seen throughout this article, nanoparticles labeled with different dyes have been employed, and their characterization did not show any significant differences when compared to the non-labeled nanoparticles. Several cargo molecules have also been loaded within the mesopores, in order to evaluate various aspects of the materials' US-responsiveness.

The US-responsiveness of UR-NPs@PEI was evaluated initially *in vial*, with a fluorescein release experiment. Taking into account that the gatekeeper copolymer shows a dual temperature-US responsiveness,[15] fluorescein loading in UR-NPs was performed at 4 °C. Under these conditions the polymer that acts as a gatekeeper presented an open or hydrophilic conformation. After the dye loading process, the temperature was increased to 50 °C, inducing the copolymer to collapse, *i.e.* change to a hydrophobic conformation, closing the pore entrances. Then, loaded UR-NPs were coated with PEI. Dye release experiments (Fig. 2) show that the behavior of the UR-NPs@PEI was similar to that of UR-NPs without coating; the presence of PEI coating did not induce any significant differences in the maximum percentage of fluorescein released with or without ultrasound (which was already reached after 16 h).[15] As commented above, before US application, the polymeric gate is collapsed at the nanoparticle surface, blocking the pores and preventing cargo release. After insonation, one of the monomers in the polymeric gate (THPMA) is cleaved, yielding hydrophilic methacrylic acid. This change in the copolymer structure induces an increase in its hydrophilicity, triggering a change of conformation towards coil-like, which allows drug release from the material. The evaluation of this change in the polymeric gate has been demonstrated in our previous work.[15] Here, we show that these engineered nanoparticles continue to behave as stimulus-responsive drug nanocarriers even though they have been coated with PEI.

In vivo ultrasound-responsiveness of this material was checked loading Calcein-AM into UR-NPs@PEI. Calcein-AM is a low-fluorescent indicator that can be converted *in vivo* to highly-fluorescent calcein due to the activity of esterases in the surrounding cells (Fig. 3A). The Calcein-AM loaded material was injected subcutaneously and bilaterally in mice, monitoring the *in vivo* fluorescence before and after US application on one of the injection sites (Fig. 3B and C). In order to point the location of the nanoparticles, Rhodamine B-labeled UR-NPs@PEI were used for these experiments. Fig. 3B corres-

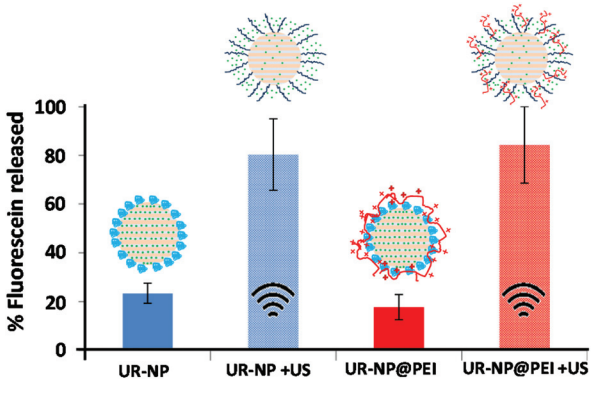

Fig. 2 Percentage of fluorescein released in PBS at 37 °C from UR-NPs and UR-NPs@PEI with or without ultrasound exposure after 16 h.

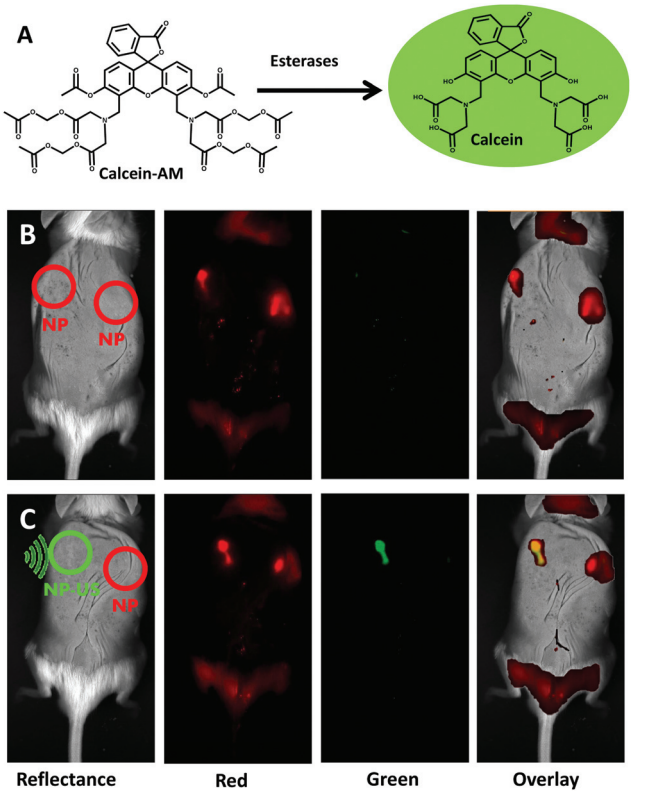

Fig. 3 Data showing the material cargo retention and release capability *in vivo*. *In vivo* fluorescence of subcutaneously injected UR-NPs@PEI (red channel) and the released cargo (green channel); scheme of green fluorescence generation by the cleavage of cargo molecules (Calcein-AM) after release, yielding fluorescent Calcein (A); *in vivo* fluorescence images of the different fluorescence channels before (B) and 100 min after ultrasound application (1 MHz, 10 min, 3 W cm^{-2}) (C).

ponds to the fluorescence before US application, showing red fluorescence, delimiting the location of NPs due to the Rhodamine B labeling. No fluorescence was observed in the green channel (therefore, there had been no cargo release). After US application (1 MHz, 3 W cm^{-2}, 10 min), red fluorescence indicated that the NPs were still present at the injection site and green fluorescence appeared only in the US-exposed area (Fig. 3C). Taking into account that Calcein-AM inside the material pores is not accessible to the esterases from the cells, the presence of green fluorescence indicates that Calcein-AM was released from the material when the gatekeeper was opened due to ultrasound exposure. On the other hand, at the injection site without US application, there was no green fluorescence, which indicates that Calcein-AM is retained inside the nanoparticle pores and not exposed to esterases. The progressive increase of green fluorescence *in vivo* at different time points after ultrasound application can be seen in Fig. S2.† These results demonstrate the capability of the UR-NPs@PEI to retain a cargo and release it when exposed to ultrasound *in vivo*.

Ultrasound-responsive nanoparticle–cell platform

After evaluating the *in vial* and *in vivo* responsiveness of UR-NPs@PEI, we tested the interaction of the UR-NPs@PEI with the DMSCs which will act as transporters to the tumor tissue. To do so, the effect of UR-NPs@PEI at different concentrations on DMSCs' viability was tested using the MTS and LDH assays (Fig. S3†). The results show no toxicity up to 200 μg mL^{-1}, and a small toxicity at higher concentrations. Therefore, a concentration of 200 μg mL^{-1} was chosen for further experiments.

Then, DMSCs were exposed to UR-NPs@PEI to study their internalization and retention in the cells. For these studies, the NPs were covalently labeled with fluorescein isothiocyanate (FITC). Fig. 4A–C show the fluorescence microscopy images of DMSCs stained with DAPI (nuclei) and Alexa Fluor®568 phalloidin (cytoplasm) after incubation with labeled nanoparticles (200 μg mL^{-1} for 2 h). As expected, microscopy images indicate that UR-NPs@PEI were internalized by the cells better than UR-NPs (Fig. 4A and B). Moreover, the UR-NPs@PEI escaped the *endo*-lysosomal compartment shortly after endocytosis, since NP fluorescence (green) and lysosomes (red) do not co-localize (Fig. 4C). This behavior can be attributed to the proton sponge effect provided by PEI.[43] Under the acidic conditions of the lysosome, PEI (and other polycationic molecules) presents a very high positive charge. This induces the entrance in the lysosomes of chloride anions, accompanied by water. The lysosomes swell until they eventually burst, releasing their contents into the cytoplasm. The quantification of UR-NPs@PEI uptake (200 μg mL^{-1} for 2 h) by DMSCs by flow cytometry indicates a more successful internalization of UR-NPs@PEI compared to the nanoparticles without PEI (Fig. 4D and S4†). The coated particles were also retained inside the cells for at least 6 days (Fig. 4E), enough for the cells to reach the tumor, according to our previous work.[35]

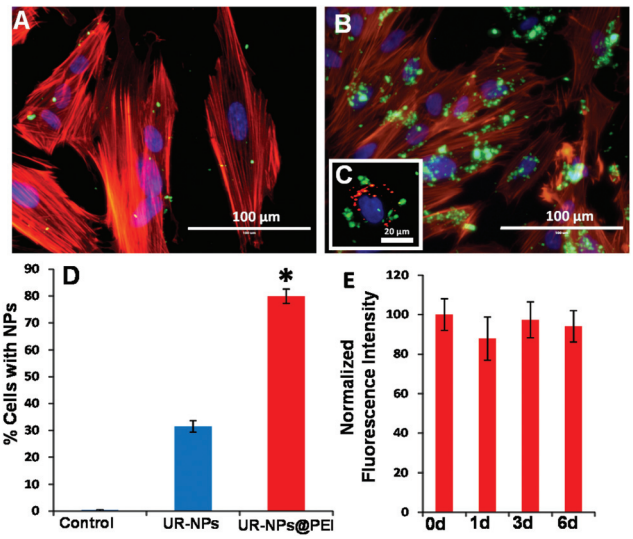

Fig. 4 Fluorescence microscopy images of NP-loaded DMSCs; blue (nucleus), red (cytoplasm), green (NPs): UR-NPs (A), UR-NPs@PEI (B); colocalization study of UR-NPs@PEI (green), nucleus (blue) and lysosomes (red) in DMSCs 2 h after internalization (C); flow-cytometry data regarding UR-NPs and UR-NPs@PEI uptake (D); flow-cytometry data regarding UR-NPs@PEI retention (E) (data are means ± SD, $N = 3$, $*p < 0.05$).

In addition, the UR-NPs@PEI retain their cargo after uptake by the DMSCs and are also able to release intracellular fluorescein after US application (Fig. 5). For this experiment, Rhodamine B-labeled nanoparticles were used to simultaneously study the location of UR-NPs@PEI (red fluorescence) and their cargo (green fluorescence). Before US exposure, red and green fluorescence colocalize, indicating that the dye is retained inside UR-NPs@PEI. After insonation (1 MHz, 3 W cm^{-2}, 5 min), a significant part of the dye diffuses out of the NPs and stains the cell cytoplasm (images taken 30 min after insonation), as a consequence of the polymeric gates changing from a closed to an open conformation (Fig. 2).

The above results show the possibility to fabricate a cell platform containing US-responsive NPs inside the DMSCs for at least 6 days. To evaluate the effect of the cell-platform as

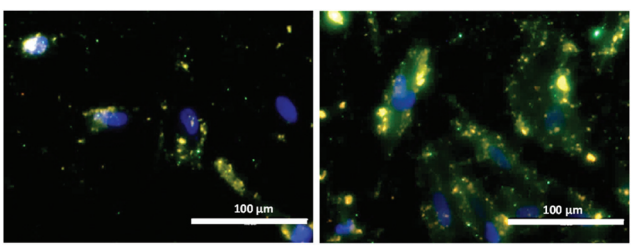

Fig. 5 Fluorescence microscopy images of DMSCs incubated with Rhodamine B-labeled UR-NPs@PEI loaded with fluorescein before (left) and after (right) ultrasound irradiation. Overlay images of three fluorescence channels: blue fluorescence (nuclei), red fluorescence (UR-NPs@PEI) and green fluorescence (fluorescein cargo). Fluorescence microscopy images taken 30 min after the US exposure was performed.

transporters of cytotoxic molecules, the UR-NPs@PEI were loaded with doxorubicin (loaded amount was 2.94 ± 0.17%). First, we incubated different concentrations of cytotoxic-loaded NPs with the DMSCs for 2 h. After this, we washed the cells to eliminate the non-internalized NPs and cell viability was evaluated after 24 and 72 h (Fig. 6). No toxicity was observed up to a concentration of 200 μg mL^{-1}. Therefore, these conditions (200 μg mL^{-1} UR-NPs@PEI for 2 h) were used for any further experiments. It is worth noting that in our previous work, we had observed significant toxicity in DMSCs 48 h after internalization caused by similar doxorubicin-loaded NPs but without stimulus-responsive gatekeepers.[35] Thus, the NPs engineered in the present work are capable of retaining the cytotoxic drug inside them, preventing a premature leakage of the doxorubicin that could damage the transporting cells before they reach their target tissue.

The next stage was to check the capability of the cell–NP platform to reach the tumor site. In this sense, we performed a standardized *in vitro* cell migration assay towards the tumor homogenate to check whether the presence of UR-NPs@PEI inside the cells has any negative impact on the DMSCs' migration capacity. The results showed a high migration capacity of DMSCs towards the tumor homogenate, which was maintained in our platform carrying UR-NPs@PEI, even if those NPs were loaded with doxorubicin (DOX-Platform) (Fig. 7). The amount of doxorubicin transported by the DOX-Platform was determined to be 0.47 ± 0.08 μg of doxorubicin per 10 000 DMSCs. The quantification of the migrated cells shows no significant difference in cell migration due to UR-NP@PEI (with or without doxorubicin). These data indicate that stimulus responsive NPs containing a cytotoxic drug can be vectorized to the tumor site by DMSCs.

Finally, in order to test whether this developed platform (UR-NPs@PEI inside DMSCs) could be useful for anticancer therapy, an *in vitro* co-culture experiment was carried out. The

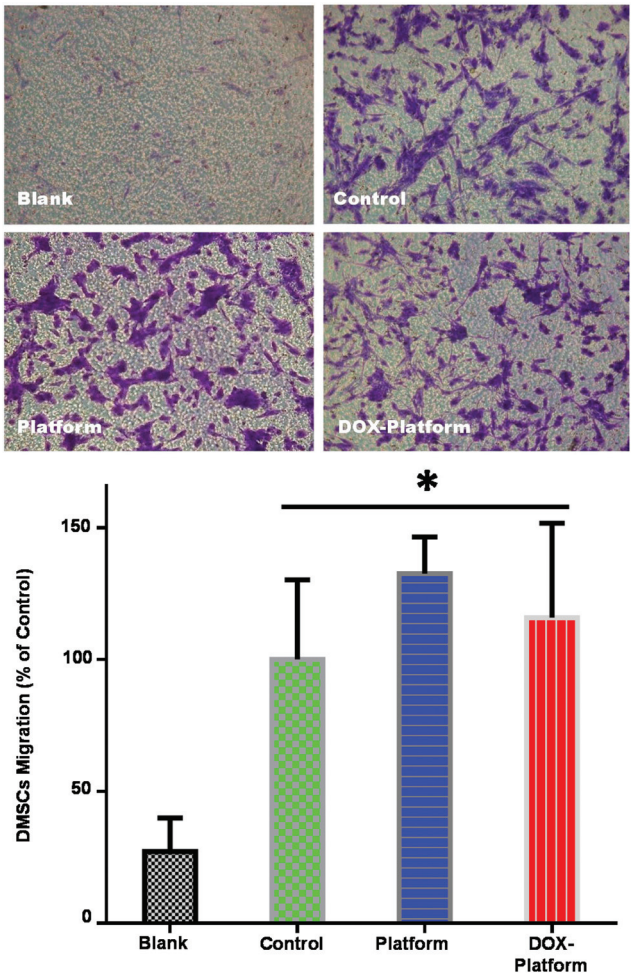

Fig. 7 *In vitro* Transwell® migration assay of DMSCs against culture medium (basal), tumor homogenate (control) and migration of DMSCs loaded with UR-NP@PEI or DOX-UR-NP@PEI against the tumour homogenate. Optical microscopy images of migrated cells (top) and quantification of migrated cells by UV-Vis spectrophotometry (bottom) (mean ± SD, $N = 3$, $*p < 0.05$).

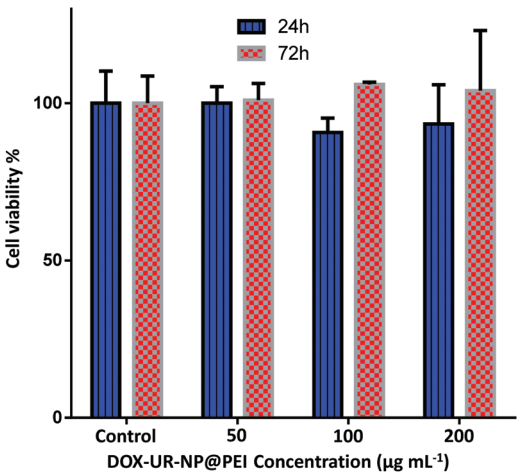

Fig. 6 Cytotoxicity assay in DMSCs of doxorubicin-loaded UR-NPs@PEI at different concentrations after 24 h and 72 h measured by using the Alamar Blue test. No significant differences were found at any of the tested concentrations.

transporting cells (DMSCs and DOX-Platform) were divided into two groups and half of the samples were exposed to US (1 MHz, 3 W cm^{-2}, 5 min). Then, the DMSCs and DOX-Platforms with/without US exposure were seeded in a Transwell® culture insert on top of a well that contained NMU cancer cells (DMSCs : NMU ratio was 1 : 2). After 24 and 48 h, the Transwell® inserts were removed and the NMU viability was evaluated by performing the Alamar Blue test. Fig. 8 shows that NMU cell viability is only affected when US is applied on DMSCs carrying doxorubicin-loaded UR-NPs@PEI, but it remains unaffected under any of the other experimental conditions. Therefore, doxorubicin remains retained in UR-NPs@PEI inside DMSCs until the platform is exposed to US. After insonation, the nanoparticles release their cargo, which can diffuse towards tumor cells, inducing their death. Furthermore, this effect appears to be dose-dependent, since the reduction in NMU cell viability is smaller when the ratio DMSC : NMU is 1 : 5 (Fig. S5†).

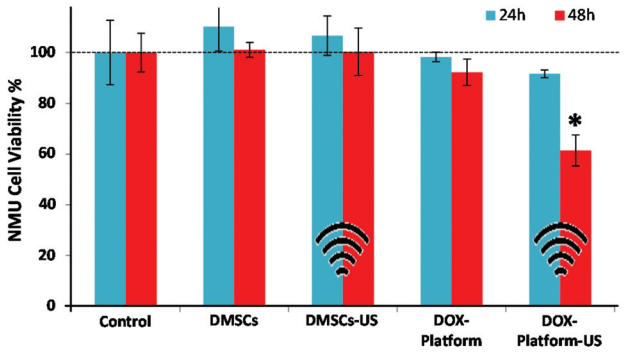

Fig. 8 Cytotoxicity assay of NMU cells after co-culture with DMSCs or with DOX-Platform (with or without ultrasound application) measured by using the Alamar Blue test. The DMSCs to NMU ratio was 1 : 2 (mean ± SD, $N = 3$, $*p < 0.05$).

These results show the possibility to introduce cytotoxic-loaded stimulus-responsive NPs in DMSCs as cell carriers. The migratory capacity of these cells to the tumor tissue was maintained in the presence of UR-NPs. This platform was activated, *i.e.* released the cytotoxic drug, just when an external stimulus was applied, in principle, when the cell platform reached the tumor tissue.

Conclusions

A cell platform to transport ultrasound-responsive nanoparticles towards tumor tissue has been developed. Experiments, both *in vial* and *in vivo*, have demonstrated the ultrasound responsiveness of the system, showing the capability to induce cargo release on-demand. These polyethylenimine-coated nanoparticles were efficiently internalized by decidua-derived mesenchymal stem cells and they were retained for at least 6 days. The nanoparticle–cell construct also presented ultrasound-responsive cargo release capability.

The tumor-tropic behavior of the cells was preserved when transporting doxorubicin-loaded nanoparticles. This doxorubicin carrying platform was able to induce the death of mammary cancer cells *in vitro* when it was exposed to ultrasound.

The obtained results indicate that this platform could be employed to transport cytotoxic drugs specifically to tumors, and release them when exposed to ultrasound.

Experimental section

Reagents and characterization techniques

The following compounds were purchased from Sigma-Aldrich Inc.: ammonium nitrate, cetyltrimethylammonium bromide (CTAB), tetraethyl orthosilicate (TEOS), methacrylic acid (MAA), pyridine, *p*-toluenesulfonic acid, toluene, dichloromethane (DCM), dihydropyran, dimethylformamide (DMF), 2-(2-methoxyethoxy)ethylmethacrylate (MEO_2MA), 4,4′-azobis (4-cyanovaleric acid) (ABCVA), diethylether, *N*,*N*′-dicyclohexylcarbodiimide (DCC), *N*-hydroxysuccinimide (NHS), phosphate-buffered solution (PBS), fluorescein sodium salt, polyethylenimine (PEI) of 1800 Da, rhodamine-B isothiocyanate and fluorescein isothiocyanate (FTIC). Calcein-AM was purchased from ThermoFisher Scientific. DMEM, penicillin–streptomycin, non-essential amino acids, and trypsin–EDTA were purchased from Invitrogen (Fisher Scientific, Madrid, Spain). Fetal bovine serum is from Biowest (LabClinics, Spain). Transwells were purchased from Nunc (Fisher Scientific, Spain). These compounds were used without further purification. Tetrahydropyranyl methacrylate (THPMA) was synthesized as described previously.[15,45]

The materials were analyzed by X-ray diffraction (XRD) in a Philips X-Pert MPD diffractometer equipped with Cu Kα radiation. Thermogravimetry and Differential Thermal Analysis (TGA/DTA) were performed in a PerkinElmer Pyris Diamond TG/DTA analyzer, with 5 °C min^{-1} heating ramps, from room temperature to 600 °C. Fourier Transformed Infrared (FTIR) spectra were obtained in a Nicolet (Thermo Fisher Scientific) Nexus spectrometer equipped with a Smart Golden Gate ATR accessory. Surface morphology was analyzed by Scanning Electron Microscopy (SEM) in a JEOL 6400 electron microscope. Transmission Electron Microscopy (TEM) was carried out with a JEOL JEM 2100 instrument operated at 200 kV, equipped with a CCD camera (KeenView Camera). Phosphotungstic acid staining was employed to detect the presence of organic matter in the hybrid materials. N_2 adsorption was carried out on a Micromeritics ASAP 2010 instrument; surface area was obtained by applying the Brunauer–Emmett–Teller (BET) method to the isotherm and the pore size distribution was determined by the Barrett–Joyner–Halenda (BJH) method from the desorption branch of the isotherm. The mesopore size was determined from the maximum of the pore size distribution curve. The *Z*-potential was measured in deionized water by means of a Zetasizer Nano ZS (Malvern Instruments) equipped with a 633 nm "red" laser.

Engineered US-responsive nanoparticles

Preparation of UR-NPs. A detailed description of the synthesis method of Ultrasonic-Responsive Nanoparticles (UR-NPs) can be found in our previous work.[15] Mesoporous silica nanoparticles were fabricated by using the modified Stöber method from TEOS in the presence of CTAB as a structure-directing agent under basic and very dilute conditions.

The random copolymer, poly(2-(2-methoxyethoxy)ethylmethacrylate-*co*-2-tetrahydropyranyl methacrylate), p(MEO_2MA-*co*-THPMA), was synthesized by free radical polymerization from 2-(2-methoxyethoxy)ethylmethacrylate, MEO_2MA, and 2-tetrahydropyranyl methacrylate, THPMA, in a MEO_2MA : THPMA ratio of *ca.* 90 : 10. The synthesis was performed at 80 °C overnight in DMF solution under an inert atmosphere.

Grafting the polymer nanogate to mesoporous silica nanoparticles to obtain UR-NPs was performed in two steps. First, the previously copolymer, p(MEO_2MA-*co*-THPMA), was

modified with an alkoxysilane(3-aminopropyl triethoxysilane) through DCC–NHS chemistry. Then, the silylated polymer was grafted to the silica nanoparticles surface through sol–gel chemistry. A ratio polymer : nanoparticles of 6 : 1 was used, and the silylated polymer was added in 3 steps to the nanoparticles.[15]

FITC and Rhodamine B-labeled UR-NPs were prepared following the same procedure but using NPs covalently labeled with the fluorophore during NP synthesis as described elsewhere.[15,35]

Preparation of UR-NPs@PEI. The synthesis of stimuli responsive nanoparticles coated with PEI (UR-NPs@PEI) was carried out by adding 5 mg of PEI to 10 mg of UR-NPs dispersed in 2 mL of PBS. The coating was carried out at 37 °C for 3 h. The product was washed several times with PBS, centrifuged and dried under vacuum at 25 °C.

Cargo loading and release

Cargo loading. 20 mg of UR-NPs were placed in a glass vial with a septum and dried at 80 °C under vacuum for 24 h. Then, the vial was placed at 4 °C with magnetic stirring and 5 mL of cargo solution (20 mg mL^{-1} fluorescein in PBS) were added and the suspension was stirred for 24 h. After this, the sample was filtered and washed twice with warm PBS (50 °C) to remove the potential fluorescein absorbed on the external surface. Note that the cargo loading was performed at 4 °C, below the lower critical solution temperature (LCST) which means that the polymer presents an extended conformation (pores opened). After loading, the temperature was increased to 50 °C (above the LCST) which induces the polymer to collapse, closing the pore entrances.[15] After this, loaded UR-NPs were coated with PEI in a similar way to that described above.

In vial cargo release. 9 mg of fluorescein-loaded nanoparticles were suspended in 1.8 mL of PBS pH 7.4 (10 mM). Then, 0.5 mL of the UR-NP suspension were placed on a Transwell® permeable support with a 0.4 μm polycarbonate membrane (3 replicas were performed). The well was filled with 1.5 mL of PBS and the suspension was stirred at 37 °C and 100 rpm during all the experiments. For the US experiments the particle suspension was subjected to US exposure (10 min at 1.3 MHz and 100 W) before placing it on the Transwell® insert. The amount of fluorescein released after 16 h was determined by fluorescence spectrometry (λ_{exc} 490, λ_{em} 514 nm).

In vivo evaluation of US responsive nanoparticles

The *in vivo* US-responsiveness of UR-NPs@PEI was evaluated on a mouse model (FVB strain). Mice were shaved and depilatory cream was employed to remove their hair in the area that was evaluated (to prevent auto-fluorescence and to apply the ultrasound gel). Nanoparticles were covalently labeled with Rhodamine B, as previously mentioned, to be able to visualize the NPs by *in vivo* fluorescence imaging (*In vivo* Xtreme®, Bruker). Loading of Calcein-AM was performed following the same procedure as previously described but using a 2 mg mL^{-1} solution of the cargo in a mixture of DMSO and PBS (the material was washed several times with PBS after cargo loading). Calcein-AM loaded nanoparticles were injected subcutaneously and bilaterally in mice (2 mg of NPs in 100 μL PBS per injection). US was applied at the left injection site (1 MHz, 3 W cm^{-2}, 10 min continuous application) and using ultrasound gel. *In vivo* fluorescence was evaluated at different wavelengths (green: λ_{exc} 490, λ_{em} 514 nm, red: λ_{exc} 540, λ_{em} 625 nm), before and after US application.

Ultrasound-responsive nanoparticle–cell platform

Human placentas from healthy mothers were obtained from the Department of Obstetrics and Gynecology under written informed consent approved by the Ethics Committee from Hospital Universitario 12 de Octubre, Madrid, Spain. Processing of placental membranes and culture of primary cells (DMSCs) were done as previously reported.[33,34]

Cellular uptake of nanoparticles. DMSCs were plated 24 h before starting the experiment in culture multiwell plates at a density of 10^4 cells per cm^2. After incubation with particles (UR-NPs and UR-NPs@PEI) in serum-free culture medium (200 μg mL^{-1}) for 2 h, the media were removed and the cells were washed with PBS three times. Then, the cells were fixed with Z-fix solution (Anatech, USA) for 15 min, permeabilized with 0.1% Triton X-100 in PBS at room temperature for 5 min and, subsequently incubated for 20 min with Alexa Fluor®568 phalloidin (Invitrogen, Spain) for staining F-actin. DAPI (4′,6-diamidino-2-phenylindole) at 1 μg mL^{-1} was used to stain and visualize the nuclei. Fluorescence microscopy was performed with an Evos® FL Cell Imaging System equipped with three LED light cubes (λ_{exc} (nm); λ_{em} (nm)): DAPI (357/44; 447/60), GFP (470/22; 525/50), RFP (531/40; 593/40) from AMG (Advance Microscopy Group). Quantitative analysis of cellular uptake was performed by flow cytometry (FACS). 200 μg mL^{-1} particles were incubated with the DMSCs for 2 h, and then removed by washing three times with PBS. Subsequently, the cells were trypsinized, collected by centrifugation and redispersed in PBS solution with trypan blue (0.5%) to remove extracellular fluorescence. The fluorescence intensity of 10 000 cells was quantified by FACS. Statistical analysis for differences between groups was carried out by the Student's *t* test.

Quantitative analysis of particle retention was performed by FACS. Particles at a concentration of 200 μg mL^{-1} were incubated with the DMSCs for 2 h, and then removed by washing three times with PBS. The cells were then cultured in fresh medium for indicated time points. Subsequently, the cells were collected by trypsinization and centrifugation, and redispersed in PBS solution with trypan blue (0.5%). The fluorescence intensity of 10 000 cells was quantified by FACS. The fluorescence intensities obtained after the first day were corrected by the cell dilution folds due to cell division.

Cytotoxicity of nanoparticles. The cytotoxicity of both UR-NPs and UR-NPs@PEI was evaluated using the following standard protocols:

Lactate dehydrogenase (LDH) activity test. Extracellular LDH activity was measured in the media using the kit for quantitative determination of LDH (Spinreact, Spain). DMSCs were incubated with different sets of NPs for 2 h at different concen-

trations in serum-free DMEM (n = 3). Then, the media were changed with fresh complete culture media and the cells were incubated for another 24 h. The culture medium was then collected to determine the extracellular LDH activity, measured by means of a spectrophotometer (at 340 nm) following the manufacturer's protocol.

MTS(3-(4,5-dimethylthiazol-2-yl)-5-(3-carboxymethoxyphenyl)-2-(4-sulfophenyl)-2H-tetrazolium) assay. The MTS reduction assay was performed using a commercial assay and following the manufacturer's protocol (CellTiter® Aqueous One Solution Cell Proliferation Assay). Briefly, DMSCs were incubated with various concentrations of NPs for 2 h in serum-free DMEM (n = 3). Then, the media were changed with fresh complete culture media and the cells were incubated for another 24 h. The medium was replaced with 600 μL culture medium including MTS, and the incubation proceeded for 3 h. The medium was then removed, and its absorption at 490 nm was measured using a spectrofluorimeter plate reader (EnSpire, PerkinElmer).

Intracellular fate of nanoparticles. For the co-localization of NPs and lysosomes, the cells were incubated with 200 μg mL^{-1} particles for 2 h. The cells were washed twice with PBS solution. Then, lysosomes were stained with the Cell Tracker® Lysosome staining kit following the manufacturer's protocol (AAT Bioquest, Inc., USA). After washing twice with PBS, fresh medium was added. The cells were fixed and stained with DAPI as previously described. Fluorescence microscopy was performed with an Evos® FL Cell Imaging System.

***In vitro* evaluation of the ultrasonic responsive cell platform.** Preparation of UR-NPs@PEI containing doxorubicin was performed by stirring 10 mg of UR-NPs in 5 mL of a solution of doxorubicin in PBS (1 mg mL^{-1}) for 24 h at 4 °C. Doxorubicin-loaded particles were washed by centrifugation and redispersion in PBS at 50 °C several times. Loaded nanoparticles were coated with PEI as previously described (DOX-UR-NPs@PEI). Quantification of doxorubicin inside DOX-UR-NPs@PEI was performed by dispersing a known amount of nanoparticles in 95% ethanol in an ultrasonic bath to force the release of the cargo, and measuring the fluorescence of doxorubicin in ethanolic solution after filtration of the nanoparticles. A calibration curve of doxorubicin fluorescence in ethanolic solution (λ_{exc} 470, λ_{em} 585 nm) was used.

The preparation of the engineered cell–NP platform was carried out by using the following procedure: DMSCs were incubated with 200 μg mL^{-1} of UR-NP@PEI (with/without DOX) for 2 h and washed with PBS to remove non-internalized nanoparticles. Quantification of doxorubicin in the DOX-Platform was carried out as described for DOX-UR-NPs@PEI, dispersing the DOX-Platform in 95% ethanol under sonication (therefore, releasing the cell content, including the nanoparticles, to the ethanolic solution) and measuring the fluorescence.

Cell viability was evaluated after 1 and 3 days by performing the Alamar Blue assay, following the manufacturer's instructions: 10% of the reagent was added to the culture medium with the DMSCs and incubated at 37 °C for 1 h. Then, fluorescence at λ_{exc} 560, λ_{em} 590 nm was measured in a spectrofluorimeter plate reader. Cell viability was then analyzed as a percentage of the control wells (DMSCs not exposed to DOX-nanoparticles).

Migration capacity towards mammary tumor homogenates. Animal care was carried out in accordance with the Royal Decree 223/1988 (BOE 8, 18) and the Ministerial Order of 13 October 1989 (BOE 8) regarding the protection of experimental animals, as well as with the European Council Directive 86/609/EEC and approved by the Committee of Ethics and Animal Welfare (CEBA) from Hospital Universitario 12 de Octubre. *N*-Nitroso-*N*-methylurea (NMU) tumors were induced in 45-day-old Sprague-Dawley female rats according to our previously published protocol.[46] The tumors were dissected out from the animals, immediately frozen in liquid nitrogen and subsequently stored at −80 °C until further use. Homogenates from those tumors were performed at 4 °C as we previously described.[34] The protein concentration was measured using the Lowry protein assay kit (Biorad, Spain) following the manufacturer's instructions.

The migration capacity of the engineered platform towards the tumor homogenate was performed using Millicell culture plate inserts with 8 μm pore polycarbonate membranes (Merck Millipore, Spain) in 24-well plates. 1.5 × 10^5 DMSCs containing UR-NPs@PEI (with/without DOX) in 300 μL of serum-free DMEM were seeded in the insert. The tumor homogenate (5 mg mL^{-1} of protein concentration) was added in the well below. Migration medium (serum-free DMEM) without tissue was used as a negative control. Migration was assessed at 24 h by the CytoSelect 24-Well Cell Migration Assay (8 μm, Colorimetric, Cell Biolabs, Bionova Cientifica, S.L., Spain). Non-migratory cells were removed from the top of the membrane and migratory cells on the bottom of the polycarbonate membrane were stained with the cell stain solution and quantified according to the manufacturer's instructions. Migratory cells were visualized (three individual fields per insert) using a light microscope under ×40 magnification objective. The color of the stained cells was subsequently extracted with the extraction solution, and quantified by absorbance at 560 nm using the multimodal plate reader Enspire (PerkinElmer). All experiments were done as a minimum in triplicate.

***In vitro* co-culture experiments.** DMSCs or the engineered DOX-Platform (UR-NPs@PEI inside DMSCs, with doxorubicin) were co-cultured with NMU rat mammary cancer cells (ATCC, LGC Standards S.L.U., Spain). NMU cells were cultured in 24-well plates at a density of 20 000 cells per well 24 h before the experiment was carried out. DMSCs were incubated with DOX-UR-NPs@PEI as previously described. After washing non-internalized nanoparticles, DMSCs (with and without NPs) were trypsinized and ultrasound was applied to some of the DMSC suspensions (1 MHz, 3 W cm^{-2}, 5 min continuous application). Then, DMSCs with or without DOX-NPs (and with or without US exposure) were seeded in Transwell® culture inserts (0.4 μm pore, polycarbonate membranes, tissue cultured treated, Costar®), in the same plate containing NMU cells, in two different DMSC : NMU ratios (1 : 2 and 1 : 5). After

1 and 2 days, the inserts were removed and NMU cell viability was analyzed by performing the Alamar Blue test, as previously described.

Ultrasonic experiments

For the *in vial* release experiments, the US experiments were performed in a commercial laboratory ultrasound apparatus (RBI, France), working at 1.3 MHz and 100 W for 10 min, under similar conditions to those described in our previous work.[15]

For the *in vivo* and *in vitro* intracellular cargo release experiments, a commercial ultrasound apparatus for application in physical therapy was used (New Pocket Sonovit, New Age Italia Srl, Italy). The parameters selected were: 1 MHz, 3 W cm^{-2}, continuous application, 5–10 min. In the *in vitro* intracellular experiments, ultrasound was applied from the top of a filled culture well through a latex membrane (ultrasound transmission gel was placed between the transducer and the latex membrane).

Acknowledgements

The authors thank the funding from the European Research Council through the Advanced Grant VERDI (ERC-2015 AdG proposal no. 694160). Financial support from Ministerio de Economía y Competitividad, (MEC), Spain (Project MAT2015-64831-R) is gratefully acknowledged. JL Paris gratefully acknowledges MEC, Spain, for his PhD grant (BES-2013-064182). This work was sponsored by grants PI11/00581; PI13/00045; PI15/01803 (Ministry of Economy, Industry and Competitiveness) and cofunded by the European Regional Development Fund, and approved by the Ethics Committee of our Institution; MULTIMAT-CHALLENGE (S2013/MIT-2862) from Comunidad de Madrid and the Neurosciences and Aging Foundation, the Francisco Soria Melguizo Foundation, Octopharma and Parkinson Madrid (PI2012/0032 and PI2013/0116).

Notes and references

1 S. Mura, J. Nicolas and P. Couvreur, *Nat. Mater.*, 2013, **12**, 991–1003.
2 A. Baeza, M. Colilla and M. Vallet-Regí, *Expert Opin. Drug Delivery*, 2015, **12**, 319–337.
3 M. Vallet-Regi, A. Rámila, R. P. del Real and J. Pérez-Pariente, *Chem. Mater.*, 2001, **13**, 308–311.
4 Z. Li, J. C. Barnes, A. Bosoy, J. F. Stoddart and J. I. Zink, *Chem. Soc. Rev.*, 2012, **41**, 2590–2605.
5 A. Baeza, M. Manzano, M. Colilla and M. Vallet-Regí, *Biomater. Sci.*, 2016, **4**, 803–813.
6 Z. Li, D. L. Clemens, B.-Y. Lee, B. J. Dillon, M. A. Horwitz and J. I. Zink, *ACS Nano*, 2015, **9**, 10778–10789.
7 Z. Luo, K. Cai, Y. Hu, L. Zhao, P. Liu, L. Duan and W. Yang, *Angew. Chem., Int. Ed.*, 2011, **50**, 640–643.
8 A. Popat, B. P. Ross, J. Liu, S. Jambhrunkar, F. Kleitz and S. Z. Qiao, *Angew. Chem., Int. Ed.*, 2012, **51**, 12486–12489.
9 Y.-Z. You, K. K. Kalebaila and S. L. Brock, *Chem. Mater.*, 2008, **20**, 3354–3359.
10 M. Martínez-Carmona, A. Baeza, M. a. Rodriguez-Milla, J. García-Castro and M. Vallet-Regí, *J. Mater. Chem. B*, 2015, **3**, 5746–5752.
11 J. Liu, C. Detrembleur, M.-C. De Pauw-Gillet, S. Mornet, C. Jérôme and E. Duguet, *Small*, 2015, **11**, 2323–2332.
12 E. Guisasola, A. Baeza, M. Talelli, D. Arcos, M. Moros, J. M. de la Fuente and M. Vallet-Regí, *Langmuir*, 2015, **31**, 12777–12782.
13 S. Carregal-Romero, P. Guardia, X. Yu, R. Hartmann, T. Pellegrino and W. J. Parak, *Nanoscale*, 2015, **7**, 570–576.
14 S.-F. Lee, X.-M. Zhu, Y.-X. J. Wang, S.-H. Xuan, Q. You, W.-H. Chan, C.-H. Wong, F. Wang, J. C. Yu, C. H. K. Cheng and K. C.-F. Leung, *ACS Appl. Mater. Interfaces*, 2013, **5**, 1566–1574.
15 J. L. Paris, M. V. Cabanas, M. Manzano and M. Vallet-Regí, *ACS Nano*, 2015, **9**, 11023–11033.
16 D. Roy, J. N. Cambre and B. S. Sumerlin, *Prog. Polym. Sci.*, 2010, **35**, 278–301.
17 A. P. Blum, J. K. Kammeyer, A. M. Rush, C. E. Callmann, M. E. Hahn and N. C. Gianneschi, *J. Am. Chem. Soc.*, 2015, **137**, 2140–2154.
18 H. Hosoya, A. S. Dobroff, W. H. P. Driessen, V. Cristini, L. M. Brinker, F. I. Staquicini, M. Cardó-Vila, S. D'Angelo, F. Ferrara, B. Proneth, Y.-S. Lin, D. R. Dunphy, P. Dogra, M. P. Melancon, R. J. Stafford, K. Miyazono, J. G. Gelovani, K. Kataoka, C. J. Brinker, R. L. Sidman, W. Arap and R. Pasqualini, *Proc. Natl. Acad. Sci. U. S. A.*, 2016, **113**, 1877–1882.
19 N. Bertrand, J. Wu, X. Xu, N. Kamaly and O. C. Farokhzad, *Adv. Drug Delivery Rev.*, 2014, **66**, 2–25.
20 J. Fang, H. Nakamura and H. Maeda, *Adv. Drug Delivery Rev.*, 2011, **63**, 136–151.
21 H. Maeda, H. Nakamura and J. Fang, *Adv. Drug Delivery Rev.*, 2013, **65**, 71–79.
22 J. W. Nichols and Y. H. Bae, *Nano Today*, 2012, **7**, 606–618.
23 I. K. Kwon, S. C. Lee, B. Han and K. Park, *J. Controlled Release*, 2012, **164**, 108–114.
24 S. Wilhelm, A. J. Tavares, Q. Dai, S. Ohta, J. Audet, H. F. Dvorak and W. C. W. Chan, *Nat. Rev. Mater.*, 2016, **1**, 16014.
25 F. Ratto, S. Centi, C. Avigo, C. Borri, F. Tatini, L. Cavigli, C. Kusmic, B. Lelli, S. Lai, S. Colagrande, F. Faita, L. Menichetti and R. Pini, *Adv. Funct. Mater.*, 2016, **26**, 7178–7185.
26 Z. Gao, L. Zhang, J. Hu and Y. Sun, *Nanomedicine*, 2013, **9**, 174–184.
27 J. M. Karp and G. S. Leng Teo, *Cell Stem Cell*, 2009, **4**, 206–216.
28 Y.-L. Hu, Y.-H. Fu, Y. Tabata and J.-Q. Gao, *J. Controlled Release*, 2010, **147**, 154–162.

29 M. Roger, A. Clavreul, M.-C. Venier-Julienne, C. Passirani, L. Sindji, P. Schiller, C. Montero-Menei and P. Menei, *Biomaterials*, 2010, **31**, 8393–8401.
30 L. Kucerova, V. Altanerova, M. Matuskova, S. Tyciakova and C. Altaner, *Cancer Res.*, 2007, **67**, 6304–6313.
31 L. S. Sasportas, R. Kasmieh, H. Wakimoto, S. Hingtgen, J. A. J. M. van de Water, G. Mohapatra, J. L. Figueiredo, R. L. Martuza, R. Weissleder and K. Shah, *Proc. Natl. Acad. Sci. U. S. A.*, 2009, **106**, 4822–4827.
32 H. Motaln, C. Schichor and T. T. Lah, *Cancer*, 2010, **116**, 2519–2530.
33 M. I. Macias, J. Grande, A. Moreno, I. Domínguez, R. Bornstein and A. I. Flores, *Am. J. Obstet. Gynecol.*, 2010, **203**, 495.
34 I. Vegh, M. Grau, M. Gracia, J. Grande, P. de la Torre and A. I. Flores, *Cancer Gene Ther.*, 2013, **20**, 8–16.
35 J. L. Paris, P. D. La Torre, M. Manzano, M. V. Cabañas, A. I. Flores and M. Vallet-Regí, *Acta Biomater.*, 2016, **33**, 275–282.
36 J. B. Engel, A. V. Schally, S. Buchholz, S. Seitz, G. Emons and O. Ortmann, *Arch. Gynecol. Obstet.*, 2012, **286**, 437–442.
37 C. E. Soma, C. Dubernet, G. Barratt, F. Nemati, M. Appel, S. Benita and P. Couvreur, *Pharm. Res.*, 1999, **16**, 1710–1716.
38 V. V. Padma, *Biomedicine*, 2015, **5**, 19.
39 C. J. Springer and I. Niculescu-Duvaz, *J. Clin. Invest.*, 2000, **105**, 1161–1167.
40 C. Peters and S. Brown, *Biosci. Rep.*, 2015, **35**, e00225–e00225.
41 H. Meng, M. Xue, T. Xia, Y.-L. Zhao, F. Tamanoi, J. F. Stoddart, J. I. Zink and A. E. Nel, *J. Am. Chem. Soc.*, 2010, **132**, 12690–12697.
42 S. Wang, P. Huang and X. Chen, *Adv. Mater.*, 2016, **28**, 7340–7364.
43 T. Xia, M. Kovochich, M. Liong, H. Meng, S. Kabehie, S. George, J. I. Zink and A. E. Nel, *ACS Nano*, 2009, **3**, 3273–3286.
44 X. Li, Y. Chen, M. Wang, Y. Ma, W. Xia and H. Gu, *Biomaterials*, 2013, **34**, 1391–1401.
45 J.-T. Lee, M. C. George, J. S. Moore and P. V. Braun, *J. Am. Chem. Soc.*, 2009, **131**, 11294–11295.
46 I. Vegh and R. E. de Salamanca, *J. Carcinog.*, 2007, **6**, 18.

Electronic Supplementary Material (ESI) for Nanoscale.

Supporting Information

Vectorization of ultrasound-responsive nanoparticles in placental mesenchymal stem cells for cancer therapy

Juan L. Paris, Paz de la Torre, M. Victoria Cabañas, Miguel Manzano, Montserrat Grau, Ana I. Flores and María Vallet-Regí*.*

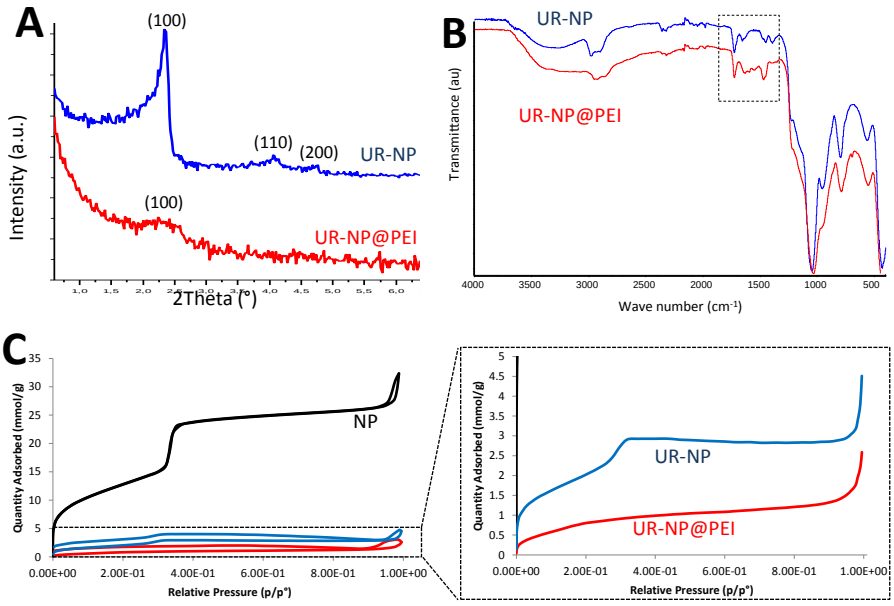

Figure S1. Characterization of Mesoporous Silica Nanoparticles: Small Angle XRD pattern (A), FTIR spectra (B) and N_2 adsorption-desorption isotherms (C).

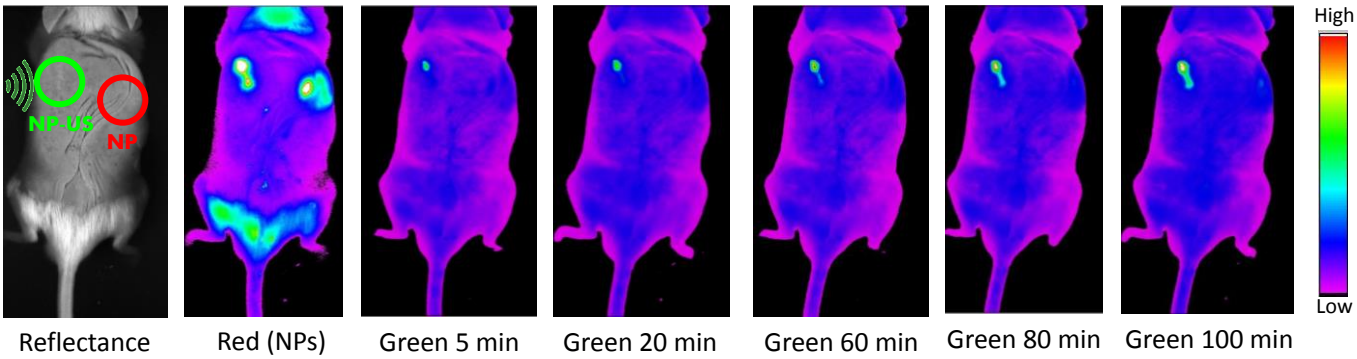

Figure S2. *In vivo* fluorescence of subcutaneously injected UR-NPs@PEI (red channel) and calcein produced after calcein-AM release at different times after ultrasound application (1 MHz, 3 W cm^{-2}, 10 min) (green channel).

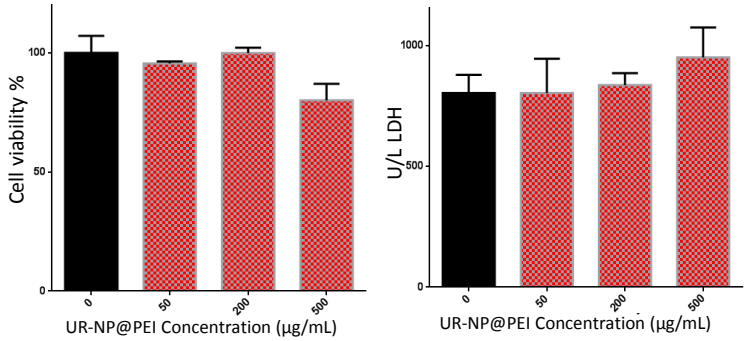

Figure S3. Cytotoxicity assay in DMSCs of UR-NP@PEI at different concentrations after 24 h measured by MTS reduction (left); LDH release by DMSCs with internalized UR-NP@PEI at different concentrations after 24 h. (Data presented as Mean ± SD, N = 3).

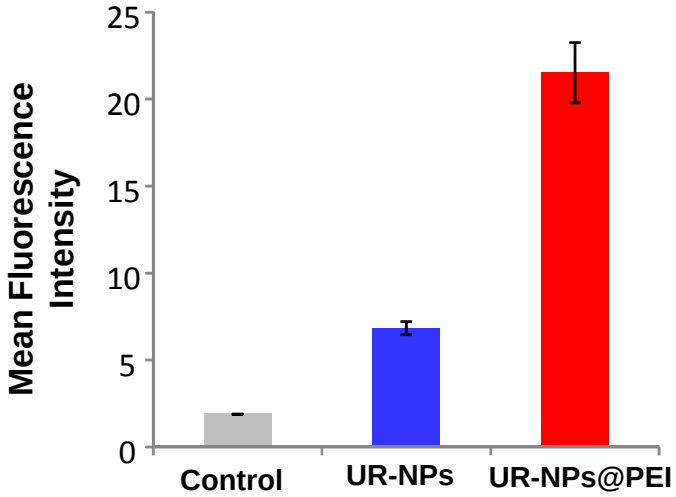

Figure S4. Flow-cytometry data regarding UR-NPs and UR-NPs@PEI uptake shown as Mean Fluorescence Intensity (a.u.). (Data presented as Mean ± SD, N = 3).

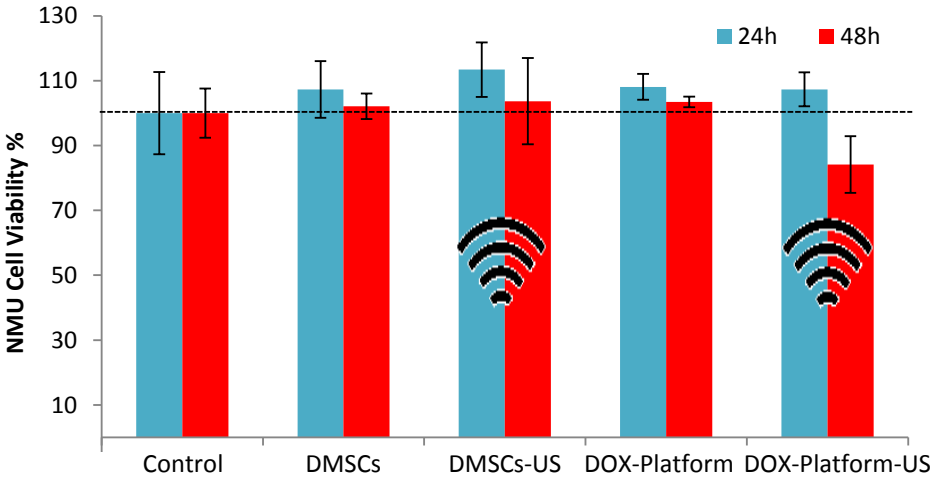

Figure S5. Cytotoxicity assay of NMU cells after co-culture with DMSCs or with DOX-Platform (with or without Ulltrasound application) measured by Alamar Blue test. DMSCs to NMU ratio was 1:5. (Data are Means ± SD, N =3).

3.3.3 Gene Transfection employing Ultrasound-responsive Mesoporous Silica Nanoparticles

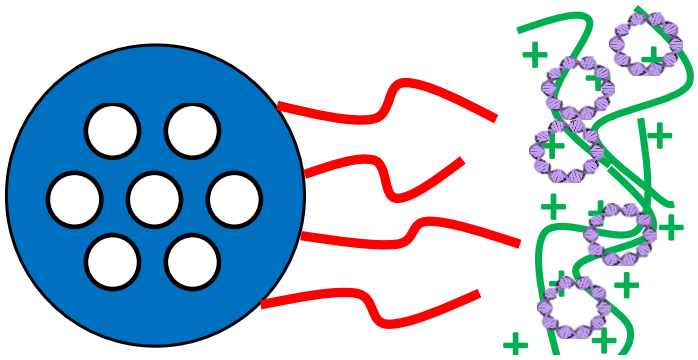

Gene Transfection employing Ultrasound-responsive Mesoporous Silica Nanoparticles

Abstract

A previously developed Ultrasound-responsive drug delivery system based on Mesoporous Silica Nanoparticles is here modified to include nucleic acids into the polymeric coating to provide gene transfection capabilities. The stimulus-responsive nanoparticles are coated with polyethylenimine with two different molecular weights. Gene transfection capacity with two different plasmids is evaluated. First, the expression of Green Fluorescent Protein is analyzed in Decidua-derived Mesenchymal Stem Cells after incubation with the nanoparticles. The most successful formulation is then employed to induce the expression of two suicide genes: cytosine deaminase and uracil phosphoribosyl transferase, which allow the cells to convert a non-toxic prodrug (5-fluorocytosine) into a toxic drug (5-Fluorouridine monophosphate). The effect of the production of the toxic final product is also evaluated in a cancer cell line (NMU cells) co-cultured with the transfected vehicle cells, Decidua-derived Mesenchymal Stem Cells.

Introduction

Stimuli-responsive nanoparticles for antitumor drug release have attracted much attention in recent years because they could significantly improve the safety profile of cancer therapies.[1] However, nanomedicine is still facing a nanoparticle delivery problem, since a low amount of nanoparticles reach the tumor tissues after systemic injection.[2] Therefore, it is necessary to develop alternative strategies to ensure that the appropriate dosage of drug can reach the target tissue.[3] In this context, cell vehicle-based approaches are amongst the most promising strategies to overcome this issue.[4–6] Mesenchymal Stem Cells are among the most studied cells for nanoparticle vectorization towards tumors.[4] Human Decidua-derived Mesenchymal Stem Cells (DMSCs) are multipotent stem cells with migratory properties towards tumor tissue, and they can also inhibit tumor progression.[7,8] We have recently reported the use of DMSCs as vehicles capable of transporting ultrasound-responsive Mesoporous Silica Nanoparticles (UR-NPs).[6,9] These UR-NPs loaded with doxorubicin (a cytotoxic drug) can be transported towards tumors inside DMSCs. Then, upon ultrasound exposure, the drug is released from the platform, killing surrounding cancer cells.[9]

Gene transfection is based on inducing or modifying the expression of different proteins through delivering nucleic acids to the target cell. Gene transfection using non-viral

vectors can be used to develop therapeutic strategies.[10] For example, cancer cell death can be induced by the expression of a toxin encoded in a suicide gene[11]. Suicide genes can act either directly, encoding a protein that is toxic, or indirectly, encoding an enzyme that can lead to the production of a toxic molecule.[11] Furthermore, vehicle cells can be transfected with suicide genes that will induce the death not only to the transfected cell, but also surrounding cancer cells,[10,12–14] in an effect known as the "bystander effect".[15] Furthermore, combined strategies in which both small therapeutic molecules, like doxorubicin, and nucleic acids, like plasmids, are delivered can drastically improve the therapeutic outcome by exploiting synergisms between both mechanisms of action.[16]

The main objective of the present work is to provide gene transfection capabilities to UR-NPs, aiming a dual therapeutic strategy. Thus, in addition to the production of a therapeutic protein by the genetically-engineered vehicle cells, an anticancer drug will also be released in the tumor. The combination of both approaches would enhance the performance of the therapeutic nanoparticle-cell platform.

Experimental section

Synthesis of UR-NPs: Ultrasound-responsive Mesoporous Silica Nanoparticles were obtained as described elsewhere, by grafting the polymeric gate poly-(2-(2methoxyethoxy)ethyl methacrylate-co-2-tetrahydropyranyl methacrylate), p(MEO_2MA-co-THPMA), to mesoporous silica nanoparticles.[17] MCM-41 type mesoporous silica nanoparticles were prepared following a modified Stöber Method, by the condensation of tetraethyl orthosilicate (TEOS) under dilute conditions in the presence of hexadecyltrimethylammonium bromide (CTAB).[17] The surfactant was removed by ionic exchange with NH_4NO_3 and the particles were collected by centrifugation and washed with ethanol.[6,17] The temperature and ultrasound-responsive copolymer p(MEO_2MA-co-THPMA) was obtained by Free Radical Polymerization of MEO_2MA and THPMA monomers (90:10 molar ratio in the final polymer). The copolymer was then grafted on the surface of Mesoporous Silica Nanoparticles by conjugating it with (3-aminopropyl)triethoxysilane (APTES) through dicyclohexylcarbodiimide/ *N*-Hydroxysuccinimide (DCC/NHS) chemistry, and then through the condensation of the APTES moieties on the silica surface.[9,17]

Polyethylenimine (PEI) coating of UR-NPs: US-responsive nanoparticles coated with PEI of different molecular weights (UR-NPs@PEI) were obtained by dissolving 5 mg of PEI (1.8 or 5 kDa) in 0.5 mL of deionized (DI) water with 3 µL of acetic acid (glacial). The PEI solution

was then diluted with 0.5 mL of 10 mM Phosphate-buffered saline (PBS) solution. That PEI solution was then added to 10 mg of UR-NPs dispersed in PBS (final volume 2 mL). The coating was carried out at 37 ºC for 3 h under orbital stirring. The product was washed several times with PBS, centrifuged and dried under vacuum at room temperature.
Z potential measurements were performed in DI water by means of a Zetasizer Nano ZS (Malvern Instruments) equipped with a 633 nm "red" laser.

Plasmid loading in the PEI coating and cell transfection: Green fluorescence protein (GFP) or cytosine deaminase: uracil phosphoribosyl transferase (CD:UPRT) plasmid was incubated with UR-NPs@PEI as follows: 7.5 µg of plasmid in Dulbecco's Modified Eagle's Medium (DMEM) were mixed with 1 mg of UR-NPs@PEI already dispersed in DMEM (total volume 1 mL), and magnetically stirred at room temperature for 15 min. The mixture was then diluted to 200 µg/mL of UR-NPs@PEI-plasmid in DMEM (without serum) and incubated with DMSCs for 2 h at 37 ºC. The transfected cells were then washed with PBS twice and incubated in complete culture medium.

Transfection with GFP plasmid was evaluated by fluorescence microscopy and flow cytometry 3 days after incubation with the nanoparticles. Fluorescence microscopy was performed with an Evos FL Cell Imaging System equipped with three Led Lights Cubes (lEX (nm); lEM (nm)): DAPI (357/44; 447/60), GFP (470/22; 525/50), RFP (531/40; 593/40) from AMG (Advance Microscopy Group). Flow cytometry was performed in a BD FACSCalibur™ cytometer, and results were processed using Flowing Software.

Cell viability after transfection with CD:UPRT plasmid was evaluated after exposing the cells to 0.05 mg/mL of 5-FC. Flow cytometry was performed using an apoptosis/necrosis staining kit (BD Pharmingen™ FITC Annexin V Apoptosis Detection Kit I, following the manufacturer´s instructions).

Coculture with NMU cells: DMSCs with UR-NPs@5PEI loaded with the CD:UPRT plasmid were co-cultured with NMU rat mammary cancer cells (ATCC, LGC Standards S.L.U.) as described elsewhere[6,9]. NMU cells were cultured in 24 well plates at a density of 20,000 cells per well. Twenty-four hours later, DMSCs (with or without nanoparticles) were seeded in Transwell® culture inserts (0.4 µm pore, polycarbonate membranes, tissue cultured treated, Costar®) in a 1:2 DMSCs:NMU ratio. After 3 days, 5-FC was added to the medium (final concentration was 0.1 mg/mL). Four days after the addition of the prodrug, the inserts were removed and the viability/proliferation of NMU cells was evaluated by Alamar Blue assay, following the manufacturer's instructions. NMU cells were also trypsinized and stained with

BD Pharmingen™ FITC Annexin V Apoptosis Detection Kit I. Then, the cells were analyzed by flow cytometry. Statistical analyses were performed by the Student's t test.

Results and Discussion

UR-NPs were obtained by grafting an ultrasound-responsive polymeric gate on the surface of mesoporous silica nanoparticles, as we have described elsewhere.[17] UR-NPs were coated with PEI, UR-NPs@PEI, to provide a positive charge on their surface, which promotes an efficient nanoparticle internalization into DMSCs.[9] A plasmid containing the genes of interest could be loaded in PEI-coated UR-NPs by inserting it into the PEI coating. The effect of PEI molecular weight on gene transfection was evaluated by using 1.8 kDa (as used for our previous work[9]) and 5 kDa linear PEIs to coat the UR-NPs (UR-NPs@1.8PEI and UR-NPS@5PEI, respectively). The change to positive values in the Z potential confirms the successful coating of UR-NPs by both types of PEI (Figure 1).

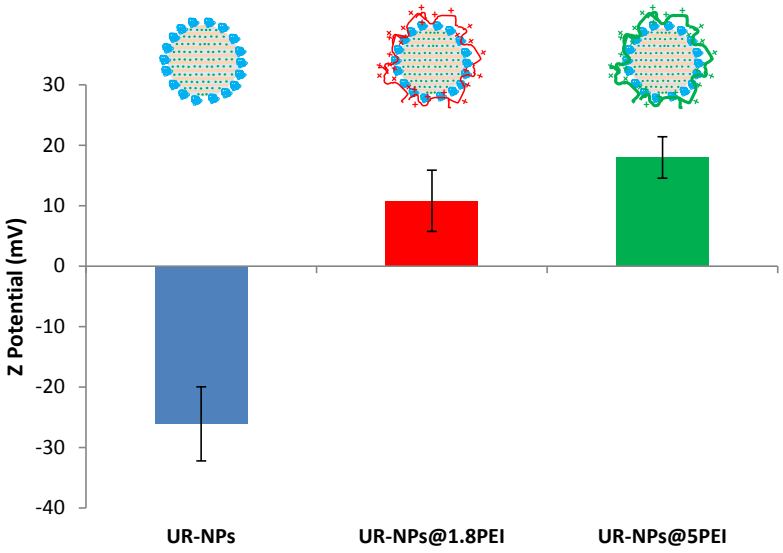

Figure 1. Z Potential values of UR-NPs without or with PEI coatings of two different molecular weights (1.8 or 5 kDa).

Gene transfection conditions were optimized employing a GFP plasmid. The expression of GFP was evaluated by fluorescence microscopy and flow cytometry. UR-NPs@PEI were stirred with the plasmid at room temperature for 15 minutes, and the mixture was then incubated with DMSCs at 37 ºC for 2 h in serum-free DMEM. Then, the non-internalized particles were removed by washing with PBS. Figure 2 shows that no significant gene expression could be achieved with the 1.8 kDa PEI. On the other hand, incubation with UR-NPs@5PEI induced the expression of GFP, as can be observed both in fluorescence

microscopy and flow cytometry. These results, showing that gene transfection efficiency of PEI is directly related to its molecular weight, are in good agreement with previous literature.[18] However, the toxicity of PEI is also related to the molecular weight,[18] and when we attempted to use a 25 kDa PEI, the vast majority of DMSCs died after incubation with the nanoparticles (data not shown), which is also in agreement with the literature. Therefore, after optimizing the conditions for our platform, 5 kDa PEI was chosen for all further experiments.

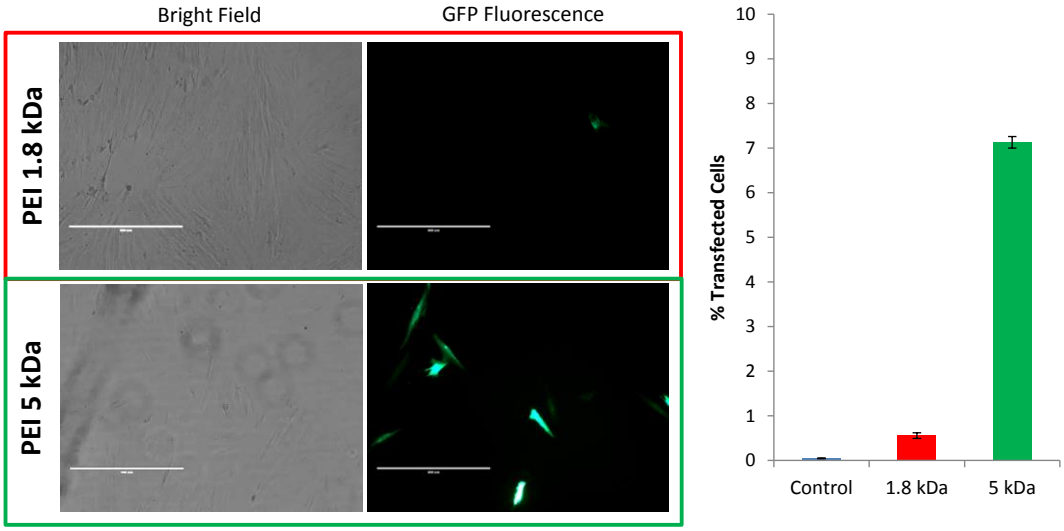

Figure 2. Fluorescence microscopy images (left) and flow cytometry (right) of DMSCs 3 days after incubation with UR-NPs@PEI carrying the plasmid of GFP.

The next step after optimizing the conditions for gene transfection using UR-NPs@5PEI, consisted on using a plasmid of therapeutic interest to further evaluate its transfection in DMSCs. We selected a commercial plasmid with two genes involved in suicide gene therapy: cytosine deaminase (CD) and uracil phosphoribosyl transferase (UPRT). CD can convert the non-toxic prodrug 5-fluorocytosine (5-FC) into toxic 5-Fluoruracil (5-FU), which is then further transformed by UPRT into the more toxic 5-Fluorouridine monophosphate (5-FUMP), an irreversible inhibitor of thymidylate synthase,[19] and consequently, generating a potent cytotoxic effect (Scheme 1).

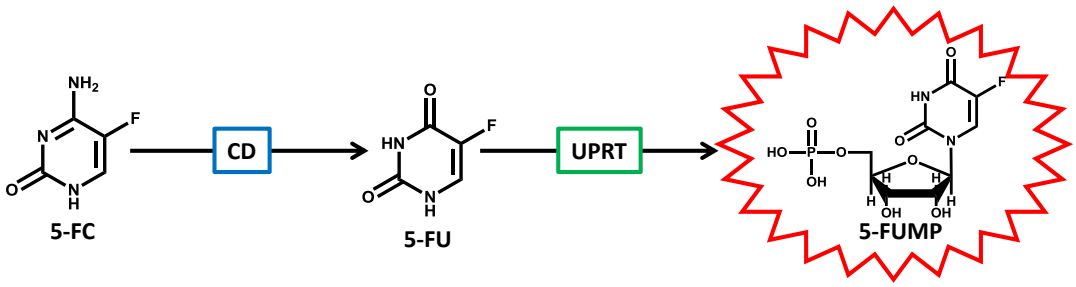

Scheme 1. Schematic representation of prodrug activation.

The plasmid containing the two suicide genes (CD:UPRT plasmid) was loaded into the UR-NPs@5PEI following the same protocol as previously described for GFP plasmid. Those plasmid-loaded nanoparticles were incubated with DMSCs for two hours, and after 3 days, 5-FC was added to the culture media of DMSCs. Same procedure was carried out on DMSCs without incubation with nanoparticles and/or without the addition of 5-FC for control. After 5 days, the viability of DMSCs was evaluated through bright field microscopy (Figure 3a), showing a significant reduction in the cell density growing on the wells that were treated with 5-FC after transfection, while no significant changes could be observed in the other experimental groups. After staining the nuclei with DAPI, apoptotic nuclei (brighter staining) could be observed by fluorescence microscopy in the transfected cells exposed to the prodrug (Figure 3b), as would be expected from the production of toxic 5-FUMP.

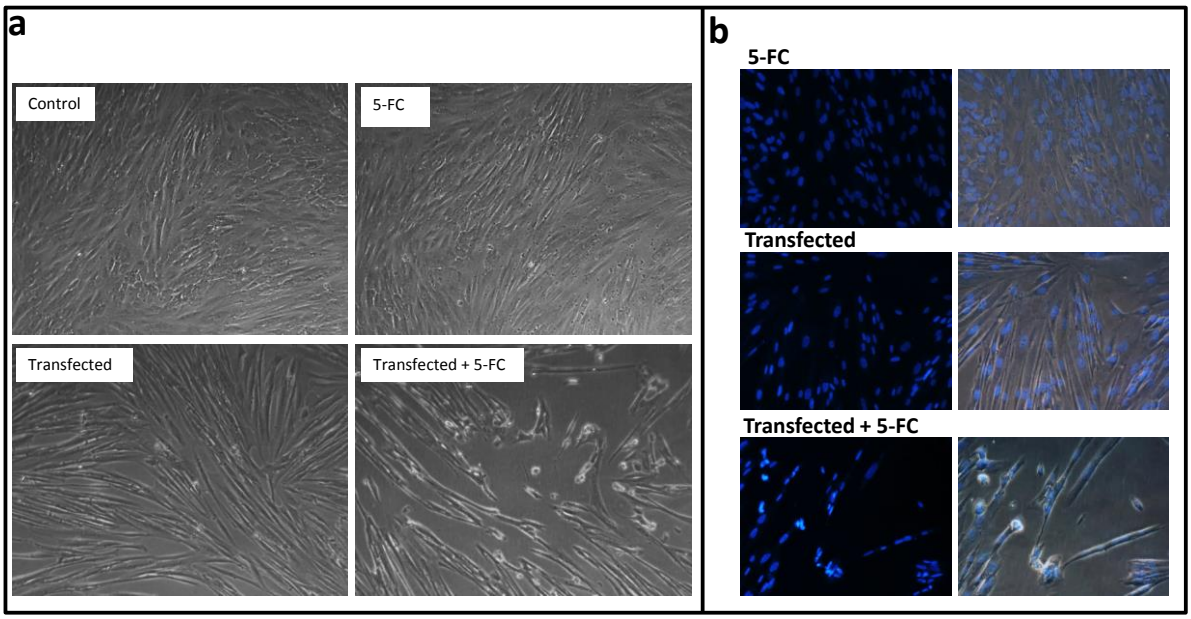

Figure 3. Bright field microscopy images showing DMSCs after different treatments with UR-NPs@5PEI carrying the plasmid with the suicide genes CD:UPRT and/or the non-toxic prodrug 5-FC (0.05 mg/mL) (a) and DAPI-stained fluorescence microscopy images of DMSCs after the same treatments showing apoptotic nuclei (brighter nuclei staining) (b).

DMSCs exposed to those treatments were also evaluated by Flow cytometry with an apoptosis-necrosis evaluation kit (Figure 4). Cells in the lower left quadrant correspond to healthy cells, lower right quadrant cells are early-apoptotic, and upper-right quadrant comprises late-apoptotic or necrotic cells. Figure 4 shows an increase in late apoptotic/necrotic cells only in the transfected cells exposed to 5-FC.

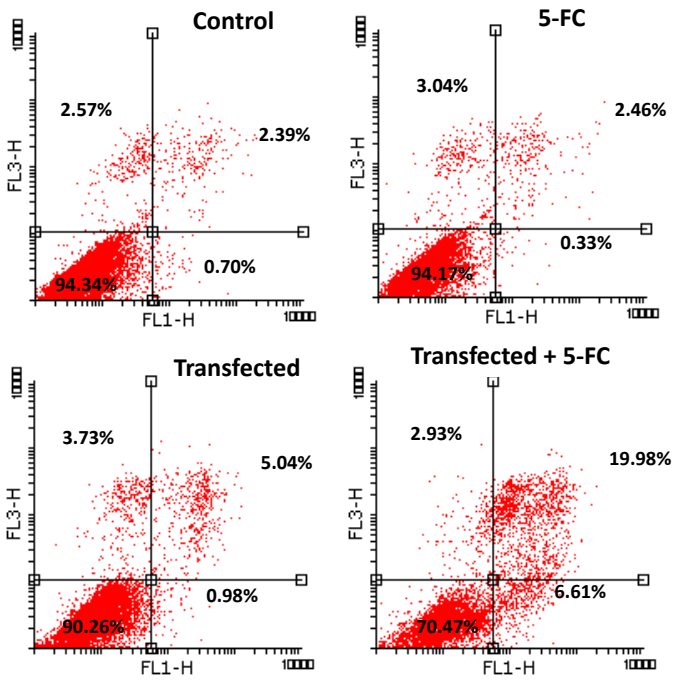

Figure 4. Flow cytometry analysis of apoptotis/necrosis in DMSCs after different treatments with nanoparticles carrying the suicide genes and/or the non-toxic prodrug 5-FC.

These results confirm the successful transfection of DMSCs with the CD:UPRT plasmid, which provides them the capability of converting non-toxic 5-FC into toxic 5-FUMP, as shown in Scheme 1. One of the main advantages of the combination of the CD and UPRT genes instead of using the CD gene alone is the increased bystander effect of 5-FUMP over 5-FU.[19]

In order to test the bystander effect in our platform, a Transwell co-culture with NMU mammary cancer cells was carried out.[6,9] DMSCs were transfected with CD:UPRT employing UR-NPs@5PEI as previously described, and they were then placed on a Transwell cell culture insert in a well containing NMU cancer cells (DMSC:NMU ratio was 1:2). Three days after transfection of the DMSCs, 5-FC was added to the culture medium, and the viability of NMU cells was evaluated 4 days after the addition of the prodrug. Figure 5 shows a significant decrease in the Alamar Blue assay of NMU cells exposed to transfected DMSCs and with 5-FC in their culture medium.

The results obtained by Alamar Blue were further confirmed by the apoptosis-necrosis results evaluated by flow cytometry, which show a significant increase in the number of early apoptotic cells in the treatment population compared to the other experimental conditions (Figure 6).

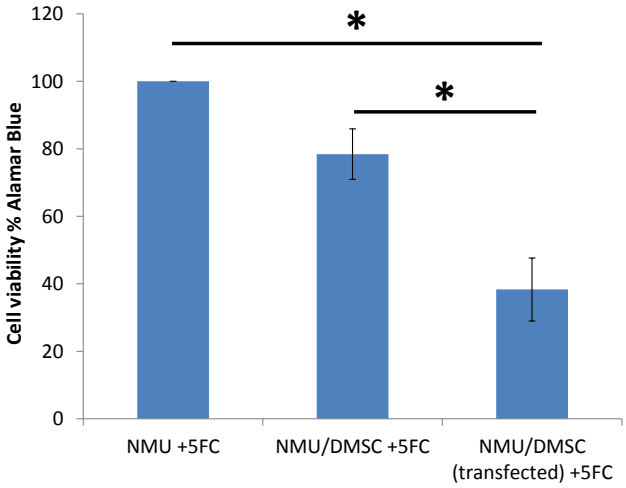

Figure 5. NMU cell viability results obtained by Alamar Blue assay in co-culture with DMSCs (without or with nanoparticle-mediated gene transfection) and exposed to 5-FC.

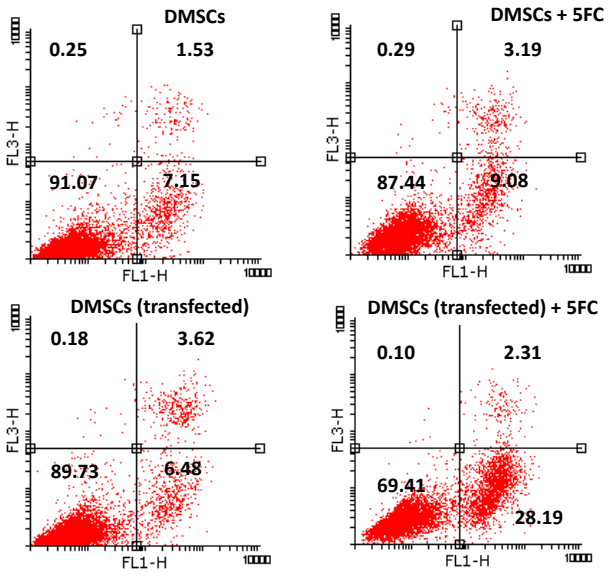

Figure 6. Apoptosis/necrosis evaluation by flow cytometry of NMU cells co-cultured with DMSCs (without or with nanoparticle-mediated gene transfection).

All of these results confirm the possibility of killing surrounding cancer cells by nanoparticle-mediated genetic engineered DMSCs. This anticancer therapeutic approach by the production of a toxic molecule by DMSCs could be further improved by the ultrasound-responsive release of another anticancer drug from our UR-NPs.[9]

Conclusions

The results obtained in this work confirm the possibility of inducing gene transfection using our previously developed US-responsive MSNs, without inducing significant toxicity to the

vehicle cells (DMSCs), by modifying the molecular weight of the PEI coating. UR-NPs@5PEI were used to transfect DMSCs with the CD:UPRT plasmid, providing them the capability of converting non-toxic 5-FC into toxic 5-FUMP. Moreover, DMSCs transfected with the CD:UPRT plasmid are capable of inducing cell death in co-cultured NMU cancer cells, when exposed to the non-toxic prodrug 5-FC.

References

1. Rahoui, N., Jiang, B., Taloub, N. & Huang, Y. D. Spatio-temporal control strategy of drug delivery systems based nano structures. *J. Control. Release* **255,** 176–201 (2017).
2. Wilhelm, S., Tavares, A. J., Dai, Q., Ohta, S., Audet, J., Dvorak, H. F. & Chan, W. C. W. Analysis of nanoparticle delivery to tumors. *Nat. Rev. Mater.* **1,** 16014 (2016).
3. Wang, S., Huang, P. & Chen, X. Hierarchical Targeting Strategy for Enhanced Tumor Tissue Accumulation/Retention and Cellular Internalization. *Adv. Mater.* **28,** 7340–7364 (2016).
4. Hu, Y.-L., Fu, Y.-H., Tabata, Y. & Gao, J.-Q. Mesenchymal stem cells: A promising targeted-delivery vehicle in cancer gene therapy. *J. Control. Release* **147,** 154–162 (2010).
5. Roger, M., Clavreul, A., Venier-Julienne, M.-C., Passirani, C., Sindji, L., Schiller, P., Montero-Menei, C. & Menei, P. Mesenchymal stem cells as cellular vehicles for delivery of nanoparticles to brain tumors. *Biomaterials* **31,** 8393–8401 (2010).
6. Paris, J. L., de la Torre, P., Manzano, M., Cabañas, M. V., Flores, A. I. & Vallet-Regí, M. Decidua-derived mesenchymal stem cells as carriers of mesoporous silica nanoparticles. In vitro and in vivo evaluation on mammary tumors. *Acta Biomater.* **33,** 275–282 (2016).
7. Vegh, I., Grau, M., Gracia, M., Grande, J., de la Torre, P. & Flores, A. I. Decidua mesenchymal stem cells migrated toward mammary tumors in vitro and in vivo affecting tumor growth and tumor development. *Cancer Gene Ther.* **20,** 8–16 (2013).
8. Macias, M. I., Grande, J., Moreno, A., Domínguez, I., Bornstein, R. & Flores, A. I. Isolation and characterization of true mesenchymal stem cells derived from human term decidua capable of multilineage differentiation into all 3 embryonic layers. *Am. J. Obstet. Gynecol.* **203,** 495.e9-495.e23 (2010).
9. Paris, J. L., de la Torre, P., Cabañas, M. V., Manzano, M., Grau, M., Flores, A. I. & Vallet-Regí, M. Vectorization of ultrasound-responsive nanoparticles in placental mesenchymal stem cells for cancer therapy. *Nanoscale* **9,** 5528–5537 (2017).
10. Roy, I., Stachowiak, M. K. & Bergey, E. J. Nonviral gene transfection nanoparticles: function and applications in the brain. *Nanomedicine Nanotechnology, Biol. Med.* **4,** 89–97 (2008).
11. Alvarez, R. D., Gomez-Navarro, J., Wang, M., Barnes, M. N., Strong, T. V., Arani, R. B., Arafat, W., Hughes, J. V., Siegal, G. P. & Curiel, D. T. Adenoviral-Mediated Suicide Gene Therapy for Ovarian Cancer. *Mol. Ther.* **2,** 524–530 (2000).
12. Kucerova, L., Matuskova, M., Pastorakova, A., Tyciakova, S., Jakubikova, J., Bohovic, R., Altanerova, V. & Altaner, C. Cytosine deaminase expressing human mesenchymal stem cells mediated tumor regression in melanoma bearing mice. *J. Gene Med.* **10,** 1071–1082 (2008).
13. Cavarretta, I. T., Altanerova, V., Matuskova, M., Kucerova, L., Culig, Z. & Altaner, C. Adipose Tissue–derived Mesenchymal Stem Cells Expressing Prodrug-converting Enzyme Inhibit Human Prostate Tumor Growth. *Mol. Ther.* **18,** 223–231 (2010).

14. You, M.-H., Kim, W.-J., Shim, W., Lee, S.-R., Lee, G., Choi, S., Kim, D.-Y., Kim, Y. M., Kim, H. & Han, S.-U. Cytosine deaminase-producing human mesenchymal stem cells mediate an antitumor effect in a mouse xenograft model. *J. Gastroenterol. Hepatol.* **24,** 1393–1400 (2009).
15. Springer, C. J. & Niculescu-Duvaz, I. Prodrug-activating systems in suicide gene therapy. *J. Clin. Invest.* **105,** 1161–1167 (2000).
16. Wang, Y., Gao, S., Ye, W.-H., Yoon, H. S. & Yang, Y.-Y. Co-delivery of drugs and DNA from cationic core–shell nanoparticles self-assembled from a biodegradable copolymer. *Nat. Mater.* **5,** 791–796 (2006).
17. Paris, J. L., Cabañas, M. V., Manzano, M. & Vallet-Regí, M. Polymer-Grafted Mesoporous Silica Nanoparticles as Ultrasound-Responsive Drug Carriers. *ACS Nano* **9,** 11023–11033 (2015).
18. Xia, T., Kovochich, M., Liong, M., Meng, H., Kabehie, S., George, S., Zink, J. I. & Nel, A. E. Polyethyleneimine Coating Enhances the Cellular Uptake of Mesoporous Silica Nanoparticles and Allows Safe Delivery of siRNA and DNA Constructs. *ACS Nano* **3,** 3273–3286 (2009).
19. Bourbeau, D., Lavoie, G., Nalbantoglu, J. & Massie, B. Suicide gene therapy with an adenovirus expressing the fusion gene CD::UPRT in human glioblastomas: different sensitivities correlate with p53 status. *J. Gene Med.* **6,** 1320–1332 (2004).

4. CONCLUSIONES

La ciencia es una forma de pensar, y no tanto un agregado de conocimientos.

Carl Sagan

Conclusiones

- Se ha conseguido controlar la liberación de fármacos desde nanopartículas de sílice mesoporosa empleando ultrasonido como estímulo.

- Se ha demostrado que la cavitación acústica juega un papel fundamental en la liberación desde el nuevo nanotransportador sensible a ultrasonido.

- La modificación de las nanopartículas sensibles a ultrasonido ha permitido mejorar su estabilidad en suspensión y proporcionar capacidad de internalización selectiva en células tumorales, algo de gran importancia para el uso de nanomedicinas en terapias oncológicas.

- Se ha conseguido inducir la internalización en células tumorales de un nuevo tipo de nanopartículas de sílice mesoporosa con vectorización jerarquizada, empleando los efectos térmicos del ultrasonido.

- Se ha demostrado la capacidad de inducir la extravasación de nanopartículas de sílice mesoporosa al ser expuestas a cavitación acústica en un modelo *in vitro*.

- Se ha comprobado la capacidad de células madre mesenquimales de placenta para captar y transportar hacia tumores nanopartículas de sílice mesoporosa.

- Por primera vez, se han transportado en un vehículo celular nanopartículas con liberación sensible a ultrasonido, mostrando su capacidad de matar células tumorales al ser expuestas al estímulo, primer paso de ensayos preclínicos antes de considerar su traslación.

- Se ha logrado inducir la expresión de un gen suicida en las células madre mesenquimales de placenta modificando la superficie de nuestras nanopartículas sensibles a ultrasonido para que actúen como agentes de transfección.

A lo largo de esta tesis se ha conseguido un control espaciotemporal de la liberación de fármacos citotóxicos, permitiendo inducir su liberación, modificar la vectorización de nanopartículas hacia tumores y controlar la liberación de agentes terapéuticos desde transportadores celulares, todo ello por medio de la combinación de ultrasonido con nanopartículas de sílice mesoporosa.

Conclusions

- Control of drug release from mesoporous silica nanoparticles has been achieved using ultrasound as a stimulus.

- Acoustic cavitation has been demonstrated to play a key role in inducing release from the new ultrasound-responsive nanocarrier.

- The modification of ultrasound-responsive nanoparticles allowed us to improve their suspension stability and to provide selective uptake by cancer cells, which is of great importance for the use of nanomedicines in cancer therapy.

- Induced internalization in cancer cells has been achieved using a new type of mesoporous silica nanoparticles with hierarchical targeting, employing the thermal effects of ultrasound.

- The possibility of inducing the extravasation of mesoporous silica nanoparticles by exposure to acoustic cavitation has been demonstrated in an *in vitro* model.

- The capacity of placental mesenchymal stem cells to load and transport mesoporous silica nanoparticles towards tumors has been proven.

- For the first time, ultrasound-sensitive nanoparticles have been transported in a cellular vehicle, showing their capacity to kill cancer cells when exposed to the stimulus, first step in preclinical studies before considering their translation.

- The expression of suicide genes in placental mesenchymal stem cells has been achieved by modifying the surface of our ultrasound-responsive nanoparticles to enable them to act as gene transfection agents.

Throughout this thesis, spatiotemporal control of cytotoxic drug release has been achieved, enabling inducing drug release, modifying nanoparticle targeting to tumors and controlling the release of therapeutic agents from cell vehicles, all of it through the combination of ultrasound and mesoporous silica nanoparticles.

ANEXOS

Anexo I. Técnicas de caracterización empleadas

Los contenidos de este anexo se han recogido en su mayor parte de descripciones presentadas por fabricantes de equipos de las diferentes técnicas, así como de otras fuentes online (tales como Malvern, Iesmat, LABTE, Linseis, ThermoFisher, LTI y otras) con el objeto de facilitar la comprensión de los datos que se pueden obtener de cada una de ellas para lectores no familiarizados con alguna de las mismas.

Dispersión de luz dinámica (DLS)

La dispersión de luz dinámica (DLS), a la que a veces se hace referencia como dispersión de luz cuasi elástica (QELS), es una técnica no destructiva y bien establecida para medir el tamaño y distribución de tamaño de moléculas y partículas típicamente en la región submicrométrica, y con la última tecnología, inferiores a 1 nm.

Las aplicaciones típicas de la dispersión de luz dinámica son la caracterización de partículas, emulsiones o moléculas que se han dispersado o disuelto en un líquido. El movimiento Browniano de las partículas o moléculas en suspensión hace que la luz láser se disperse en diferentes intensidades. Con el análisis de estas fluctuaciones en la intensidad se obtiene la velocidad del movimiento Browniano, y por lo tanto, del tamaño de partícula mediante la relación de Stokes-Einstein.

Potencial Z

El potencial Z es una medida de la magnitud de la repulsión o atracción entre las partículas. Su medida proporciona una idea detallada de los mecanismos de dispersión y es la clave del control de dispersión electrostático. Valores positivos o negativos del potencial Z de una suspensión de nanopartículas proporcionan una idea del valor de la carga superficial de dichas nanopartículas en el medio en que se encuentran dispersas.

El potencial Z es un parámetro extremadamente importante en una gran variedad de actividades industriales como las bebidas, cerámica, farmacéutica, medicina, procesado mineral o tratamiento de aguas. Muchas industrias usan grandes cantidades de agua, que pueden ser contaminadas durante el proceso de producción. El potencial Z puede ser usado para optimizar el uso de floculantes excesivamente caros y la velocidad del proceso de floculación.

Porosimetría de adsorción de nitrógeno

La adsorción física o fisisorción de gases es una técnica de análisis de propiedades texturales (superficie específica, volumen y tamaño de poros) basada en la interacción que tiene lugar entre un gas (adsorbato) y el sólido que se quiere caracterizar (adsorbente). La porosimetría manométrica está basada en la medida de la presión reinante en el equilibrio, registrada a una temperatura determinada (77 K), para el sistema adsorbato-adsorbente considerado. Así, los resultados del análisis de fisisorción de gases están condicionados por la calidad en la medida de presión. El resultado de estos análisis es la 'isoterma de adsorción-desorción', que consiste en una serie de datos que relacionan el volumen de gas (en nuestro caso nitrógeno) retenido por la superficie del sólido a caracterizar en función de las condiciones de presión. La interpretación de estas isotermas mediante diferentes modelos matemáticos permite obtener valores para las propiedades texturales. Las propiedades que caracterizan texturalmente a un sólido son varias, aunque las más empleadas suelen ser:

- Superficie específica. Hace referencia al desarrollo superficial del sólido por unidad de masa y suele expresarse como m^2/g. La medida de esta propiedad se lleva a cabo en el rango intermedio de presiones, empleando modelos matemáticos como el B.E.T. (Brunauer-Emmett-Teller).
- Volumen total de poros. Se refiere al volumen ocupado por adsorbato, dentro del adsorbente, a una presión determinada (habitualmente cercana a $p/p^0=1$). Se trata de una medida directa, sin utilización de un modelo matemático, y expresa el volumen que ocupan los poros en una unidad másica de sólido. Habitualmente se expresa como cm^3/g.
- Distribución de tamaños de poro. Consiste en expresar el volumen de poro frente al tamaño de poro al que se adscribe. No es una medida directa, sino la consecuencia de aplicar modelos matemáticos más o menos complejos. En el caso de esta tesis doctoral, se ha empleado el modelo Barret-Joyner-Halenda (BJH). Es posiblemente el método más empleado para el cálculo de distribuciones de tamaños de poro en el rango de los mesoporos (2-50 nm) con geometría cilíndrica.

Análisis termogravimétrico (TGA)

La termogravimetría (TG) es una técnica en la que la masa de una muestra es monitorizada en función de la temperatura, a medida que se somete a dicha muestra a una rampa de calentamiento programada en una atmósfera controlada. Esta técnica ofrece la determinación cuantitativa de composiciones de materiales. Se trata de un método de análisis común en la industria química y farmacéutica. El análisis termogravimétrico (TGA) se realiza en polímeros, alimentos, productos farmacéuticos, así como muchos otros materiales.

Espectrofotometría ultravioleta-visible (UV-Vis)

La espectrofotometría ultravioleta-visible es una espectroscopia de emisión de fotones y una espectrofotometría. Utiliza radiación electromagnética (luz) de las regiones visible, ultravioleta cercana (UV) e infrarroja cercana (NIR) del espectro electromagnético, es decir, una longitud de onda entre 380 nm y 780 nm. La radiación absorbida por las moléculas desde esta región del espectro provoca transiciones electrónicas que pueden ser cuantificadas.

La espectroscopia UV-visible se utiliza para identificar algunos grupos funcionales de moléculas y de manera general en la determinación cuantitativa de los componentes de soluciones de iones de metales de transición y compuestos orgánicos altamente conjugados. Se utiliza extensivamente en laboratorios de química y bioquímica para determinar pequeñas cantidades de cierta sustancia, como las trazas de metales en aleaciones o la concentración de ciertos fármacos.

Espectroscopía y microscopía de fluorescencia

La espectrometría de fluorescencia (también llamada fluorometría o espectrofluorimetría) es un tipo de espectroscopia electromagnética que analiza la fluorescencia de una muestra. Se trata de utilizar un haz de luz, por lo general luz ultravioleta, que excita los electrones de las moléculas de ciertos compuestos y provoca que emitan luz de una menor energía, generalmente luz visible (aunque no necesariamente). Los dispositivos que miden la fluorescencia se llaman fluorímetros.

En la espectroscopia de fluorescencia, primero se excita la muestra mediante la absorción de un fotón de luz, desde su estado electrónico basal a uno de los distintos

estados vibracionales del estado electrónico excitado. Las colisiones con otras moléculas causan que la molécula excitada pierda energía vibracional hasta que alcanza el estado vibracional más bajo del estado electrónico excitado. La molécula desciende luego a uno de los distintos niveles de vibración del estado electrónico basal, emitiendo un fotón en el proceso. Como las moléculas pueden caer a cualquiera de los diferentes niveles de vibración en el estado basal, los fotones emitidos tendrán diferentes energías y, por lo tanto, frecuencias. Así pues, mediante el análisis de las diferentes frecuencias de luz emitida por espectrometría de fluorescencia, junto con sus intensidades relativas, se puede determinar la estructura de los diferentes niveles de vibración.

En un experimento típico, se miden las diferentes frecuencias de luz fluorescente emitida por una muestra, manteniendo la luz de excitación a una longitud de onda constante. A esto se le llama espectro de emisión. Un espectro de excitación se mide mediante el registro de una serie de espectros de emisión utilizando luz de diferentes longitudes de onda.

El mismo principio físico de fluorescencia se emplea en la microscopía de fluorescencia. El microscopio de fluorescencia es una variación del microscopio de luz ultravioleta en el que los objetos son iluminados por rayos de una determinada longitud de onda. La imagen observada es el resultado de la radiación electromagnética emitida por las moléculas que han absorbido la excitación primaria y reemitido una luz con mayor longitud de onda. Para dejar pasar sólo la emisión secundaria deseada, se deben colocar filtros apropiados debajo del condensador y encima del objetivo. Se usa para detectar sustancias con autofluorescencia o sustancias marcadas con fluorocromos.

Espectroscopía de resonancia magnética nuclear (NMR)

La espectroscopía de resonancia magnética nuclear (NMR) es una técnica empleada principalmente en la elucidación de estructuras moleculares, aunque también se puede emplear con fines cuantitativos y en estudios cinéticos y termodinámicos.

Algunos núcleos atómicos sometidos a un campo magnético externo absorben radiación electromagnética en la región de las frecuencias de radio o radiofrecuencias. Como la frecuencia exacta de esta absorción depende del entorno de estos núcleos, se puede emplear para determinar la estructura de la molécula en donde se encuentran estos. Para que se pueda emplear la técnica los núcleos deben tener un momento magnético distinto de cero. Esta condición no la cumplen los núcleos con número

másico y número atómico par. Los núcleos más importantes en química orgánica son: ^{1}H, ^{13}C, ^{31}P, ^{19}F y ^{15}N.

Se prefieren los núcleos de número cuántico de espín nuclear igual a 1/2, ya que carecen de un momento cuadrupolar eléctrico que produce un ensanchamiento de las señales de RMN. También es mejor que el isótopo sea abundante en la naturaleza, ya que la intensidad de la señal dependerá de la concentración de esos núcleos activos. Por eso, uno de los más útiles en la elucidación de estructuras es el ^{1}H, dando lugar a la espectroscopia de resonancia magnética nuclear de protón. También es importante en química orgánica el ^{13}C, aunque se trata de un núcleo poco abundante y poco sensible.

La técnica se ha empleado en química orgánica, química inorgánica y bioquímica. La misma tecnología también ha terminado por extenderse a otros campos, por ejemplo en medicina, en donde se obtienen imágenes por resonancia magnética.

Espectroscopía de infrarrojo con transformada de Fourier (FTIR)

La espectroscopia de absorción infrarroja con transformada de Fourier (FTIR) es el método utilizado para determinar las estructuras de moléculas con características de absorción de la radiación infrarroja según su vibración molecular. La región IR va de 12.800 a 10 cm^{-1} y se puede dividir en IR cercano (NIR) (12.800-4000 cm^{-1}), IR medio (4.000-400 cm^{-1}) e IR lejano o FAR-IR (50-400 cm^{-1}). El espectro vibracional de una molécula se considera una propiedad física única y por tanto, característica de esta molécula. Así, entre otras aplicaciones, el espectro IR se puede usar como "huella dactilar" en la identificación de muestras desconocidas mediante la comparación con espectros de referencia

Una de las grandes ventajas de la espectroscopia FTIR es su versatilidad, ya que permite estudiar prácticamente cualquier muestra con independencia del estado en que se encuentre: líquidos, disoluciones, polímeros, geles, fibras, films, gases o superficies son algunos ejemplos. Es posible trabajar tanto en transmisión, como en reflectancia total atenuada (ATR).

Difracción de rayos X (XRD)

La difracción de rayos X es uno de los fenómenos físicos que se producen al interaccionar un haz de rayos X, de una determinada longitud de onda, con una estructura ordenada. La difracción de rayos X se basa en la dispersión coherente del haz

de rayos X por parte de la materia (se mantiene la longitud de onda de la radiación) y en la interferencia constructiva de las ondas que están en fase y que se dispersan en determinadas direcciones del espacio.

El fenómeno de la difracción puede describirse con la Ley de Bragg, que predice la dirección en la que se da interferencia constructiva entre haces de rayos X dispersados coherentemente por un cristal: $n\lambda=2d\text{sen}\theta$.

La difracción de rayos en muestra policristalina permite abordar la identificación de fases cristalinas (puesto que todas las estructuras cristalinas poseen su difractograma característico) tanto en su aspecto cualitativo como cuantitativo. En el caso de materiales mesoporosos tipo MCM-41, la XRD a bajo ángulo permite evaluar la estructura ordenada de los poros del material.

Microscopía electrónica de barrido (SEM)

La microscopía electrónica de barrido (SEM) es una técnica de microscopía electrónica capaz de producir imágenes de alta resolución de la superficie de una muestra utilizando las interacciones electrón-materia. Utiliza un haz de electrones en lugar de un haz de luz para formar una imagen. Los microscopios de SEM poseen una gran profundidad de campo, que permite enfocar a la vez gran parte de la muestra. También producen imágenes de alta resolución, de forma que las características más ínfimas de la muestra pueden ser examinadas con gran amplificación. La preparación de las muestras es relativamente fácil ya que la mayoría de los microscopios de SEM sólo requieren que estas sean conductoras. La muestra generalmente se recubre con una capa de carbono o una capa delgada de un metal, como el oro, para darle carácter conductor. Posteriormente, se barre la superficie con electrones acelerados que viajan a través del cañón. Un detector formado por lentes basadas en electroimanes, mide la cantidad e intensidad de los electrones que devuelve la muestra, siendo capaz de mostrar figuras en tres dimensiones mediante imagen digital.

Microscopía electrónica de transmisión (TEM)

El microscopio electrónico de transmisión es un instrumento que aprovecha los fenómenos físico-atómicos que se producen cuando un haz de electrones suficientemente acelerado colisiona con una muestra delgada convenientemente preparada. Cuando los electrones colisionan con la muestra, en función de su grosor y

del tipo de átomos que la forman, parte de ellos son dispersados selectivamente, es decir, hay una gradación entre los electrones que la atraviesan directamente y los que son totalmente desviados. Todos ellos son conducidos y modulados por unas lentes para formar una imagen final sobre un dispositivo de carga acoplada que puede tener miles de aumentos con una definición inalcanzable para cualquier otro instrumento. La información que se obtiene es una imagen con distintas intensidades de gris que se corresponden al grado de dispersión de los electrones incidentes.

La imagen de TEM tal como se ha descrito ofrece información sobre la estructura de la muestra, tanto si ésta es amorfa o cristalina. Además, si la muestra es cristalina o posee porosidad ordenada, es decir, si hay una estructura de planos periódica, puede ocurrir que varias familias de esos planos cumplan la condición de Bragg y difracten de forma coherente la onda electrónica incidente. Esto da lugar a un diagrama de difracción, que es una imagen de distintos puntos ordenados respecto a un punto central (electrones transmitidos no desviados) que nos aportan información sobre la orientación y estructura del/los cristales presentes.

Cromatografía por permeación de gel (GPC)

La cromatografía por permeación de gel (GPC) es una técnica analítica que separa macromoléculas disueltas por tamaño con base en su elución desde columnas llenas de un gel poroso. Cuando la GPC se usa con dispersión de luz, viscómetro y detectores de concentración (lo que se conoce como detección triple), puede medir el peso molecular absoluto, el tamaño molecular y la viscosidad intrínseca, y generar información sobre la estructura macromolecular, la conformación, la agregación y la ramificación. Mediante el uso de GPC para medir el peso molecular y las otras propiedades, los científicos pueden caracterizar moléculas como polímeros sintéticos y polímeros naturales como los polisacáridos.

Citometría de flujo

El termino citometría de flujo se define como una tecnología que mide células a su paso por un fluido en una serie de detectores, esto es, una suspensión celular se inyecta al fluido laminar donde las células pasan una después de la otra a través de un capilar y llegan hasta un rayo láser. Cuando este rayo incide en una célula, la luz de excitación sale hacia delante y hacia los lados de la célula y esto genera información. La luz

dispersada hacia delante posee información sobre el tamaño de la célula. La luz dispersada hacia los lados provee información sobre la granularidad, tamaño y morfología celular. Si la célula va marcada con un fluoróforo o es autofluorescente, la luz fluorescente se procesa, a través de los distintos fotomultiplicadores, en el sistema procesador de datos y los resultados son analizados por el software del citómetro.

La ventaja analítica de la citometría de flujo tiene como base la habilidad de hacer mediciones cuantitativas y multiparamétricas en un número estadísticamente adecuado de células para definir las propiedades de una población celular o de las subpoblaciones que la componen. Para llevar a cabo todo esto los equipos necesitan un sistema combinado de flujo, óptica y electrónica. El sistema de fluido introduce y restringe a las células para su análisis individual, el sistema óptico excita la muestra y colecta las señales de luz provenientes de la misma y el sistema electrónico convierte la señal óptica en una señal electrónica y la digitaliza para el análisis en el ordenador.

Anexo II. Publicaciones realizadas durante la tesis doctoral.

1. Martínez-Vázquez, F. J., Cabañas, M. V., **Paris, J. L**., Lozano, D. & Vallet-Regí, M. Fabrication of novel Si-doped hydroxyapatite/gelatine scaffolds by rapid prototyping for drug delivery and bone regeneration. Acta Biomater. 15, 200–209 (2015). Nº citas= 45. IF= 6.008.
2. **Paris, J. L**., Román, J., Manzano, M., Cabañas, M. V. & Vallet-Regí, M. Tuning dual-drug release from composite scaffolds for bone regeneration. Int. J. Pharm. 486, 30–37 (2015). Nº citas= 11. IF= 3.994.
3. **Paris, J. L**., Cabañas, M. V., Manzano, M. & Vallet-Regí, M. Polymer-Grafted Mesoporous Silica Nanoparticles as Ultrasound-Responsive Drug Carriers. ACS Nano 9, 11023–11033 (2015). Nº citas= 78. IF= 13.334.
4. **Paris, J. L**., de la Torre, P., Manzano, M., Cabañas, M. V., Flores, A. I. & Vallet-Regí, M. Decidua-derived mesenchymal stem cells as carriers of mesoporous silica nanoparticles. *In vitro* and *in vivo* evaluation on mammary tumors. Acta Biomater. 33, 275–82 (2016). Nº citas= 4. IF= 6.319.
5. **Paris, J. L**., Colilla, M., Izquierdo-Barba, I., Manzano, M. & Vallet-Regí, M. Tuning mesoporous silica dissolution in physiological environments: a review. J. Mater. Sci. 52, 8761–8771 (2017). IF= 2.599.
6. Rwei, A. Y.[1], **Paris, J. L.[1]**, Wang, B., Wang, W., Axon, C. D., Vallet-Regí, M., Langer, R. & Kohane, D. S. Ultrasound-triggered local anaesthesia. Nat. Biomed. Eng. 1, 644–653 (2017). *(Destacado como portada).*
7. **Paris, J. L**., de la Torre, P., Cabañas, M. V., Manzano, M., Grau, M., Flores, A. I. & Vallet-Regí, M. Vectorization of ultrasound-responsive nanoparticles in placental mesenchymal stem cells for cancer therapy. Nanoscale 9, 5528–5537 (2017). Nº citas= 2. IF= 7.367.
8. **Paris, J. L**.[1]; Mannaris, C. [1]; Cabañas, M. V.; Carlisle, R.; Manzano, M.; Vallet-Regí, M.; Coussios, C.C. Ultrasound-Mediated Cavitation-Enhanced Extravasation of Mesoporous Silica Nanoparticles for Controlled-Release Drug Delivery. Chem. Eng. J. (2017). Enviado.
9. **Paris, J**. **L.;** Vallet-Regí, M. Nanostructures for imaging, medical diagnostics and therapy. 2017, aceptado para su publicación como capítulo de libro en "Handbook of nanoparticles and architectural nanostructured materials", de la editorial Elsevier.

[1] Co-primer autor.

Esta tesis doctoral se centra en el estudio de nanopartículas de sílice mesoporosa (MSNs) en combinación con ultrasonido (US) para su uso en biomedicina, y más concretamente, en el contexto de la oncología. Primero, se ha llevado a cabo el desarrollo y la evaluación de nanopartículas de sílice mesoporosa con liberación de fármacos inducida por US. Posteriormente, se plantean dos tipos de aproximaciones para lograr el transporte selectivo de estas nanopartículas hacia tumores, bien mediante estrategias físico-químicas de vectorización o bien empleando como vehículos de las nanopartículas células capaces de migrar al tejido tumoral.